TO FLEE, OR NOT TO FLEE?

Using innate defensive behaviours to investigate rapid perceptual decision-making through subcortical circuits in mouse models of autism.

by

Laura Burnett
January, 2023

A thesis submitted to the
Graduate School
of the
Institute of Science and Technology Austria
in partial fulfilment of the requirements
for the degree of
Doctor of Philosophy

Committee in charge:

Professor Beatriz Vicoso, Chair
Professor Maximilian Jösch (Supervisor)
Professor Ryuichi Shigemoto (Internal)
Professor Mark Hübener (External)

The thesis of Laura Burnett, titled "*To flee, or not to flee? Using innate defensive behaviours to investigate rapid perceptual decision-making through subcortical circuits in mouse models of autism.*", is approved by:

Supervisor: Maximilian Jösch, ISTA, Klosterneuburg, Austria

Signature: _____

Committee Member: Ryuichi Shigemoto, ISTA, Klosterneuburg, Austria

Signature: _____

Committee Member: Mark Hübener, Max Planck Institute for Biological Intelligence, Martinsried, Germany

Signature: _____

Defence Chair: Beatriz Vicoso, ISTA, Klosterneuburg, Austria

Signature: _____

Signed page is on file

ISTA Thesis, ISSN: 2663-337X

I hereby declare that this thesis is my own work and that it does not contain other people's work without this being so stated; this thesis does not contain my previous work without this being stated, and the bibliography contains all the literature that I used in writing the dissertation.

I declare that this is a true copy of my thesis, including any final revisions, as approved by my thesis committee, and that this thesis has not been submitted for a higher degree to any other university or institution.

I certify that any republication of materials presented in this thesis has been approved by the relevant publishers and co-authors.

Signature: _____

Laura Burnett

January, 2023

Signed page is on file

Abstract

The process of detecting and evaluating sensory information to guide behaviour is termed perceptual decision-making (PDM), and is critical for the ability of an organism to interact with its external world. Individuals with autism, a neurodevelopmental condition primarily characterised by social and communication difficulties, frequently exhibit altered sensory processing and PDM difficulties are widely reported. Recent technological advancements have pushed forward our understanding of the genetic changes accompanying this condition, however our understanding of how these mutations affect the function of specific neuronal circuits and bring about the corresponding behavioural changes remains limited. Here, we use an innate PDM task, the looming avoidance response (LAR) paradigm, to identify a convergent behavioural abnormality across three molecularly distinct genetic mouse models of autism (*Cul3*, *Setd5* and *Ptchd1)*. Although mutant mice can rapidly detect threatening visual stimuli, their responses are consistently delayed, requiring longer to initiate an appropriate response than their wild-type siblings. Mutant animals show abnormal adaptation in both their stimulus-evoked escape responses and exploratory dynamics following repeated stimulus presentations. Similarly delayed behavioural responses are observed in wild-type animals when faced with more ambiguous threats, suggesting the mutant phenotype could arise from a dysfunction in the flexible control of this PDM process.

Our knowledge of the core neuronal circuitry mediating the LAR facilitated a detailed dissection of the neuronal mechanisms underlying the behavioural impairment. *In vivo* extracellular recording revealed that visual responses were unaffected within a key brain region for the rapid processing of visual threats, the superior colliculus (SC), indicating that the behavioural delay was unlikely to originate from sensory impairments. Delayed behavioural responses were recapitulated in the *Setd5* model following optogenetic stimulation of the excitatory output neurons of the SC, which are known to mediate escape initiation through the activation of cells in the underlying dorsal periaqueductal grey (dPAG). *In vitro* patch-clamp recordings of dPAG cells uncovered a stark hypoexcitability phenotype in two out of the three genetic models investigated (*Setd5* and *Ptchd1*), that in *Setd5,* is mediated by the misregulation of voltage-gated potassium channels. Overall, our results show that the ability to use visual information to drive efficient escape responses is impaired in three diverse genetic mouse models of autism and that, in one of the models studied, this behavioural delay likely originates from differences in the intrinsic excitability of a key subcortical node, the dPAG. Furthermore, this work showcases the use of an innate behavioural paradigm to mechanistically dissect PDM processes in autism.

Acknowledgments

First and foremost, I would like to thank *Max Jösch* for his supervision, support and encouragement throughout the PhD process, and for taking me on to begin with. Thank you for giving me the freedom to pursue this project and the opportunity to learn from you.

I would also like to thank the following people:

Peter Koppensteiner for offering his unparalleled patching prowess and professionalism to the project. The contribution of his work to this project cannot be understated.

Olga Symonova for her incredible computational abilities, kindness and generosity. She has been instrumental in the development of my computational skills and I feel fortunate to have her as both a friend and a colleague.

Tomás Vega-Zuniga for his assistance with the *in vivo* recordings, his anatomical knowledge and unmatched sense of humour.

Tomás Masson for his help with the western blot experiments and all members of the *Neuroethology group*, past and present: *Divyansh Gupta*, *Victoria Pokusaeva*, *Eleonora Quiroli*, *Roshan Satapathy*, *Florian Schmidt*, *Toni Sumser* and *Ece Sönmez*, for their valuable feedback, discussions and fun times both inside and outside the lab.

Gaia Novarino for her generosity in establishing this collaborative project and continued support from its conception. Thanks also to multiple members of her group for their assistance in obtaining animals and resources and helpful discussions.

Ryuichi Shigemoto for his contributions to the project and his support throughout and his former PostDoc, *Felipe Fredes*, for teaching me how to perform the mouse surgeries and his general advice on the project at the beginning.

Freyja Langer and *Michael Schunn* for their invaluable work in generating, maintaining and supporting our mouse colonies.

Our A2Ps over the years: *Lena Marr*, *Mariam Mosiashvili* and especially *Rita Six* for providing invaluable organisational assistance.

I would also like to thank my previous mentors: *Joanne Britto*, *Heather Young*, *Conor McCann* and *Robert Beattie* who all showed me incredible kindness and generosity and who inspired, encouraged and supported me in pursuing a PhD, or scientific research in general.

For the personal support they have provided, I would like to thank my friends, both in Vienna and further afield, especially *Chloe*, *Chiara*, *Ella*, *Anna*, *Jasmin* and *Giulia*, for the spontaneous facetimes, erratic voice notes and the endless cups of tea.

Last but not least, I would like to thank my *family* for their continued love and support, especially my *parents*, without whose countless sacrifices I would almost certainly not be here writing this, and *Michele*, for supporting me, believing in me and feeding me through it all.

*

This work received great assistance from the Scientific Service Units of IST Austria (ISTA) through resources provided by the Lab Support Facility, the Imaging and Optics Facility, the Machine Shop Unit and the Preclinical Facility and was supported by a European Research Council (ERC) Starting Grant 756502 (*Daphne*).

About the Author

Laura Burnett completed a BSc and a MSc in Natural Sciences at University College London (UCL), UK. The third year of her undergraduate was spent at the University of Melbourne, Australia, before returning to London to complete her MSc at the UCL Institute of Child Health. She joined the ISTA graduate school in September 2016, became part of the Neuroethology group in July 2017 and has since been working on investigating how rapid perceptual decision-making through subcortical circuits is affected in mouse models of autism. During her PhD, Laura has presented her research at the 2019 'Federation for European Neuroscience (FENS) Winter School for Instinctive and Innate Behaviours' at Sölden, Austria, the '2019 Color Vision' conference at Janelia Farm Research Campus, USA, the Austrian Neuroscience Association (ANA) 2021 Meeting in Salzburg, Austria, the International Winter Neuroscience Conference (INWC) 2022 in Sölden, Austria and two FENS Forums in 2020 and 2022.

List of Collaborators and Publications

Peter Koppensteiner performed all *in vitro* patch clamp experiments and helped analyse the data.

Olga Symonova assisted in the construction of the experimental setups and generated scripts for stimulus control and data analysis.

Tomás Masson performed the western blot analysis of $K_v1.1$ protein content.

Tomas Vega-Zuniga designed and built the *in vivo* electrophysiology setup.

Ximena Contreras, *Thomas Rülicke* and *Gaia Novarino* generated the *Ptchd1* mouse line.

The results presented in this thesis have been posted on the BioRXiv preprint server in the following manuscript:

Subcortical circuit dysfunctions delay perceptual decision-making in autism models. **Burnett LE**, Koppensteiner P., Symonova O., Masson T., Vega-Zuniga T., Contreras X., Rülicke T., Shigemoto R., Novarino G., Jösch M. (2022) *bioRxiv*.
doi: https://doi.org/10.1101/2022.10.11.51169

Table of Contents

List of Figures

List of Abbreviations

1-EBIO	1-ethyl-2-benzimidazolinone
2AFC	Two alternative forced choice
ACSF	Artificial cerebrospinal fluid
α-DTX	alpha-Dendrotoxin
ADHD	Attention deficit hyperactivity disorder
ASD	Autism spectrum disorders
BK	Calcium-activated large-conductance
BLA	Basolateral amygdala
BSA	Bovine serum albumin
CeA	Central nucleus of the amygdala
ChR2	Channelrhodopsin-2
C_m	Membrane capacitance
CMNF	Constrained non-negative matrix factorisation
CNO	Clozapine N-Oxide
CNV	Copy number variants
CSD	Current source density
CTX	Cortex
Cul3	Cullin-3
DABCO	1,4,-diazabicyclooctane
DAPI	4’,6-diamidino-2-phenylindole
DiI	1,1'-dioctadecyl-3,3,3',3'-tetramethylindocarbocyanine perchlorate
dLGN	Dorsal lateral geniculate nucleus
dlPAG	Dorsolateral periaqueductal grey
dmPAG	Dorsomedial periaqueductal grey
DREADDS	Designer Receptors Exclusively Activated By Designer Drugs
dSC	Deep superior colliculus
DSI	Direction selectivity index
EEG	Electroencephalogram
ER	Endoplasmic reticulum
fAHP	Fast-afterhyperpolarisation potential
FID	Flight initiation distance
fMRI	Functional magnetic resonance imaging
GABA	γ-Aminobutyric acid
GRIN	Graded index
Hdac3	Histone deacetylase 3
ID	Inflection depth
i.p.	Intraperitoneal
iPSC	Induced pluripotent stem cells
IQR	Interquartile range
IR	Infra-red
iSC	Intermediate superior colliculus
KP	Kynurenine pathway
Kv	Voltage-gated potassium channels
LAR	Looming avoidance response
LED	Light emitting diode
LGN	Lateral geniculate nucleus
LIP	Lateral intraparietal area
lPAG	Lateral periaqueductal grey
LTP	Long term potentiation

MEG	Magnetoencephalography
MD	Mediodorsal thalamus
MT	Medial temporal area
NF	Narrow field
NMDA	N-methyl-D-aspartate
OT	Optic tectum
P2N	Peak-to-noise
Paf1	Polymerase-associated factor 1
PAG	Periaqueductal grey
PBGN	Parabigeminal nucleus
PD	Perceptual decision
PDM	Perceptual decision-making
PFA	Paraformaldehyde
PFC	Prefrontal cortex
PSD	Postsynaptic density
Ptchd1	Patched domain containing 1
Pulv	Pulvinar
PV	Parvalbumin
rDNA	Ribosomal deoxyribonucleic acid
R_{in}	Input resistance
RF	Receptive field
RGC	Retinal ganglion cell
RMP	Resting membrane potential
SAI	Stratum album intermediale
SAP	Stratum album profudum
SEM	Standard error of the mean
sEPSC	Spontaneous excitatory postsynaptic current
Setd5	SET-domain containing 5
s.c.	Subcutaneous
SC	Superior colliculus
SGI	Stratum griseum intermediate
SGP	Stratum griseum profundum
SGS	Stratum griseum superior
SO	Stratum opticum
SK	Small-conductance calcium-activated
sSC	Superficial superior colliculus
STA	Spike-triggered average
τ	Membrane time constant (tau)
T_d	Trajectory directedness
TRN	Thalamic reticular nucleus
V1	Primary visual cortex
vLGN	Ventral lateral geniculate nucleus
vlPAG	Ventrolateral periaqueductal grey
VR	Visually-responsive
VTA	Ventral tegmental area
WCC	Weak central coherence
WF	Wide-field
ZETA	Zenith of Event-based Time-locked Anomalies
ZO	Stratum zonale

1 Introduction

The phenomenon of behaviour is the outcome of the iterative process of evolution that has enabled complex organisms to interact with, and respond to, external features within their environment. Over the course of evolution, organisms developed the ability to convert the detection of certain external phenomena into interpretable signals through which meaningful information could be inferred. Organisms that developed specialised biological systems for detecting physical stimuli within the environment were preferentially selected for, thanks to the survival advantage this newfound knowledge provided. Their ability to gather knowledge about the presence, location and identity of objects around them enabled the expression of increasingly sophisticated motor behaviours that in turn, further shaped the development of their sensory processing systems. Initial motor responses to the detection of stimuli were reactive and stereotyped. Some of these reflexive responses bestowed a level of survival fitness upon the host individuals that they were meticulously selected for, and conserved over time, to give rise to what we see today as 'instinctive' behaviours. Instinctive behaviours include actions critical to reproductive success, growth or survival. These stimulus-response routines became 'hard-wired' into animals' neural circuits, overcoming the need for prior experience or training. Evolutionary pressures, however, encouraged the expansion of the behavioural repertoire from these reactive motor actions to flexible, adaptive responses that could be fine-tuned to match the externally changing environment and fluctuating internal needs. Although this gave rise to a huge increase in behavioural flexibility, it simultaneously brought about the challenge of discriminating, evaluating and determining the most appropriate choice for the current situation, among a selection of potential options. This process of detecting and evaluating sensory information to make an informed decision about how to behaviourally respond is defined as **perceptual decision-making** (PDM), and describes the pervasive process guiding many of the conscious and nonconscious tasks performed by living organisms throughout life.

The research in this thesis centres specifically on the investigation of the **rapid PDM** processes that generate behavioural responses to **imminent threats**. It focuses on the neurodevelopmental condition **autism,** characterised by abnormal perception, attention and cognition, all of which are foundational to PDM, to shed light on neuronal pathways and biophysical mechanisms required for proper PDM. Here I aim to examine these questions using a **comparative approach** across three distinct genetic mouse models of autism. It is hoped that through a systematic behavioural and neuronal analysis of these animals we might learn more about the biology of PDM, as well as how PDM differences arise in autism. In this introduction, I will first introduce how sensory, and specifically visual, information is used by animals and humans to drive behaviour. I will then describe how visually-guided defensive behaviours have been used to model and examine PDM in animal models, and will outline what is known about the circuits regulating these behaviours in mammals. Lastly, I will introduce the neurodevelopmental condition, autism, and will present the current knowledge on altered perceptual decision-making in both affected human individuals and animal models of this condition.

1.1 How is visual information used to drive behaviour?

The origin of any perceptual decision (PD) is the detection of sensory information in the external world. Sensory systems have evolved to detect, and make the most of, all forms of sensory information available to them and perceptual decisions can rely on information arising from any sensory modality. The selective identification of chemical cues in the air, the localisation of a particular auditory cue or even the detection of physical vibrations or proprioceptive pressure signals can be used to inform a behavioural response. While each of these modalities have their own unique advantages and limitations for detecting useful information from the environment, this thesis is primarily focussed on understanding how vision, and visual cues, are used to guide an organism's behaviour.

The ubiquitous presence and extensive reach of light from the sun, has resulted in many of earth's terrestrial and shallow-dwelling aquatic animals developing a reliance on visual cues to gather information about the world around them. Rhythmic fluctuations in environmental luminance provided a sensory scaffold on which early organisms could sync their activity and orient themselves in time and space and reflexive, phototactic responses are likely the earliest visually-driven behaviours. Although these behaviours only required crude detectors of global illumination, across millennia the visual sensory systems of organisms refined their ability to resolve detailed properties of visual stimuli with exquisite sensitivity, acuity and speed. This perceptual advancement meant that detailed information about external objects could be acquired rapidly and accurately from a distance. Dangerous terrains could be avoided, food could be foraged for, mates could be signalled to and threats could be detected at range.

However, this newfound abundance in perceptual detail brought with it a corresponding increase in the computational complexity of identifying, classifying and evaluating the collection of stimuli present within the visual scene. Which part of the visual scene should an organism preferentially attend to? What visual features will be most informative in driving an organism's behavioural decisions? To overcome this problem, nervous systems developed mechanisms by which they could automatically process incoming visual information, to rapidly discriminate the relevant signals, from irrelevant ones. The saliency, or importance, of a visual feature could be determined by several mechanisms and the process of selecting the most important visual feature to then subject to further processing, is referred to as selective attention. This process is thought to occur in neural circuits downstream of the primary sense organs, and involves the ongoing integration of both 'bottom-up' and 'top-down' inputs to the incoming visual signal for the selection of an appropriate attentional target. 'Top-down' inputs arise from higher brain areas that impart contextual information about the current situation, needs or past experiences of an organism in order to infer the most appropriate stimulus to target future actions (Gilbert and Li 2013). Top-down modulation by higher, mainly cortical brain areas, has the ability to alter the visual signal arising directly from the retina, and at all stages downstream. This modulation can bias the representation of certain visual features, objects or spatial regions according to the behavioural context and is critical for the formation

of adaptive behaviour. These sorts of projections are required for assigning value or meaning to novel visual stimuli over development, and for the ability of these values to be evaluated, updated and even extrapolated to new stimuli over time. In general, perceptual processing that undergoes top-down modulation requires longer timescales to generate an informed decision than the bottom-up mechanisms described below but it benefits from the acquisition of information accrued through past experiences.

Bottom-up influences on selective attention refer to the intrinsic association of certain, often simplistic, features of visual stimuli that imbue a generalisable message of importance. The size, shape, motion, colour or position of a visual stimulus can all be inherently salient to an organism and can rapidly shift critical processing capabilities towards the further examination of this object. The gestalt presentation of the stimulus and its surroundings can also instil a level of saliency that is not achieved by the stimulus alone (Kofka, 1935). For example, the presentation of a single horizontal bar among a collection of vertical bars is inherently salient, whilst the presentation of that bar alone, or with other horizontal bars is not (Fig. 1.1). Many intrinsic, or innate behavioural responses to visual stimuli often rely on bottom-up forms of visual attention since they are often more rapidly processed and do not require wider contextual or evaluative cues. Different types of these behaviours can be seen in a wide variety of life on earth and to all types of visual features. For example, toads will selectively perform hunting behaviours towards the presentation of a moving horizontal, but not vertical bar (Ewert 1987). While, the detection of specific colour cues will drive aggressive behaviours in English robins. Typically, these aggressive behaviours are generated in response to the detection of the bright red plumage of a competing conspecific, however experiments showed that they can also be produced solely in the presence of an inanimate tuft of red feathers (Lack 1939).

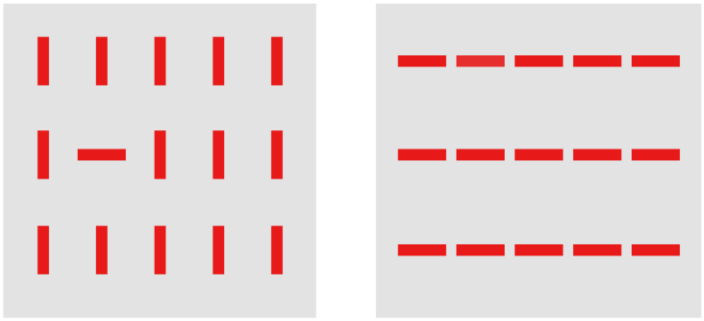

Fig. 1.1 Bottom-up attentional mechanisms.

Gestalt perception involves the understanding of a pattern or object as a whole, rather than the sum of its parts (Kofka, 1935). The visual system's gestalt perceptual organisation of visual stimuli generates an innate bottom-up attentional mechanism whenever single elements within an image are incongruent with the global image or pattern being presented. For example, the same horizontal bar presented within a group of vertical bars (left) is inherently more salient than the same bar presented within a group of identical horizontal bars (right).

Moving objects are inherently salient since they indicate a change in the external world. Orienting responses to visual motion cues are found in every animal group with non-primitive eyes, and play a crucial role in course stabilisation and navigation (Srinivasan et al. 1999). Flying insects, such as *Drosophila melanogaster*, use full-field visual motion cues to gather information about their position in space and adjust their course control parameters appropriately (Hausen and Egelhaaf 1989; Borst 2014). While many predatory animals, such as snakes and chameleons, use motion cues to detect and plan attack strategies towards prey (Flanders 1985; Ketter-Katz et al. 2020; Bothe et al. 2019). Although certain features of visual motion are of behavioural importance only to specific species, others represent features of universal significance and mediate conserved behavioural responses across the animal kingdom. One such stimulus is the rapid expansion of an image on the retina that signals an approaching object, possibly a predator or an obstacle, on a collision course with the observer. This type of visual cue is referred to as a 'looming' stimulus and triggers bottom-up attentional mechanisms across species (see section 1.2.3). Responding to approaching threats is crucial to an organism's survival and the specific use of visual cues is advantageous in that objects can be identified over large distances and with a high temporal precision (Inman 2020). For this reason, neural circuits that mediate rapid defensive responses to threats upon the detection of specific visual cues are highly conserved across evolution.

1.2 Defensive behaviours as perceptual decision-making processes.

Once a visual threat has been detected, a decision must be made as to how to respond. A defensive behaviour is an action that 'aims to minimise the chances of being harmed' (Evans et al. 2019). Although the ability to generate the individual defensive behaviours is hard-wired and innate, the decision to initiate a response and the process of selecting and performing the chosen defensive behaviour is necessarily flexible and adaptive. The performance of the response is known to depend on specific features of the threatened target, the threat, as well as the ongoing environmental conditions, internal state and past experiences of the individual. In this section, I will discuss how these decision processes have been investigated in the past and the factors that are known to influence them. I will introduce and focus on the use of a specific behavioural paradigm - the looming avoidance response (LAR) - since it forms the basis of most of the experimental work done in this thesis.

1.2.1 To flee, or not to flee? The detection and perception of threats.

Given the importance of responding to visual threats to the survival of an organism, visual systems have been primed to respond with a sensitivity that is both critical to early stimulus detection and simultaneously fallible to activation by innocuous, but statistically similar stimuli. Therefore, upon visual detection of a potential threat, an organism must perform an initial classification operation which can be subdivided into a perceptual evaluation (Is there an object present?) and a value-based evaluation (Is the object a threat?). The outcome of this classification is often linked to the activation of the bottom-up attentional mechanisms described in the section above. Many features of visual threats; bright colours, large sizes or approaching motion, inherently trigger an alerting response in animals that cause the animal to cease its ongoing activity and perform further sensory sampling of the environment. Often at this initial stage, and especially in situations where the quality of the sensory information is low, or ambiguous, and the existence of the threat is uncertain, animals often perform risk assessment behaviours (Blanchard et al. 2001; Blanchard et al. 2011). Cessation of movement enables animals to improve their sampling of sensory information whilst additionally decreasing their saliency to potential predators. This additional acquisition of information is often critical in determining if the signal requires further action.

Sometimes, distinct objects can generate qualitatively similar retinal images and therefore will be registered with a certain level of ambiguity in downstream processing circuits. As mentioned in the previous section, often the gestalt configuration of the object in its environment or the combination of multiple visual features are required to accurately interpret both the identity and the contextual value of the observed object. A stimulus with the same statistics but in a different context may not be classified as a threat and so will not generate a response. This was a key finding of seminal works in the field of neuroethology[1] (Tinbergen 1939; Lorenz 1939), where birds presented with an asymmetric, bird-shaped stimulus would escape only when the stimulus was moved in one direction, but not the other (Fig. 1.2). Whilst the shape itself was not inherently aversive, the combination of the shape, with the aerial location of presentation and the kinetics of movement was sufficient to 'release' the evoked defensive response.

[1] See Schleidt et al. (2011) for a detailed review of this topic.

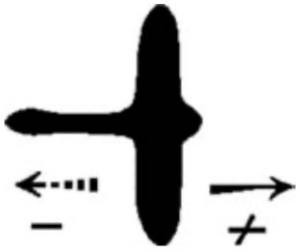

Fig. 1.2 Perceived movement affects the ability of an asymmetric visual stimulus to trigger defensive responses in birds.

The presentation of the above stimulus to a group of chickens did not trigger a defensive response when moved in the direction to the left ('-' symbol), but it did when moved to the right ('+' symbol). It is thought that this is because leftward motion mimics the movements of a long-necked, non-threatening species while rightward motion gives the silhouette of a short-necked, predatory bird species flying overhead. Figure adapted from Tinbergen (1951).

An influential theory applying an economical cost-benefit analysis to the generation of escape behaviours (Ydenberg and Dill 1986) can also be applied to the decision-making process underlying the choice to respond to a stimulus at all. This model attempts to describe the factors underlying the decision to initiate an escape response at varying levels of danger. It models the decision-making process as a continuous evaluation of the relative costs and gains associated with responding or remaining. Applied to the situation whereby an organism detects a potential threat, generating an errant 'false positive' response to an innocuous stimulus would result in the unnecessary cessation of other, potentially critical, resource acquisition activities such as foraging, mate selection or territory defence and the needless expenditure of energy. All factors which present a significant fitness cost to the individual. At the same time, not responding to a real threat would result in the increased risk of serious injury, and in the most extreme case, death.

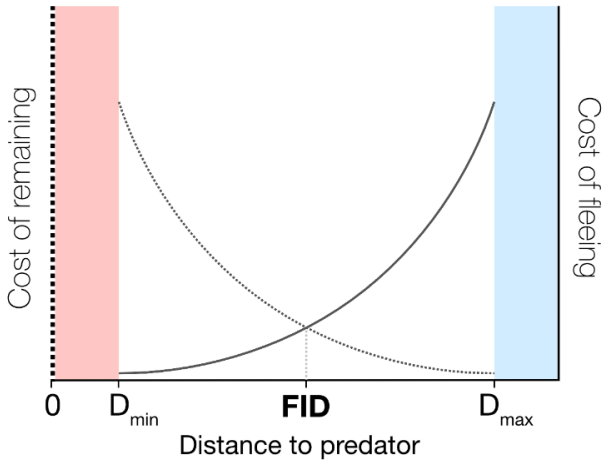

Fig. 1.3 Modification of the Ydenberg and Dill (1986) economic model of flight initiation distance.

This graphical model represents the idea that the intersection of the two lines predicts the optimal distance at which an animal should initiate an escape response, the flight initiation distance (FID), in order to minimise the overall costs to the animal. The cost of remaining (dashed line) increases, and the cost of fleeing (solid line)

decreases as the distance to an approaching predator decreases (left side of graph). Blumstein (2003) further proposed that two critical distances exist (Dmin and Dmax) which creates three zones of response. The first (red box, left side, D<Dmin) represents distances at which animals will always respond to threats, the second (middle, Dmin<D<Dmax) represents distances at which animals will dynamically optimise their responses based on this cost-benefit analysis and the third (blue box, right side, D>Dmax) which represents distances at which animals will not respond to the detection of threats by fleeing. Adapted from (Ydenberg and Dill 1986; Blumstein 2003).

This graphical model produced (Fig. 1.3) predicted that it is only when the cost of not responding and the cost of responding are equal (at the intersection of the lines), that an animal should respond. Critically, they also determined that the interaction between these two competing options generates an optimal distance, the flight initiation distance (FID), between the threat and the individual at which a response should be generated. This theory was notable in its deviation from the previously held belief that detection and reaction occur simultaneously in animals when exposed to threats. Instead, it proposed that the time between detection of the stimulus and the initiation of a response was a critical period of active deliberation where the animal is continually choosing which behaviour to perform. Despite emphasising the deliberate nature of the evaluation, the authors do note that such a decision is not necessarily made cognitively, but emerges from the perceived evaluation of the threat imminence and the associated costs of reacting.

1.2.2 Behavioural choice - the selection and execution of a suitable defence strategy.

Once it has been determined that a threat is present, the next step is determining which of the available behavioural responses provides the maximum probability of a favourable outcome, in this case, survival. The selection of a specific defensive course of action relies on both the perceptual evaluation of the sensory stimulus and the additional evaluation of the external environment and the likely outcomes of each of the chosen behavioural strategies. Whereas (Ydenberg and Dill 1986) examined the influence of the threat distance on the timing of response initiation, another influential theory (Blanchard and Blanchard 1989) aimed to explain the simultaneous role of threat distance and escape availability on the choice and intensity of a range of defensive behaviours (Fig. 1.4). A symmetric graph reflects the shared convergence of defensive behaviours towards defensive attack as the threat intensity increases, with either reflection representing the choice of flight or freezing as the chosen behaviours in the presence or absence of an escape route, respectively. The influence of environmental conditions, for example the presence or availability of a refuge (Blanchard et al. 1986; Vale et al. 2017), was shown to affect the selection of defensive behaviour. In the absence of a suitable or attainable refuge, escape was considered futile and rats and mice were more likely to elicit freezing behaviours to visual threats. In line with this idea, animals that naturally inhabit open environments that lack close access to shelter, were observed to more frequently perform freezing behaviours in response to threats (Edut and Eilam 2003).

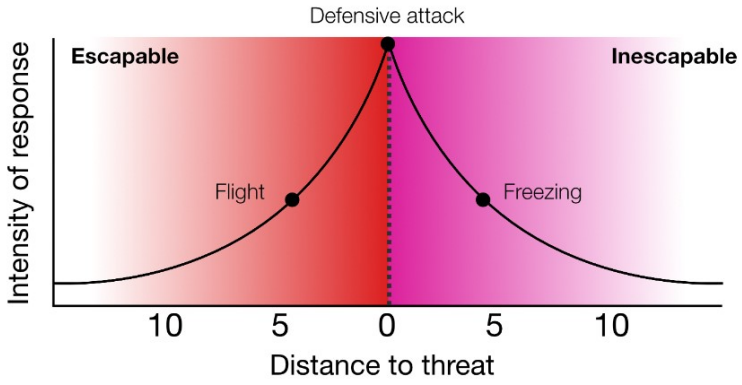

Fig. 1.4 Summary of the Blanchard and Blanchard model (1989) describing defensive behaviour as the combination of both the distance to the threat and the availability of an escape route.

The selection of a flight or freezing behaviour is dependent upon the availability of an escape route (left side, red gradient), or not (right side, pink gradient). The intensity of the behavioural response is also correlated with the distance of the threat from the observer. Shorter defensive distances in both situations give rise to more aggressive responses such as defensive attack. Modified from Blanchard and Blanchard (1989).

The perceptual evaluation of a stimulus also critically determines the selection of a specific behaviour, the decision of when to initiate the behaviour and how to perform it. Depending on the type of visual threat detected, the same organism with fixed environmental conditions can select different defensive strategies. It is important to note that defensive behaviours are not single, fixed motor programmes but are actually composed of sequential, distinct behavioural events, as exemplified in the Blanchard & Blanchard model (1986) for rodents. However, this parcellation of behaviour can be observed in the defensive behaviours of organisms across the animal kingdom. It is evident in the distinct stages of evasive flight take off in *Drosophila* (Card and Dickinson 2008; von Reyn et al. 2014), the compound escape sequence of crayfish (Reichert and Wine 1982) and the subsequent inking then escaping behaviour observed in threatened squids (Hikidi et al. 2020). The selection, organisation and timing of these discrete behavioural syllables can optimise the outcome success by generating a contextually-tailored response. In chaffinches, the detection of two equally threatening stimuli, that of a sparrowhawk or a woodpigeon, gave rise to slightly different defensive behaviours (Cresswell et al. 2009). Whilst the chaffinches would generate an initial freeze before escaping when presented with the woodpigeon, they would escape immediately when presented with the hawk stimulus. Response kinematics are also strongly linked to the perceptual evaluation of the threat stimulus. Even larger prey, such as *Squalus acanthias*, a type of shark that is predated upon by larger apex predators, alter their turning speed and escape acceleration in response to the speed, size and approach orientation of a threat (Seamone et al. 2014).

1.2.3 The looming avoidance response as an innate PDM process

Historically, responses to visual threats have been examined in laboratory settings using visual stimuli that involve either the presence of a real threat (i.e. a live predator (Dunkeld and Bower 1980; Deng et al. 2016; Masferrer et al. 2020; Tsutsui-Kimura et al. 2022), an artificial replica of a real threat (Xie et al. 2022; Tsutsui-Kimura et al. 2022), images of a threatening object (Coker-Appiah et al. 2013) or shapes that either reduce the image to its outlining silhouette (Tinbergen 1939) or capture a low-level feature that is known to be innately-aversive (Yilmaz

and Meister 2013; Temizer et al. 2015)). Although all methods have their advantages, the latter, most reductionist method offers the most experimental power through the ability to tightly map the influence of specific statistics of the stimulus to the observed response. The visual looming stimulus is a key example of this type of stimulus. Looming stimuli are often graphically represented as the presentation of a 2D dark expanding disc and represent an approaching object on a collision course with the observer. This stimulus has been enthusiastically adopted by research groups in recent years due to its robust evocation of a defensive behavioural response, termed the looming avoidance response (LAR). Behavioural readouts of defensive reactions and neural responses to looming visual stimuli have been observed across the animal kingdom, from insects (Gabbiani et al. 2002), praying mantids (Yamawaki and Toh 2009), locusts (Gabbiani, Krapp, and Laurent 1999), crustaceans (Oliva et al. 2007; Smolka et al. 2011), birds (Wang et al. 1993; Wu et al. 2005), frogs (Lettvin et al. 1959), fish (Temizer et al. 2015; Filosa et al. 2016; Otero Coronel et al. 2020) and mammals (including mice: Yilmaz and Meister 2013; Shang et al. 2015; Evans et al. 2018; Shang et al. 2018; primates: Schiff et al. 1962; King and Cowey 1992; Cléry et al. 2020 and humans: Ball and Tronick 1971; Hu et al. 2017). The rapid decision to initiate a defensive response, and the selection of the appropriate action and performance parameters has been considered an innate form of a "Go/No-Go" task commonly used in studies of PDM (see Fig. 1.5, Juavinett et al. 2018).

Upon detection of a looming visual stimulus, laboratory mice must decide whether to freeze, flee, fight or ignore the stimulus. The decision to respond to the presence of a looming stimulus has been experimentally tested by exposing laboratory mice to the sequential looming stimuli of different contrasts, to generate threat detection scenarios with varying degrees of certainty (Evans et al. 2018). By evaluating the stimulus-induced escape probability, the authors showed that the lower contrast, more ambiguous stimuli, were less likely to trigger a defensive escape response. Yilmaz and Meister (2013) probed how the perceptual evaluation of the stimulus features influenced the decision to respond and observed that although dark, expanding overhead discs could readily evoke escape (and less frequently, freezing) response, light expanding discs, dark receding discs or static dark discs did not elicit defensive behaviours. Perception of the visual threat features can also affect the selection of distinct behavioural response strategies. De Franceschi et al. (2016) observed robust segregation of defensive responses in mice depending on whether they were presented with a looming or panning dark disc stimulus. Furthermore, the selective expression of flight, freezing or exploratory rearing was shown to be influenced by both the size and velocity of the looming stimulus (Yilmaz and Meister 2013; Yang et al. 2020). In mice, stimulus features were also directly correlated to the intensity and vigour with which the chosen behaviour was elicited, with higher contrast stimuli leading to faster and more vigorous escape responses (Evans et al. 2018). The precise topological features of the looming stimulus used could also affect the escape response parameters (Huang et al. 2020).

The use of this particular behavioural paradigm has been highlighted for its unique position among available behavioural tests for its intersection of ethological validity, simplicity, robustness and the compatibility of the stimulus-response relationship (Fig. 1.5, Juavinett et al. 2018). Moreover, the rigorous work of the field in dissecting the particular circuits that mediate and modulate this response has generated an anatomical and mechanistic framework upon which discrete behaviours can be mapped to both their relevant phases in the PDM process and underlying neural circuits. In the following section, I will outline what is known about the

circuits that control the generation of defensive behaviours to visual threats in mammals, with a specific emphasis on the midbrain circuits known to play a critical role in the generation of escape responses.

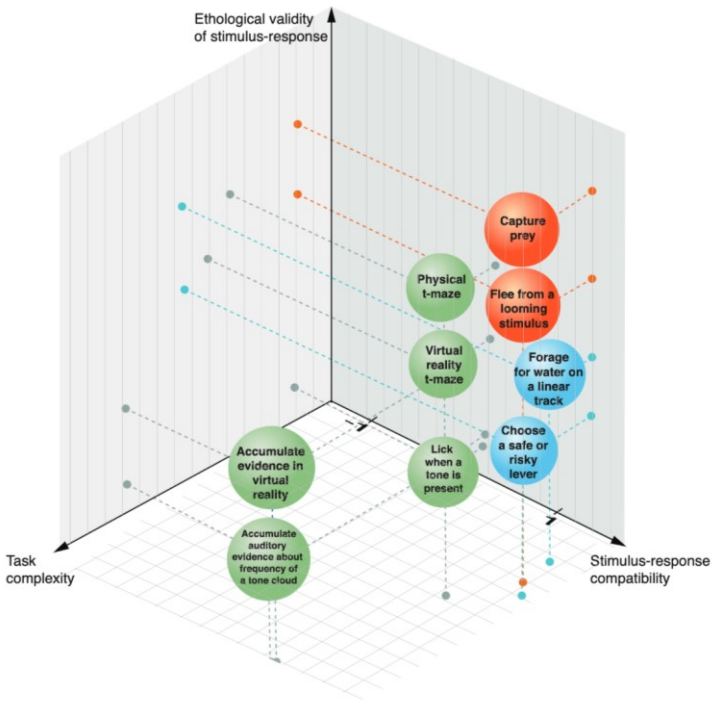

Fig. 1.5 Utility of the LAR paradigm in PDM research.

Different behavioural tasks used in the study of PDM have different strengths and limitations. The looming avoidance response (orange circle in the top right) is an attractive paradigm to use given its high ethological validity, strong stimulus-response compatibility and low task complexity. These features are graphically represented here by the position of this circle along the three axes of requirements for experimental perceptual decision-making tasks. Figure adapted from Juavinett et al. (2018).

1.3 Midbrain circuits for visually-evoked defensive behaviours

The widespread threat of predation and the importance of detecting objects on a directed collision course has led to the conserved generation of neural circuits linking the detection of visual threats with the initiation of defensive behaviours across species. Attempts have been made in different animal systems to link the specific behavioural components of the PDM response to their underlying neural circuits. In this case, these components can be defined as: the detection of the stimulus, the evaluation of the sensory information, the selection of an appropriate action and the initiation of a motor response. Looming stimuli have been shown to evoke defensive behavioural responses at incredibly short latencies (<250 ms). This means that this remarkable feat of detecting, evaluating, selecting and initiating must all occur within, quite literally, the blink of an eye[2]. This rapid processing speed implies certain limitations on either the physical size or transduction speed of the underlying circuitry. Numerous studies have determined several key nodes which form a core neural circuit that is responsible for the generation of this sensorimotor transformation which includes: the retina (detection), the superior colliculus (evaluation) and the periaqueductal grey (selection and initiation). For the sake of clarity, this section is focussed on outlining the mammalian, and in particular, the rodent system since it is the system under investigation in this study. Where possible, I will try and bridge what is known about the rodent nervous system with our current understanding of the circuits involved in humans.

1.3.1. The superior colliculus (SC)

In mammals, there exist two major neural pathways through which visual information is processed (Fig. 1.6). The first, the retino-geniculo-cortical pathway sends information from the retina to the dorsal lateral geniculate nucleus (dLGN) before transmitting this information to the primary visual cortex (V1) for more detailed analysis within cortical visual processing circuits. The more recent evolution of this visual pathway, the relative contribution of retinal projections along this route and its specific role in image-forming vision has led to this pathway receiving a more rigorous investigation in humans and non-human primates, especially with regards to its role in vision-based PDM (Wyart and Tallon-Baudry 2009; Siegel et al. 2011; Lorteije et al. 2015; Burgess et al. 2017; Odoemene et al. 2018; Wilming et al. 2020).

The second pathway is the retinocollicular pathway that comprises the direct connection from the output retinal ganglion cells (RGCs) to the SC. This pathway is known to have evolved first, and also develops first in both mice and humans (Stein 1984). The emergence of visually-driven activity within the superior colliculus is thought to guide the development of both visual and multisensory representation within higher cortical regions (Rowland et al. 2007). Situated on the dorsal surface of the brain, the mammalian superior colliculus (SC) (and its non-mammalian homologue, the optic tectum (OT)) is a midbrain structure conserved across vertebrates. Its laminated organisation and dense connectivity with numerous and widespread

[2] Human blinks are thought to last ~300ms (Kwon et al. 2013).

brain regions facilitate its role in multisensory integration and the selective filtering of sensory information for the generation of oriented behavioural responses. The specific connections that dictate the weighting and type of sensory information it receives varies from species to species, and is directly affected by the organism's perceptual capabilities (their *Umwelt,* von Uexküll 2013) and ethological requirements. Although the exact proportion of all retinal outputs targeting the SC varies, from 70-90 % in rodents (May 2006; Ellis et al. 2016) to 50 % in cats (Wässle and Illing 1980) and 10 % in primates (Cowey and Perry 1980), its role in visually-guided orienting responses and subconscious visual processing is widely accepted (Allen et al. 2021; Krauzlis et al. 2013).

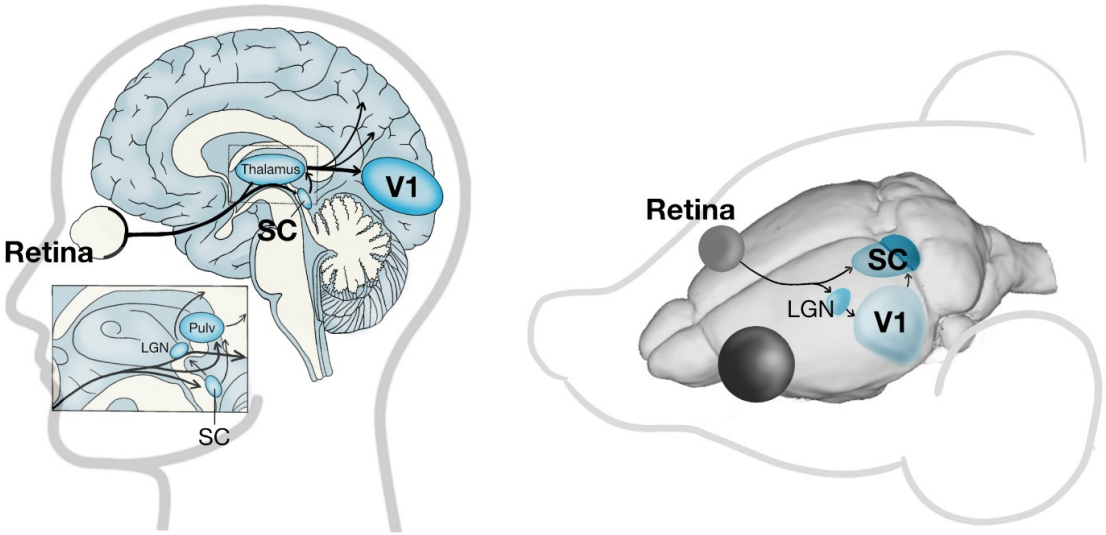

Fig. 1.6 The main visual processing pathways in humans and mice.

In both humans (left) and mice (right) there exist two core visual processing pathways. The first, the retino-geniculo-cortical pathway sends visual information through the lateral geniculate nucleus (LGN) in the thalamus to the primary visual cortex (V1) and to other higher cortical areas. The second, the retinocollicular pathway sends visual information directly from the retina to the superior colliculus (SC). Left image adapted from Tamietto and de Gelder (2010).

1.3.1.1 Structure, function and anatomy of the mammalian SC

The rodent SC is made up of seven anatomically discrete layers with distinct cyto-, myelo-, receptor and synaptic architectures, diverse functions and differing afferent and efferent connections. The dorsalmost region of the SC, of which more than half is covered by overlying cortex, is referred to as the superficial layer (sSC) and which itself is subdivided into the zonal (SZ), superficial grey (SGS) and the optic layer (SO). The remaining two-thirds of the SC are often grouped together as the deep layers of the SC (dSC) whilst others prefer to further subdivide the region into separate intermediate (iSC) and deep layers (dSC), with both subregions consisting of a soma-rich grey layer (SGI and SGP) and a fibre-rich white layer (SAI and SAP), respectively (Fig. 1.7).

The SC is a bilateral structure that, in mice, receives input almost exclusively from the contralateral retina with projections travelling through the underlying SO before reaching their targets in the SGS and SZ (Fig. 1.7a, Drager and Hubel (1975)). In animals with more binocular overlap, like monkeys, contralateral projections are still dominant although ipsilateral projections exist and can be observed as patches distributed within the SGS (Pollack and Hickey 1979). In mice, the majority (>80%, Ellis et al. 2016) of RGCs project to the SC, terminating in a retinotopic manner and with an average convergence of 5.5 RGCs onto a single SC neuron (Chandrasekaran et al. 2007). The inputs of functionally-distinct RGCs segregate into distinct regions of the sSC (Inayat et al. 2015; Ellis et al. 2016), and selectively target sSC cells with specific downstream targets, indicating a projection-specific logic to the SC sampling of visual inputs in the retina (Reinhard et al. 2019).

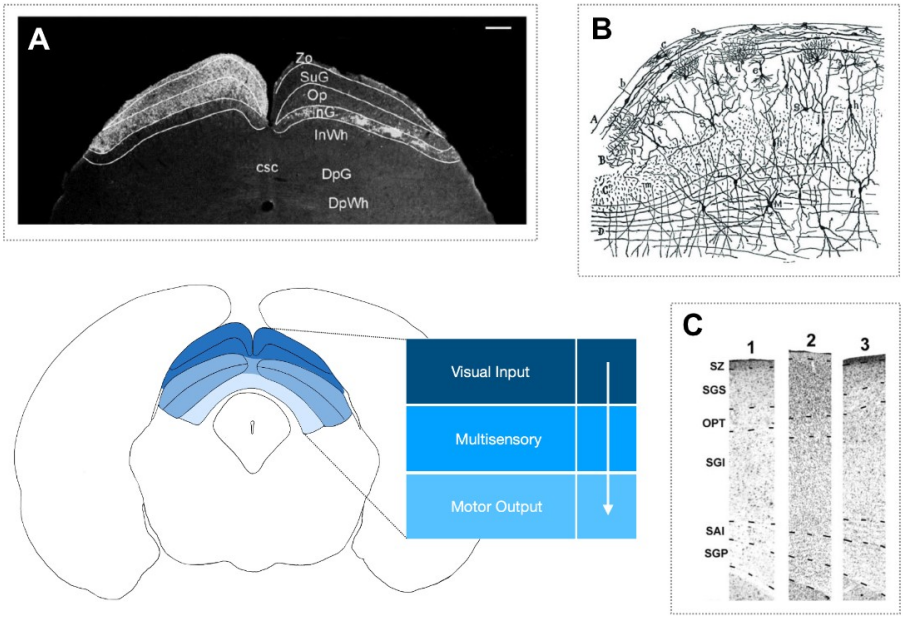

Fig. 1.7 Structure and layered organisation of the superior colliculus (SC).

A, Laminar organisation of the SC superimposed onto the visualisation of retinotectal projections. Shown is a darkfield micrograph of the mouse SC after intraocular injection of cholera toxin β-subunit into the right eye. Contralateral projections can be seen terminating mainly in the ZO, SGS (here SuG) and SO (here Op), whilst ipsilateral projections can be seen as discrete patches in the SO and SGI (here InG). Modified from Morin and Studholme (2014). A simplified schematic of the laminar organisation of the SC is represented in the image beneath. The visual (dark), multisensory (mid) and motor (light) layers are represented with different shades of blue**. B**, A drawing by Santiago Ramón y Cajal of a coronal section of rabbit SC, stained using the Golgi method. The drawing shows the diverse cell types and dendritic branching morphologies of the cells in one hemisphere. Image taken from Ramón y Cajal (1909) reprinted in Isa and Hall (2009). **C**, Vertical sections of the cytoarchitecture of cat (1), squirrel (2) and macaque *M.fascicularis* (3) SC, stained with cresyl violet. While the laminar structure is conserved, the relative size of the respective layers differs across species. Figures A-C, modified from May (2006).

The SC also receives visual input from the retino-geniculo-cortical pathway via input from primary visual cortex (V1). Across species, the majority of these inputs originate from layer

V cells, with some projections originating from layer IV in V1 (macaque: Lock et al. 2003; cat: Kawamura and Konno 1979; rat: Sefton et al. 1981). These inputs have been found to modulate visual responses within the sSC without directly affecting the tuning properties of the cells (Wang et al. 2010; Zhao et al. 2014; Ahmadlou, Tafreshiha, and Heimel 2017). One study even observed the selective, and extensive, targeting of V1 inputs onto the dendrites of one class of sSC neurons (Masterson et al. 2019), that they suggested could be responsible for the previously-described V1-mediated arrest behaviours (Liang et al. 2015; Zingg et al. 2017). Inversely, multiple recent studies have also highlighted the ability of the SC to modulate visual responses within the cortex (Ahmadlou et al. 2018; Beltramo and Scanziani 2019; Ruediger and Scanziani 2020; Fang et al. 2020).

Electrophysiological recordings have uncovered the visual response properties of cells within the sSC. The majority of the visually responsive cells exhibit ON-OFF centre receptive fields (indicating that they express biphasic responses to the sequential increase and then decrease of light) with largely overlapping ON/OFF subregions (Wang et al. 2010; Franceschi and Solomon 2018). Meanwhile, *in vivo* two-photon imaging of the mouse sSC revealed a columnar organisation of cells with similar orientation tuning (Feinberg and Meister 2015; Ahmadlou and Heimel 2015). Subpopulations of cells exhibit direction selectivity (Inayat et al. 2015), that was found to be inherited directly from the retina (Shi et al. 2017), however, these cells were not similarly arranged in columns. Interestingly, the primate sSC noticeably lacks cells with strong feature selectivity (Ito and Feldheim 2018). It is thought that the sSC cells may function more as 'event detectors', whereas feature-specific, image-forming visual processing is thought to occur in cortical visual areas. Attempts have been made to classify the cell types within the sSC of mice based on distinct morphological, functional or molecular features with differing results. Selective activation of genetically-targeted sSC cell populations using a combination of functional ultrasound imaging (fUSI) and optogenetics enabled functional segregation of some of these cell types based on the behavioural responses evoked and downstream circuits activated (Sans-Dublanc et al. 2021). The number of classes varies from five based on somatodendritic morphology (May 2006), four found through functional characterisation (Gale and Murphy 2014), while ten distinct groups were identified by screening for molecular markers (Byun et al. 2016). The principal classes appear to be wide-field (WF), narrow-field (NF), horizontal and stellate cells (May 2006), whose names refer to the general shape of their dendritic arborizations (Fig. 1.8).

These visually-responsive cells are largely excitatory, glutamatergic cells, with the horizontal subclass of cells comprising the only group that expresses the inhibitory neurotransmitter, γ-Aminobutyric acid (GABA). These inhibitory interneurons have large dendrites that spread horizontally across the medial-lateral and rostral-caudal axes of the SC. They are thought to respond most strongly to large, static objects. They send inhibitory projections to the LGN and the parabigeminal nucleus (PBGN, a 'satellite' cholinergic nucleus that projects back to the SC), as well as to cells locally within the SC. By comparison, stellate cells have small and multipolar dendritic arbours, as their name would suggest. They similarly project to the LGN and PBGN, but send excitatory, not inhibitory signals in response to small, stationary objects. NF cells also send excitatory projections to the PBGN, but crucially they are the only cells

thought to send direct projections to cells located ventrally with the dSC. They also preferentially respond to small, static visual stimuli, but often show direction selectivity unlike stellate cells. NF cells exhibit a more bipolar orientation of their dendrites in the dorsal-ventral axis. Lastly, there exist large, WF cells with vast dendritic arbours that stretch across the sSC. Their expansive dendritic morphology enables these cells to pool visual inputs from large areas of the visual scene, thanks to the topographic organisation of visual inputs that will be discussed below. Their shape facilitates their function since they preferentially respond to small stimuli moving slowly across the visual scene. They appear to send projections selectively to the lateral posterior nucleus of the thalamus (LP, homologue of the pulvinar in humans).

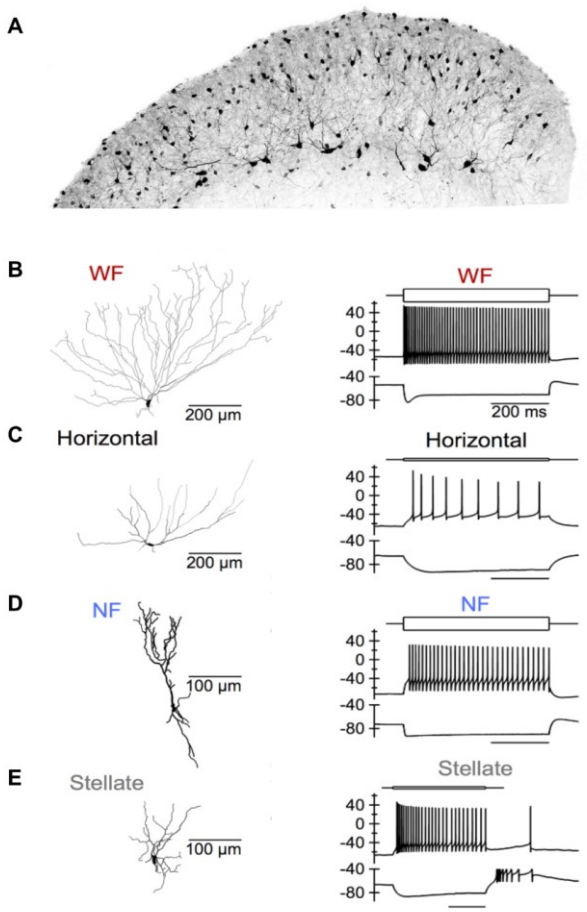

Fig. 1.8 Functional cell types within the sSC in mice.

A, Confocal micrograph of one sSC hemisphere in a Tac1-Cre;Ai95 mouse, showing the diversity of cell type morphologies and the orientation of the dendrite with respect to the SC surface. **B**, Tracing of an example biocytin-filled neuron from the WF class (left) and an example trace showing an example response to current injection. The black line above the trace indicates the current amplitude and duration. **C**, **D** and **E**, as for **B** but for the horizontal class, NF and stellate class, respectively. Current steps were 500 ms and 600 pA for the WF and NF cell examples and 100 pA for the horizontal and stellate cell examples. Figures B-E, adapted from Gale and Murphy (2014).

The topographic organisation of visual inputs to the sSC facilitates the proposed role of the SC in selective attention and the selection of targets for further visual inspection. Direct electrical stimulation or optical activation of cells within the SC evokes directed behavioural responses (Sahibzada et al. 1986; Dean et al. 1989). These oriented sensorimotor transformations are made possible by the alignment of overlapping layers of retinotopically-organised sensory maps across the dorsal-ventral axis of the SC. Resulting in neurons sensitive to sensory stimuli of different modalities, but with receptive fields located in overlapping regions of space, arranged in vertical columns across the SC layers. These maps are the result of the dense, and often reciprocal, ascending and descending afferents to the dSC layers from both cortical and subcortical regions conveying information about auditory, somatosensory and motor functions (Dräger and Hubel 1976). Similar to the orientation columns observed in the predominantly visually-responsive sSC, orderly genetically-defined anatomical modules of iSC cells were found to discretely represent directed head movements in space (Masullo et al. 2019). This functional segregation of the SC into spatial columns and sensory sheets hints at a high level of coordination between cells and circuits within the SC itself (Fig. 1.9).

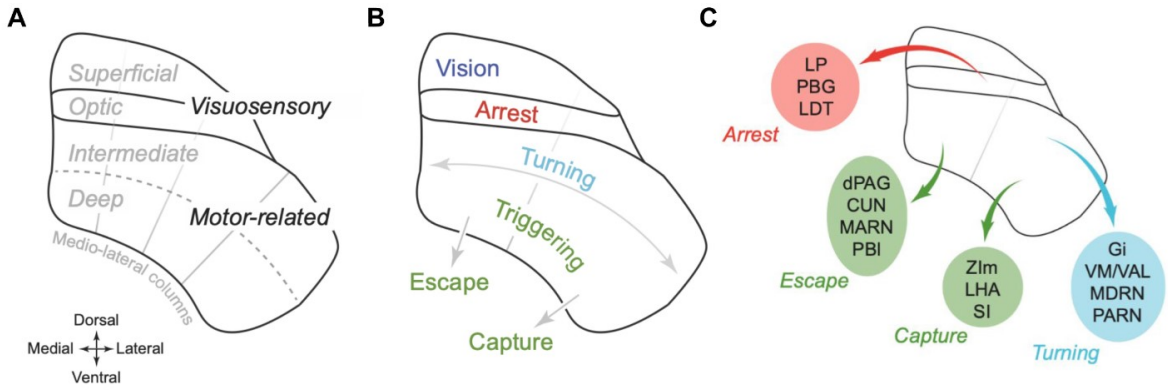

Fig. 1.9 Dorsal-ventral sensory-motor segregation and medial-lateral response segregation in the SC.

A, Schematic of the laminar and columnar structure of the SC. **B**, Proposed functional organisation of the SC based on the dorsal-ventral region. **C**, Summary of some of the major outputs of the SC involved in the generation of the behaviours mentioned in **B**. CUN, cuneiform nucleus; D-HVAs, higher visual areas (dorsal stream); DN, dentate nucleus; dPAG, dorsal PAG; FN, fastigial nucleus; Gi, gigantocellular nucleus; IP, interposed nucleus; LDT, laterodorsal tegmental nucleus; LHA, lateral hypothalamus; LP, lateral posterior nucleus of the thalamus; LS, lateral septal nucleus; MARN, magnocellular reticular nucleus; MDRN, medullary reticular nucleus; MOp, primary motor area; MOs, secondary motor area; PARN, parvicellular reticular nucleus; PBG, parabigeminal nucleus; PBl, lateral parabrachial nucleus; SI, substantia innominata; SNr, substantia nigra (reticular part); VAL, ventral anterior-lateral complex of the thalamus; V-HVAs, higher visual areas (ventral stream); VISp, primary visual area; VM, ventral medial nucleus of the thalamus; VMHdm/c, ventromedial hypothalamic nucleus (dorsomedial/central part); VMHvl, ventromedial hypothalamic nucleus (ventrolateral part); ZIm, zona incerta (medial part). Adapted from Wheatcroft, Saleem, and Solomon (2022).

The dSC cells are in general more heterogeneous, with diverse multipolar morphologies, than their sSC counterparts (Mooney et al. 1992; Evans et al. 2018). Dense, reciprocal connectivity between dSC neurons facilitates the recurrent build up in SC activity during the evaluation of

sensory stimuli (Mooney et al. 1992; Evans et al. 2018). This functional build-up of neural activity can then send signals to a wide range of downstream targets which can be grouped into two main categories. The first option is to further influence sensory processing through the activation of ascending thalamic pathways that recruit the basal ganglia and cortical areas (May 2006; Benavidez et al. 2021). The second option would be to activate descending pathways through midbrain and brainstem regions, including the medullary, pontine and cuneiform nuclei, the PBGN, the mesencephalic reticular formation and the periaqueductal grey, to target downstream motor circuits (Sparks and Hartwich-Young 1989; Benavidez et al. 2021; Wheatcroft et al. 2022).

In humans and non-human primates, the primary function linked to the SC is visual attention and specifically, the control of gaze and eye movements (Sparks 1986; Platt et al. 2003; Schneider and Kastner 2005; Müller et al. 2005). Various indirect connections from the SC have been identified in primates that link the SC with higher cortical areas strongly linked to gaze control, such as the frontal eye fields, via the pulvinar, lateral intraparietal area (LIP) and the mediodorsal thalamus (MD), and the medial temporal area (MT) through the inferior pulvinar. Other connections link the SC directly to motor generation circuits in the basal ganglia and through the pontine nuclei to the cerebellum (Wurtz and Albano 1980; Moschovakis 1996; Krauzlis et al. 2013). Akin to the two visual processing pathways in mice that are described at the beginning of this section, humans contain two homologous pathways: the ventral “What?” pathway that is primarily responsible for image-forming and detailed vision and the dorsal “Where?” pathway that processes visual information related to global processing of the visual scene, as well as moving objects and emotional cues. The SC belongs to the dorsal pathway and is responsible for innate behaviours such as attention to faces (Nguyen et al. 2014), socially-motivated approach (Solié et al. 2022) and innate fear (Maior et al. 2012; Wang et al. 2020).

1.3.1.2 The role of the superior colliculus in mediating defensive behaviour

The ability to generate orienting responses is perhaps the most well-studied and understood behaviour mediated by the SC. Evoked orienting responses are generated through SC stimulation that are related to the size of the animal and proportional to the strength of stimulation. Defensive responses, other than orienting movements, were first observed to be mediated by SC activation in rats in the early 1960’s (Olds and Olds 1962), and were later evoked through various forms of neuronal activation in the 1980’s (Sahibzada et al. 1986; Dean et al. 1988). These early studies, as well as others (Dean et al. 1989; Vargas et al. 2000), observed that it was possible to evoke different defensive behaviours by targeting different areas and modulating the strength of SC stimulation. These behaviours ranged in intensity from freezing and flinching, to jumping and running. It was later determined that the medial and lateral divisions of the SC were individually responsible for the generation of approach and avoidance behaviours, respectively (Comoli et al. 2003; Furigo et al. 2010).

While the role of the SC in generating the motor response of defensive behaviours was widely acknowledged, it took an influential lesion study in wild rats to demonstrate the critical

involvement of the SC in the specific detection of visual threats (Blanchard et al. 1981). In this study it was observed that lesioned rats would not respond, by either escaping or orienting, to the approach of an experimenter however they would generate rapid escape responses upon physical contact. Appreciation of the role of the SC in mediating the processing of threatening visual stimuli was further strengthened by the discovery of approach sensitive neurons in numerous mammalian systems (Westby et al. 1990; Liu et al. 2011; Zhao et al. 2014; Shang et al. 2015; Franceschi and Solomon 2018; Lee et al. 2020), including humans (Billington et al. 2011). In rodent models, specific collicular-targeting retinal ganglion cell types were found to show strong and selective responses to looming stimuli (Münch et al. 2009; Zhang et al. 2012). Recent, targeted investigation of the necessity and specific role of certain RGC subtypes that target the SC unveiled a genetically-defined subtype that is both necessary and sufficient for looming evoked fear responses (Wang et al. 2021) and the selective loss of flight but not freezing responses to looming stimuli after the functional ablation of another subtype (Lees et al. 2020).

Within the SC itself, specific microcircuits and cell types have been identified as mediating distinct components of defensive responses to looming stimuli. Shang et al. (2015) revealed an unexpectedly excitatory, parvalbumin population of SC cells that specifically drive escape responses to looming stimuli. A follow-up study (Shang et al. 2018) proposed that the specific connection of these neurons with downstream structures, the parabigeminal nucleus (PBGN) and the lateral posterior nucleus (LP) generated the divergent presentation of escape and freezing behaviours to this stimulus, respectively. However, later works debated the necessity of the PBGN connection, suggesting that antidromic activation of SC neurons projecting to both the PBGN and the PAG could have resulted in the observed escape responses (Evans et al. 2018). Another study linked the SC-LP connection to the specific generation of threat-induced freezing responses (Wei et al. 2015). A seminal study in the field used *in vivo* calcium imaging techniques in freely moving and *in vivo* silicon probe recordings in awake, head-fixed animals, to observe the temporally-aligned activation of excitatory glutamatergic cells within the medial SC (mSC) in response to the onset of a looming stimulus (Evans et al. 2018). They further found that targeted activation of the same cell population using excitatory optogenetics evoked graded defensive escape behaviours in freely-moving animals, and that while chemical ablation of the SC or PAG abolished looming-evoked escape responses, ablation of the amygdala, PBGN or visual cortex did not. Overall, this study outlined the critical role of the SC, and also the PAG, in driving escape responses to visual looming stimuli.

Modulation of the behavioural responses and neural responses to visual threats in the sSC has been observed through the activation of inputs from both cortical and subcortical brain regions. As mentioned, although not sufficient to drive escape responses, V1 inputs to the SC evoked bright-light induced arrest behaviours (Liang et al. 2015) and sophisticated transsynaptic viral tagging and subsequent optogenetic activation of SC neurons receiving V1 input elicited freezing behaviour (Zingg et al. 2017). Silencing of V1 inputs to visually-responsive SC cells reduced the magnitude but not the selectivity of the cells to the looming stimulus (Zhao et al. 2014). More recently, it was shown that activation of inhibitory thalamic inputs from the ventral LGN (vLGN) suppressed visual responses within the SC and suppressed both looming-

evoked escape (Fratzl et al. 2021) and freezing (Salay and Huberman 2021) responses. Many open questions still remain about the specific role and the detailed evaluation of visual, especially threatening, stimuli that occurs within the SC circuits. How much of the threat signal is inherited from the properties of the RGCs that initiate the SC responses? Are there different filtering networks within the SC that are separated already at the level of the retinal inputs to streamline the generation of targeted behavioural responses? Or does the SC simply give a general signal of 'threat' and the action selection occurs at a later node in the pathway?

1.3.2 The periaqueductal grey (PAG)

1.3.2.1 Overview of the PAG

Enveloping the aqueduct of Sylvius, the aptly named periaqueductal grey is an elongated midbrain structure running along the brain's rostral-caudal axis. Similarly to the SC, the PAG is highly conserved across evolution, likely due to its key role in many fundamental behaviours related to survival. It has been most studied in connection to its role in the transmission and modulation of pain but has also been investigated for its links to autonomic control of cardiovascular function, micturition, vocalisation (Gruber-Dujardin 2010) and of relevance to this thesis, defensive responses to threats. It is commonly divided into four subregions, namely the dorsomedial (dmPAG), dorsolateral (dlPAG), lateral (lPAG) and ventrolateral (vlPAG), that represent distinct columns running parallel to the aqueduct (Fig. 1.11). However, more detailed classifications have been suggested. A recent attempt to systematically differentiate PAG subregions used single-cell RNA sequencing to isolate more than 100 transcriptomic subtypes that were later assembled into 19 spatially-distinct metaclusters, whose activation mapped onto a range of instinctive behaviours (Vaughn et al. 2022). Cytoarchitecturally, the PAG is relatively homogeneous with mostly small- to medium-sized cells (5 - 40 μm in diameter), with soma that generally increase with distance from the aqueduct and fusiform, triangular or stellate morphologies (Mantyh 1982). The principal neurotransmitter is glutamate, although neurons that utilise GABA, opioids (particularly enkephalin), substance P and neurotensin are also present (Benarroch 2012).

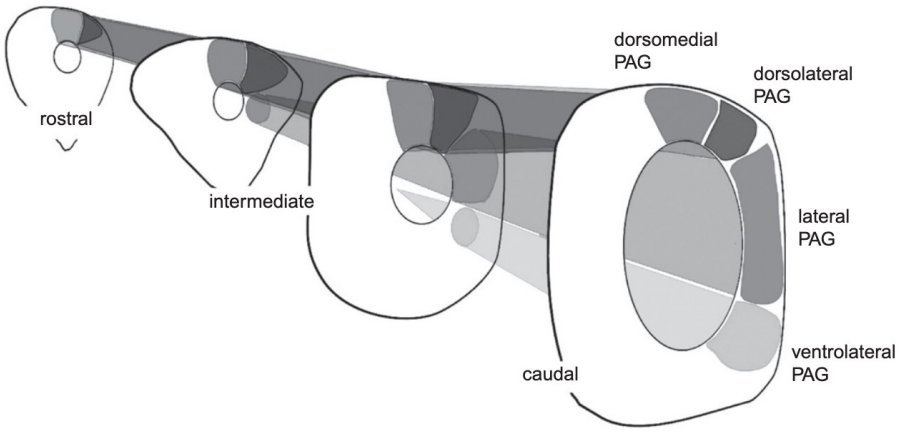

Fig. 1.10 The columnar organisation of the PAG.

The dorsal-ventral segregation of the PAG into functional columns. Dorsal regions (dmPAG and dlPAG) are predominantly thought to be involved with the generation of active defensive responses, such as escape, while lateral and ventral regions control passive defensive behaviours like freezing. Figure from Gruber-Dujardin (2010), modified from Bandler and Shipley (1994).

The PAG receives widespread inputs from forebrain, brainstem and sensory neurons of the dorsal horn and trigeminal nucleus that have distinct patterns of termination within the separate functional columns. From the forebrain, the anterior cingulate gyrus targets dmPAG, lPAG, vlPAG, while the medial wall of the PFC targets dlPAG (An et al. 1998). Targeted rabies tracing recently showed that cortical inputs exclusively target glutamatergic, and not inhibitory, PAG cells (Franklin et al. 2017). While the PAG also receives input from the amygdala and numerous hypothalamic nuclei, including the medial preoptic, anterior, periventricular, ventromedial, posterior, supramammillary nuclei and lateral hypothalamus (Vianna and Brandão 2003). Consistent with its role in pain processing, the ventral PAG receives ascending spinal afferents from trigeminal nuclei. The PAG sends ascending afferent connections to the forebrain, including the thalamus and hypothalamus, which further project to the prefrontal cortex, amygdala and basal ganglia. Apart from the dlPAG - all other regions target the lower brainstem, most of which are premotor areas that then in turn project to sensory, motor or autonomic nuclei of the brainstem and spinal cord (Holstege et al. 1996). A human study of patients undergoing deep brain stimulation in the PAG for neuropathic pain revealed connections of the dPAG with ventral posterior thalamus, primary somatosensory cortex, ipsilateral dorsomedial medulla and the cerebellum (Sillery et al. 2005), indicating a mixture of conserved and distinct anatomical connections in humans and animal models studied.

1.3.2.2 A general role for the PAG in defensive behaviour

Positioned at the interface of the brain's sensory, limbic areas and locomotor control centres, the PAG has long been considered a prime candidate in mediating defensive behaviours to threats (Lefler et al. 2020). The general role of the PAG in the generation of defensive behaviour was first suggested by Hunsperger (1956). These early experiments showed that defensive hissing and fighting in cats could be evoked by PAG stimulation, even after the

extensive lesioning of the amygdala and hypothalamus, whilst the same behaviours that could also be elicited by electrical stimulation of these areas were suppressed by lesioning the PAG (Hunsperger 1956; Molina and Hunsperger 1962). These results were later corroborated by numerous further studies that confirmed both the ability to drive defensive behaviour through PAG activation, and the corresponding loss of these same behaviours through target lesions across a range of animal species (Blanchard et al. 1981; Behbehani 1995; Vargas et al. 2000; Bittencourt et al. 2004; Tovote et al. 2016). Corresponding human studies support a conserved role of the PAG in responses to threats. Functional imaging studies have revealed a preferential activation of the PAG during reactive fear, especially in situations of imminent danger that require fast reactions (Mobbs et al. 2007; Rigoli et al. 2016; Wendt et al. 2017; Terburg et al. 2018; Qi et al. 2018). Interestingly, greater PAG activation was observed using fMRI in humans to looming threatening, rather than neutral, images (Coker-Appiah et al. 2013). Meanwhile, electrical stimulation of the PAG in human patients evokes sensations of fear, panic and impending death (Nashold et al. 1969; Amano et al. 1978, 1982; De Oca et al. 1998).

Our understanding of the specific contribution of PAG subdivisions in mediating defensive behaviour has evolved in recent decades thanks to increasingly targeted experimental approaches. The selective activation of PAG subregions gave rise to the idea of a functional division of the PAG along its dorsal-ventral axis. The dorsal regions of the PAG are thought to be primarily involved in the generation of 'active' defensive responses - i.e. escape, jumping, defensive attack, tachycardia and hypertension; whilst the ventral regions play a larger role in mediating 'passive' responses such as freezing or immobility, analgesia, bradycardia and hypotension (Bolles and Fanselow 1980; Bandler and Depaulis 1991; Fanselow 1991; De Oca et al. 1998). With the advent of targeted genetic approaches, the contribution of specific groups of cells within these regions could be dissected leading to ever more detailed understanding of cellular contributions. Optogenetic activation of glutamatergic cells within the d/dlPAG predominantly resulted in escape with the occasional expression of freezing, whilst activation of this cell population in the vlPAG robustly drove freezing (Tovote et al. 2016; Assareh et al. 2016; Evans et al. 2018).

1.3.2.3 Selection of a defensive action within the PAG

The observation of various forms of defensive response elicited by PAG stimulation intuitively fostered speculation about the potential mechanisms by which action selection could be resolved and controlled within the PAG. In line with early ethological studies (Blanchard and Blanchard 1989), defensive behaviours are hierarchically recruited to incremental increases in the level of PAG activation. Within the dPAG, the application of higher levels of electrical current shifted the expression of the evoked defensive behaviour from freezing to fleeing in freely-behaving rats (Vianna and Brandão 2003; Bittencourt et al. 2004; Assareh et al. 2016) and increased optogenetic stimulation of excitatory neurons in the dPAG increased the reaction time and maximum speed reached during the evoked flight (Evans et al. 2018). Human imaging studies have also revealed increases in the blood-oxygen-level dependent (BOLD) activity within the PAG as innately threatening visual stimuli become more imminent (Mobbs et al.

2007; Coker-Appiah et al. 2013). These results suggest the existence of a graded relationship between circuit activation and behavioural expression.

Complementary to this view, is the idea that selective, and potentially sequential, activation of distinct circuits and ensembles of cells within the PAG is responsible for the flexible expression of distinct behavioural choices. This idea is strengthened by the observation that within subregions of the PAG, distinct cell populations are active during discrete components of the behavioural interaction with a threat, namely threat detection, risk assessment and flight (Deng et al. 2016; Reis et al. 2021; La-Vu et al. 2022). Of note, is the presence of local reciprocally-inhibited microcircuits within the PAG responsible for the activation of distinct motor behaviours (Tovote et al. 2016). This circuit motif presents a potential mechanism by which the mutual inhibition and disinhibition of discrete PAG ensembles could mediate the behavioural switching between active and passive defensive responses. Specifically, this study found that the the selection of freezing over escape is implemented through the selective disinhibition of specific cells within vlPAG together with the simultaneous inhibition of PAG ensembles responsible for driving escape responses. Unlike escape, which is widely thought to be exclusively driven through the dPAG, freezing can be observed through the activation of both the dorsal and ventral regions of the PAG. It is thought that distinct circuits are responsible for different forms of freezing: the active immobility to an inescapable threat, the post-escape recuperative quiescence, or the arresting behaviour linked to risk assessment.

These experiments were fundamental in developing the idea that external inputs might exert a level of control over the promotion of specific behavioural strategies, whilst the selection of the appropriate action and circuits is arbitrated through tightly-controlled lateral inhibition of cellular ensembles within the PAG. This idea is supported by studies showing that the activation of select inputs from lateral hypothalamus, zona incerta or central amygdala populations to the l/vlPAG was shown to precisely modify the selection of active and passive behaviours (Fadok et al. 2017; Li et al. 2018; Chou et al. 2018). Moreover, the idea that competition between mutually exclusive circuits drives action selection was observed in the promotion of freezing behaviour in response to the selective inhibition of excitatory cells within the dPAG (Lefler et al. 2020). Defensive action selection is also modulated by inputs from the prefrontal cortex that suppress dPAG activity and promote the expression of social defeat (Franklin et al. 2017), and serotonergic inputs from the raphe nuclei that are specifically activated in situations of high threat to promote the selection of escape (Seo et al. 2019).

It is likely that the recruitment of specific neural circuits is required to select between competing escape behaviours, whilst the graded level of circuit activation might act to shift the intensity of expression of the chosen behaviour. It has been difficult to disentangle if the PAG circuitry also contributes to the evaluative component of threat response or if it is purely an action selection switchboard for the gating and commanding of distinct defensive behaviours. Interestingly, ascending projections from the PAG to higher areas suggest a further role of PAG activity in the adaptation of fear responses. The ability of the dlPAG in inhibiting forebrain activity in response to extreme risk suggests the PAG could be playing a further role in the development of contextual fear memories (De Oca et al. 1998)

1.4 Autism: Perceptual decision-making and response to threats in models of neurodiversity.

Having discussed in detail the critical importance of perceptual decision-making (PDM) and specifically the ability to generate rapid defensive responses to visual threats, I will now introduce the neurodevelopmental condition autism, including the specific autism-risk genes that are the focus of this study, and will briefly outline what is known about how visual processing and PDM are affected in autism.

1.4.1 Autism: a short introduction

The term 'autism' is used to describe a complex neurodevelopmental condition with a heterogeneous genetic and non-genetic aetiology, that affects an estimated 1-2 % of the global population, with an average male to female bias of 4-5:1 (Wiśniowiecka-Kowalnik and Nowakowska 2019). The condition was first described by the austro-american psychiatrist Leo Kanner in 1943 (Kanner, 1943)[3]. It is syndromic in that it is characterised by the consistent expression of several core symptoms: deficits in social interaction and communication, and restricted and repetitive interests and behaviours. However, these core symptoms are almost always expressed with co-occurring mental and physical health conditions. Common comorbidities include intellectual disability, gastrointestinal disturbances, sleep abnormalities, motor impairments, epilepsy and sensory processing and attentional differences (Al-Beltagi 2021). Autistic individuals can present with one, or several of these co-occurring conditions simultaneously or consecutively, and can be expressed with varying degrees of severity that can fluctuate over the course of the individual's lifetime.

Whilst the aetiology of autism is still largely unknown, it is widely accepted that both genetic and non-genetic factors contribute to the development of the disorder. Autism's strong genetic component was revealed through a number of family and twin studies; with genes implicated in syndromic forms of autism first identified in the 1990s, whilst the identification of rare, but highly penetrant genomic copy number variants (CNV) occurred in the 2000s (Hulbert and Jiang 2016). More recently, the widespread analysis of genetic variability between patients and their unaffected family members through the use of microarray, whole-exome sequencing and whole-genome sequencing technologies has unveiled a number of rare, *de novo*, genomic variants in hundreds of genes (de la Torre-Ubieta et al. 2016). Despite challenges in establishing a causal role for many of these sequence variants, a subset group of candidate 'autism-risk' genes emerged through the repeated identification of distinct, *de novo* mutations at different loci within the same gene in affected individuals but not in controls. Notably, these gene variants that confer high penetrance for autism only occur in a small subset of the

[3] Kanner first published a systematic description of common characteristics among eleven children with "autistic disturbance of affective content" in 1943, yet the condition was only officially entered into the Diagnostics and Statistics Manual (DSM-3) in 1980.

population with autism - fewer than 2 % of individuals with the condition - suggesting a complex and polygenic genetic aetiology of autism. Despite this however, diverse genetic mutations converge on common downstream effects and signalling pathways. Thus, the study of monogenic mouse models with targeted mutations in the homologous 'risk' genes may prove fruitful in identifying common neurobiological pathways affected by different autism-associated mutations, as well as the specific contribution of these mutations to the autistic-like traits observed in animals (Crawley 2012).

1.4.2 Sensory processing, visual attention and decision-making in autism

Previously listed as some of the most frequently expressing comorbidities (>90 %, Marco et al. 2011; de la Torre-Ubieta et al. 2016), sensory processing abnormalities, encompassing both hyper- and hypo-sensitivity to sensory stimuli, are now integrated into the core diagnostic features of autism (Shapse 2008). These differences range from mild to severe and can occur in the processing of stimuli from any modality, including chemosensory (Endevelt-Shapira et al. 2018), tactile (Balasco et al. 2019; Espenhahn et al. 2021; Salkić et al. 2022), auditory (Remington and Fairnie 2017; Rotschafer 2021) and visual (Robertson and Baron-Cohen 2017; Bakroon and Lakshminarayanan 2016). Our understanding of the specific alterations in sensory processing capabilities in autistic individuals is mixed however, and studies utilising diverse experimental paradigms have found autistic individuals can display typical, superior or reduced sensory detection sensitivities when compared to neurotypical individuals. Gaze and attentional abnormalities have been linked to autism since its first description (Kanner 1943), however, it is commonly observed that many autistic individuals exhibit excellent visual processing abilities (Baron-Cohen et al. 2009). Enhanced perception has been observed to local visual features and fine details (Dakin and Frith 2005), whilst the processing of faces appears to be atypical (Dalton et al. 2005; Kleinhans et al. 2011; Senju et al. 2011; Campatelli et al. 2013; Keehn et al. 2015). The processing of visual motion also seems to be affected (Gepner et al. 1995; Milne et al. 2002; Blake et al. 2003; Kogan et al. 2004; Annaz et al. 2010, 2012; Manning et al. 2022), however other studies have highlighted that there might be a specific difficulting in processing the motion of complex, but not simple visual stimuli (Bertone et al. 2005; Foss-Feig et al. 2013).

Understanding the potential perceptual differences in autism will necessarily require an understanding of how stimulus selection and other attentional processes are affected. Differences in both attentional shifting between stimuli and selective attention in general have been observed in autistic individuals. Abnormal attentional disengagement has been proposed as one of the earliest diagnostic symptom to emerge in infants (Elsabbagh et al. 2013; Sacrey et al. 2014) and has similarly been shown in behavioural readouts and functional EEG recordings in adults (Courchesne et al. 1994; Kawakubo et al. 2007). Meanwhile, it is widely observed that the selection of appropriate targets of fixation is abnormal in autism. One of the most established ideas concerning this inappropriate visual selection is that there exists a bias for local over global processing of visual scenes, resulting in a "difficulty to see the forest for the trees" (Robertson and Baron-Cohen 2017). This idea is most clearly outlined in the 'Weak

Central Coherence' (WCC) theory of visual perception in autism (Frith and Happé 1994), and was also found to be the inverse of the global-to-local form of visual processing commonly observed in neurotypical individuals (Happé and Frith 2006; Van der Hallen et al. 2015; Guy et al. 2019). Altered visual search strategies (Wang et al. 2015) and added difficulties in selecting appropriate visual targets when presented with crowded visual scenes have been frequently described in studies of humans with autism (Burack 1994; Remington et al. 2009; Remington et al. 2012; Keehn et al. 2013; Wang et al. 2020). Inappropriate target selection has also been suggested to result from the overactivation of certain sensory circuits that 'capture' the attentional load from other forms of visual processing. This led to the 'Intense World Theory' of perception in autism (Markram 2007), which proposes that excessive neuronal processing and overactivation of certain circuits results in local circuit hyper-reactivity, which in turn gives rise to the emergence of hyper-perception and hyper-attention.

The specific investigation of *perceptual* decision-making in autism has largely centred around the use of visual discrimination tasks that incorporate a saccadic or physical motor action to signal the chosen target. As mentioned above, many of these studies have yielded conflicting and contradictory results with studies relying on the discrimination of visual motion or orientation indicating a mixture of enhanced (Foss-Feig et al. 2013; Dickinson et al. 2016), reduced (Pirrone et al. 2017) and unchanged (Manning et al. 2022) PDM abilities in autistic individuals. Many contributing factors, such as the temporal predictability of stimulus presentation (Kunchulia et al. 2019) and past behavioural choices (Feigin et al. 2021) have also been shown to affect PDM in autism. Overall, it has been proposed that differences in perception and sensory evaluation in autism arise from an imbalance, and overuse of, incoming sensory information over stored knowledge generated through experience (Pellicano and Burr 2012). This "Bayesian hypothesis" of perceptual decision-making in autism has received a lot of attention in recent years and has attempted to integrate several features of abnormal perceptual and action regulation in autism (Lawson et al. 2014; Palmer et al. 2017; Qi et al. 2018; Amoruso et al. 2019; Mirza et al. 2019; Manning et al. 2022).

Linking the behavioural differences observed in human studies to the underlying circuit and cellular mechanisms have proved challenging. Whilst fMRI and EEG/MEG studies have facilitated the detection of large scale changes in neural activity across large areas they are fundamentally limited in their spatial resolution and interpretability (Summerfield and Blangero 2017). Relevant to this thesis, the specific contribution of the SC or the PAG is difficult to determine due to the current difficulties in isolating and recording from these regions with commonly used recording systems such as fMRI (Jure 2019). For this reason, cortical brain regions have been most linked to perceptual or attentional changes in autism, such as the lateral prefrontal cortex, the frontal eye fields, the lateral intraparietal cortex, anterior insular cortex and the primary visual and extrastriate visual cortices (Dinstein et al. 2012; Ibrahim et al. 2019; Chung and Son 2020; Keehn et al. 2020). Overall, ethical and logistical difficulties in monitoring and recording neural activity in humans has meant that attempts to understand the detailed neurophysiological changes in autism have often made use of animal models, especially genetically-modified mouse models carrying homologous mutations to those found in human patients (Crawley 2012; Del Pino et al. 2018). Rodent

genetic models of autism have revealed similar auditory (Scott et al. 2018; Razak et al. 2021), tactile (Orefice et al. 2016) and visual (Wells et al. 2016; Goel et al. 2018; Felgerolle et al. 2019; Cheng et al. 2020) sensory deficits to those seen in human patients. Similar to human studies, rodent studies have largely focussed on investigating the role of cortical and thalamic brain regions in generating these sensory differences. Functionally, these studies have observed altered neuronal responses to selected features of visual stimuli, such as motion (Felgerolle et al. 2019) or orientation (Goel et al. 2018) in visual cortices. Moreover, the worsened performance of these animals in common experimental PDM paradigms, such as two alternative forced choice (2AFC) paradigms in which individuals must perceptually evaluate a specific feature of two visual stimuli before selecting the appropriate target and performing a signalling action, have identified candidate cellular or circuit phenomena affected in these mice, however they are often limited by the difficulty in interpreting both the behaviour and neural activity recorded (Wells et al. 2016, Goel et al. 2018, Felgerolle et al. 2019).

Difficulties with decision-making in general have been widely reported in first hand accounts of individuals with autism (Grandin 2000; Lawson 2001; Sainsbury 2009) with common descriptions of feeling overwhelmed, exhausted and paralysed by the process of decision-making, even in seemingly trivial situations such as deciding what to eat or wear. These reports suggest PDM difficulties may have pervasive, knock-on effects on many aspects of autistic individuals' everyday lives. Reports from family members (Frost and Shows 1993; Johnson et al. 2006) and teachers (Winter 2011) are consistent with these autobiographical accounts, indicating that simple tasks are more stressful, take longer and lead to greater levels of indecisiveness in general in autistic children and adolescents. A study on decision-making in autism revealed that autistic participants more frequently reported difficulties in decision-making than their neurotypical peers (Luke et al. 2012). Decisions that need to be made quickly or require a change in routine were reported as particularly difficult. The extent to which decision-making is affected in autism and the neurobiological mechanisms through which these difficulties emerge are still unclear.

1.4.3 Responses to visual threats in autism.

Relevant to the focus of this thesis, it should be noted that the specific response of autistic individuals to threats, including visual threats, also appear to be different to those performed by neurotypical individuals. Overall, it appears that although affected individuals may attend less to threatening visual cues (Macari et al. 2021), their emotional fear responses are actually increased, with some even suggesting a threat-detection advantage in autism (Krysko and Rutherford 2009). High levels of anxiety, phobias and fear in general have been well reported in the autistic population (Evans et al. 2005) and has led to the idea that dysfunction of a critical brain region for the processing and generation of fear responses, the amygdala, is a central feature of autism (Baron-Cohen et al. 2000). Correspondingly, enhanced behavioural responses to naturally or conditioned fearful stimuli as well as amygdala hyperexcitability have been observed in animal models of autism (Markram et al. 2008 ; Fricano-Kugler et al. 2019).

Defensive responses, characterised as evasive head or body movements, to looming or rapidly approaching visual stimuli were observed in human infants as early as 1971 (Ball and Tronick 1971; Dunkeld and Bower 1980; Billington et al. 2011; Vagnoni et al. 2012; Coker-Appiah et al. 2013; Dunkeld and Bower 1980), whilst similar avoidance responses were observed in macaque even earlier (Schiff et al. 1962) and have been seen in mice as early as postnatal day 14 (P14) (Chen et al. 2022). Only one study, to the best of my knowledge, has assessed the behavioural responses of any animal model of autism to the looming avoidance response (LAR) paradigm (Hu et al. 2017). This study discovered impaired looming-evoked responses in the valproic acid model of autism. They suggested that abnormal connectivity between the SC and the basolateral amygdala (BLA), through the lateral posterior nucleus (LP) were the source of the deficit. Interestingly, they observed corresponding looming-evoked behavioural impairments in autistic children.

1.4.4 The contribution of the SC and PAG to the pathophysiology of autism.

The potential contribution of superior colliculus dysfunction to the generation of a number of the behavioural phenotypes observed in autism has recently been speculated (Jure 2019, 2022). Often overlooked for brain regions linked to higher-level cognitive and emotional processing, the recognition of a striking overlap between the functional roles carried out by the SC and the phenotypic expression in autism has spurred researchers towards an investigation of this area in the condition. Many of the critical sensory and attentional roles mentioned in the sections above are strongly linked to SC function: bottom-up attentional mechanisms (Amso et al. 2014), the control of gaze and eye movements (Akechi et al. 2014; Hadjikhani et al. 2017; Madipakkam et al. 2017), nonconscious visual processing of faces and motion (Kleinhans et al. 2011) and multisensory processing (Panagiotidi et al. 2017; Siemann et al. 2020) are all found to be disrupted in autism. Several studies have identified structural and functional changes in SC function in humans with an ASD (Hu et al. 2017; Yiting Huang et al. 2022). While differences in SC circuit organisation and function (Kay et al. 2018) as well as impairments in related behavioural responses (Dendrinos et al. 2011) have been identified in both genetic and non-genetic mouse models of autism. Functionally, these studies identified wider visual receptive fields (Dendrinos et al. 2011) and altered feature-selectivity to visual stimuli in the SC (Kay et al. 2018).

The early development of the SC and its greater role in early visual processing suggests a potentially larger role for the SC in ASD aetiology through its potential contribution to higher-circuit formation and widespread brain development. It has been indirectly suggested that early social visual experiences can epigenetically influence the formation of subcortical-cortical brain networks through the activation of subcortical visual circuits that are highly-receptive to visual input (Johnson et al. 2005; Klin et al. 2015; Salva et al. 2015). The SC's prominent role in many forms of sensory processing, and its central position at the interface of subcortical and cortical networks mean that its selective disruption could have far-reaching and cascading effects on numerous downstream structures that are reliant on SC input for their own function (Thye et al. 2018).

The periaqueductal grey has received limited attention in connection with the phenotypic expression and pathophysiology of autism. To the best of our knowledge, only one study has directly linked a genetic mutation linked to autism to PAG dysfunction (Anstey et al. 2022). This study linked an observed overreaction to somatosensory stimuli to PAG hyperexcitability in the *Nlgn3*$^{-/Y}$ genetic rat model of autism. However, as mentioned in section 1.3.2, the PAG plays a diverse role in many factors that are affected in autism such as pain, anxiety, reactive responses to threats and a number of autonomic processes. The PAG is positioned at the critical interface between sensory processing circuits and motor control centres, and as such could have an influential role in the overall performance of many sensory-driven behaviours.

*

The research in this thesis centres upon the examination of the behavioural and neuronal responses of three distinct monogenic mouse models of autism to an innately threatening, looming visual stimulus. In the next three subsections I will briefly introduce each of the autism-risk genes under investigation and outline what is known about the molecular and behavioural effects of their mutation in mice.

1.4.5 The *Setd5* model of autism

The discovery of the human gene, *SETD5*, as a candidate gene for the development of neurodevelopmental conditions such as autism originated from a large-scale genomic screening of almost 1000 individuals with intellectual disability (Grozeva et al. 2014). Numerous *de novo*, loss of function (LoF) variants were identified by whole-exome sequencing and through individual case reports (Green, Willoughby, and Balasubramanian 2017; Fernandes et al. 2018; Chiang, Shumakova, and Greenfield 2020), that indicated a strong link between these mutations and intellectual disability[4], craniofacial abnormalities and attentional difficulties. The gene, SET[5]-domain containing 5 (*SETD5*), belongs to the SET-domain containing gene family that encodes histone-modifying proteins. In general, mutations in the gene seem to have a higher penetrance in males with the mutation, whilst affected females had a more heterogeneous phenotypic expression overall (Fernandes et al. 2018). It is widely expressed in tissues across the body, with a strong expression in the brain, during both development and across adulthood. It is thought to play a critical role during development since mouse models with the full deletion are lethal at early embryonic stages. *In silico* analysis predicted the potential role of the functional protein encoded by this gene to be the epigenetic regulation of

[4] 0.7% of individuals with idiopathic intellectual disability had heterozygous mutations in SETD5 (Fernandes et al. 2018)

[5] The SET domain is a protein domain that typically has methyltransferase activity. It was first identified in the Drosophila Su(var)3-9 and 'Enhancer of zeste' proteins, from which the acronym SET is derived [Su(var)3-9, Enhancer-of-zeste and Trithorax] (Dillon et al. 2005).

gene expression through histone methyltransferase activity (Kuechler et al. 2015). The Setd5 protein interacts with two regulatory complexes, histone deacetylase3 (Hdac3) and polymerase-associated factor 1 (Paf1), to regulate gene transcription (Deliu et al. 2018), and (Nakagawa et al. 2020) uncovered the particular role of Setd5 in removing the regulatory protein TIP5 to enable the transcription of ribosomal protein genes and rDNA.

Recent studies, enlisting a mutant mouse model with haploinsufficiency in the mouse homologue, *Setd5,* have investigated the molecular mechanism of action of this mutation and have characterised the relevant behavioural phenotypes of this mouse line (Deliu et al. 2018; Moore et al. 2019; Nakagawa et al. 2020). Mutant mice were born with craniofacial abnormalities, as well as skin pigmentation differences and occasional eye defects, indicators of aberrant head and trunk neural crest proliferation and cell-fate determination. All three studies found significant changes in gene expression in embryonic (E9.5: Deliu et al. 2018, E18.5: Moore et al. 2019) and adult (Nakagawa et al. 2020) brain tissue. Although the gross brain morphology of *Setd5*$^{+/-}$ mice was indistinguishable from their wild-type siblings, there was a pronounced shift in the expression of neuronal-related genes compared to other cell lineages.

Functionally, the *Setd5*$^{+/-}$ mutation was found to perturb neural network activity and synchrony in cultured cortical tissues, and these cultured neurons exhibited altered morphological features, including reduced dendritic branching and smaller soma sizes (Moore et al. 2019). Additionally, *in vitro* recordings of hippocampal slices from *Setd5*$^{+/+}$ and *Setd5*$^{+/-}$ littermates revealed increased early and late long term potentiation (LTP) of synaptic transmission at CA3-CA1 synapses after high frequency stimulation in the *Setd5*$^{+/-}$ compared to their wildtype littermates (Deliu et al. 2018). These neural changes were in line with behavioural observations suggesting enhanced memory retention in *Setd5*$^{+/-}$ mice, both through sustained freezing in a contextual fear conditioning paradigm and better discrimination indices in a novel object location memory test. Despite the enhanced memory retention observed in *Setd5*$^{+/-}$ mice, these animals showed no difference in their acquisition of contextual fear memories, suggesting these animals do not exhibit altered proprioceptive sensitivity (Deliu et al. 2018). Interestingly, this study also observed differences in the transcriptional profile of neural tissue in the mutant animals after behavioural training, especially in genes linked to synaptic plasticity and learning.

Poor nest building abilities but intact social interaction and social novelty responses were consistently observed across the studies. However, while two of the studies observed a clear hyperexcitability phenotype and thigmotaxis of the *Setd5*$^{+/-}$ mice during open field observation (Moore et al. 2019; Nakagawa et al. 2020), Deliu et al. (2018) found no difference in the exploratory or locomotor abilities of the mutant animals. Two studies presented conflicting reports on the ability of the *Setd5*$^{+/-}$ mice to form and extinguish conditioned fear memories, with Deliu et al. (2018) describing an intact fear memory acquisition, but enhanced fear retention in *Setd5*$^{+/-}$, whilst Nakagawa et al. (2020) observed deficits in both the acquisition and retention of a conditioned freezing response to a foot shock.

1.4.6 The Ptchd1 model of autism

The human *PTCHD1* gene encodes a transmembrane protein consisting of 12 transmembrane helices, containing a patched-related domain and a sterol-binding site. The gene is highly conserved in a wide range of species from nematodes to humans, suggesting an important role across biological systems (Noor et al. 2010). *PTCHD1* is located on the small arm of the X chromosome and is highly expressed in nervous tissue during development, especially between embryonic day 9.5 (E9.5) and postnatal day 1 (P1), and in adulthood. Strong expression is seen in the hippocampus and thalamic reticular nucleus, with the highest level in adulthood found in the cerebellum and pituitary gland (Pastore et al. 2022). Mutations in the *PTCHD1* gene are thought to occur in ~1 % of the population with autism and intellectual disability (Marshall et al. 2008). Whilst mutations in the gene are thought to show a strong penetrance, phenotypic screening of families with CNV in the *PTCHD1* gene revealed a 40% chance of expressing autism-like behaviours in those carrying mutations in the gene (Chaudhry et al. 2015). Despite diverse phenotypic presentations, hypotonia and motor incoordination were characterised as the only consistent neurological findings in this comparative analysis, while other studies have indicated ADHD-like behaviours.

The similarity of the amino acid structure, as well as the presence of the sterol-binding site led to initial hypotheses that the encoded protein acts as a receptor for Sonic hedgehog (Shh); a key signalling pathway during development that is critical for brain and neural tube formation (Marshall et al. 2008; Noor et al. 2010; Chaudhry et al. 2015). However, this proposed role was later disproved by further studies. Tora et al. (2017) identified a critical interaction of Ptchd1 with several postsynaptic density (PSD) proteins, including PSD95, and the Retromer complex, suggesting Ptchd1 has a key role in endosomal sorting within dendritic spines. This hypothesis was later confirmed by a separate study which further identified inefficient trafficking of the protein to the membrane, with aberrant expression of the protein within the endoplasmic reticulum (ER) in cell cultures with mutations in PTCHD1 (Halewa et al. 2021). A further molecular role for Ptchd1 was hypothesised by Murakami et al. (2019) recently who linked mutations in *Ptchd1* to an overactivation of the kynurenine pathway (KP) and proposed that higher levels of KP metabolites in both the plasma and the brain could be used as a potential biomarker for the condition.

Mouse models carrying mutations in the mouse homologue *Ptchd1* revealed conserved hyperactivity and ADHD-like behaviours in affected male mice, as well as locomotor impairments, sleep disruptions and hyperaggression (Wells et al. 2016; Ung et al. 2018; Nakajima et al. 2019). Profound functional disruptions in the balance of excitatory and inhibitory signalling in hippocampal neurons were also observed (Tora et al. 2017), together with a 33% reduction in dentate granule cell excitatory spine density (Ung et al. 2018). Sensory processing through the thalamic reticular nucleus (TRN) was shown to be impaired to both visual (Wells et al. 2016) and auditory (Nakajima et al. 2019) stimuli. These processing deficits seemed to be ameliorated by the application of 1-ethyl-2-benzimidazolinOne (EBIO), a SK potassium channel positive allosteric modulator. In both cases however, additional perturbations in thalamic-projecting prefrontal circuits were shown to result in impaired higher-

level executive control of thalamic sensory filtering. The hypofunction of neuronal populations were also observed in induced pluripotent stem cell (iPSC) cultures derived from patients with *PTCHD1* mutations, with these cultured populations exhibiting reduced mini excitatory postsynaptic currents (EPSCs) and N-methyl-D-aspartate (NMDA) receptor hypofunction (Ross et al. 2020).

1.4.7 The *Cul3* model of autism

CUL3 encodes for Cullin-3 (Cul3), a core member of the E3-ubiquitin ligase complex. Found ubiquitously throughout the cell, it plays a crucial role in regulating cellular protein composition through the controlled recognition and recruitment of target substrates for breakdown through the ubiquitin-dependent proteasomal degradation pathway. This targeting specificity is accomplished through the unique combination of adaptor and substrate recognition sites possessed by each member of the Cullin protein family. It is an evolutionarily conserved protein involved in a wide range of cellular and biological functions including growth, cell cycle and cytoskeletal dynamics, cell signalling and transcriptional regulation (Singer et al. 1999). Its disruption has been linked to a wide range of cellular and system pathologies (Andérica-Romero et al. 2013). *Cul3* is found abundantly in both human and mouse tissues and is highly expressed in the brain. Molecularly, Cul3 has a specific role in regulating cytoskeletal dynamics and cell migration during development through the specific regulation of the protein Plastin3 (Pl3) that cell-autonomously regulates actin cytoskeleton organisation (Morandell et al. 2021) and through RhoA signalling (Amar et al. 2021).

The identification of *CUL3* as a top-ranking autism-risk gene was found through the recurrent identification of *de novo* loss-of-function mutations on the Cullin 3 (*Cul3*) gene by large-scale unbiased genetic screening of autism patients (O'Roak et al. 2012; Kong et al. 2012) and new CNV are being repeatedly identified in patients with autism, intellectual disability and schizophrenia (Wang et al. 2016; Nakashima et al. 2020; Iwafuchi et al. 2021). Individuals with mutations in the *CUL3* genes often co-present with ID, ADHD, sleep disturbances, motor deficits, dysmorphic facial features and seizures. Similar to *Setd5* and *Ptchd1*, the homozygous loss of *Cul3* is lethal at early embryonic stages. This lethality occurs at E7.5 in mice and has been found to be due to the accumulation of the cell cycle regulator Cyclin E, (Singer et al. 1999). For this reason, haploinsufficient mouse models have been generated to study the developmental and cellular effects of reduced Cul3 protein content.

Social and cognitive impairments have been widely observed in studies of these mouse models (Dong et al. 2020; Rapanelli et al. 2021; Morandell et al. 2021; Amar et al. 2021), as well as changes in neural transmission and altered excitability in hippocampal and cortical neurons. However, conflicting effects on excitatory-inhibitory (E-I) balance were observed, with (Dong et al. 2020) describing an increase in the E-I ratio whilst (Morandell et al. 2021) describe a decrease in E-I activity changes. *Cul3* deficiency was found to disrupt glutamatergic presynaptic transmission due to an imbalance of protein synthesis and degradation, resulting in

hyperexcitability of glutamatergic hippocampal pyramidal neurons (Dong et al. 2020). The specific reduction of *Cul3* in cortical tissues decreased PFC spine density and led to NMDA receptor hypofunction (Rapanelli et al. 2021). Whilst, reduced spontaneous network activity was observed in layer II/III cortical cells in the absence of morphological alterations (Morandell et al. 2021). These differences could be explained by the different brain regions investigated, hippocampus CA1 pyramidal cells and cortical layer II and III cells, or the method of driving the *Cul3* mutation in the different mouse lines.

Conflicting effects were also observed with respect to the locomotor and exploratory ability of the animals. Dong et al. (2020) described the expression of anxiety behaviours without any chances in the locomotor or exploratory behaviour, whilst both Rapanelli et al. (2021) and Amar et al. (2021) observed hyperactivity but intact motor coordination and Morandell et al. (2021) reported a number of motor abnormalities including altered gait dynamics, impaired hindlimb clasping and abnormal motor learning dynamics, without any difference in anxiety or exploration. The acquisition of fear memories appears intact although the strong retention of conditioned fear responses after extinction training suggests mutant animals exhibit a reduced ability to extinguish aversive memories (Morandell et al. 2021). Interestingly, the selective reduction of *Cul3* in either cortical or striatal brain structures led to distinct behavioural deficits in social interactions or repetitive and restricted behaviours, respectively (Rapanelli et al. 2021). Visual processing or attentional abnormalities have not been investigated in either humans or mice with mutations in the *CUL3*/*Cul3* gene.

1.5 Aims of this study

Give all that was mentioned above, this project aims to:

1 - Investigate whether mouse models of autism exhibit altered rapid perceptual decision making. Specifically, whether they are able to perform an appropriate defensive behaviour upon exposure to an innately threatening visual stimulus.

And if so, to:

2 - Describe the nature of the behavioural differences observed in the autism mouse models.
3 - Isolate the exact node(s) along this circuit where functional differences emerge.
4 - Determine the electrophysiological nature of these differences and possibly their molecular origins and functional significance in normal circuit function.

2 Methods

2.1 Animals

The study was discussed and approved by the institutional ethics committee of the Institute of Science and Technology Austria (ISTA) in accordance with good scientific practice guidelines and national legislation under license numbers BMWF-68.205/0023-II/3b/2014 and 66.018/0017-WF/V/3b/2017. Male and female adult (>5 weeks old) *Setd5*, *Setd5* ::*Emx1*-Cre, *Setd5* ::VGluT2-ires-Cre, *Cul3*, *Cul3* ::*Emx1*-Cre, *Ptchd1* mice were housed under a 12h light/dark cycle (lights on at 07:00), with food and water available *ad libitum*. The animals were housed in groups of 2-6 animals per cage and were tested during the light phase. Animals used for the *in vivo* electrophysiological recordings or freely-moving optogenetics experiments were group housed before surgery and individually housed after the surgery. Mice were chosen based on genotypes. Sex-matched animal pairs of control-mutant siblings from the same litters were compared to decrease variance due to age, environment and genetic background in all behavioural and *in vivo* electrophysiological recordings. Sex and age-matched animals were used for the *in vitro* patch clamp recordings.

2.2 Behavioural assay

2.2.1 Experimental setup

All behavioural experiments were performed at mesopic light levels, in a square, black box made from an IR-transparent Perspex material (W: 32 cm x L: 32 cm x H: 32 cm, Fig. 2.1). The arena contained a shelter with two entrance ports, made of the same material (9 cm x 9 cm x 3 cm), positioned in one corner. One wall of the box was intentionally 2 cm shorter to allow for ventilation and for the optic fibre to pass through for optogenetic experiments. A plastic screen covered with a plastic sheet with a matte grey surface was placed as a lid on top of the box, and a modified Texas Instruments DLP projector (DLP CR4500EVM) back-projected a grey background. The blue LED was exchanged for a high-power UV-LED (ProLight 1W UV LED, peak 405 nm) to improve the differential stimulation of S pigments. The entire behavioural chamber was illuminated with IR light (SIL 616.21, Sanitas) and experiments were recorded with a near-IR camera (acA1920-150um, Basler, 60 Hz) from below the centre of the arena. The entire apparatus was housed within a sound-deadening, light-proof cabinet.

Video recording, visual and optogenetic stimulation were controlled using custom software written in MATLAB (Mathworks, Inc.), python and arduino. This pipeline conducted several steps of image processing analysis of the behavioural video frames, including erosion and dilation steps to remove the optic-fibre patch cord, outline of the shelter and arena edges, to track the centre-of-mass coordinate position of the animal in real-time which was then used to control the timing of the sensory and optogenetic stimulation. A red square was presented off-screen in the corner of the projected image every 5th frame. An optical filter, positioned in front of the projector, reflected this red light back into a photodiode which then sent a signal to an arduino board (Uno) to trigger the behavioural camera. The timing of these events were

recorded through the arduino board, logged and used for later synchronisation of the stimulus and behavioural videos. For each experiment, a folder of jpg images (416 x 416 pixel resolution; later converted into AVI video files for storage) and log files containing information about the stimulus parameters, tracking data and analog synchronisation signals were saved.

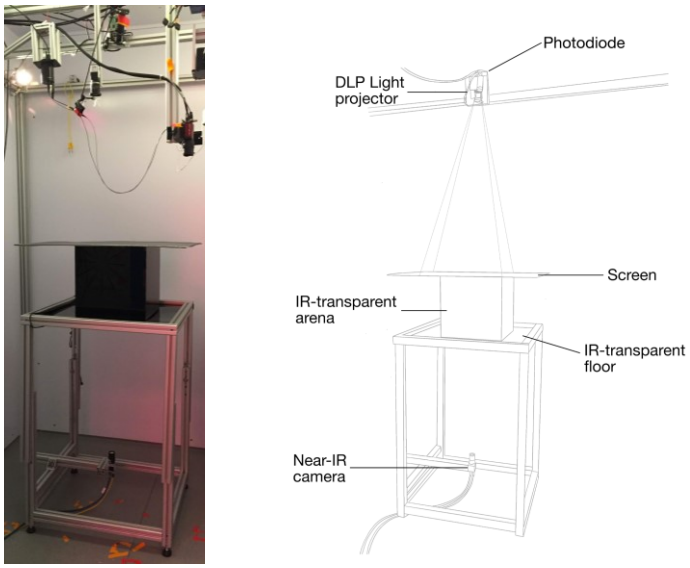

Figure. 2.1 Behavioural setup used to perform the looming avoidance response (LAR) paradigm.
Left, photograph of the behavioural arena. Right, diagram of the components visible in the photograph to the left.

2.2.2 Protocols

All animals were habituated to the test arena at least one day before testing and were allowed to explore the arena for at least 20 mins. The first 10 min of this exploration time was recorded and used to analyse the animals' exploratory behaviour. Animals were transferred to the arena from their home cages using a cardboard roll to minimise experimenter handling and avoid additional stress for the animals.

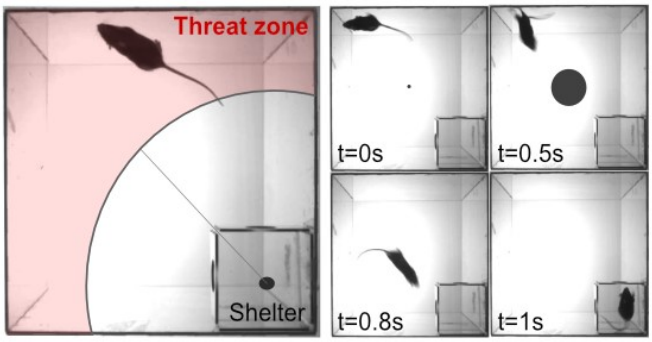

Figure. 2.2 Example video frames during a looming avoidance response (LAR) trial.

Left, video frames from a single trial of the looming avoidance response (LAR) paradigm showing the location of the shelter and the threat zone in red. Right, frames from a trial, covering one second after the triggering of the looming stimulus, t = 0 s.

2.2.2.1 Looming avoidance response - standard protocol

For the looming avoidance response (LAR) paradigm, responses were tested over five consecutive days. On each test day the animals were given 10 min to acclimatise to the arena, after which they were subjected to 3 test trials, with a 3 min interval between each trial. Each trial lasted 180 s, within which the central position of the mouse was tracked online (Python) and was used to trigger the visual stimuli in a closed-loop manner whenever the mouse crossed a designated threshold distance (10 cm) from the centre of the shelter. Stimuli were presented with a minimum stimulus interval of 30 s. A typical experiment lasted ~30 min and the entire arena was cleaned with 70 % ethanol between animals.

2.2.2.2 Reward trials

In preparation for the reward trials, after the 4th day of testing a small piece of banana chip was placed in the opposite corner of the arena to the shelter and the mice were free to explore the arena without triggering any loom stimuli (Fig. 2.3). The animals were left to explore until they successfully acquired the banana chip, after which time both the mouse and the chip were placed back in their home cage. The reward trial then took place after the 5th day of testing. A new small piece of banana chip was again placed in the opposite corner of the arena and the animals were free to explore, however this time whenever the mouse passed the threshold distance from the shelter a looming stimulus would start, with no inter-stimulus interval.

Figure. 2.3 Example video frame during a looming avoidance response (LAR) 'reward' trial, showing the location of the food reward in one corner of the arena.

Video frame from a reward trial showing the location of the food reward within the threat zone.

2.2.2.3 Different contrast trials

For different contrast experiments, animals were acclimatised to the arena as in the standard LAR paradigm and were then presented with looming stimuli of 20, 50 or 98 % contrast in a

pseudorandom order upon crossing the trigger threshold. The background luminosity remained constant while the luminance of the disc was increased to generate low contrast stimuli.

2.2.2.4 Learned suppression of escape

Learned suppression of escape (LSE) experiments were conducted as in (Lenzi et al. 2022). Naive mice were habituated to the arena for 10 minutes before the shelter was removed from the arena and a series of 8 blocks of 3 loom stimuli were presented to the mice with 40 s intervals. The luminance of the black disc remained constant but the luminosity of the background increased with each block and for the preceding 40 s period. Once all the looms had been presented, the shelter was returned to the arena and the mice were given an additional 7 min in the arena before they were tested with the standard high contrast loom stimuli.

2.2.3 Visual stimuli

Stimuli were created and presented using custom-made scripts in MATLAB (MathWorks, Inc.), using the Psychophysics Toolbox extensions. The standard stimulus consisted of a dark disc on a grey background presented on the lid over the centre of the arena,that reached a maximum size of 40 deg/visual angle. The disc expanded over 500 ms at a speed of 80 deg s-1 and then remained at this size for 250 ms before disappearing and a new expanding disc immediately appearing. A maximum of 5 expanding discs were shown in a single loom bout and the luminance of the background remained constant throughout. A red rectangle was presented along one side of the projected image every 5th frame, onto an out-of-view section of the arena lid, for post-hoc synchronisation (See *Methods 2.2.1*).

2.2.4 Analysis of behavioural data

Behavioural experiments, the initial tracking and analysis of the escape behaviour were done blind through automatic analysis scripts and the genotypes were added later when pooling the animals' data together. Behaviour metrics were calculated both by pooling trials across all animals and also by calculating the average per mouse and computing an average across all mouse averages. Detailed explanations of the use of the specific analyses are mentioned in the text.

2.2.4.1 Analysis of behavioural responses to the looming stimulus

LAR responses were assessed by analysing a peri-stimulus period starting from 3 s before the stimulus until 10 s after the stimulus onset. Responses were classified as successful escapes if the mouse returned to the shelter within 7 s after stimulus onset and reached a maximum speed of >20 cm s-1 in travelling back to the shelter. The maximum escape speed was calculated as the peak value of the speed trace between the onset of the escape and entry into the shelter. The reaction time of the mouse was calculated as the time from stimulus onset til the mouse reached the maximum speed during its escape back to the shelter. This reaction time was then used to group the responses of the animals depending on which loom presentation the peak of their escape response was recorded. The number of looms triggered is the total number of loom stimuli (bouts) triggered across the 5 days of testing, not including the reward trial. The Log10(ΔSpeed) was calculated as the logarithmic of the ratio between the average speed in the

time 300-800 ms after the start of the stimulus and the average speed in the peristimulus period ±50ms around the start of the stimulus. For the analysis of the response dynamics during the reward trials, only trials where the animals made a noticeable escape back to the shelter were included. Four *Setd5*$^{+/-}$ trials were removed from the final analysis because the mouse was interacting with the banana chip reward during the stimulus presentation and no obvious detection of the stimulus occurred, therefore a reliable response could not be determined.

2.2.4.2 Analysis of exploratory behaviour

Exploratory behavioural metrics were calculated from videos of the first 10 minutes of the acclimatisation period starting from when the mice were placed within the arena. A shelter exit was defined as an episode where the centre-of-mass of the mouse was recorded as having crossed the shelter edge limit, and had moved from inside to outside the shelter. Manual quality checking confirmed that this reliably detected the movement of the entire body of the mouse outside of the shelter, and did not assign risk assessment behaviours, such as nose or head pokes, as exits.The maximum distance travelled during an exit was defined as the maximal distance reached in a straight line between the centre of the mouse and the centre of the shelter. The exit duration was defined as the time between when the full body of the mouse crossed over (in-to-out)until it re-crossed (out-to-in) the shelter boundary. The interbout interval during exploration was the time between subsequent shelter exits. The centre position of the mouse, [X_m, Y_m], was used to quantify the percentage of the 10 minutes recorded that the mouse was either outside of the shelter, in the centre of the area (defined as a circular area, centred on the middle of the arena, [X_c, Y_c], with a 7 cm radius) or at the edge of the area (defined as outside of a circular area, centred on [X_c, Y_c] with a 14 cm radius, Fig. 2.4).

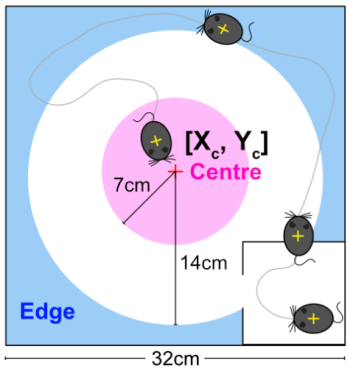

Figure. 2.4 Schematic of how the exploratory behavioural parameters were calculated from the behavioural video frames.

Schematic describing how certain features of the exploratory behaviour were analysed. The area of the arena classified as 'the centre' was defined as the area inside a circle of 7 cm radius from the coordinate centre of the arena of the arena [X_c, Y_c]. The 'edge' of the arena was classified as the space outside of a circle of 14 cm diameter centred on [X_c, Y_c].

2.2.4.3 Analysis of head direction

To understand the effect of certain parameters of the mouse's position and spatial location within the arena on it's LAR response we calculated the distance of the mouse from shelter

(defined as the straight line distance between [X_m, Y_m] and [X_s, Y_s]) and the heading angle of the mouse at the time of stimulus start. This parameter was defined as the angle (BÂC) between point B: the tip of the mouse's snout, A: the position between the two back paws of the mouse and C: the centre of the shelter [X_s,Y_s] (Fig. 2.5). The position of the individual body parts of the mouse were extracted using DeepLabCut tracking (Mathis et al. 2018) on the behavioural video frames.

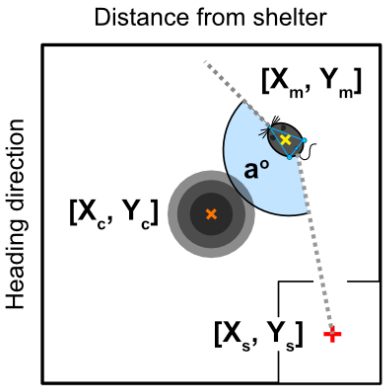

Figure 2.5 Schematic of how positional control variables were calculated.
Schematic describing how the distance from the shelter (difference between centre of the mouse ([Xm, Ym], yellow cross, and the centre of the shelter ([Xs, Ys], red cross), distance from the loom (difference between centre of the mouse ([Xm, Ym], yellow cross, and the centre of the arena ([Xc, Yc], orange cross) and the heading direction (Angle ABC where A is the tip of the mouse's nose (blue dot), B is the centre position between the back two paws (blue dot) and C is the centre of the shelter ([Xs, Ys], red cross); 0o would be facing the centre of the shelter) are calculated.

2.2.4.4 Analysis of trajectory directedness

The trajectory directedness of individual escapes was defined as (1 - ($d-d_{min}$/$d+d_{min}$)), where d is the cumulative displacement of the mouse from it's position at the time of the stimulus, [X_m,Y_m], start till when the centre of the mouse's body re-enters the shelter, and d_{min} is the straight line distance between [X_m, Y_m] and [X_s, Y_s] (Fig. 2.6). The distance from the loom was calculated as the straight distance between the centre of the arena [X_c, Y_c], and the centre of the mouse [X_m, Y_m].

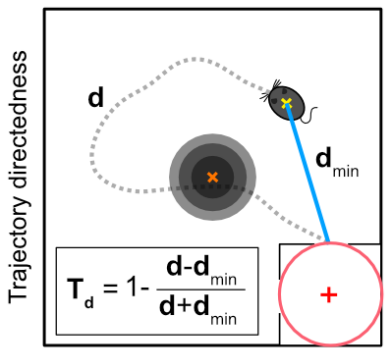

Figure 2.6 Schematic of how the directedness of the escape trajectory was calculated.

Schematic describing how trajectory directedness (Td) is calculated from the minimum euclidean distance of the mouse from the edge of the shelter at the initiation of the stimulus (d_{min}) and the cumulative sum of the total distance travelled by the mouse before it re-enters the shelter (d). Yellow cross is the coordinate centre of the mouse, orange cross is the coordinate centre of the arena where the looming stimulus is presented, red cross is the coordinate centre of the shelter.

2.3 Viruses

The viruses used in this study were adeno-associated virus (AAV) AAV9-EF1a-DIO-hChR2(E123T)T159C)-EYFP-WPRE-hGH (1×10^{13} viral genomes per ml (vg ml-1), Addgene 35509) for optogenetic activation and AAV9-Syn-Flex-GCaMP6m-WPRE-SV40 (1×10^{13} vg/ml, Addgene 100838) for control experiments.

2.4 General surgical procedures

Animals were anaesthetised with an intraperitoneal (i.p.) injection of ketamine (95 mg kg-1) and xylazine (4.5 mg kg-1), followed by metamizol (20 mg kg-1, i.p.), buprenorphine (0.05 mg kg-1, i.p.) and meloxicam (2 mg kg-1, subcutaneous (s.c.)). If needed, isoflurane (0.5-2 % in oxygen, 0.8 l min-1) was used to maintain anaesthesia. Fur on the top of the head was removed with an electric hair remover (Braun Precision Trimmer, PT 5010), then the mice were placed in a stereotaxic frame (Model 962, Kopf Instruments) and fixed using the ear bars. Eyes were protected using eye cream (Oleo Vital) and a topical analgesic (Xylocain 2%-Gel) was applied to the skin with a q-tip before incising the skin. The skin was resected by 2-4mm to make room for the affixation of the optic fibre or head plates, a few drops of saline were applied to facilitate the removal of the fascia and periosteum overlying the bone. The position of bregma and lambda were located and the skull was levelled as needed. Craniotomies of ~1mm diameter were made using 0.5mm burrs (Fine Science Tools) and a dental drill (Foredom, HP4-917). Viral vectors were delivered using pulled pipettes (World Precision Instruments, 1.4mm OD, 0.53mm ID, #504949) made with a micropipette puller (DMZ Zeitz-puller, Germany), backfilled with mineral oil and frontfilled and delivered using an automatic injector system (World Precision Instruments, Nanoliter 2010). The pipette was zeroed once it touched the surface of the brain, then lowered manually at ~ 500 µm min^{-1}. Once the target location had been determined, the pipette was retracted by 25 µm before the virus was delivered at 20 nl min-1. The pipette remained in this location for 10-15 minutes before withdrawal. The skin was closed after surgery using surgical glue (Vetbond, 3M, #1469SB) and upon completion of the procedure mice were administered with 500 µl of sterile saline (s.c.) and remained under observation on the heat plate until small movements could be detected, only then were they returned to their home cages for full recovery.

2.4.1 Additional surgical procedures for optic fibre implantation.

For optogenetics experiments, one optic fibre (400 µm-diameter, CFMC54L02, ThorLabs) was implanted per animal, into the medial posterior corner of the left superior colliculus, 250 µm dorsal to the injection site. Care was taken to effectively remove the dura before lowering the fibre to avoid pushing, and not penetrating the brain tissue. The surface of the skull was cleaned

and dried before small etching marks were made in a hashed pattern to improve affixation of the cement to the skull. Fibres were affixed using light-curing glue (Optibond Universal, Kerr Dental) and dental cement (SuperBond C&B Kit, Hentschel-Dental), and the skin was closed around the implant with surgical glue (Vetbond, 3M, #1469SB).

2.4.2 Additional surgical procedures for head plate affixation.

For *in vivo* head-fixed electrophysiological recordings, mice were implanted with a custom-designed head plate over a ~0.5-1 mm diameter craniotomy (left hemisphere, AP: 0.4 to -0.4, ML: 0.4 to 0.8 from lambda). This headplate was designed with specific features such as a serrated anterior edge to improve surface area for the cement to attach to, a small 'handle' to the side for ease of attaching the headplate to the holder in the setup and small raised grooves that fit in a 'lock-and-key' fashion to the holder for better stability when initially fixing the animal. A second craniotomy (~0.5mm) was made anterior to bregma on the right hemisphere, where a reference gold pin was implanted and lowered until it touched the brain surface. Both were cemented to the skull using light-curing glue (Optibond Universal, Kerr Dental) and dental cement (SuperBond C&B Kit, Hentschel-Dental), with the headplate additionally fixed using Charisma Flow (Kulzer GmBH). The craniotomy was covered with Kwik-Cast (World Precision Instruments) to protect the underlying tissue before recording.

2.5 Manipulation of neuronal activity *in vivo* - Optogenetics

Setd5$^{+/+}$::*VGluT2*-ires-Cre and *Setd5*$^{+/-}$::*VGluT2*-ires-Cre sex-matched sibling mice were injected with AAV9-DIO-ChR2-eYFP (see Viruses) into the right dmSC (75-100 nl, ML:-0.5, AP: -0.5 to -0.7, DV: -1.45 to -1.6, mm from bregma). Control mice were injected with 100 nl of AAV9-Flex-GCaMP6m into the right dmSC at the same coordinates.

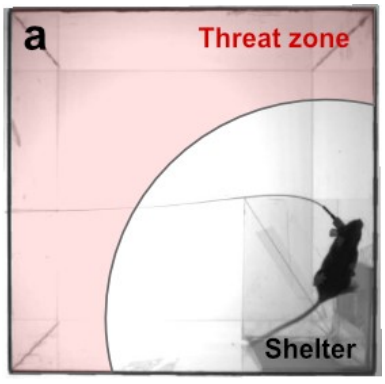

Figure. 2.7 Example video frames during a trial testing the effects of optogenetic activation of dmSC vGlut2⁺ cells.

Example video frame during an optogenetics trial showing the different shelter and the attachment of the patch cable to the implanted optic fibre.

2.5.1 Experimental paradigm

The same behavioural arena was used for the optogenetic activation experiments except with the addition of a black piece of perspex (9cm x 5cm) positioned 10 cm above the floor, replacing the closed shelter used in the standard LAR trials. Preliminary experiments revealed that animals reliably generated escape responses towards this shelter in response to looming stimuli, despite its more open configuration. At least two weeks after the surgery, mice were acclimatised to the arena, similarly as in the LAR procedure, but with the addition of the attachment of the fibre optic patch cable (200 μm, 0.48 NA, Doric Lenses). The cable was attached via a rotary joint (RJ1, ThorLabs) to allow for unrestrained movement and minimal handling of the animals.

Once the trial began, mice were photostimulated (473 nm, 10 light pulses of 10 ms at 10 Hz; Shanghai Dream Lasers Technology) if they passed the threshold distance (10cm) from the shelter, with a minimum inter-stimulus interval of 30s. The initial laser intensity was set to a low irradiance (0.01-0.1mW mm^{-2}) that did not evoke an observable behavioural response, however after at least 3 trials (180 s each, with a maximum 5 triggers per trial) at each intensity the irradiance was increased by (0.25-0.5 mW mm^{-2}). Laser power never exceeded 12 mW mm^{-2}. Two mice never elicited an observable escape behaviour, and post-processing histological analysis revealed mislocalised viral expression in these animals, and they, along with their matched siblings, were excluded from further analyses.

2.5.2 Analysis of behavioural responses

Trials were pooled across animals for each genotype, binned according to the stimulation parameters used in the trials and were fitted with logistic functions to generate psychometric curves. Initially, the stimulation intensity was normalised to the intensity for each animal that reliably evoked escape responses with the aim to account for variabilities in virus infection and expression or light transmission. After consideration, however, we did not continue with this normalisation since we thought that in this particular situation, there might be a significant difference in the level of light stimulation required to drive the circuitry and by normalising each animal to its maximum we might be obscuring this variation across the genotypes.

As with the LAR trials, escapes were automatically classified as trials in which the animals returned to the shelter within 7s of optogenetic stimulation and with a speed of > 20 cm s^{-1}. Reaction time was again calculated as the time from the onset of the stimulation, in this case the light stimulation, and the time at which the animal reached its maximum speed. The vigour of the response was calculated as the maximum speed reached between light onset and the return of the animal to the shelter. The slope and 95% confidence intervals for the logistic fits to the response parameters were calculated and two-way repeated measures ANOVA tests were used to isolate the effect of genotype, laser power and their interaction on the specific variables. The data of the Log10(ΔSpeed) across laser powers was further analysed by a multiple comparisons analysis of the output of the repeated-measures ANOVA, with Bonferroni correction to investigate the values of light stimulation the elicited significant differences between the genotypes. See the statistics table for more details.

2.6 Recording extracellular neuronal activity in vivo - Silicon probe recordings.

2.6.1 Experimental setup

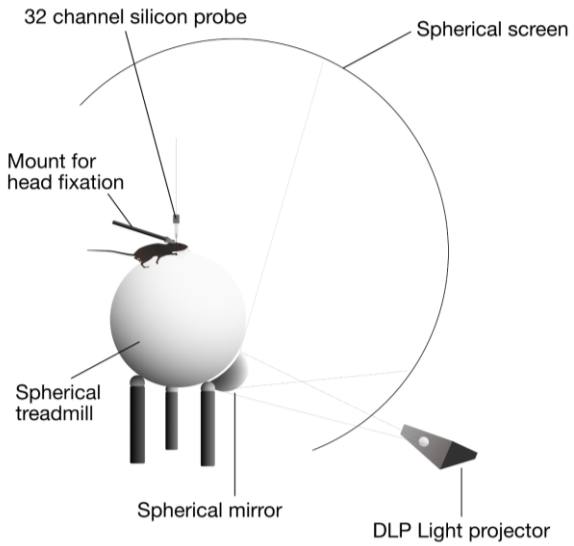

Figure. 2.8 The setup used to record extracellularly within the superior colliculus *in vivo* in head-fixed animals.

2.6.2 Data acquisition

A 32-channel silicon probe (NeuroNexus, USA, A32-OM32) was used to record extracellular spikes from different depths of the SC in *Setd5*$^{+/+}$ (n = 3), *Setd5*$^{+/-}$ (n = 3), *Cul3*$^{+/+}$ (n = 3), *Cul3*$^{+/-}$ (n = 3), *Ptchd1*$^{Y/+}$ (n = 3) and *Ptchd1*$^{Y/-}$ (n = 3) sex-matched sibling mice. At least 24-hours after surgery, mice were placed on a suspended spherical treadmill (polystyrene, 20 cm diameter) and head-fixed within a toroidal screen covering 190º of visual angle which was illuminated by a DLP-light projector (Blue LED exchanged for UV 405nm, 60 Hz refresh rate) reflecting off a spherical mirror in front of the screen (see diagram in Fig. 2.8). An infra-red (IR) light was positioned towards the animal, and its behaviour was recorded from the reflection of the animal in an IR-reflective heat mirror positioned 30 cm from the face of the mouse and 35 cm from the camera by a near-IR camera (Basler, acA1920-150um, 30 Hz). Prior to recording, the probe was coated with DiI (1 mM in ethanol, Merck, #42364) for later histological confirmation of the recording site and a wire was connected to the ground pin for both an external reference and grounding.

Once the animal was positioned within the arena and fixed using the head plate the kwik-cast seal was removed, revealing the brain surface and the confluence of the overlying superior sagittal and the left transverse sinus. Care was taken to position the probe as posteriorly and as medially as possible without damaging the sinuses or other blood vessels. The position of the probe was zeroed when the tip touched the surface of the brain, then was slowly lowered (1 µm s^{-1}) into the overlying cortex and the underlying SC to sequential depths between 1.2-2.2 mm. The recording was started 15 min after reaching the desired depth to allow for stabilisation of the probe. Separate recordings were made at 3-4 depths per animal, with 250 µm intervals between recording sites, to sample from cells across the depth of the SC. Each recording took

~30 min, with the animal in the setup for ~180-210 min in total. Data was recorded at 20 kHz (PCIe-6321, National instruments and Intan board RHD2000 Evaluation Board version 1.0).

2.6.3 Visual stimuli

Sensory stimuli were made using the Psychophysics Toolbox extensions in MATLAB (Mathworks) and presented and synchronised using custom-made LabVIEW software (2015), 64-bit, National Instruments). Frames were presented at a refresh rate of 60 Hz. At each depth, the mice were exposed to one 20 min presentation of a full field shifting spatiotemporal white-noise stimulus (20 Hz update for 10 min, see (Gupta et al. 2022) in order to assess receptive fields, and two repetitions of the remaining stimuli (5 x loom bouts, moving bars, moving gratings, full field flash). The checker size was 6.56 deg^2 and the entire grid was shifted between 0 and 3.25 deg in both x- and y-axis after every frame.
Each presentation would start with a uniform grey screen (60s, green and UV LED intensities were set to match the sun spectrum from a mouse opsin perspective), followed by the first presentation of the looming stimulus then the other stimuli in a pseudorandom order. Each stimulus was separated by a 30 s grey screen gap. Auditory monitoring of responses to a flashing point stimulus was used in real-time to gauge the rough centre of the receptive fields of the neurons being recorded, and the location of the looming stimulus was positioned to overlap with this position. The looming stimulus consisted of 10 repetitions of 5 sequential, individual looming stimuli (a loom bout), as previously described in the behavioural experiments. These loom bouts would be presented with intervals of pseudorandom lengths between 10-30s with a grey screen in between. To assess direction selectivity, the mice were presented with full-field moving square gratings (1.5 cycles s-1 temporal frequency and 0.3 cycles deg-1 spatial frequency) or a wide dark bar (38 deg s-1 speed, 6.5 deg width) in four orientations, drifting in eight different directions (separated by 45 deg) repeated twice for each orientation. Full field ON-OFF flashes were presented in blocks of 10 repetitions of 0.5s OFF-1s ON-0.5s OFF stimuli.

2.6.4 Analysis

2.6.4.1 Preprocessing

Initial analysis was performed in MATLAB R2018b and later in MATLAB R2019a. Raw voltage traces were high-pass filtered (300 Hz) and spikes were detected and sorted using Kilosort2 (https://github.com/cortex-lab/Kilosort) and Phy (Rossant et al. 2016**)** as previously described (Pachitariu et al. 2016), followed by manual curation. Firing rates histograms were calculated as the average firing rate across 16.7 ms time bins. Analog input channels (Photodiode, camera trigger) were extracted in MATLAB (MathWorks, Inc.) and arduino were recorded at a 20 kHz sample rate and were used for offline synchronisation. Custom-made scripts in MATLAB were used to extract the time points of the visual stimulus onsets and were later matched to the corresponding video frames.

2.6.4.2 Determining the surface of the superior colliculus

The initial SC location was determined in real-time by auditory monitoring of multi-unit activity to a flashing stimulus and was later confirmed offline using a current source density

analysis of the raw recording (Stitt et al. 2013) combined with histological reconstruction of the probe location visualised with DiI. CSD profiles were calculated for each recording and were used to align the depth of the units across recordings and across animals. The transition point between an overlying source and underlying sink was taken as the boundary between the stratum griseum superficiale (SGS) and the stratum opticum (SO). The boundary between the superficial (sSC) and intermediate/deep superior colliculus (idSC) was defined as 100 µm below this inflection depth (ID), taking into account the thickness of the SO. sSC was defined as 300 µm above the ID to 100 µm below the ID, and i/dSC was defined as the area below 100 µm below the ID. Only units identified as within the sSC and units with at least 2 spikes within the entire stimulus presentation were used for analysis. For all analyses spikes were sorted into peristimulus periods based on synchronisation with the stimulus frames and firing-rate histograms were calculated over 16.7 ms time bins.

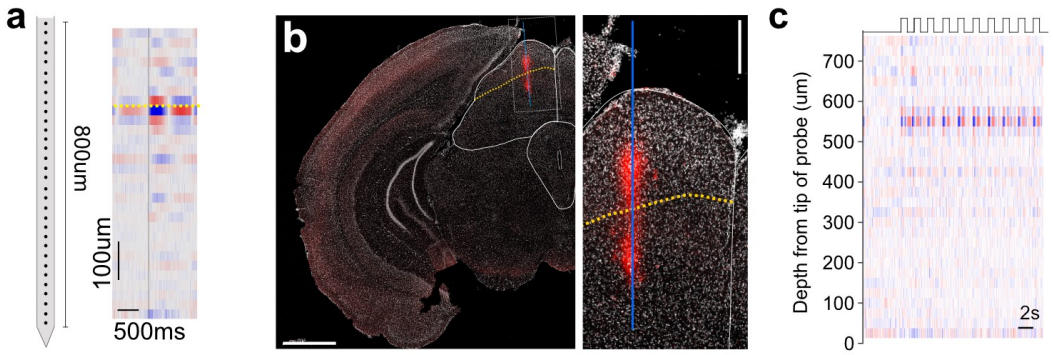

Figure. 2.9 Using current source density (CSD) analysis to determine the depth of the surface of the superior colliculus.

a, Schematic of the 32-channel silicon probe used to record extracellular activity aligned with the current source density analysis of a single flash stimulus averaged over 10 presentations. Black vertical line represents the stimulus onset, yellow dotted line marks the inflection depth separating the current source and sink. **b**, Histological reconstruction of the probe position marked with DiI (120 µm coronal section, scale bar: 1000 µm) with a close-up (scale bar: 250 µm). Yellow dotted line as in (**a**). **c**, Current source density analysis from a single recording showing the current source and sink values in response to 10 flash stimulus repetitions.

2.6.4.3 Analysis of baseline firing properties

The baseline firing properties of the cells recorded were determined by analysing their responses to a full field grey screen during the first 60 s of recording. The baseline firing rate per animal was calculated as the mean firing rate across this 60 s period across cells located within the 1000 µm below the sSC surface. The maximum firing rate was calculated as the maximum firing rate recorded over the 16.7 ms bins during this grey screen presentation.

2.6.4.4 Analysis of flash responses

Responses to a single flash stimulus (0.5 s OFF; 1 s ON; 0.5 s OFF) were generated by averaging the firing-rate histograms across 10 repetitions of the stimulus. The responsiveness of single units was defined based on the *p*-value generated from running a ZETA test (Montijn et al. 2021) on the average firing rate histograms during the stimulus. The 30 s period of grey screen before the stimulus was used as baseline and the period with the 2 s flash stimulus as

the response time. Clustering of responsive units was done using a K-means analysis and the number of clusters was determined by identifying the elbow point when analysing the Calinski-Harabasz index. Clustering was done with units from both genotypes pooled together, then later split based on genotype to assess the proportion of units from each genotype that are classified into each cluster. The proportion of flash responsive cells for *Ptchd1* and *Cul3* animals were determined for each animal by dividing the number of sSC units that were $p < 0.05$ by the total number of sSC units found.

2.6.4.5 Analysis of loom responses

Responses to a single loom stimulus were obtained by averaging the responses to the first loom of the loom bout stimulus (consisting of 5 consecutive looms) across 10 repetitions. Responsiveness was again defined as units having a *p*-value (determined using the ZETA test) of <0.05, with the 30s of grey screen preceding the loom stimulus as baseline, and the 0.7 s of first loom presentation as the response time. The average firing rate was calculated as the overall average of the mean firing-rate recorded across each of the 5 loom presentations individually for 10 repetitions. Maximum firing was similarly calculated as the mean maximum firing during each of the 5 looms, averaged across the 10 repetitions. The time-to-peak was calculated as the mean of the time to the peak firing within each of the 5 looms, averaged over the 10 repetitions. The time to the peak firing was calculated as the time from stimulus onset to the time when the activity of the unit reached its peak firing rate over the course of the loom stimulus.

2.6.4.6 Analysis of shifting white noise stimuli

To further analyse the visual receptive fields (RFs) of the units recorded we analysed their responses to a shifting white noise stimulus (Gupta et al. 2022) and calculated them as spike-triggered averages. The location of the centre of the receptive field was estimated by finding the pixel with the highest variance over a peri-spike time period and the final RF was cropped to 160 x 160 pixels, centred on this pixel of highest variance. To find the signal-to-noise ratio (SNR) for each neuron, we first found the difference between the square of the pixel value at the receptive field centre and the variance of all the values in a 5 pixels border around the edge of the RF. The $\log_{10}$ of this value was then multiplied by 10 to obtain the SNR value. Visually-responsive neurons were defined as those with SNRs in the 80th percentile of the SNRs of all sSC units (from all animals pooled together) or above. The centre of the RF was assigned as ON or OFF based on the sign of the mean of the central pixel at the centre of the receptive field. The proportion of OFF RFs was calculated as the ratio between visually-responsive cells with OFF RFs and the total number of visually-responsive cells in the sSC. The radius of the RF centre was calculated as the width at half of the peak value of the spatial RF profile. The average radius of the receptive fields of an animal was calculated using only the visually-responsive units. Temporal receptive fields were clustered similarly to flash responses, using K-means analysis to cluster the responses, with the number of clusters determined using the Calinski-Harabasz index.

2.6.4.7 Analysis of responses to moving bars and gratings

For each direction the mean across trials was calculated and normalised to the baseline firing in the 30 s before stimulus onset. The preferred direction (D_p) was defined as the direction with the greatest normalised response and the non-preferred direction (D_{np}) was taken as 180 degrees from that angle. The direction selectivity index (DSI) was then computed as $(D_p-D_{np})/(D_p+D_{np})$ with values falling in a range from 1 (reflecting high direction selectivity) to 0 (reflecting low direction selectivity). Units were defined as being 'direction selective' (DS) if their DSI was in the 80th percentile or higher out of all units recorded (pooled across all animals) within the sSC. The proportion of direction selective cells per animal was found by quantifying the proportion of DS sSC units divided by all sSC units recorded for that animal.

2.6.4.8 Head-fixed behavioural analysis

The motion of the animal was determined by sorting the difference between pixels in neighbouring frames with a K-means analysis into two groups. This analysis reliably filtered the frames into categories based on the level of similarity between adjacent frames and was confirmed by manual inspection of the sorted frames. The proportion of time each animal spent running was calculated as the proportion of frames that were registered as 'moving' over the total number of frames. The pupillary light reflex (PLR) of the animals was assessed by tracking the change in pupil size across the repetitions of the flash stimulus. A deep neural network approach for markerless tracking (Mathis et al. 2018) was used to extract points around the pupil. The diameter of the pupil was then calculated by fitting an ellipse to these points. Since we observed, and it is known, that the size of the pupil is greatly affected by locomotion, when analysing the PLR we only included repetitions in which the mice were running. An animal was considered to be running during a repetition if the mouse was classified as 'moving' in over half of the video frames covering that repetition.

2.7 In vitro electrophysiological recordings

2.7.1 Protocol

Mice were deeply anesthetized via intraperitoneal (i.p.) injection of ketamine (95 mg kg-1) and xylazine (4.5 mg kg-1), followed by transcardial perfusion with ice-cold, oxygenated (95 % O2, 5 % CO2) artificial cerebrospinal fluid (ACSF) containing (in mM): 118 NaCl, 2.5 KCl, 1.25 NaH2PO4, 1.5 MgSO4, 1 CaCl2, 10 Glucose, 3 Myo-inositol, 30 Sucrose, 30 NaHCO3; pH = 7.4. The brain was rapidly excised and coronal sections of 300 µm thickness containing the SC and PAG were cut using a Linear-Pro7 vibratome (Dosaka, Japan). Slices were left to recover for 20 min at 35°C, followed by a slow cool down to room temperature (RT) over 40 – 60 min. After recovery, one slice was transferred to the recording chamber (RC-26GLP, Warner Instruments, Holliston, MA, USA) and superfused with ACSF containing 2 mM CaCl2 and 20 µM bicuculline methiodide (Tocris) at a rate of 3 – 4 ml/min at RT. In experiments using 100 nM α-dendrotoxin (Alomone Labs, Jerusalem, Israel), 0.1% bovine serum albumin (BSA) was added to the ACSF. Glass pipettes (B150-86-10, Sutter Instrument, Novato, CA, USA) with resistances of 3 – 4 MΩ were crafted using a P1000 horizontal pipette puller (Sutter Instrument) and filled with internal solution containing (in mM): 130 K-Gluconate, 10 KCl, 5 MgCl2, 5 MgATP, 0.2 NaGTP, 0.5 EGTA, 5 HEPES; pH 7.4 adjusted with KOH. Biocytin

(0.2 – 0.3 %) was added to the internal solution for post hoc morphological reconstruction. Neurons of the dPAG or the dmSC were visually identified using an infrared differential interference contrast video system in a BX51 microscope (Olympus, Tokyo, Japan). Electrical signals were acquired at 20 – 50 kHz and filtered at 4 kHz using a Multiclamp 700B amplifier (Molecular Devices, San Jose, CA, USA) connected to a Digidata 1440A digitizer (Molecular Devices) with pClamp10 software (Molecular Devices). Spontaneous excitatory postsynaptic currents (sEPSCs) were recorded at –60 mV for at least 1 min. Intrinsic membrane properties and neuronal excitability were measured in current clamp mode by applying current steps from –20 to 200 pA for 1 s in 10 pA increments. Access resistance was constantly monitored between protocols and recordings with access resistances exceeding 20 MΩ or with changes in access resistance or holding current by more than 20% were discarded. After recordings, the pipette was carefully withdrawn and the slice was transferred to 4% paraformaldehyde (PFA) in PBS solution.

2.7.2 Analysis

Whole-cell recordings were analysed in Clampfit (Molecular Devices) and MiniAnalysis Program (Synaptosoft). Resting membrane potential (RMP) was measured as the average membrane potential prior to current-injection. Input resistance (R_{in}) was calculated from the slope of the linear fit of the hyperpolarizing current/voltage relationship. Membrane time constant τ was measured from the exponential fit of the membrane potential change in response to a –10 or –20 pA current-injection. Membrane capacitance (C_m) was calculated from Cm = τ/Rin. Action potential firing was quantified in Clampfit using the event detection function. Phase-plane plots were performed to investigate the dynamic changes in the membrane potential over time (dV/dt) and were generated using the spikes from the first current step necessary to elicit action potentials (rheobase current). Soma size was calculated by fitting an oval to the projected image (63X) of the neurons and calculating the area of that oval.

2.8 Histology

For fluorescent immunostainings and histological confirmation of fibre and probe locations, adult *Setd5*$^{+/+}$ and *Setd5*$^{+/-}$ mice were transcardially perfused with 4 % paraformaldehyde (PFA) and their brains were dissected, post-fixed overnight in 4 % PFA, washed with 1X PBS, dehydrated in a 30 % sucrose solution and sectioned with a freezing microtome (SM2010R, Leica) to 100 µm (for probe/fibre confirmation) and 40 µm (for immunostainings) thick slices. For histological confirmation of probe and fibre locations, the sections were rinsed in PBS, stained with 4',6-diamidino-2-phenylindole (DAPI; 2uM in PBS) and mounted on Superfrost glass slides in a mounting medium containing 1,4,-diazabicyclooctane (DABCO; Sigma, D27802) and Mowiol 4-88 (Sigma, 81381). For Kv1.1 immunostainings, tissue was rinsed and then blocked for 1 hour at room temperature in a buffer solution containing 10% normal donkey serum (Abcam, ab7475), 0.1 % Triton X-100 in PBS. Primary antibodies (Kv1.1, Rabbit, 1:200; Rb-Af400, Frontier Institute) were diluted in a blocking buffer and incubated for 48 hours at 4 °C. The tissue was then rinsed 3 times in PBS and left overnight to wash at 4 °C. Secondary antibodies (Alexa-594 Donkey anti-rabbit, 1:1000; R37119, Thermo Fisher) were diluted in 1X PBS and incubated for 2 hours at room temperature in the dark, before being

washed three more times in 1X PBS before being counter-stained with DAPI and mounted as for histological sections described above. Sections were imaged with either a confocal microscope (LSM800, Zeiss), at 63X or 20X magnification, or a wide-field microscope (VS120, Olympus), at 10X magnification. For comparison between the Kv1.1 expression in *Setd5*$^{+/+}$ and *Setd5*$^{+/-}$ tissue 30 µm stacks were imaged with 1 µm sections at 63X magnification, or 55µm stacks were imaged with 2µm sections at 20X magnification, and the same laser power settings were used for all images at a given magnification. For visualisation of the dPAG/dmSC cells recorded *in vitro* tissue sections were washed in 1X PBS for 10 minutes then a solution of Streptavidin (1:100, 1 mg/ml, Thermo Fisher Scientific, S11227) in PBS with 0.3% Triton-X was added and the samples were left at 4 ºC overnight. The tissue was then washed three times with PBS, mounted into a custom designed chamber for thick slices and imaged with a confocal microscope (LSM800, Zeiss) at 20X (90 µm projection, 2 µm sections) and 40X (50 µm projection, 1 µm sections).

2.9 Western blot

Tissue samples from the superior colliculus, periaqueductal grey (PAG) and cortex were dissected from *Setd5*$^{+/+}$ (n = 3) and *Setd5*$^{+/-}$ (n = 3) adult (6-7 weeks) mice. PAG tissue was dissected using a 2 mm diameter biopsy punch (ID: 2 mm, OD: 3 mm, Fine Science Tools, 18035-02). Each purification was performed independently three times and samples were stored at -80ºC until further processing. Samples were Dounce homogenised 15 times with 300 µL RIPA buffer (50 mM Tris-HCl, 150 mM NaCl, 0.5 % sodium deoxycholate, 1 % Triton-X, 0.2 % SDS, completeTM protease inhibitor cocktail (Roche) and and 1 mM phenylmethylsulfonyl fluoride (PMSF, Sigma)) using the loose pestle and sonicated for 10 seconds. The lysed samples were centrifuged for 20 min at 16000 g and the supernatant was stored at -80oC. Total protein concentration was determined using the BCA protein assay (Pierce). Proteins were boiled for 5 min in Laemmli sample buffer before being separated at 200V for 40 min using TGX stain-free precast gels (Bio-Rad). Stain-free protein gels were activated with UV light for 5 min and then transferred to PVDF membranes (Bio-Rad) using a turbo transfer system (Bio-Rad). Membranes were blocked for 1 hour in TBST (Tris-buffered saline with 0.1 % Tween 20) supplemented with 5 % bovine serum albumin (Sigma) and then incubated overnight at 4ºC with anti-Kv1.1 primary antibody (Rb-Af400, Frontier Institute, 1:100). After primary antibody incubation, membranes were washed four times with TBST for 5 min and then incubated with anti-rabbit IRDye 800CW (LI-COR Biosciences, dilution 1:4000) for 1 hour at room temperature. Bio-Rad ChemiDoc MP system was used for imaging and acquisition.

2.10 Statistics

Analyses were performed in custom-written MATLAB (2019a) scripts (MathWorks, Inc.). Shapiro-Wilk and Levene's tests were used to test the normality and the equal variances of the datasets, respectively and parametric or non-parametric tests were used accordingly. All statistical tests are reported in the text and appropriate figure legends ($* \ p < 0.05$, $* * \ p < 0.01$, $* * * \ p < 0.001$). In bar plots the mean ± s.e.m. are shown, unless otherwise stated. Boxplots display the median and IQR.

Preface to chapters 3 & 4

The classification of autism as a syndrome highlights the key role of identifying common behavioural phenotypes in defining and diagnosing the condition. Despite the integral role of behavioural phenotypes in the diagnosis of autism and our understanding of the implications of the disorder, detailed behavioural analyses often take a secondary role in studies focussed on understanding the molecular aetiology of the condition. In this thesis, we aim to put behaviour at the forefront of the investigation by taking a top-down neuroethological approach to the study of neuropsychiatric disorders.

The following chapters contain the results from experiments that aim to identify if behavioural differences are present in diverse genetic mouse models of autism to an innate, visually-driven PDM task. **Chapter 3** sets out to determine if a behavioural difference can be observed in any of the models and will aim to comprehensively analyse the responses performed. While, **Chapter 4** will look in detail at the evolution of these perceptually-driven behaviours in wild-type and mutant animals over time. By comparing a single behaviour across multiple genetic models, we hope to explore how diverse mutations linked to autism that affect diverse cellular and molecular functions can ultimately give rise to qualitatively similar changes in behaviour.

3 The looming avoidance response (LAR) paradigm reveals delayed perceptual decision-making in mouse models of autism.

We sought to investigate if the LAR paradigm be used to assess functional differences in perceptual decision-making (PDM) within mouse models of autism and the potential contribution of subcortical sensorimotor circuits, through the SC and PAG, to the pathophysiology of the PDM differences observed in humans. Previous work revealed that mice displayed innate defensive behaviours in response to rapidly expanding overhead dots in laboratory settings (Yilmaz and Meister 2013). The simplicity, specificity and experimental tractability of this experimental paradigm enabled further investigation to isolate the specific neural circuits underlying the generation of this behaviour (Evans et al. 2018). This work identified the SC and PAG as the key circuit loci required for the sensorimotor transformation underlying this response. Well-described differences in multiple aspects of PDM have been identified in autistic individuals and related animal models, which led us to hypothesise that genetic mouse models of autism might present with different behavioural responses to the LAR paradigm than their wild-type siblings, and that the specific differences in the expression of these behaviours could be used to investigate what role these subcortical circuits play in some of the maladaptive behaviours observed in autism.

3.1 Defensive responses to the looming stimulus are slower and less vigorous in *Setd5*$^{+/-}$, *Cul3*$^{+/-}$ and *Ptchd1*$^{Y/-}$ mice.

To investigate perceptual decision-making in mouse models of autism we utilised the looming avoidance response (LAR) paradigm which involves the presentation of an overhead, expanding dark disc. This visual stimulus is innately aversive to many organisms as it mimics a rapidly approaching object or an impending aerial predator. This paradigm presents many advantages as a tool to investigate perceptual decision-making since it is developmentally-hardwired, making it robust and importantly does not depend on the ability of the animals to learn the correct response. Its sole reliance on the visual modality allows for an in depth dissection of how visual information is used by the brain to drive behaviour, and the stimulus itself is easily manipulated experimentally which enables the contribution of specific stimulus features to the response to be investigated in detail.

In our assay, mice were placed in a square arena with a shelter in one corner. A grey, back projected screen formed a lid with three of the four walls of the arena, 32cm above the arena floor and provided a low-level of illumination, similar to mesopic light levels (Fig. 2.1). Animals were given at least 10 minutes to acclimatise to the arena in which they were able to spontaneously explore. The animal's movements were tracked online from below through the IR-transparent floor, and the entire behavioural chamber was illuminated by IR light. After the acclimatisation period, each mouse then underwent three LAR trials, during which time if the centre of the mouse crossed the threshold distance (10cm) from the edge of the shelter, a

looming stimulus would be presented in the centre of the arena lid above. Frame-by-frame analysis of the behavioural videos revealed a sequence of behavioural actions that reflected a successful escape to the overhead threat (Fig. 3.1).

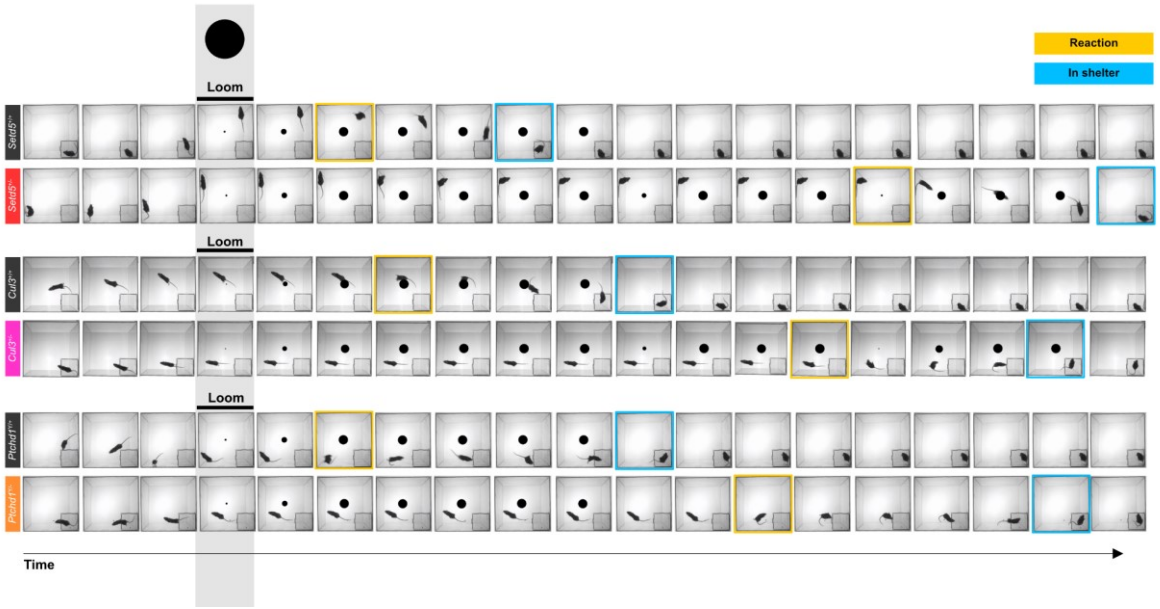

Figure 3.1 Behavioural video frames of example wild-type and heterozygous animals from each model during a LAR trial.

All animals showed an initial arrest response, which could range in duration from milliseconds to seconds, upon detection of the looming stimulus. This response involved an interruption of ongoing movement and some animals showed signs of small head or upper body movements, potentially indicating the need for further risk assessment. Typical wild-type escape responses were rapidly followed by the orienting of the mouse towards the shelter, a full-body turn and the uninterrupted movement of the animal in a straight line towards the shelter (yellow reaction frames highlighted in Fig. 3.1). Despite previous reports (de Franceschi et al. 2016, Salay et al. 2018, Shang et al. 2018) studying the different defensive strategies used by mice, we never observed any jumping, sustained freezing or tail-rattling in our standard LAR trials. Reaction times were calculated as the time from the initiation of the looming stimulus and the time of the maximum speed during the escape response, and the frame where the centre of mass of the animal was fully inside the shelter was used to determine the termination of the escape response. Upon reaching the shelter, animals usually remained immobile with a curled posture for a variable period of time before resuming movement, first within the shelter and later during exploration bouts outside of the shelter. Many animals displayed a significant increase in head-poke and risk assessment behaviours (data not shown), whilst remaining predominantly inside the shelter, after initial exposure to the looming stimulus.

In order to reliably compare the behavioural responses of animals, we presented wild-type and haploinsufficient sibling pairs of the *Setd5*, *Ptchd1* and *Cul3* genetic mouse models of autism with the same sequence of high contrast looming stimuli. As expected from numerous previous studies, the wild-type mice displayed robust responses with the stereotypical sequence of behaviours mentioned above. All animals tested initiated a rapid escape response upon detection of the looming stimulus (P_{wt} escape = 100%, n = 14, 61 trials) and the initiation of the escape occurred almost exclusively during the expansion of the first disc in the sequence of five (P_{wt} escape within 1st loom = 93%, n = 14, 55 trials, Fig. 3.2).

Remarkably, although the mutant siblings reliably generated a robust escape response (P_{het} escape = 92%, n = 14, 224 trials) with the same stereotyped behavioural sequence, the latency to initiate the escape was considerably more variable and there was a much lower probability of them initiating their escape during the first disc expansion (P_{het} escape within 1st loom = 38%, n= 14, 38 trials, Fig. 3.2).

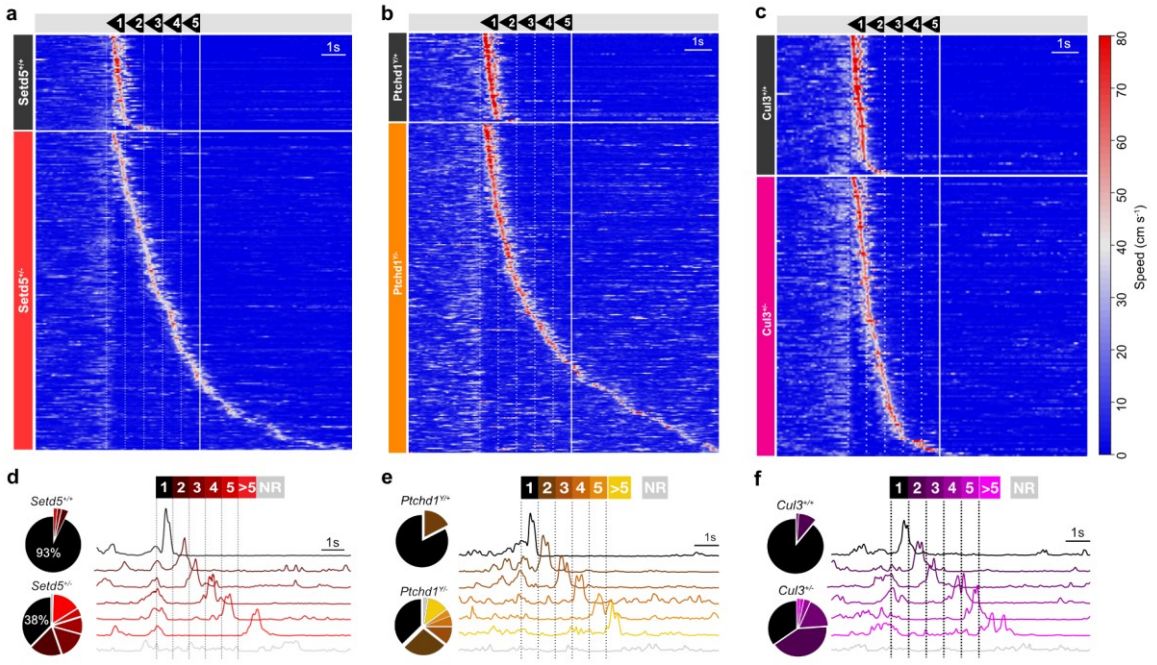

Figure. 3.2 Mice haploinsufficient in *Setd5*, *Cul3* or *Ptchd1* have wider variability in their time to react to the looming stimulus.

a, Raster plot of mouse speed in response to the looming stimuli (white, dotted vertical lines denote the start of each loom; solid white line denotes the end of the stimulus) for *Setd5*$^{+/+}$ (top, n = 14, 60 trials) and *Setd5*$^{+/-}$ (bottom, n = 14,198 trials), sorted by reaction time. **b**, Raster plot of mouse speed in response to looming stimuli (white, dotted vertical lines denote the start of each loom; white solid line denotes the end of the stimulus) for *Ptchd1*$^{Y/+}$ (top, n = 9, 49 trials) and *Ptchd1*$^{Y/-}$ (bottom, n = 9, 259 trials), sorted by reaction time. **c**, Raster plot of mouse speed in response to the looming stimuli (white, dotted vertical lines denote the start of each loom; white solid line denotes the end of the stimulus) for *Cul3*$^{+/+}$ (top, n = 10, 61 trials) and *Cul3*$^{+/-}$ (bottom, n = 10, 112 trials), sorted by reaction time. **d**, Trials sorted by whether the mice responded within 1 of the 5-loom stimuli, after the 5th, or not at all. Left, distribution of trials into these categories (*Setd5*$^{+/+}$, top and *Setd5*$^{+/-}$, bottom). Proportion of trials where mice escaped within the first loom: *Setd5*$^{+/+}$, 0.93, 56 of 61 trials; *Setd5*$^{+/-}$, 0.374, 84 of 224 trials, $P < 0.001$, two-sample paired Wilcoxon signed rank tests. Distribution of trials into the different categories: *Setd5*$^{+/+}$ versus

Setd5$^{+/-}$, P < 0.001, two-sample Kolmogorov-smirnov test. Right, example speed traces from *Setd5*$^{+/-}$ trials within each loom category. The colour of the trace indicates the category the trial belongs to. **e**, Trials sorted by whether the mice responded within 1 of the 5-loom stimuli, after the 5th, or not at all. Left, distribution of trials into these categories (*Ptchd1*$^{Y/+}$, top and *Ptchd1*$^{Y/-}$, bottom). Proportion of trials where mice escaped within the first loom: *Ptchd1*$^{Y/+}$, 0.826, 40 of 49 trials; *Ptchd1*$^{Y/-}$, 0.374, 97 of 259 trials, P = 0.004, two-sample paired Wilcoxon signed rank tests. Distribution of trials into the different categories: P < 0.001, *Ptchd1*$^{Y/+}$ versus *Ptchd1*$^{Y/-}$, two-sample Kolmogorov-smirnov test. Right, example speed traces from *Ptchd1*$^{Y/-}$ trials within each loom category. The colour of the trace indicates the category the trial belongs to. **f**, Trials sorted by whether the mice responded within 1 of the 5-loom stimuli, after the 5th, or not at all. Left, distribution of trials into these categories (*Cul3*$^{+/+}$, top and *Cul3*$^{+/-}$, bottom). Proportion of trials where mice escaped within the first loom: *Cul3*$^{+/+}$, 0.892, 56 of 63 trials; *Cul3*$^{+/-}$, 0.347, 42 of 121 trials, P < 0.001, two-sample paired Wilcoxon signed rank tests. Distribution of trials into the different categories: *Cul3*$^{+/+}$ versus *Cul3*$^{+/-}$, P < 0.001, two-sample Kolmogorov-smirnov test. Right, example speed traces from *Cul3*$^{+/-}$ trials within each loom category. The colour of the trace indicates the category the trial belongs to.

When looking at the response variables of the escape trials, per animal, the mutant animals had on average markedly slower reaction times than their wild-type siblings (Fig. 3.3a-c, left panels), but also reached significantly slower maximum speeds during their escape (Fig. 3.3a-c, right panels). Previous work has proposed that the maximum escape speed can be used as a proxy for the vigour of the response to the stimulus, since lower contrast stimuli, or repeated exposure to the stimuli lead to slower reaction times and decreased maximal speeds (Evans et al. 2018; Lenzi et al. 2022).

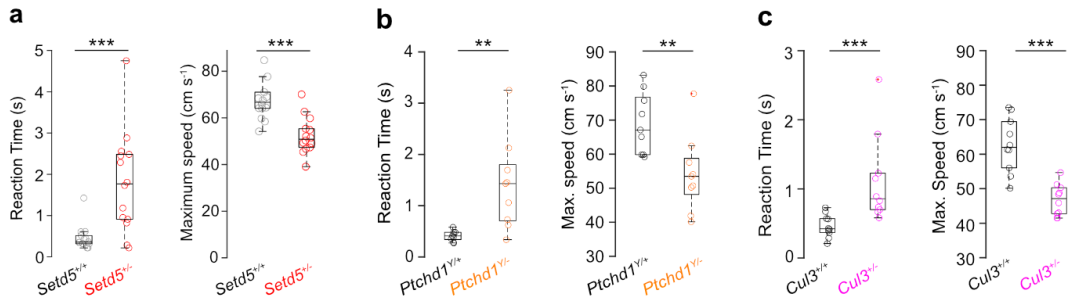

Figure 3.3 Reaction time and the maximum speed reached during escape are slower in heterozygous mice.

a, Mean reaction time (left) and maximum escape speed (right) per animal, for all trials where the mouse performed an escape to the shelter (Reaction time: *Setd5*$^{+/+}$, n = 14, 0.458 s; *Setd5*$^{+/-}$, n = 14, 1.88 s, P = 0.001. Maximum escape speed: *Setd5*$^{+/+}$, n = 14, 68.4 cms^{-1}; *Setd5*$^{+/-}$, n = 14, 51.6cms^{-1}, P < 0.001). **b**, Mean reaction time (left) and maximum escape speed (right) per animal, for all trials where the mouse performed an escape to the shelter (Reaction time: *Ptchd1*$^{Y/+}$, n = 9, 0.411s; *Ptchd1*$^{Y/-}$, n = 9, 1.41 s, P = 0.002. Maximum escape speed: *Ptchd1*$^{Y/+}$, n = 9, 69.1 cm s^{-1}; *Ptchd1*$^{Y/-}$, n = 9, 54.2 cms^{-1}, P = 0.005). **c**, Mean reaction time (left) and maximum escape speed (right) per animal, for all trials where the mice performed an escape to the shelter. (Reaction time: *Cul3*$^{+/+}$, n=10, 0.464 s; *Cul3*$^{+/-}$, n=10, 1.11 s, P < 0.001. Maximum escape speed: *Cul3*$^{+/+}$, n = 10, 62.7 cms^{-1}; *Cul3*$^{+/-}$, n = 10, 46.8 cm s^{-1}, P < 0.001). P-values are two-sample paired Wilcoxon signed rank tests. Box-and-whisker plots show median, IQR and range. Plotted points represent average values, across all trials where the mice perform an escape to the shelter, for individual animals.

It could be that slower overall reaction time observed in the mutant animals could be due to the animals choosing to elicit an alternative escape mode that might confer a survival advantage despite being slower overall, such as the use of a zig-zag escape trajectory. By aligning the peri-stimulus velocity traces of the animals to the point of their maximum speed we could qualitatively assess that animals from both genotypes were performing escapes with similar

overall response kinetics (Fig. 3.4). The immediate acceleration was similar for both genotypes, suggesting that it is not an implicit motor deficit in initiating an escape that is leading to the delay in overall reaction time. Analysing the latency between stimulus onset and the point of maximum speed, for all trials pooled by genotype, highlighted the larger distribution in the time to initiate a response in mutant animals.

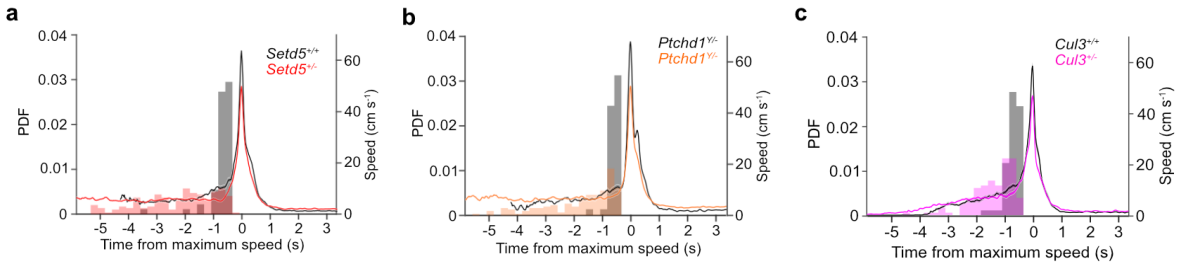

Figure 3.4 All genotypes show similar escape kinetics when aligned to the point of maximum speed.

Average speed response profiles aligned to the time of maximum speed, across all wild-type and mutant trials where mice escape to the shelter with probability density function histograms of the time when the looming stimulus started with respect to the time of maximum speed. **a**, *Setd5*$^{+/+}$, n = 14, 61 trials; *Setd5*$^{+/-}$, n = 14, 198 trials, $p < 0.001$. **b**, *Ptchd1*$^{Y/+}$, n = 9, 49 trials, black; *Ptchd1*$^{Y/-}$, n = 9, 212 trials, orange, $p < 0.001$. **c**, *Cul3*$^{+/+}$, n = 10, 61 trials, black; *Cul3*$^{+/-}$, n = 10, 112 trials, magenta, $p < 0.001$. *p*-values are two-sample kolmogorov-smirnov tests.

Given these results, we hypothesised that for all animals, once the decision to escape had been made, there would be no difference in the dynamics of the escape response. To test this, we selected only the trials from both wild-type and mutant animals where the animals initiated their response within the first disc expansion (Fig. 3.5). When comparing the average response profiles of these trials for both genotypes, several differences between the genetic models became apparent. Firstly, the mean response of the aligned trials resulted in very similar kinetic response profiles between the wild-type and mutant animals in the *Setd5* and *Ptchd1* models (Fig. 3.5a,c), whilst the average response profile for the *Cul3*$^{+/-}$ animals was still delayed with respect to their wild-type siblings (Fig. 3.5e). This suggests that, at least for *Cul3*$^{+/-}$ animals, they may possess underlying motor difficulties that impair their ability to generate a comparable escape response to their wild-type siblings.

Previous work has linked increasing uncertainty about the stimulus (i.e. by varying stimulus contrast) with both slower reaction times and slower maximal escape speeds. By looking at the maximum speed reached during only the trials where the animals responded within the first disc expansion, we were able to disentangle the effect of the slower reaction time and the slower escape vigour. We noticed that all models retained slower escape vigours, even when isolating these 'early responding' trials (Fig. 3.5b,d,f). Indicating that even when the decision to escape was made with a similar latency, the mutant animals did not escape with a comparable vigour when averaging across all trials.

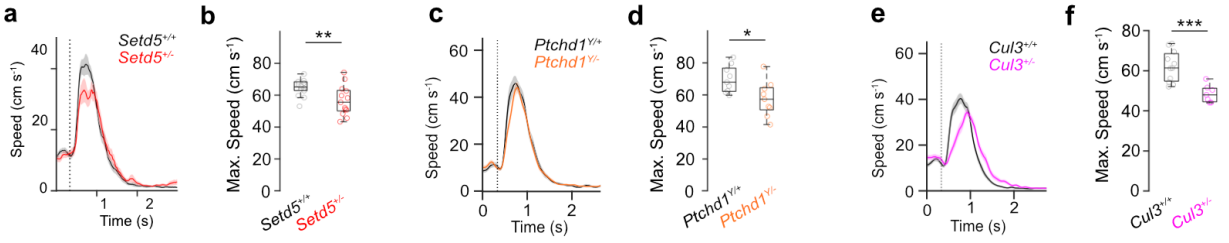

Figure 3.5 *Setd5*$^{+/-}$, *Cul3*$^{+/-}$ and *Ptchd1*$^{Y/-}$ do not reach the same maximum escape speed, even if they react within the first loom presentation.

a, Mean speed response profile of all trials from *Setd5*$^{+/+}$ (n = 14, 55 trials) and *Setd5*$^{+/-}$ (n = 14, 38 trials) animals where the animals responded within the presentation of the first loom stimulus aligned to the onset of the first loom presentation (vertical dotted line). Shaded areas represent the standard error of the mean. **b**, Maximum escape speed during trials where the animals responded within the first loom presentation of *Setd5*$^{+/+}$ (n = 14, 55 trials, 67.6 cms^{-1}) and *Setd5*$^{+/-}$ (n = 14, 38 trials, 56.6 cms^{-1}) for trials where the mice respond within the first loom presentation (P = 0.009, two-sample paired Wilcoxon signed rank test). **c**-**d**, as for **a**-**b** for *Ptchd1* (*Ptchd1*$^{Y/+}$, n = 9, 69.8cms^{-1}; *Ptchd1*$^{Y/-}$, n = 9, 57.6 cms^{-1}; P = 0.024, two-sample paired Wilcoxon signed rank test) and **e**-**f**, *Cul3* (*Cul3*$^{+/+}$, n = 10, 55 trials, 59.6 cms-1; *Cul3*$^{+/-}$, n = 10, 41 trials, 45.8 cms-1; P < 0.001, two-sample paired Wilcoxon signed rank test), respectively. Box-and-whisker plots show median, IQR and range. Plotted points represent average values, across trials, for individual animals.

However, since the previous analyses have used values generated by pooling the animal averages of the response variables across all trials, they are confounded by any effects of adaptation that might be occurring due to repeated exposures to the stimulus, an effect that has been observed before in previous studies (Lenzi et al. 2022). To separate these effects and to determine if the mutant animals were slower even to the very first exposure to the stimulus, we compared the response kinetics of the wild-type and mutant animals to their very first stimulus presentations (Fig. 3.6). Here, we observed that in both the *Setd5* and *Ptchd1* models, the heterozygous animals did not display slower maximum escape speeds to the first presentation, indicating that the differences in response vigour observed when examining trials across all days of testing likely arise from adaptation to the stimulus over time. Mutant animals did however, still exhibit slower reaction times even at the first presentation of the stimulus. This implies that the overall differences in reaction time are mediated by intrinsic factors, which could be further influenced by, but are independent of, adaptation to the stimulus. *Cul3*$^{+/-}$ animals, by comparison, showed a non-significant difference in their reaction times during the first loom presentation but retained the slower maximal escape speeds. These results could be the result of previously described stride and gait defects in these animals (Morandell et al. 2021), and indicate that intrinsic locomotor impairments limit the ability of the mice to generate appropriately vigorous escapes.

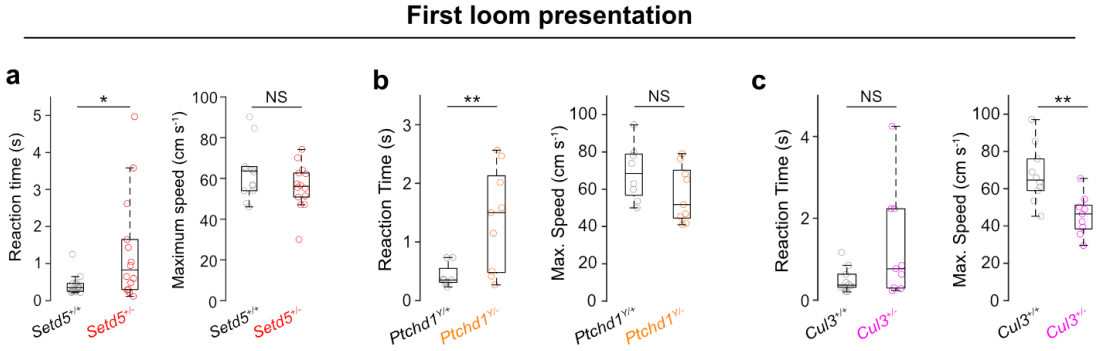

Figure 3.6 Reaction time and escape vigour to the very first loom presentation.

a, Median reaction time (left) and maximum escape speed (right) per animal, for the responses to the first ever loom presentation (Reaction time: *Setd5*$^{+/+}$, n = 14, 0.49s; *Setd5*$^{+/-}$, n = 14, 1.41s, p = 0.046. Maximum escape speed: *Setd5*$^{+/+}$, n = 14, 67.2 cms^{-1}; *Setd5*$^{+/-}$, n = 14, 56.1 cms^{-1}, p = 0.167). **b**, as for **a** but for *Ptchd1* animals (Reaction time: *Ptchd1*$^{Y/+}$, n = 9, 0.42s; *Ptchd1*$^{Y/-}$, n = 9, 1.39s, p = 0.014. Maximum escape speed: *Ptchd1*$^{Y/+}$, n = 9, 69.1 cms^{-1}; *Ptchd1*$^{Y/-}$, n = 9, 57.6 cms^{-1}, p = 0.139). **c**, as for **a** but for *Cul3* animals (Reaction time: *Cul3*$^{+/+}$, n = 10, 0.45s; *Cul3*$^{+/-}$, n = 10, 1.26s, p = 0.117. Maximum escape speed: *Cul3*$^{+/+}$, n =10, 67.5 cms^{-1}; *Cul3*$^{+/-}$, n = 10, 45.8 cms^{-1}, p = 0.003). All p-values are two-sample paired Wilcoxon signed rank tests. Box-and-whisker plots show median, IQR and range. Plotted points represent the values from the single trials for individual animals.

In order to test whether the delay in generating an escape response was due to the mutant animals simply detecting the stimulus later than their wild-type siblings, we examined the immediate responses of the animals following stimulus onset (Fig. 3.7). To quantify this specific behaviour we generated a variable '$\text{Log}_{10}(\Delta$ speed)' that was calculated as the logarithmic of the ratio between the animal's speed immediately after stimulus onset versus its baseline speed at stimulus onset. The speed after was calculated as the average speed in the 300-800 ms following the stimulus onset, and the baseline speed was the average speed of the animal in the peristimulus period ∓50ms around the start of the stimulus. Positive values of this variable would indicate an increase in speed in the time immediately following the stimulus onset, zero would indicate there was no change in the kinetics of the animal and negative values imply a reduction in the speed of the animal in this time. As expected, the wild-type animals showed largely positive values of this variable, indicating a rapid increase in their speed immediately following the onset of the stimulus. The heterozygous animals, however, showed largely negative values of this variable showing that they frequently present a rapid reduction in their speed following the appearance of the looming stimulus. These trends were clearly noticeable in all three mouse models.

By plotting the value of the $\text{Log}_{10}(\Delta$ speed) variable versus the maximum speed reached during each trial, we were able to observe that even though the mutant animals showed an initial

reduction in their speed, they later reached maximum speeds similar to those reached by the wild-type animals. This fact indicates that the mutant animals are not performing the well-described defensive freezing behaviour (Yilmaz et al. 2013, De Franceschi et al. 2016, Shang et al. 2018), but are instead exhibiting a response characterised by two parts: an initial rapid reduction in speed upon stimulus detection, an 'arrest', followed by a subsequent high speed, directed escape response back to the shelter. We are confident of this classification, since the described freezing response is defined as a prolonged period of immobility across tens of seconds, with the complete cessation of all movement. The arrest behaviour we observed in the mutant animals occurred on the timescale of 1-10 seconds and in many cases, small movements of the head or front paws were observed. These small movements also led us to think of this arrest behaviour as indicative of a period of ongoing threat evaluation as previously described in wild-type animals to more ambiguous stimuli (Evans et al. 2018). Altogether, this suggests that the delay in generating a LAR arises from difficulties in the evaluation or action selection components of the perceptual decision, and not the initial detection of the stimulus.

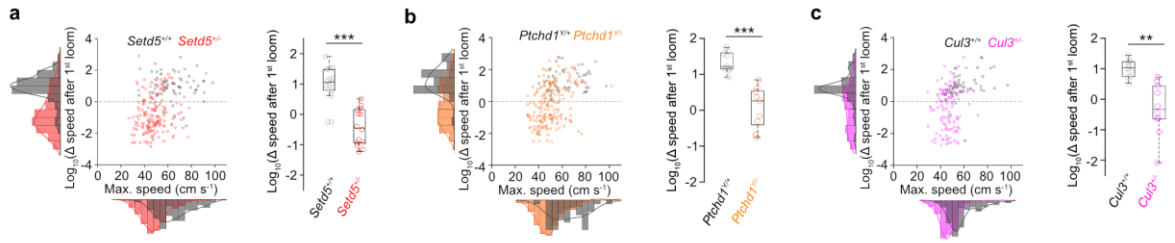

Figure 3.7 Mutant animals exhibit an arrest immediately after loom presentation but before initiating their escape response.

a, left, scatter-hist plot of the log_{10}(change in speed upon the 1st loom presentation) (*x*-axis, see methods) and the maximum speed reached during the escape (*y*-axis). Trials from all animals of the same genotype are pooled together and each point represents a single trial (*Setd5*$^{+/+}$, n = 14, 61 trials; *Setd5*$^{+/-}$, n = 14, 198 trials. Log_{10}(ΔSpeed), $p < 0.001$, two-sample kolmogorov-smirnov test; maximum escape speed, $p < 0.001$, two-sample kolmogorov-smirnov test). Right, summary of the average log_{10}(ΔSpeed) per animal (*Setd5*$^{+/+}$, n = 14, log_{10}(ΔSpeed) = 0.979; *Setd5*$^{+/-}$, n = 14, log_{10}(ΔSpeed) = -0.423, $p < 0.001$, two-sample paired Wilcoxon signed rank tests). Plotted points represent the average value across all trials where the mice performed an escape behaviour for individual animals. **b**, as for **a** but for *Ptchd1* animals. (*Ptchd1*$^{Y/+}$, n = 9, 49 trials; *Ptchd1*$^{Y/-}$, n = 9, 212 trials. Log_{10}(ΔSpeed), $p < 0.001$, two-sample kolmogorov-smirnov test; maximum escape speed, $p < 0.001$, two-sample kolmogorov-smirnov test). Right, summary of the average log_{10}(ΔSpeed) per animal (*Ptchd1*$^{Y/+}$, n = 9, log_{10}(ΔSpeed) = 1.37; *Ptchd1*$^{Y/-}$, n = 9, log_{10}(ΔSpeed) = -0.131, $p < 0.001$, two-sample paired Wilcoxon signed rank tests). **c**, as for **a** but for *Cul3*. (*Cul3*$^{+/+}$, n = 10, 63 trials; *Cul3*$^{+/-}$, n = 10, 121 trials. Log_{10}(ΔSpeed), $p < 0.001$, two-sample kolmogorov-smirnov test; maximum escape speed, $p < 0.001$, two-sample kolmogorov-smirnov test). Right, summary of the average log_{10}(ΔSpeed) per animal (*Cul3*$^{+/+}$, n = 10, log_{10}(ΔSpeed) = 0.910; *Cul3*$^{+/-}$, n = 10, log_{10}(ΔSpeed) = -0.353, $p < 0.001$, two-sample paired Wilcoxon signed rank tests). Box-and-whisker plots show median, IQR and range.

3.2 Conditional ablation of *Setd5* in the cortex and hippocampus does not recapitulate full knockout delay.

Delayed cognition in autistic individuals is predominantly believed to derive from differences in cortical processing. For this reason, a large percentage of the animal research has focused

on investigating the role of cortical structures in the generation of abnormal behaviours. Even though escape responses to looming stimuli are predominantly mediated via subcortical circuits, efferent projections from cortical regions could be affecting the evoked behavioural response through modulatory influences. Cortical projections from V1 to the sSC neurons were able to modulate the magnitude of visual responses of these cells (Zhao et al. 2014) and can directly promote the generation of arrest behaviours in mice (Liang et al. 2015). For this reason we decided to investigate whether selective haploinsufficiency of the *Setd5* and *Cul3* genes in only cortical and hippocampal brain structures would recapitulate the phenotypic delay observed in the full knockout. To do this we used the conditional transgenic mice: *Setd5*$^{+/fl}$; *Emx1*-Cre and *Cul3*$^{+/fl}$;*Emx1*-Cre. Unfortunately, a conditional *Ptchd1* mouse line is currently unavailable.

The selective reduction in *Setd5* in the cortex and hippocampus did not recapitulate the behavioural effects observed in the full knockout (Fig. 3.8). In contrast, the mutant siblings were indistinguishable from their wild-type siblings in any of the assessed variables. They generated escape responses within the first loom at levels almost identical to their wild-type siblings (Fig. 3.8b. *Setd5*$^{+/+}$;*Emx1*-Cre, 87%, *Setd5*$^{+/fl}$;*Emx1*-Cre, 88%), had comparable maximal speeds (Fig. 3.8d, middle. *Setd5*$^{+/+}$;*Emx1*-Cre, 61.1 cm s^{-1}, *Setd5*$^{+/fl}$;*Emx1*-Cre, 66.4 cm s^{-1}, $p = 0.295$) and reaction times (Fig. 3.8d, left. *Setd5*$^{+/+}$;*Emx1*-Cre, 0.591 s, *Setd5*$^{+/fl}$;*Emx1*-Cre, 0.506 s, $p = 0.469$) and didn't preferentially perform the arrest behaviour frequently observed in the full knockouts (Fig. 3.8d, right. *Setd5*$^{+/+}$;*Emx1*-Cre, 0.930, *Setd5*$^{+/fl}$;*Emx1*-Cre, 0.991, $p > 0.995$).

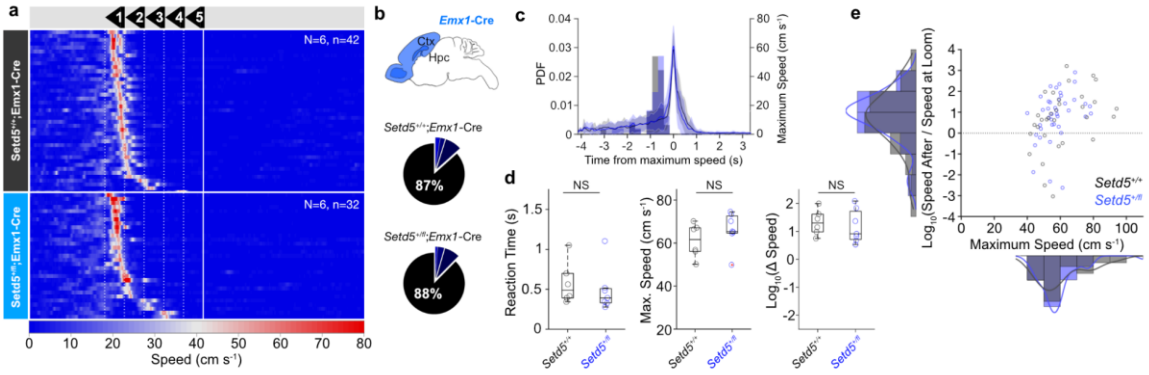

Figure 3.8 Escape response properties in *Setd5*$^{+/fl}$::*Emx1*-Cre mice.

a, Raster plot of mouse speed in response to the looming stimuli (white, dotted vertical lines denote the start of each loom; white solid line denotes the end of the stimulus) for *Setd5*$^{+/+}$; *Emx1*-Cre (top, n = 6, 42 trials) and *Setd5*$^{+/fl}$; *Emx1*-Cre (bottom, n = 6, 32 trials), sorted by reaction time. **b**, Pictorial representation of the expression of *Emx1* in a sagittal section of a mouse brain, showing the localisation of the expression to the cortex and hippocampus (blue, top). Proportion of trials in which the mice respond within each loom for *Setd5*$^{+/+}$; *Emx1*-Cre (middle) and *Setd5*$^{+/fl}$; *Emx1*-Cre mice (bottom). There is no significant difference in the proportion of trials in which the mice respond within the 1st loom (*Setd5*$^{+/+}$;*Emx1*-Cre, n = 6, 0.866. *Setd5*$^{+/fl}$;*Emx1*-Cre, n = 6, 0.8764, $p = 0.760$, two-sample Wilcoxon's ranked sum (RS) test. Distribution of number of looms to escape across all trials, *Setd5*$^{+/+}$;*Emx1*-Cre, 32 trials, *Setd5*$^{+/fl}$;*Emx1*-Cre, 42 trials, $p = 0.960$, two-sample Kolmogorov-Smirnov (KS) test). **c**, Mean speed response profile of all trials where mice escape to the shelter for *Setd5*$^{+/+}$;*Emx1*-Cre (black) and *Setd5*$^{+/fl}$;*Emx1*-Cre (blue) showing similar escape kinetics, with a histogram of the distribution of the start of the loom stimulus aligned to the peak of the escape response (*Setd5*$^{+/+}$;*Emx1*-Cre, 32 trials, -0.633 s; *Setd5*$^{+/fl}$;*Emx1*-Cre, 42 trials, -0.700 s, $p = 0.773$, two-sample KS test). **d**, No significant difference in reaction time (*Setd5*$^{+/+}$;*Emx1*-

Cre, n = 6, 0.591 s; *Setd5*$^{+/fl}$;*Emx1*-Cre, n = 6, 0.506 s, $p = 0.468$, Wilcoxon's RS test), escape vigour (*Setd5*$^{+/+}$;*Emx1*-Cre, n = 6, 61.1 cms^{-1}; *Setd5*$^{+/fl}$;*Emx1*-Cre, n = 6, 66.4 cms^{-1}, $p = 0.295$, Wilcoxon's RS test) or $\log_{10}$(ΔSpeed) (*Setd5*$^{+/+}$;*Emx1*-Cre, n = 6, $\log_{10}$(ΔSpeed) = 0.929; Setd5$^{+/fl}$;Emx1-Cre, n = 6, $\log_{10}$(ΔSpeed) = 0.990, $p > 0.995$, Wilcoxon's RS test). Plotted points represent the average value across all trials where the mice performed an escape behaviour for individual animals. Box-and-whisker plots show median, IQR and range. **e**, Relationship between $\log_{10}$(ΔSpeed) and the maximum speed reached during the escape. $\log_{10}$(ΔSpeed): *Setd5*$^{+/+}$;*Emx1*-Cre, 42 trials, 0.829; *Setd5*$^{+/fl}$;*Emx1*-Cre, 32 trials, 0.677, $p = 0.598$, two-sample KS test. Maximum escape speed: *Setd5*$^{+/+}$;*Emx1*-Cre, 42 trials, 58.8 cm s^{-1}, *Setd5*$^{+/fl}$; *Emx1*-Cre, 32 trials, 61.0 cm s^{1}, $p = 0.675$, two-sample KS test). Trials from animals of the same genotype are pooled together and each point represents a single trial.

The conditional *Cul3* model however, retained some of the behavioural differences observed in the full knockout. The conditional animals still presented with slower maximal escape speeds, similar to that of the full knockout (*Cul3*$^{+/-}$, 46.8 cm s^{-1}), that were significantly different to their wild-type siblings (Fig. 3.9d, middle, *Cul3*$^{+/+}$;*Emx1*-Cre, 56.9 cm s^{-1}, *Cul3*$^{+/fl}$;*Emx1*-Cre, 47.6 cm s^{-1}, p = 0.030, Wilcoxon's rank sum test). On average, haploinsufficient conditional animals reacted within the first loom presentation at a level midway between those observed for the wild-type and full knockout animals (Fig. 3.2f, Fig. 3.9b, *Cul3*$^{+/+}$, 89%; *Cul3*$^{+/-}$, 35%; *Cul3*$^{+/fl}$;*Emx1*-Cre, 65%). Similarly, the conditional knockouts showed a slower, but not significant, reaction time on average than their wild-type siblings (Fig. 3.9d, left. *Cul3*$^{+/+}$;*Emx1*-Cre, 0.504 s, *Cul3*$^{+/fl}$;*Emx1*-Cre, 0.792 s, p = 0.174, two-tailed *t*-test). These results indicate different influences of cortical areas in the observed behavioural phenotypes in the *Cul3*$^{+/-}$ and *Setd5*$^{+/-}$ models. Whereas the delayed responses observed in the *Setd5* model appear to be independent of cortical dysfunctions, the persistent, if weaker, phenotypic differences observed in the conditional *Cul3* model suggest that cortical areas could be responsible for at least some of the behavioural delay.

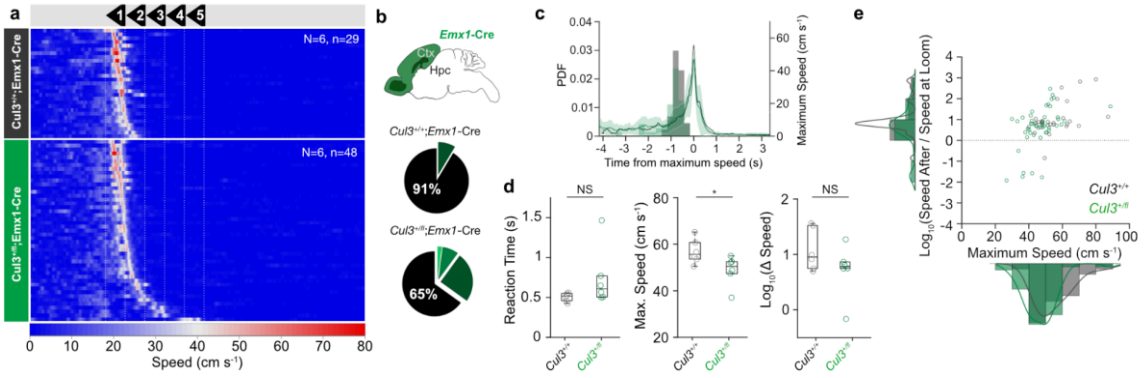

Figure 3.9 Escape response properties in *Cul3*$^{+/fl}$;*Emx1*-Cre mice.

a, Raster plot of mouse speed in response to the looming stimuli (white, dotted vertical lines denote the start of each loom; white solid line denotes the end of the stimulus) for *Cul3*$^{+/+}$;*Emx1*-Cre (top, n = 6, 29 trials) and *Cul3*$^{+/fl}$; *Emx1*-Cre (bottom, n = 6, 48 trials), sorted by reaction time. **b**, Pictorial representation of the expression of *Emx1* in a sagittal section of a mouse brain, showing the localisation of the expression to the cortex and hippocampus (green, top). Proportion of trials in which the mice respond within each loom for *Cul3*$^{+/+}$; *Emx1*-Cre (middle) and *Cul3*$^{+/fl}$; *Emx1*-Cre mice (bottom). There is no significant difference in the proportion of trials in which the mice respond within the 1st loom (*Cul3*$^{+/+}$;*Emx1*-Cre, n = 6, 0.914; *Cul3*$^{+/fl}$;*Emx1*-Cre, n = 6, 0.651, $p = 0.052$, two-sample Wilcoxon's signed-rank (RS) test. Distribution of number of looms to escape across all trials, *Cul3*$^{+/+}$;*Emx1*-Cre, 29 trials, *Cul3*$^{+/fl}$;*Emx1*-Cre, 48 trials, $p = 0.115$, two-sample Kolmogorov-Smirnov (KS) test). **c**, Mean speed response profile of all trials where mice escape to the shelter for *Cul3*$^{+/+}$;*Emx1*-Cre (black) and *Cul3*$^{+/fl}$;*Emx1*-Cre

(green) showing similar escape kinetics, with a histogram of the distribution of the start of the loom stimulus aligned to the peak of the escape response (*Cul3*$^{+/+}$;*Emx1*-Cre, 29 trials, -0.518 s; *Cul3*$^{+/fl}$;*Emx1*-Cre, 48 trials, -0.835 s, p = 0.037, two-sample KS test). **d**, No significant difference in reaction time (*Cul3*$^{+/+}$;*Emx1*-Cre, n = 6, 0.504 s; *Cul3*$^{+/fl}$;*Emx1*-Cre, n = 6, 0.792 s, p = 0.052, Wilcoxon's RS test) or $\log_{10}$(ΔSpeed) (*Cul3*$^{+/+}$;*Emx1*-Cre, n = 6, $\log_{10}$(ΔSpeed) = 1.07; *Cul3*$^{+/fl}$;Emx1-Cre, n = 6, $\log_{10}$(ΔSpeed) = 0.706, p = 0.429, Wilcoxon's RS test). However, there remains a significant difference in the escape vigour (*Cul3*$^{+/+}$;*Emx1*-Cre, n = 6, 56.9 cms^{-1}; *Cul3*$^{+/fl}$;*Emx1*-Cre, n = 6, 47.6 cms^{-1}, p = 0.017, Wilcoxon's RS test). Plotted points represent the average value across all trials where the mice performed an escape behaviour for individual animals. Box-and-whisker plots show median, IQR and range. **e**, Relationship between $\log_{10}$(ΔSpeed) and the maximum speed reached during the escape. Log_{10}(ΔSpeed): *Cul3*$^{+/+}$;*Emx1*-Cre, 29 trials, $\log_{10}$(ΔSpeed) = 1.09; *Cul3*$^{+/fl}$;*Emx1*-Cre, 48 trials, $\log_{10}$(ΔSpeed) = 0.639, p = 0.073, two-sample KS test. Maximum escape speed: *Cul3*$^{+/+}$;*Emx1*-Cre, 29 trials, 55.5 cm s^{-1}, *Cul3*$^{+/fl}$; *Emx1*-Cre, 48 trials, 46.9 cm s^{1}, p = 0.013, two-sample KS test). Trials from animals of the same genotype are pooled together and each point represents a single trial.

3.3 Delayed escape responses in mutant animals are not due to positional or locomotor differences.

The expression of different defensive behaviours to visual threats can be affected by various features of the physical environment or the animal's locomotion that are difficult to control for. For this reason, we further analysed the escape response data and specifically investigated the relationship between the response variables (reaction time and escape vigour) and the distance of the mouse from the shelter, the speed of the mouse and the heading angle of the mouse at the time of stimulus onset. We additionally investigated the relationship between these variables and the ability of individual mice to generate directed trajectories towards the shelter.

3.3.1 Distance from the shelter and from the loom.

Previous work in rodents has demonstrated that spatial awareness of the availability or perceived distance from a position of safety will modulate the type and certain features of the defensive behaviour performed (Blanchard et al. 1976; Edut and Eilam 2003; Vale et al. 2017). To ensure that the delayed responses of the mutant animals were not the result of consistent presentation of the looming stimulus at farther distances from the shelter than their wild-type siblings, we investigated the relationship between the escape response variables and the centre-of-mass position of the animal at the time when the looming stimulus started (Fig. 2.5). The average distance from the shelter did not differ between genotypes when analysed per animal across all trials (Fig. 3.10a-c), nor in the distribution of the values from all trials pooled across animals (Fig. 3.10d-f) for any of the three models tested. These results indicated that the observed perceptual delay could not be explained by differences in the distance of the animals from the shelter at the time of the stimulus onset.

Even though there was no difference between the genotypes in their average distance from the shelter, we still decided to investigate if this parameter differentially affects the response kinetics of the wild-type and mutant mice. We observed no correlation between the distance of the mouse from the shelter and the reaction time for either genotype in all three models (Fig. 3.10g-i). However, the maximum speed reached during the escape was positively correlated to

the distance of the animal from the shelter in all three wild-type cohorts (Fig. 3.10j-l). Both *Setd5* and *Cul3* mutant animals also show positive correlations between the distance from the shelter and their maximum speed, although the strength of the correlation is not as strong as for their wild-type siblings (Fig. 3.10j,l), although this wasn't observed for *Ptchd1* mutants (Fig. 3.10k).

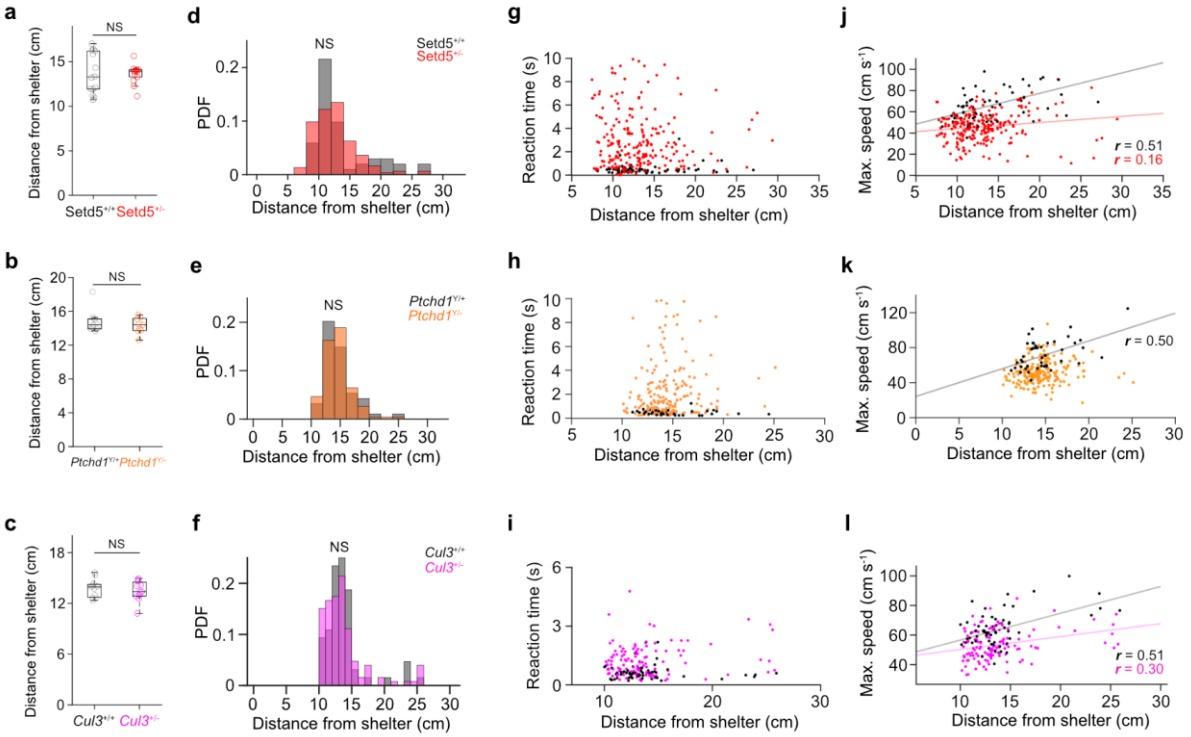

Figure 3.10 Escape response variables with respect to the distance of the centre of the mouse from the shelter at the time of the loom presentation.

a-**c**, No difference in the median distance from the shelter when the looming stimulus is triggered, between wild-type and mutant animals from any of the models tested. **a**, *Setd5*$^{+/+}$, n = 14, 13.2 cm; *Setd5*$^{+/-}$, n = 14, 13.7 cm, $p = 0.341$; **b**, *Ptchd1*$^{Y/+}$, n = 9, 14.8 cm; *Ptchd1*$^{Y/-}$, n = 9, 14.3 cm, $p = 0.796$; **c,** *Cul3*$^{+/+}$, n = 10, 13.8 cm; *Cul3*$^{+/-}$, n = 10, 13.5 cm, $p = 0.896$. *p*-values from wilcoxon's ranked sum (RS) tests. Plotted points represent the average value across all trials where the mice performed an escape behaviour for individual animals. Box-and-whisker plots show median, IQR and range. **d**-**f**, No difference in the distribution of the probability density function of distances from the shelter when the looming stimulus is triggered, across all trials, pooled by genotype, analysed by two-way Kolmogorov-smirnov tests. **d,** *Setd5*$^{+/+}$ versus *Setd5*$^{+/-}$, $p = 0.325$. **e,** *Ptchd1*$^{Y/+}$ versus *Ptchd1*$^{Y/-}$, $p = 0.878$; **f**, *Cul3*$^{+/+}$ versus *Cul3*$^{+/-}$, $p = 0.518$. **g**-**i**, No significant correlation between the distance to the shelter and the reaction time for all trials, analysed using a Pearson's correlation analysis. **g**, *Setd5*$^{+/+}$, $p = 0.443$; *Setd5*$^{+/-}$, $p = 0.778$; **h**, *Ptchd1*$^{Y/+}$, $p = 0.719$; *Ptchd1*$^{Y/-}$, $p = 0.083$; **i**, *Cul3*$^{+/+}$, p = 0.678 ; *Cul3*$^{+/-}$, $p = 0.273$. The values from each trial are plotted as single points. **j**-**l**, Significant, and positive correlations between the distance to the shelter and the maximum escape speed reached during trials for animals from all genotypes, except *Ptchd1*$^{Y/-}$, analysed using a Pearson's correlation analysis. **j,** black, *Setd5*$^{+/+}$, $r = 0.51$, $p < 0.001$; red, *Setd5*$^{+/-}$, $r = 0.16$, $p = 0.016$; **k**, *Ptchd1*$^{Y/+}$, black, $r = 0.50$, $p < 0.001$; *Ptchd1*$^{Y/-}$, orange, $r = 0.12$, $p = 0.083$**; l**, *Cul3*$^{+/+}$, $r = 0.51$, $p < 0.001$; *Cul3*$^{+/-}$, magenta, $r = 0.30$, $p = 0.002$. The values from each trial are plotted as single points. Trend lines are only drawn for significant correlations.

These results suggest that, in general, all animals are likely not reaching their maximal velocity during the escape responses due to the small size of the arena, since when the animals travel further distances they are able to build up higher maximum speeds. However, whereas in wild-

type animals the maximum speed generated is strongly linked to the length of the traversable distance to the shelter, it is less tightly linked in the mutant animals.

3.3.2. Speed of the mouse at the loom

Since the mutant animals from all three models reacted with slower vigours overall, we wondered whether this could be due to the animals moving slower overall and especially at the time of stimulus onset. Moreover, the probability of freezing versus fleeing in Drosophila was found to be dependent on the speed of the fly at the time when the stimulus started (Zacarias et al. 2018). We looked at the average instantaneous speed of the animals across all trials and could not find a difference in the mean values between genotypes (Fig. 3.11a-c) or in the distribution of these values across all trials, pooled by genotype (Fig. 3.11d-f). We can conclude that in these experiments differences in the instantaneous speed of the animals was not the cause of delayed perceptual decisions in the mutant animals.

We again were interested in the influence of this behavioural variable on the outcome of the escape response however and looked at the correlations between this value per trial and the respective reaction time (Fig. 3.11g-i) and maximum speed generated (Fig.3.11j-l). No correlation was found between any variable for any genotype in any of the models, except for a weak negative correlation between the reaction time in *Cul3*$^{+/-}$ mice (Fig. 3.11i, pink, $r = -0.17$, $p = 0.047$, Pearson's r). This result indicates that for *Cul3*$^{+/-}$ animals they are able to react faster to the looming stimulus if they are moving at a faster speed to begin with. This could be due to issues in building up speed from an initially slower starting speed, in line with the motor deficits described previously and mentioned above (Morandell et al. 2021).

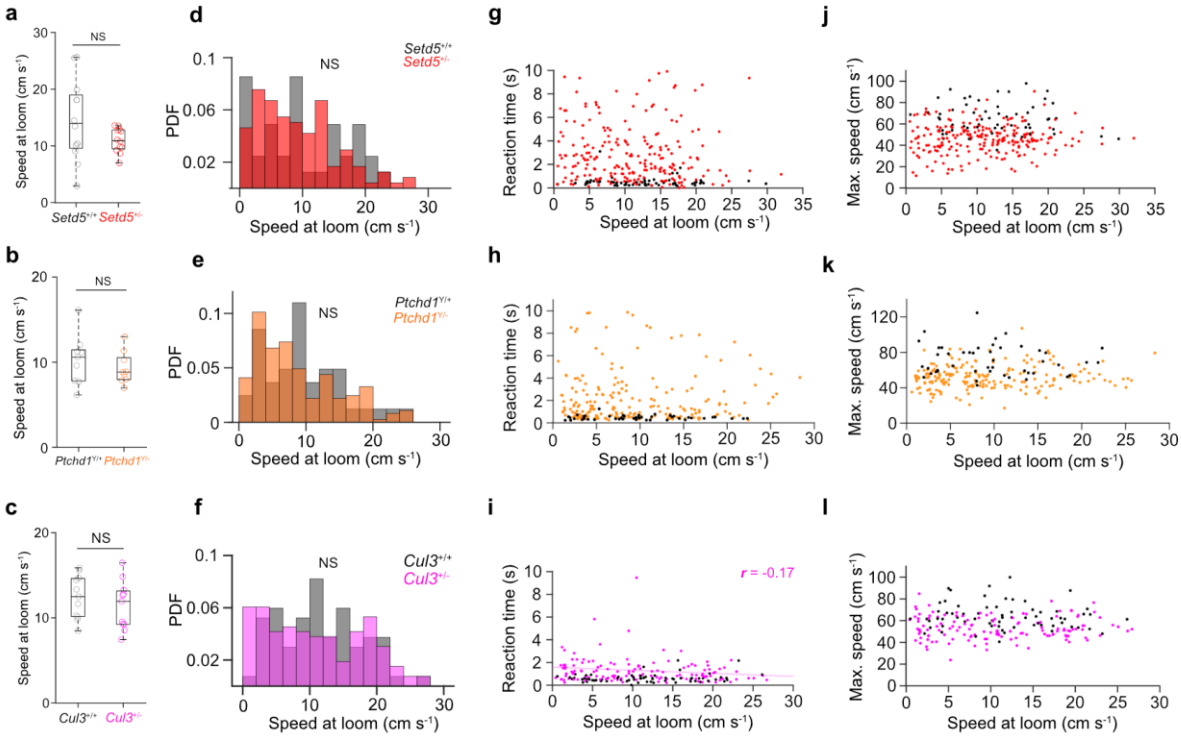

Figure 3.11 Escape response variables with respect to the speed of the mouse at the time of the loom presentation.

a-**c**, No difference in the median instantaneous speed of the mouse when the looming stimulus is triggered, between wild-type and mutant animals from any of the models tested. **a**, *Setd5*$^{+/+}$, n = 14, 15.1 cm s^{-1}; *Setd5*$^{+/-}$, n = 14,12.0 cm s^{-1}, $p = 0.312$; **b**, *Ptchd1*$^{Y/+}$, n = 9, 10.3 cm s^{-1}; *Ptchd1*$^{Y/-}$, n = 9, 9.30 cm s^{-1}, $p = 0.667$; **c,** *Cul3*$^{+/+}$, n = 10, 12.4 cm s^{-1}, *Cul3*$^{+/-}$, n = 10, 11.4 cm s^{-1}, $p = 0.393$. *p*-values from Wilcoxon's ranked-sum tests. Plotted points represent the average value across all trials where the mice performed an escape behaviour for individual animals. Box-and-whisker plots show median, IQR and range. **d**-**f**, No difference in the distribution of the probability density function of instantaneous speeds when the looming stimulus is triggered, across all trials, pooled by genotype, analysed by two-way Kolmogorov-smirnov tests. **d,** *Setd5*$^{+/+}$ versus *Setd5*$^{+/-}$, $p = 0.086$; **e,** *Ptchd1*$^{Y/+}$ versus *Ptchd1*$^{Y/-}$, $p = 0.070$; **f**, *Cul3*$^{+/+}$ versus *Cul3*$^{+/-}$, $p = 0.231$. **g**-**i**, No significant correlation between the instantaneous speed and the reaction time for all genotypes, except *Cul3*$^{+/-}$, when analysed using a Pearson's correlation analysis**.** **g**, *Setd5*$^{+/+}$, $p = 0.197$; *Setd5*$^{+/-}$, $p = 0.112$; **h**, *Ptchd1*$^{Y/+}$, $p = 0.762$; *Ptchd1*$^{Y/-}$, $p = 0.711$; **i**, *Cul3*$^{+/+}$, $p = 0.153$; *Cul3*$^{+/-}$, pink, $r = -0.17$, $p = 0.047$. The values from each trial are plotted as single points. **j**-**l**, No significant correlation between the instantaneous speed and the maximum escape speed reached during trials for animals from all genotypes when analysed using a Pearson's correlation analysis**.** **j,** *Setd5*$^{+/+}$, $p = 0.592$; *Setd5*$^{+/-}$, $p = 0.580$; **k**, *Ptchd1*$^{Y/+}$, $p = 0.517$; *Ptchd1*$^{Y/-}$, $p = 0.087$; **l**, *Cul3*$^{+/+}$, $p = 0.424$; *Cul3*$^{+/-}$, $p = 0.943$. The values from each trial are plotted as single points. Trend lines are only drawn for significant correlations.

3.3.3 Angle at loom.

We next decided to investigate whether differences in the heading direction of the animals could lead to slower reaction times in the mutant animals. We hypothesised that trials where the animals were facing away from the shelter would have slower reaction times since the animals would be required to make a full 180° turn, as opposed to if they were directly facing the shelter, and that if there were uncontrolled for differences in the probability of facing a specific direction between the genotypes then this could be having a significant effect on the

results. In our analysis we defined 0º as directly facing the shelter and 180º as facing away from the shelter.

Once again however, we could observe no significant difference in the average heading angle of the mice at the time of stimulus onset either in the mean value per genotype, derived from the average value across all trials per animal (Fig. 3.12a-c), or in the distribution of heading angles between genotypes from all trials pooled together for *Setd5* and *Cul3* (Fig. 3.12d,f). We did observe a small difference in the distribution of the heading angle across all trials pooled together for the *Ptchd1* lines however (Fig. 3.12e**,** *Ptchd1*$^{Y/+}$ versus *Ptchd1*$^{Y/-}$, p = 0.023, KS test)

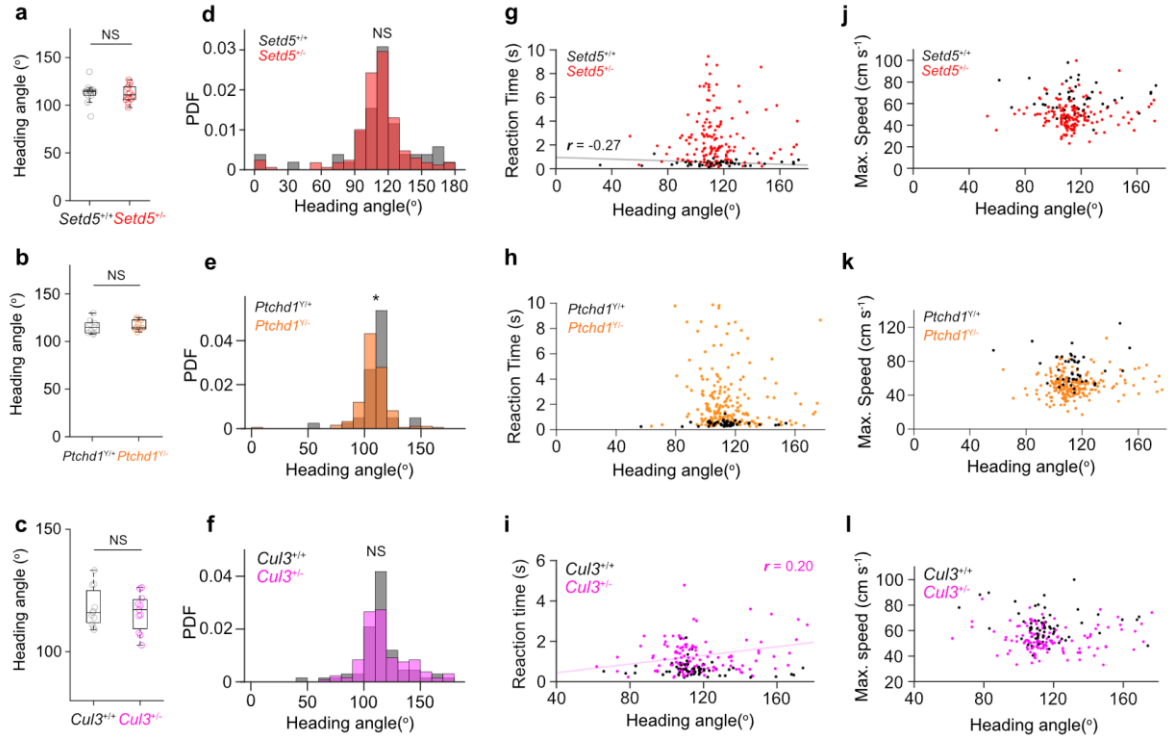

Figure 3.12 Escape response variables with respect to the heading angle of the mouse at the time of the loom presentation.

a-c, No difference in the median heading angle of the mouse when the looming stimulus is triggered, between wild-type and mutant animals from any of the models tested. **a**, *Setd5*$^{+/+}$, n = 14, 114º; *Setd5*$^{+/-}$, n = 14, 111º, *p* = 0.194; **b**, *Ptchd1*$^{Y/+}$, n = 9, 116º; *Ptchd1*$^{Y/-}$, n = 9, 117º, *p* = 0.436; **c,** *Cul3*$^{+/+}$, n = 10, 118º, *Cul3*$^{+/-}$, n = 10, 116º, *p* = 0.793. *p*-values from Wilcoxon's ranked-sum tests. Plotted points represent the average value across all trials where the mice performed an escape behaviour for individual animals. Box-and-whisker plots show median, IQR and range. **d-f**, No difference in the distribution of the probability density function of heading angle when the looming stimulus is triggered, across all trials, pooled by genotype when analysed by two-way Kolmogorov-smirnov tests, for *Setd5* and *Cul3* animals, but there is for *Ptchd1* animals. **d,** *Setd5*$^{+/+}$ versus *Setd5*$^{+/-}$, *p* = 0.994; **e,** *Ptchd1*$^{Y/+}$ versus *Ptchd1*$^{Y/-}$, *p* = 0.023; **f**, *Cul3*$^{+/+}$ versus *Cul3*$^{+/-}$, *p* = 0.621. **g-i**, Heading angle is negatively correlated with reaction time in *Setd5*$^{+/+}$ animals and positively correlated in *Cul3*$^{+/-}$ animals. There is no significant correlation between these values for the other genotypes investigated when analysed using a Pearson's correlation analysis**.** **g**, *Setd5*$^{+/+}$, black, *r* = -0.37, p = 0.014; *Setd5*$^{+/-}$, p = 0.333; **h**, *Ptchd1*$^{Y/+}$, p = 0.483 ; *Ptchd1*$^{Y/-}$, p = 0.577; **i**, *Cul3*$^{+/+}$, p = 0.158 ; *Cul3*$^{+/-}$, pink, *r* = 0.20, p = 0.022. The values from each trial are plotted as single points. **j-l**, No significant correlation between the heading angle and the maximum escape speed reached during trials for animals from all genotypes when analysed using a Pearson's correlation analysis**. j,** *Setd5*$^{+/+}$ p = 0.635;

Setd5$^{+/-}$, p = 0.188; **k**, *Ptchd1*$^{Y/+}$, p = 0.997; *Ptchd1*$^{Y/-}$, p = 0.324; **l**, *Cul3*$^{+/+}$, p = 0.294; *Cul3*$^{+/-}$, p = 0.978. The values from each trial are plotted as single points. Trend lines are only drawn for significant correlations.

Despite not observing a difference in the distribution of angles between the genotypes, we still investigated the influence of this variable on both the reaction time and maximum escape speed. Interestingly, we observed a negative correlation between reaction time and heading angle in *Setd5*$^{+/+}$ animals (Fig. 3.12g, black, r = -0.37, p = 0.014, Pearson's r), suggesting that for these wild-type animals they were actually faster at responding to the looming stimulus if they were facing away from the shelter. A limitation of this variable is that it does not include positional information about the location of the animal within the arena and the direction the animal is facing. Another interesting observation was that *Cul3*$^{+/-}$ mice were the only cohort of animals that showed a positive correlation between heading angle and reaction time (Fig. 3.12i, pink, r = 0.20, p = 0.022, Pearson's r). They were the only group of animals that displayed the hypothesised behaviour and were slower in reacting to the stimulus if they had to make a larger turn to orient themselves back towards the shelter. This result again exemplifies the potential impact of motor impairments on the expression of this behaviour. No group of animals showed any correlation between the heading angle and the maximum escape speed reached (Fig. 3.12j-l).

Overall, we can conclude that, in this study, differences in the average distance from the shelter, the instantaneous speed or the heading angle at stimulus onset between genotypes did not influence the differences in reaction time and maximum escape speed observed between these groups in response to the looming stimulus. We can conclude however that: firstly, the value of the maximum speed of the response is most affected by the distance that exists between the animal and the shelter and secondly, that the ability of *Cul3*$^{+/-}$ animals to generate a rapid response to the looming stimulus is affected by both their instantaneous speed and heading angle. This result in particular hints that the previously described motor impairments might be impacting the initial generation of the escape response in this model.

3.3.4 Trajectory analysis

Animals familiarised to a behavioural arena build a cognitive spatial map of the environment to guide later behavioural responses. Previous work has shown that animals can quickly learn about the specific features of an environment to generate the most direct escape trajectory back to a position of safety (Vale et al. 2017). We were interested in understanding if the mutant animals in our three models showed differences in their ability to generate directed trajectories back to the shelter. To do this we generated a variable T_d, which we defined as: $T_d = (1 - (d-d_{min}/d+d_{min}))$, where d is the cumulative displacement of the animal from stimulus onset until it crosses the shelter boundary and d_{min} is the minimum Euclidean distance between the position of the mouse at stimulus onset and the shelter boundary. A difference-sum ratio of these values was subtracted from one in order to generate values in which higher numbers represented more direct trajectories.

We first investigated whether the mutant and wild-type animals of each model would show differences in the average of these values across all trials. By calculating the average value of trajectory directedness across all trials for each animal we were able to observe significant differences between wild-type and mutant animals in both the *Ptchd1* and *Setd5* models (Fig. 3.13a,b), indicating that on average, mutant *Setd5* and *Ptchd1* animals performed less directed escapes back to the shelter than their wild-type siblings. This difference was not observed when looking at the average values for *Cul3*$^{+/+}$ and *Cul3*$^{+/-}$ (Fig. 3.13c). The overall distribution of T_d values across all trials was significantly different between wild-type and mutant animals in all three models however (Fig. 3.13d-f), with *Setd5* and *Ptchd1* showing much flatter distributions that are more shifted towards lower T_d values than the wild-type distributions.

We then analysed whether animals that displayed, on average, less directed trajectories also showed slower reaction times and maximum escape speeds too. Analysis of each animal's average reaction time and T_d revealed significant negative correlations for the mutant animals in all three models (Fig. 3.13g-i). No correlation was found between T_d and reaction time in any of the wild-type groups. In addition, no relationship was found between T_d and the maximum escape speed reached for *Setd5* or *Cul3* animals, however a significant positive correlation was found between *Ptchd1*$^{Y/-}$ animals (Fig. 3.13k, orange, $r = 0.75$, $p = 0.020$, Pearson's r). These results suggest that in the *Ptchd1* model, mutant animals that on average show less direct escapes back to the shelter also respond with the longest latency and the least vigour.

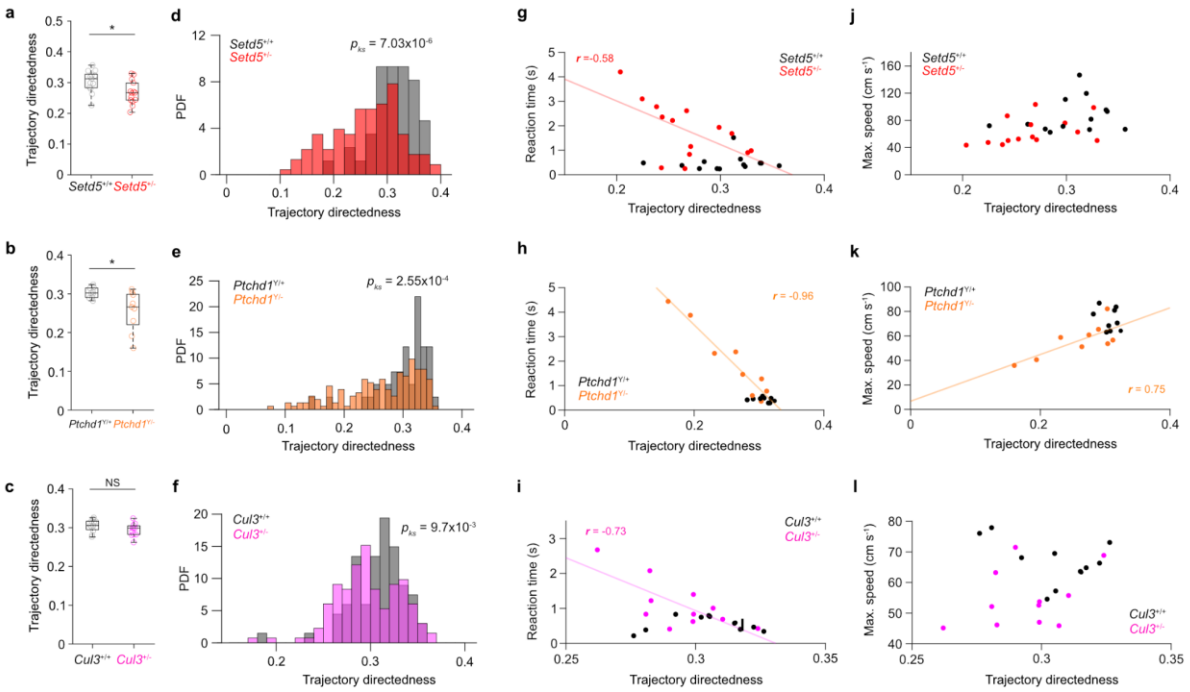

Figure 3.13 Escape response variables with respect to the directedness of the escape trajectories.

a-c, Significant difference in the median value of escape trajectory directedness between *Setd5* and *Ptchd1* wild-type and mutant animals, but not for *Cul3* animals. **a**, *Setd5*$^{+/+}$, n = 14, 0.305; *Setd5*$^{+/-}$, n = 14, 0.261, $p = 0.030$; **b**, *Ptchd1*$^{Y/+}$, n = 9, 0.303; *Ptchd1*$^{Y/-}$, n = 9, 0.255, $p = 0.019$; **c,** *Cul3*$^{+/+}$, n = 10, 0.305, *Cul3*$^{+/-}$, n = 10, 0.294,

p = 0.168. p-values from Wilcoxon's ranked-sum tests. Plotted points represent the average value across all trials where the mice performed an escape behaviour for individual animals. Box-and-whisker plots show median, IQR and range. **d**-**f**, Significant differences in the distribution of the probability density function of trajectory directedness across all trials, pooled by genotype when analysed by two-way Kolmogorov-smirnov tests for all three models. **d,** *Setd5*$^{+/+}$ versus *Setd5*$^{+/-}$, $p < 0.0014$; **e,** *Ptchd1*$^{Y/+}$ versus *Ptchd1*$^{Y/-}$, $p < 0.001$; **f**, *Cul3*$^{+/+}$ versus *Cul3*$^{+/-}$, $p = 0.010$. **g**-**i**, Trajectory directedness is negatively correlated with reaction time for mutant animals from all three models, but there is no significant correlation between these variables in the wild-type animals when analysed using a Pearson's correlation analysis**. g**, *Setd5*$^{+/+}$, p = 0.780; *Setd5*$^{+/-}$, red, r = -0.58, p = 0.029; **h**, *Ptchd1*$^{Y/+}$, p = 0.404 ; *Ptchd1*$^{Y/-}$, orange, r = -0.96, p < 0.001; **i**, *Cul3*$^{+/+}$, p = 0.827 ; *Cul3*$^{+/-}$, pink, r = -0.73, p = 0.012. The average value across all trials from each animal is plotted as a single point. **j**-**l**, *Ptchd1*$^{Y/-}$ animals show a positive correlation between trajectory directedness and maximum escape vigour, but none of the other genotypes do when analysed using Pearson's correlation analysis. **j,** *Setd5*$^{+/+}$ p = 0.425; *Setd5*$^{+/-}$, p = 0.142; **k**, *Ptchd1*$^{Y/+}$, p = 0.418; *Ptchd1*$^{Y/-}$, orange, r = 0.75, p = 0.020; **l**, *Cul3*$^{+/+}$, p = 0.201; *Cul3*$^{+/-}$, p = 0.303. The average value across all trials for each animal is plotted as a single point. Trend lines are only drawn for significant correlations.

From analysing the trajectories of animals on their first and last day of testing (Fig. 3.14), we can see that the value of trajectory directedness is influenced by adaptation to the looming stimulus across days. Wild-type animals make similar escape trajectories, with a high level of directedness on both the first and last day of testing (black, left panels in 3.14a-f). In the mutant animals, both the *Setd5*$^{+/-}$ and *Ptchd1*$^{Y/-}$ animals have less direct trajectories than their wild-type littermates already on the first day, and they seem to get less directed over time (right panels in Fig. 3.14a-d). The effect appears to be more pronounced for the *Ptchd1*$^{Y/-}$ animals. *Cul3*$^{+/-}$ animals appear to make slightly less directed escape trajectories than their wild-type companions, however this is less pronounced than in the other two models (left panels, Fig. 3.14e-f).

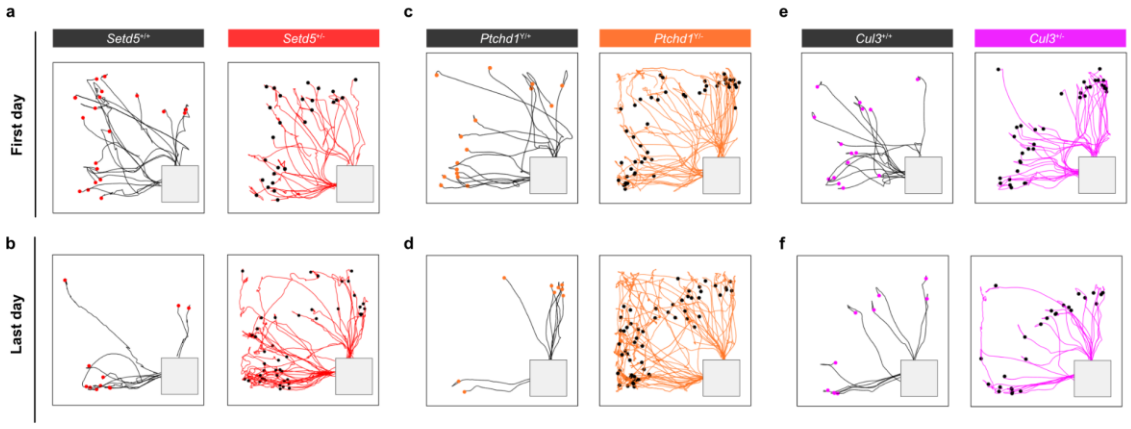

Figure 3.14 Escape trajectories of *Setd5*, *Cul3* and *Ptchd1* animals on the first and the last day of testing.

a, Escape path trajectories of *Setd5*$^{+/+}$ (left, black lines) and *Setd5*$^{+/-}$ (right, red lines) during the first day of testing. The filled circles represent the position of the animal when the looming stimulus was triggered. **b**, as for **a** but for trials on the last day of testing. **c**-**d**, as for **a**-**b** but for *Ptchd1*, mutant animals' trajectories are shown in orange. **e**-**f**, as for **a**-**b** but for *Cul3*, mutant animals' trajectories are shown in magenta.

3.3.5 Baseline locomotor abilities

Lastly, we investigated whether different locomotor activity levels at baseline could account for the slower reaction times and vigour observed in the mutant animals (Fig. 3.15). We found no differences in the average or the maximum speed reached during the exploration times in either the *Setd5* (Fig 3.15a, b) or the *Cul3* models (Fig 3.15e,f). There was also no difference observed in the maximum speed reached by either of the genotypes in the Ptchd1 model (Fig 3.15d). However, *Ptchd1*$^{Y/-}$ animals did exhibit a hyperactive phenotype during the exploration period (Fig 3.15c**)**, which is in line with results from previously published reports on another *Ptchd1* knockout mouse model (Filges et al. 2011; Chaudhry et al. 2015; Wells et al. 2016) and what is known about the behaviours observed in humans with mutations in this gene (Chaudhry et al. 2015). It is interesting to observe that the *Ptchd1* animals exhibit slower reaction times and maximal escape speeds despite showing higher levels of baseline activity.

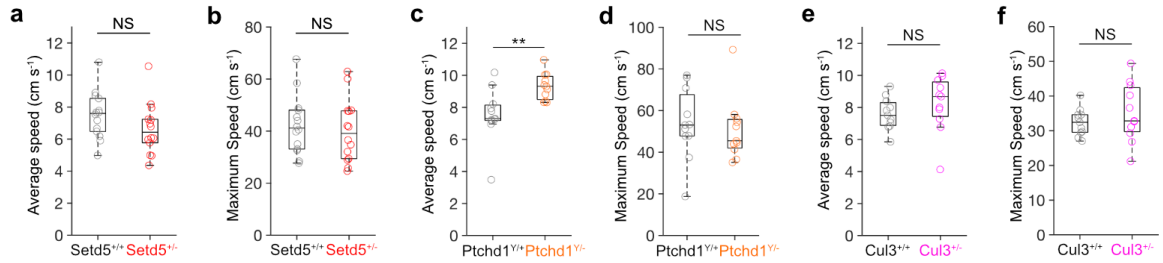

Figure 3.15 Baseline locomotor abilities of the three mouse models during acclimatisation.

Setd5$^{+/-}$ and *Cul3*$^{+/-}$ animals show similar baseline locomotor abilities to their wild-type siblings. **a**, average speed: *Setd5*$^{+/+}$, 7.50 cms^{-1}; *Setd5*$^{+/-}$, 6.65 cms^{-1}, p = 0.151; **b**, maximum speed: *Setd5*$^{+/+}$, 42.2 cms^{-1}; *Setd5*$^{+/-}$, 40.2 cms^{-1}, P = 0.642. **e**, average speed: *Cul3*$^{+/+}$, 7.60 cms^{-1}; *Cul3*$^{+/-}$, 8.23 cms^{-1}, p = 0.3055; **f**, maximum speed: *Cul3*$^{+/+}$, 32.5 cms^{-1}; *Cul3*$^{+/-}$, 35.2 cms^{-1}, p = 0.430. Whereas *Ptchd1*$^{Y/-}$ show an increased average speed during the pre-loom exploration (**c**, *Ptchd1*$^{Y/-}$, 9.31 cms^{-1}; *Ptchd1*$^{Y/+}$, 7.53 cms^{-1}, p = 0.003) but reached similar maximum speeds (**d**, *Ptchd1*$^{Y/+}$, 53.7 cms^{-1}; *Ptchd1*$^{Y/-}$, 50.7 cms^{-1}, p = 0.393). Plotted points represent the average value across all trials where the mice performed an escape behaviour for individual animals. Box-and-whisker plots show median, IQR and range. p values are from two-sample Wilcoxon's signed-rank tests.

3.4 Delayed responses are not sex-specific.

Since previous reports had observed a sexually-dimorphic expression of certain autism-like behaviours in the *Setd5* mouse model (Deliu et al. 2018), with females presenting with a stronger behavioural phenotype than males, we conducted most of the initial behavioural experiments in female *Setd5* mice. We repeated the same LAR experiments but with male wild-type and mutant sibling pairs (Fig. 3.16) and observed very similar delays in both the reaction time and the maximum escape speed for the mutant animals as in the female pairs that we tested (Fig. 3.1, 3.2, 3.3). Male *Setd5*$^{+/-}$ animals responded to the stimulus within the first loom presentation 32% of the time (Fig. 3.16b), similar to the 38% for the female mice (Fig. 3.2d). They also had similar reaction times to the loom (Fig. 3.16c, *Setd5*$^{+/-}$ females, 1.88s, n = 14; *Setd5*$^{+/-}$ males, 2.35s, n = 4, p = 0.03, RS test), maximum escape speeds (Fig. 3.16c, *Setd5*$^{+/-}$

females, 51.6 cm s^{-1}, n = 14; *Setd5*$^{+/-}$ males, 49.9 cm s^{-1}, n = 4, p < 0.001, RS test) and average Log_{10}(ΔSpeed), (Fig. 3.16f, *Setd5*$^{+/-}$ females, 0.42, n = 14; *Setd5*$^{+/-}$ males, -0.17, n = 4, p = 0.010, RS test). Altogether, these results indicate that the delay in reaction time and reduced escape vigour observed in the *Setd5*$^{+/-}$ animals is independent of the sex of the animal. Both male and female mice were tested in the *Cul3* model, and no significant differences were found in the responses of either sex (data not shown). Since *Ptchd1* is an X-linked gene, the effect of this mutation can only be observed in male mice.

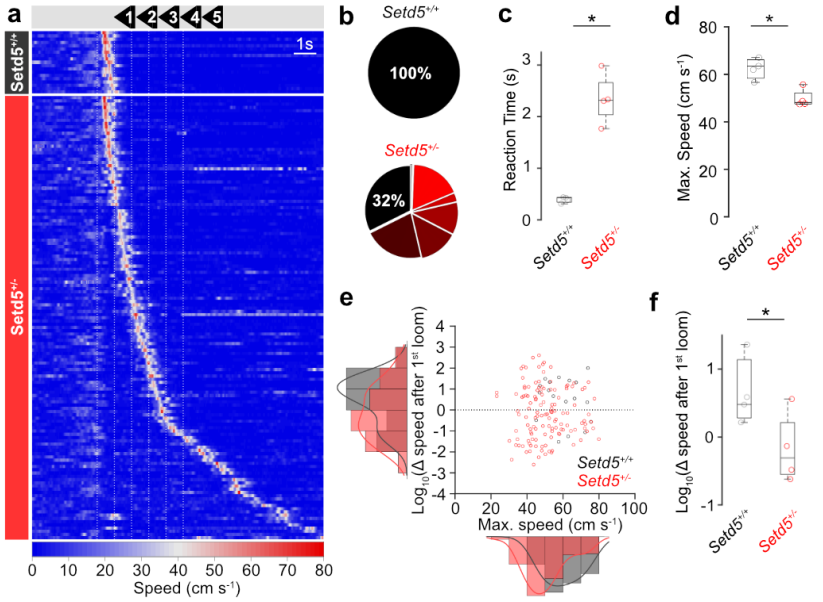

Figure 3.16 Comparable escape delay and reduced vigour in male *Setd5*$^{+/-}$ mice

a, Raster plot of mouse speed in response to the looming stimuli (white, dotted vertical lines denote the start of each loom; white solid line denotes the end of the stimulus) for *Setd5*$^{+/+}$ (top, n = 4, 18 trials) and *Setd5*$^{+/-}$ (bottom, n = 4, 144 trials), sorted by reaction time. **b**, Summary of the proportion of trials in which the mice respond within each loom for *Setd5*$^{+/+}$ (top) and *Setd5*$^{+/-}$ mice (bottom). Proportion of trials where mice escaped within the first loom: *Setd5*$^{+/+}$, 1.00; *Setd5*$^{+/-}$, 0.324, p = 0.028. Distribution of number of looms to escape, *Setd5*$^{+/+}$, 18 trials, *Setd5*$^{+/-}$, 144 trials, P < 0.001. **c**, Summary of the average reaction time per animal (*Setd5*$^{+/+}$, 18 trials, 0.394 s; *Setd5*$^{+/-}$, 130 trials, 2.10 s, p = 0.029). **d**, Summary of the average maximum escape speed per animal (*Setd5*$^{+/+}$, n = 18, 63.3 cms^{-1}; *Setd5*$^{+/-}$, n = 130, 49.9 cms^{-1}, p = 0.047). **e**, Scatter-hist plot of the log_{10}(change in speed upon the 1st loom presentation) (x-axis, see methods) and the maximum speed reached during the escape (y-axis), (Log_{10}(ΔSpeed): *Setd5*$^{+/+}$, 18 trials, 0.622; *Setd5*$^{+/-}$, 144 trials, -0.128, P = 0.008; Maximum Escape Speed; *Setd5*$^{+/+}$, 18 trials, 59.7 cms^{-1}; *Setd5*$^{+/-}$, 144 trials, 49.6 cms^{-1}, P = 0.005). **f**, Summary of the average Log_{10}(ΔSpeed) per animal for *Setd5*$^{+/+}$ (0.684) and *Setd5*$^{+/-}$ (-0.169, p = 0.048). Plotted points represent the average value across all escape trials for individual animals. Box-and-whisker plots show median, IQR and range. Shaded areas show s.e.m. p-values: Wilcoxon's test, P-values: two-sample KS test.

3.5 Summary

In conclusion, using the LAR paradigm we were able to identify and describe conserved behavioural differences in a rapid PDM process across three molecularly distinct mouse models of autism. Mutant animals from these mouse models exhibited a consistent delay in the initiation of an escape response to the innately-threatening expanding disc stimulus due to an

increased pre-escape risk assessment period, and performed less vigorous escapes overall. These differences do not appear to arise from overall differences in the position of the mutant animals from the shelter, their heading direction, their speed at the time of stimulus exposure or their baseline locomotion. *Setd5*$^{+/-}$ and *Ptchd1*$^{Y/-}$ animals perform less directed escapes back to the shelter than their wild-type siblings, while *Cul3*$^{+/-}$ animals do not. In the *Setd5*$^{+/-}$ animals, their behavioural delay does not appear to originate from cortical regions since the behavioural differences were not recapitulated in a forebrain-specific conditional knockout model, and is independent of the sex of the animals.

4 ASD mouse models exhibit altered behavioural adaptation to threatening visual stimuli.

As demonstrated in Chapter 3, the expression of an escape response to a visual threat is both robust and flexible. Learning is not required to perform an effective escape to a looming stimulus (Chen et al. 2022; Heinemans & Moita 2022), however the response can be influenced by prior exposure to the looming stimulus or other threats (Ellard 1996; Gibson et al. 2015; Evans 2017; Evans et al. 2018; Lenzi et al. 2022; Marquez-Legorreta et al. 2022). Studies have primarily investigated the effect of recent experience - and hence short term memory - on the expression of responses to the looming stimulus on the adaptation of the LAR (Evans et al. 2018; Lenzi et al. 2022) or adaptation in the neural responses to the visual stimulus itself (Lee et al. 2020) within the same experimental session. However, it is not known how behavioural responses to the looming stimulus adapt over longer time periods, e.g. multiple days. We decided to analyse the LAR dynamics of wild-type and mutant animals across multiple days of testing. Given that behavioural inflexibility and resistance to change are well-described, diagnostic features in autistic individuals and numerous studies have observed altered neuronal homeostasis in animal models of autism, we hypothesised that the mutant animals may present with altered adaptation dynamics to their wild-type siblings.

4.1 Repeated exposure to the looming stimulus differentially affects exploration in wild-type and mutant mice.

In natural environments, the ability to form spatial memories about the location of past threats is crucial to prevent repeated exposure to these potentially harmful stimuli. Animals often avoid locations where they have previously encountered threats and alter their exploration strategies accordingly. Similar behaviours have been observed in studies investigating the short-term effects of threat exposure on rodents (Evans et al. 2018; Lenzi et al. 2022), where animals exhibit place avoidance to the area of the arena where the stimulus was triggered and become more fearful of novel stimuli. Before we investigated the adaptation of the exploration strategies of these animals in response to threat exposure, we wanted to assess if there were intrinsic differences in these behaviours in the three mutant models. We focused on four key features of the exploratory behaviour observed during the acclimatisation: the number of exits from the shelter, the maximum distance from the shelter during the exploration of the arena, the time between successive exits from the shelter and the time spent outside the shelter in a single exit. For both the *Setd5*$^{+/-}$ and *Cul3*$^{+/-}$ animals, there was no difference between the wild-type and mutant animals in the pre-exposure exploratory behaviour (Fig. 4.1a-d, i-l). The wild-type and mutant animals were similarly inclined to explore the arena and exhibited similar strategies in doing so. In contrast, and in accordance with the hyperactivity observed in Fig. 3.15, *Ptchd1*$^{Y/-}$ animals displayed different exploratory strategies to their wild-type littermates, (Fig. 4.1e-h). They performed significantly more exits from the shelter with shorter intervals between subsequent exits, these exits were shorter in duration and on average they travelled less far than their wild-type siblings.

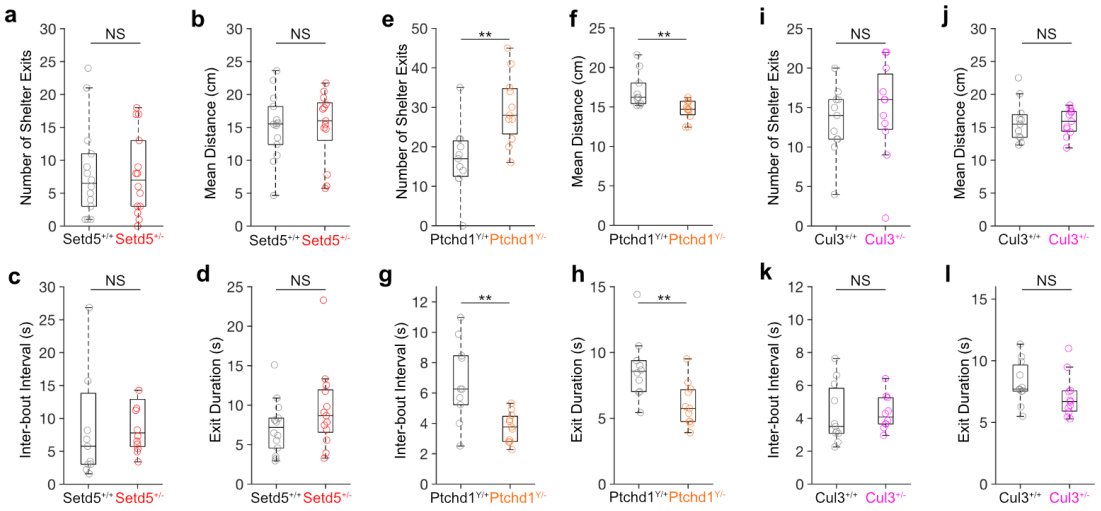

Figure 4.1 Exploration strategies and shelter exit activity of the three mouse models before loom exposure.

Exploratory behaviour during acclimatisation in *Setd5*, *Cul3* and *Ptchd1* mice. No significant difference in behaviour in *Setd5*$^{+/-}$ animals: number of shelter exits (**a**, *Setd5*$^{+/+}$, 8.14; *Setd5*$^{+/-}$, 7.88, $p > 0.999$), mean distance travelled during exit (**b**, *Setd5*$^{+/+}$, 15.2 cm; *Setd5*$^{+/-}$, 15.1 cm, p = 0.981), average inter-bout interval (**c**, *Setd5*$^{+/+}$, 10.1 s; *Setd5*$^{+/-}$, 13.5 s, $p = 0.230$) and average exit duration (**d**, *Setd5*$^{+/+}$, 7.18 s; *Setd5*$^{+/-}$, 9.50 s, $p = 0.198$). *Ptchd1*$^{Y/-}$ mice were hyperactive in their exploration of the arena compared to their wild-type siblings (**e**, number of exits: *Ptchd1*$^{Y/+}$, 17.0, *Ptchd1*$^{Y/-}$, 29.5, $p = 0.003$; distance travelled during exit: **f**, *Ptchd1*$^{Y/+}$, 17.1 cm, *Ptchd1*$^{Y/-}$, 14.6 cm, $p = 0.004$; interbout interval: **g**, *Ptchd1*$^{Y/+}$, 6.76 s, *Ptchd1*$^{Y/-}$, 3.75 s, $p = 0.007$; exit duration: **h**, *Ptchd1*$^{Y/+}$, 8.78 s, *Ptchd1*$^{Y/-}$, 6.05 s, $p = 0.007$). No significant difference in behaviour in *Cul3*$^{+/-}$ animals: number of shelter exits (**i**, *Cul3*$^{+/+}$, 13.3, *Cul3*$^{+/-}$, 14.7, $p = 0.526$), mean distance travelled during exit (**j**, *Cul3*$^{+/+}$, 15.8 cm, *Cul3*$^{+/-}$, 15.7 cm, $p = 0.9448$), average inter-bout interval (**k**, *Cul3*$^{+/+}$, 4.26 s, *Cul3*$^{+/-}$, 4.33 s, $p = 0.5035$) and average exit duration (**l**, *Cul3*$^{+/+}$, 8.23 s, *Cul3*$^{+/-}$, 7.12 s, $p = 0.066$). Box-and-whisker plots show median, IQR and range. *p*-values are two-sample Wilcoxon's ranked-sum tests. Number of animals: *Setd5*$^{+/+}$, n = 14; *Setd5*$^{+/-}$, n = 14; *Cul3*$^{+/+}$, n = 10; *Cul3*$^{+/-}$, n =10; *Ptchd1*$^{Y/+}$, n = 9; *Ptchd1*$^{Y/-}$, n = 9 for all plots. Plotted points represent the variable values across the pre-loom acclimatisation period for individual animals.

Despite the differences in the exploration activities in *Ptchd1*$^{Y/-}$ mice, all animals covered similar areas within the arena and spent similar proportions of the total acclimatisation time outside the shelter and in the centre, or at the edge of the arena (Fig. 4.2).

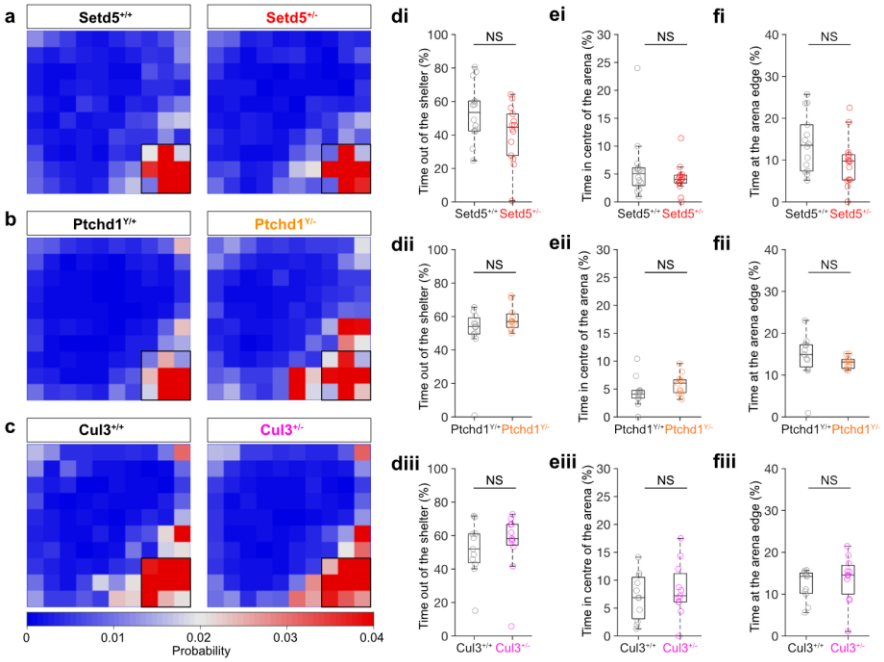

Figure 4.2 Place preference of Setd5, Ptchd1 and Cul3 animals before loom exposure.

a-**c**, Heatmaps of the place preference of willdtype (left column) and mutant (right column) animals from the three models during open field acclimatisation before loom exposure. **d**, Time spent out of the shelter (**i**, *Setd5*$^{+/+}$, 53.5 %; *Setd5*$^{+/-}$, 40.9 %, $p = 0.062$; **ii**, *Ptchd1*$^{Y/+}$, 50.5 %; *Ptchd1*$^{Y/-}$, 58.9 %, $p = 0.148$; **iii**, *Cul3*$^{+/+}$, 51.7 %; *Cul3*$^{+/-}$, 55.6 %, $p = 0.4307$). **e**, Time spent in the centre of the arena (**i**, *Setd5*$^{+/+}$, 6.00 %; *Setd5*$^{+/-}$, 4.20 %, $p = 0.448$; **ii**, *Ptchd1*$^{Y/+}$, 4.46 %; *Ptchd1*$^{Y/-}$, 5.86 %, $p = 0.170$; **iii**, *Cul3*$^{+/+}$, 7.10 %; *Cul3*$^{+/-}$, 8.32 %, $p = 0.5323$). **f**, Time spent at the edge of the arena (**i**, *Setd5*$^{+/+}$, 13.9 %; *Setd5*$^{+/-}$, 9.47 %, $p = 0.076$; **ii**, *Ptchd1*$^{Y/+}$, 14.3 %; *Ptchd1*$^{Y/-}$, 13.0 %, $p = 0.148$; **iii**, *Cul3*$^{+/+}$, 12.2 %; *Cul3*$^{+/-}$, 13.6 %, $p = 0.480$). Box-and-whisker plots show median, IQR and range. *p*-values: Wilcoxon's test. Number of animals: *Setd5*$^{+/+}$, n = 14; *Setd5*$^{+/-}$, n = 14; *Cul3*$^{+/+}$, n = 10; *Cul3*$^{+/-}$, n =10; *Ptchd1*$^{Y/+}$, n = 9; *Ptchd1*$^{Y/-}$, n = 9 for all plots. Plotted points represent the variable values across the pre-loom acclimatisation period for individual animals.

We next investigated how these exploration strategies changed over multiple days of exposure to the looming stimulus and whether this innately aversive stimulus could induce aversion to the area within which the stimulus is triggered. We quantified the movements of the animals across the entire experiment, looking specifically at how often they left the shelter, for how long and how far they would travel during an exploration. Over the course of the testing period, mutant mice from all three models, on average, exited the shelter significantly more (Fig. 4.3a-f), and correspondingly, also triggered significantly more looms (Fig. 4.3g-i) than their wild-type siblings.

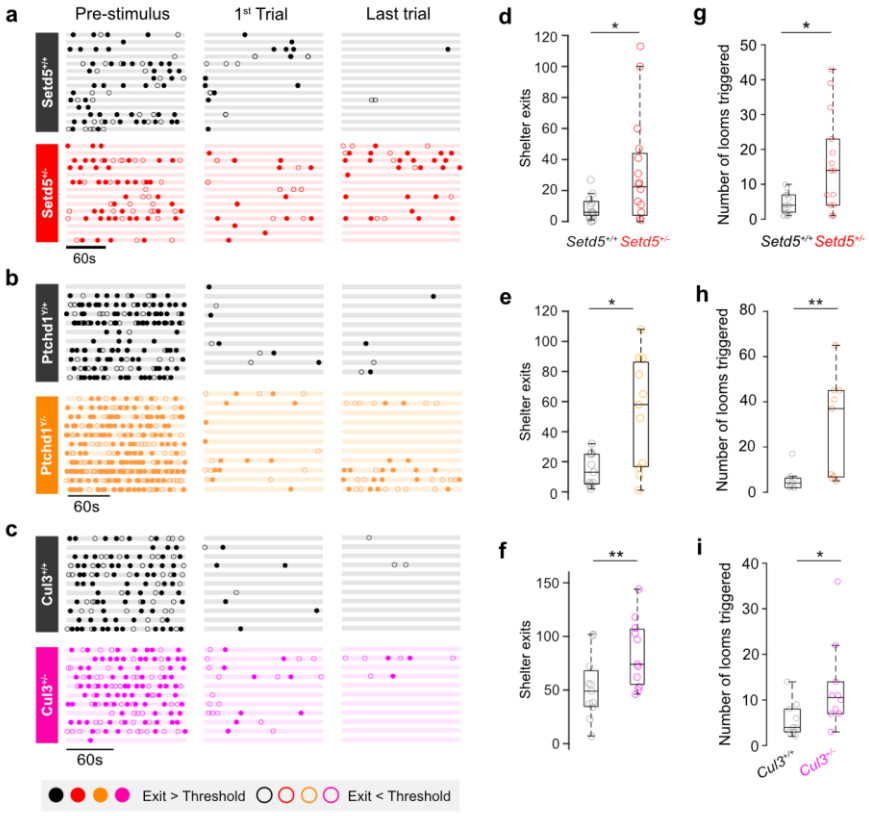

Figure 4.3 Mutant animals exit the shelter more and trigger more looms over the five days of testing.

a-c, Exploratory behaviour during pre-loom acclimatisation (left column), first (centre) and last (right) trial of the LAR paradigm. Each row represents one animal, filled and open dots represent exits into the threat zone or not, respectively. **d-f**, Summary of mean total shelter exits across the 5 test days (**d**, Setd5$^{+/+,}$ 6.0; Setd5$^{+/-}$, 24.5, p = 0.019; **e**, *Ptchd1*$^{Y/+}$, 15 exits; *Ptchd1*$^{Y/-}$, 53 exits, p = 0.025; **f**, *Cul3*$^{+/+}$, 47 exits; *Cul3*$^{+/-}$, 89 exits, p = 0.006). **g-i**, Total number of looms triggered per animal (**g**, *Setd5*$^{+/+}$, 4.4 looms; *Setd5*$^{+/-}$, 16.0 looms, p = 0.013; **h**, *Ptchd1*$^{Y/+}$, 5.4 looms; *Ptchd1*$^{Y/-}$, 28.8 looms, p = 0.004; **i**, *Cul3*$^{+/+}$, 5.6 looms; *Cul3*$^{+/-}$, 12.9 looms, p = 0.023). p-values are Wilcoxon's ranked-sum test. Box-and-whisker plots show median, IQR and range. Number of animals: *Setd5*$^{+/+}$, n = 14; *Setd5*$^{+/-}$, n = 14; *Cul3*$^{+/+}$, n = 10; *Cul3*$^{+/-}$, n =10; *Ptchd1*$^{Y/+}$, n = 9; *Ptchd1*$^{Y/-}$, n = 9 for all plots. Plotted points represent the average variable value across all escape trials for individual animals.

Further analysis of the exploration strategies of the animals across days revealed a significant drop in exploration by all animals following the initial exposure to the looming stimulus, as demonstrated by the drop in shelter exits (Fig. 4.4a-c) distance travelled (Fig. 4.4d-f) and exit duration (Fig. 4.4g-i) across all models from Day 0 to Day 1. In general, these values remained relatively stable and didn't return to the naive levels observed during the acclimatisation period. This implies that in all animals, repeated exposure to the looming stimulus has long term effects on exploratory behaviour.

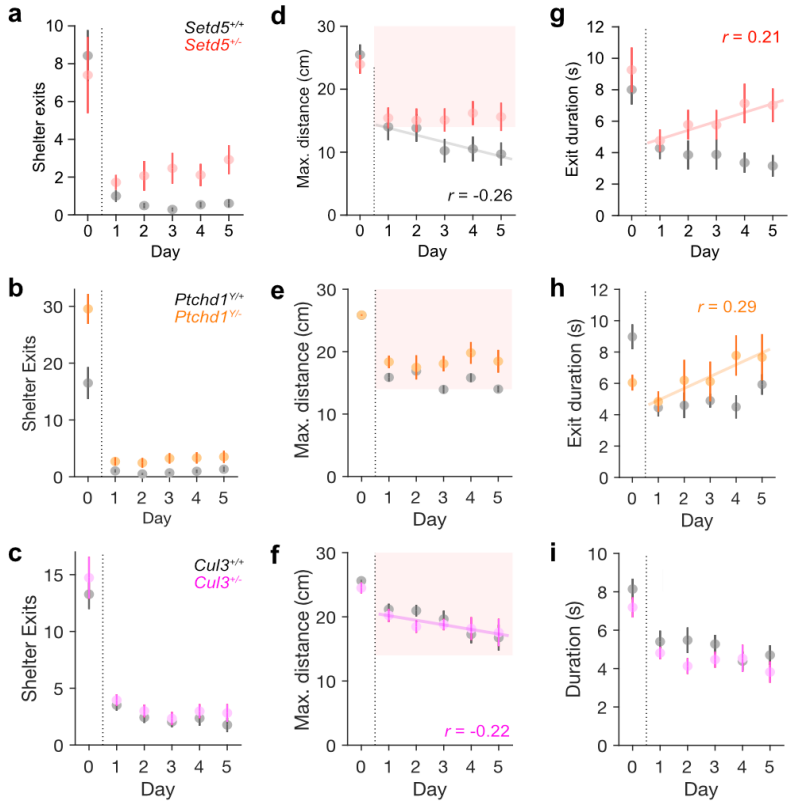

Figure 4.4 Exploration strategies of wild-type and mutant animals across days - both before (Day 0) and after (Days 1-5) threat exposure.

Adaptation in exploratory shelter exits, average maximum distance during exploratory bouts and shelter exit duration across days. **a**-**c**, Correlation between the number of shelter exits and the day, for days after loom exposure, assessed by a Pearson's correlation analysis. **a**, *Setd5*$^{+/+}$: p = 0.219, *Setd5*$^{+/-}$: p = 0.497; **b**, *Ptchd1*$^{Y/+}$, **p** = 0.135; *Ptchd1*$^{Y/-}$, p = 0.194; **c**, *Cul3*$^{+/+}$, p = 0.289; *Cul3*$^{+/-}$, p = 0.125. **d**-**f**, Correlation between the maximum distance travelled during a shelter exit and the day, for days after loom exposure, assessed by a Pearson's correlation analysis. **d**, *Setd5*$^{+/+}$: r = -0.26, p = 0.037, *Setd5*$^{+/-}$: p = 0.792; **e**, *Ptchd1*$^{Y/+}$, p = 0.135; *Ptchd1*$^{Y/-}$, p = 0.194; **f**, *Cul3*$^{+/+}$, p = 0.480; *Cul3*$^{+/-}$, r = -0.08, p = 0.034. Shaded areas in **d**-**f** represent the threat zone. **g**-**i**, Correlation between the average exit duration and the day, for days after loom exposure, assessed by a Pearson's correlation analysis. **g**, *Setd5*$^{+/+}$: p = 0.497, *Setd5*$^{+/-}$: r = 0.21, p = 0.019; **h**, *Ptchd1*$^{Y/+}$, p = 0.214; *Ptchd1*$^{Y/-}$, r = 0.29, p = 0.002; **i**, *Cul3*$^{+/+}$, p = 0.755; *Cul3*$^{+/-}$, p = 0.393. Trend lines are only drawn for significant correlations. Number of animals: *Setd5*$^{+/+}$, n = 14; *Setd5*$^{+/-}$, n = 14; *Cul3*$^{+/+}$, n = 10; *Cul3*$^{+/-}$, n =10; *Ptchd1*$^{Y/+}$, n = 9; *Ptchd1*$^{Y/-}$, n = 9 for all plots.

All wild-type animals exhibited experience-dependent reductions in their exploration, as expected and reflective of the aforementioned sensitisation to high contrast, highly-threatening, visual stimuli previously reported (Evans 2017); staying closer, making fewer exits and staying outside the shelter for a shorter period than during the pre-stimulus exploration time. Sensitisation was clearly seen in the behaviour of the *Setd5*$^{+/+}$ animals in particular, with the different exploratory behavioural parameters all showing negative trends across the test days. The exit distance in particular showed a significant negative correlation (r = -0.26, p = 0.037, Pearson's r) across days indicative of the development of place aversion towards the threat zone.

Both *Setd5*$^{+/-}$ and *Ptchd1*$^{Y/-}$ animals on the other hand, despite showing an initial drop in exploration on the first day of exposure, showed no signs of sensitisation to the looming stimulus. By contrast, over subsequent days both mutant models started showing adaptation to the stimulus; incrementally increasing their levels of exploration (Fig. 4.4a,b) and increasing the time they spent outside the shelter before returning to safety (Fig. 4.4g, *Setd5*$^{+/-}$, r = 0.21, p = 0.019; h, *Ptchd1*$^{Y/-}$, *r* = 0.29, p = 0.002). It is not clear whether the renewed exploration in the *Setd5*$^{+/-}$ and *Ptchd1*$^{Y/-}$ animals is indicative of repetitive motor behaviours, similar to those described in autistic individuals, or a perceived reduction in threat level of the looming stimulus. Interestingly, in a place avoidance paradigm, it was previously shown that *Setd5*$^{+/-}$ animals did not form the typical place avoidance to a particular food port that generates a typically aversive air puff (Deliu et al. 2018). Suggesting the possibility that the threat valence, and hence the perceived threat level, of sensory stimuli are weighted differently in *Setd5*$^{+/-}$ as opposed to their wildtype siblings. *Cul3*$^{+/-}$ animals did not show similar increases in arena exploration across days. Instead their exploratory behaviour during the loom trials was a lot more similar to that of the three wild-type cohorts. Their exploration remained low and they also showed increasing place aversion to the threat zone by reducing the maximum distance from the shelter that they would cover across days (Fig. 4.4f, *Cul3*$^{+/-}$, *r* = -0.22, p = 0.034, Pearson's *r*).

4.2 Response adaptation across repeated presentations of the looming stimulus

It was previously reported that repeated exposure to a series of looming stimuli modulates the kinetics of the escape response elicited by a subsequent looming stimulus. The use of multiple high contrast stimuli shortly before testing the LAR resulted in sensitisation of the escape response, with faster reaction times and more vigorous escape speeds (Evans 2017). Whereas, the presentation of multiple looming stimuli of low or variable contrast led to slower reaction times, lower escape probabilities and less vigorous escape speeds to subsequent high contrast stimuli (Evans 2017; Lenzi et al. 2022). We were interested in investigating whether this adaptive process also occurred over the longer timescales used in this paradigm, and whether both wild-type and mutants would exhibit the same adaptation dynamics. To assess this, we analysed the total looms triggered, the average reaction time and average maximum escape speed reached for each animal per day.

Looking across all days, all mutant models consistently triggered more looms (Fig. 4.5a-c), took longer to react to the stimulus (Fig. 4.5d-f) and reached slower maximum escape speeds (Fig. 4.5g-i) than their wild-type littermates. Both the *Setd5*$^{+/-}$ and *Ptchd1*$^{Y/-}$ animals increased the number of looming stimuli they triggered over subsequent days, in line with their successive uptake in exploration (Fig. 4.4). Additionally, both models exhibited strong adaptation to their escape responses as evidenced by the significant trend in the extension of their reaction times across test days (Fig. 4.5d, *Setd5*$^{+/-}$, *r* = 0.26, p < 0.001; e, *Ptchd1*$^{Y/-}$, *r* = 0.32, p < 0.001). The maximum escape speed in *Setd5*$^{+/-}$ mice also showed a significant negative correlation with test day (Fig. 4.5g, *Setd5*$^{+/-}$, *r* = -0.22, p = 0.002), while the maximum speed reached by *Ptchd1*$^{Y/-}$

mice remained relatively stable across days (Fig. 4.5h). *Cul3*$^{+/-}$ animals showed consistently slower reaction times and maximum speeds compared to their wild-type siblings; these parameters did not change across testing days as in the other two models. Interestingly, the *Cul3* wild-type cohort also exhibited adaptation of their escape response across days (Fig. 4.5f, reaction time, *Cul3*$^{+/+}$, $r = 0.31$, p = 0.012; i, maximum speed, *Cul3*$^{+/+}$, $r = -0.27$, p = 0.034), even so, their reaction time and escape vigour remained faster and more vigorous than their *Cul3*$^{+/-}$ siblings even on the last day of testing . The kinetics of the escape responses of the *Setd5*$^{+/+}$ and *Ptchd1*$^{Y/+}$ animals were consistently fast across days however and showed no sign of adaptation.

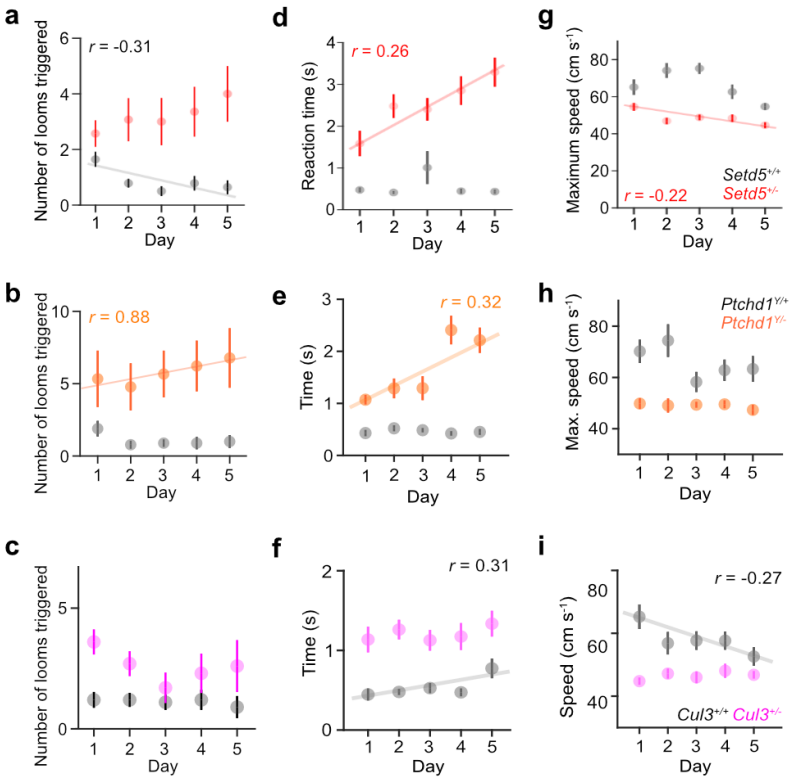

Figure 4.5 Altered escape response adaptation in mutant animals.

a-**c**, Correlation between the number of looms triggered and test day, assessed by a Pearson's correlation analysis. **a**, *Setd5*$^{+/+}$: r = -0.31, $p = 0.009$; *Setd5*$^{+/-}$: $p = 0.219$; **b**, *Ptchd1*$^{Y/+}$, $p = 0.305$; *Ptchd1*$^{Y/-}$, r = 0.88, $p = 0.047$; **c**, *Cul3*$^{+/+}$, $p = 0.068$; *Cul3*$^{+/-}$, $p = 0.379$. **d**-**f**, Correlation between the average reaction time and test day, assessed by a Pearson's correlation analysis. **d**, *Setd5*$^{+/+}$: $p = 0.890$, *Setd5*$^{+/-}$: r = 0.26, $p = 0.001$; **e**, *Ptchd1*$^{Y/+}$, $p = 0.841$; *Ptchd1*$^{Y/-}$, r = 0.32, $p = 0.001$; **f**, *Cul3*$^{+/+}$, r = 0.31, $p = 0.012$; *Cul3*$^{+/-}$, $p = 0.233$. **g**-**i**, Correlation between the average maximum escape speed and test day, assessed by a Pearson's correlation analysis. **g**, *Setd5*$^{+/+}$: $p = 0.121$, *Setd5*$^{+/-}$: r = -0.22, $p = 0.002$; **h**, *Ptchd1*$^{Y/+}$, $p = 0.078$; *Ptchd1*$^{Y/-}$, $p = 0.557$; **i**, *Cul3*$^{+/+}$, r = -0.27, $p = 0.034$; *Cul3*$^{+/-}$, $p = 0.171$. Trend lines are only drawn for significant correlations. Number of animals: *Setd5*$^{+/+}$, n = 14; *Setd5*$^{+/-}$, n = 14; *Cul3*$^{+/+}$, n = 10; *Cul3*$^{+/-}$, n =10; *Ptchd1*$^{Y/+}$, n = 9; *Ptchd1*$^{Y/-}$, n = 9 for all plots.

Similar to our investigation into the correlation between the ability of individual animals to generate directed escape trajectories and the average escape response variables of those animals (Fig. 3.13), we were interested in understanding if the variation in the average reaction time

and escape vigour of animals was linked to the development of place avoidance in these animals. To investigate this, we analysed the correlation between the total number of shelter exits made per animal across all five days of testing and their average reaction time and maximum escape speed. We discovered a strong correlation between the total number of exits and reaction time (Fig. 4.6a, *Setd5*$^{+/-}$, $r = 0.76$, $p = 0.002$; c, *Ptchd1*$^{Y/-}$, $r = 0.79$, $p = 0.012$, Pearson's r) for both the *Setd5*$^{+/-}$ and *Ptchd1*$^{Y/-}$ animals, indicating that the animals that had the greatest exploratory drive or weakest aversion to the threat zone, were the slowest in generating an escape response to the stimulus. A negative correlation was observed between this exploratory behaviour and the maximum escape speed reached for *Ptchd1*$^{Y/-}$ animals too (Fig. 4.6d, *Ptchd1*$^{Y/-}$, $r = -0.89$, $p = 0.006$). No correlation was observed between exploratory activity and reaction variables in the *Cul3*$^{+/-}$ animals, nor in any of the wild-type animals.

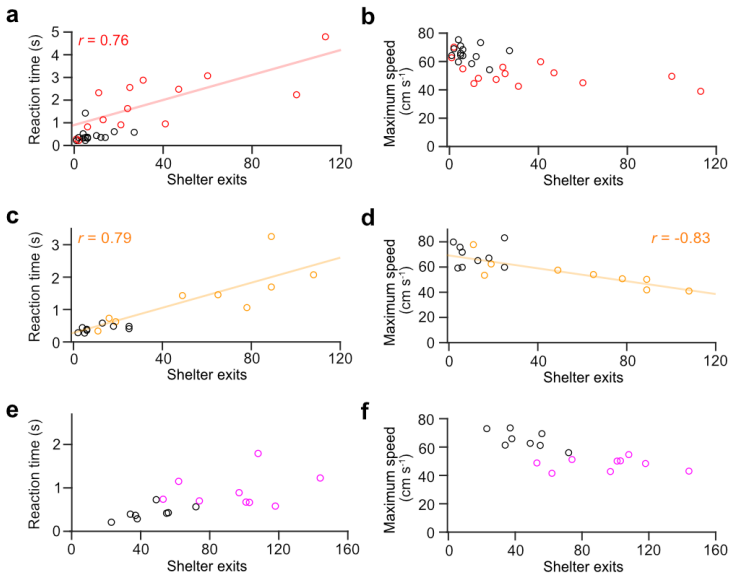

Figure 4.6 Relationship between the total shelter exits made versus the average reaction time per animal.

Relationship between the number of shelter exits and the average reaction time per animal, analysed by Pearson's correlation (**a**, *Setd5*$^{+/+}$, $p = 0.626$; *Setd5*$^{+/-}$, $r = 0.76$, $p = 0.002$; **c**, *Ptchd1*$^{Y/+}$, $p = 0.126$; *Ptchd1*$^{Y/-}$, $r = 0.76$, $p = 0.012$; **e**, *Cul3*$^{+/+}$, $p = 0.078$; *Cul3*$^{+/-}$, $r = 0.76$, $p = 0.571$). Relationship between the number of shelter exits and the maximum escape speed per animal, analysed by Pearson's correlation (**b**, *Setd5*$^{+/+}$, $p = 0.547$; *Setd5*$^{+/-}$, $p = 0.053$; **d**, *Ptchd1*$^{Y/+}$, $p = 0.963$; *Ptchd1*$^{Y/-}$, $r = -0.83$, $p = 0.006$; **f**, *Cul3*$^{+/+}$, $p = 0.069$; *Cul3*$^{+/-}$, $r = 0.76$, $p = 0.977$). Trend lines are only drawn for significant correlations. Number of animals: *Setd5*$^{+/+}$, n = 14; *Setd5*$^{+/-}$, n = 14; *Cul3*$^{+/+}$, n = 10; *Cul3*$^{+/-}$, n =10; *Ptchd1*$^{Y/+}$, n = 9; *Ptchd1*$^{Y/-}$, n = 9 for all plots.

4.3 Response adaptation in the presence of a reward

The decision to generate an escape response is necessarily based upon a trade off between competing behaviours - namely, a behaviour that minimises the potential harm inflicted upon the individual and a behaviour that could result in potential gain through the acquisition of resources (Ydenberg and Dill 1986). Previous studies have used the presence of neutral objects, such as empty petri dishes, located within the threat zone of the arena to encourage exploration from the animals (Evans et al. 2018). However, how the presence of a rewarding stimulus

would impact defensive responses is not well understood. We attempted to investigate if a food reward, located within the threat zone of the arena, would result in delayed reaction times to the stimulus since it presented a new, and potentially more appealing, competing behaviour from which to choose.

Animals were introduced to the presence, and location, of the food reward at the end of the fourth day of testing. The animals were allowed to explore the environment, and to retrieve the food reward, without triggering any looming stimuli. For some animals it took a while to overcome the place aversion they had developed for the threat zone, with many generating spontaneous escapes back to the shelter in absence of any looming stimulus (data not shown). However, eventually all mice retrieved the food reward and the mouse and the reward were both placed back into their home cages overnight. The mice were then tested the next day and once again presented with the food reward in the far corner of the arena. During these 'reward trials' we observed that some of the wild-type animals were sufficiently interested in the food reward to attempt to retrieve it, making targeted trajectories across the arena in the direction of the reward. Upon activation of the looming stimulus, however, the *Setd5*$^{+/+}$ and *Cul3*$^{+/+}$ mice rapidly evoked an escape response and did not make another attempt to retrieve the reward within the time limit of the trial (3 minutes). The *Ptchd1*$^{Y/+}$ animals on the other hand did generate several, targeted attempts, all of which resulted in escapes back to the shelter. The reaction time of the escapes of these animals were positively correlated with the loom presentation, indicating a rapid adaptation to the looming stimulus when in the presence of a reward (Fig. 4.7hi, *Ptchd1*$^{Y/+}$, $r = 0.81$, $p = 0.002$). It must be noted that fewer *Ptchd1* animals were tested in these experiments and repetition of these experiments with this model would be useful. For both the *Setd5*$^{+/+}$ and *Cul3*$^{+/+}$ animals, only one or two looming stimuli were triggered in the presence of the reward, so it was not possible to investigate any potential effect of the reward's presence on adaptation to the stimulus.

Almost all *Setd5*$^{+/-}$, *Ptchd1*$^{Y/-}$ and *Cul3*$^{+/-}$ mice made multiple attempts to retrieve the reward. They exited the shelter more often and were more likely to leave the shelter again after having re-entered after an escape response. Whilst the outward trajectories of the mutant animals were almost always directed towards the reward, their escape trajectories often included exploratory steps in the direction of the reward, after arresting in response to the onset of the stimulus (Fig. 4.7a,e,i). Since multiple mice made many attempts to retrieve the reward, we were able to investigate the adaptation of the escape kinetics in response to repeated presentations of the stimulus in quick succession. The reaction time of the *Setd5*$^{+/-}$ mice was similar, but shifted in scale, to that observed in the *Ptchd1*$^{Y/+}$ mice (Fig. 4.7dii, *Setd5*$^{+/-}$, $r = 0.83$, $p < 0.001$, Pearson's *r*), with the time to react to the looming stimulus slowing, on average, with each successive presentation. Both *Ptchd1*$^{Y/-}$ and *Cul3*$^{+/-}$ animals also showed a trend towards increasing reaction times with repeated presentations, but these results were not significant. The maximum speed generated in the escape remained constant across presentations for both *Setd5*$^{+/-}$ and *Cul3*$^{+/-}$ but decreased for the *Ptchd1*$^{Y/-}$ mice (Fig. 4.7hii, *Ptchd1*$^{Y/-}$, $r = -0.72$, $p = 0.004$). Similar to the trends in exploratory behaviour and reaction kinetics discussed above, the *Cul3*$^{+/-}$ showed a weaker phenotype to the *Setd5*$^{+/-}$ and *Ptchd1*$^{Y/-}$ models, making fewer attempts and showing less adaptation over time (Fig. 4.7i-l).

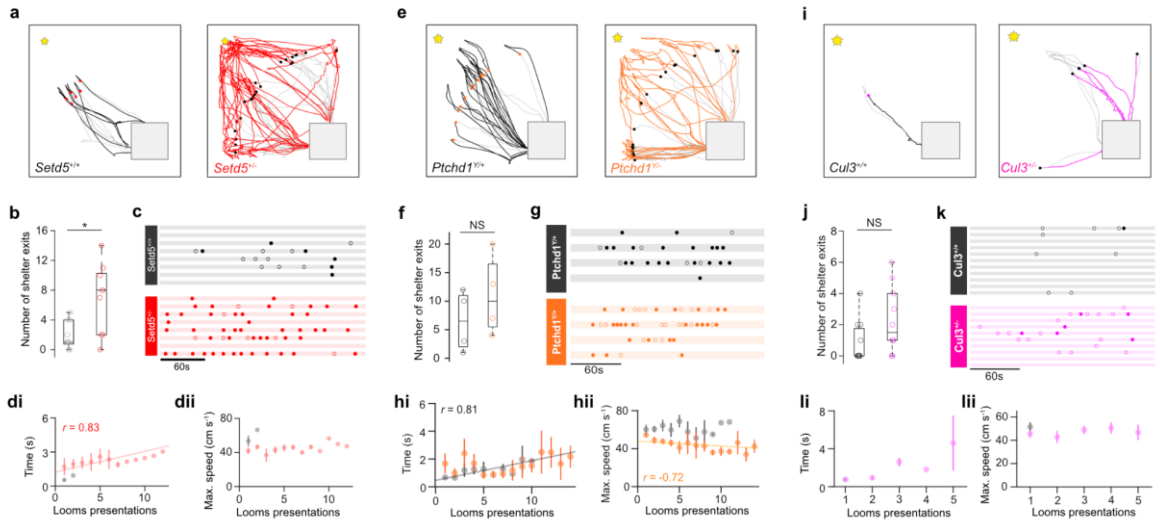

Figure 4.7 Escape response to *Setd5*, *Ptchd1* and *Cul3* mice to the looming stimulus in the presence of a food reward.

Example trajectories during the reward trials showing the position of the mouse for the 3 s before triggering the loom (light grey) and for the 6 s following the stimulus start (coloured) for *Setd5* (**a**), *Ptchd1* (**e**) and *Cul3* (**i**). Filled dots represent the position of the mouse when the stimulus was triggered, grey square is the shelter, the yellow star shows the position of the food reward. **b**, Number of shelter exits per animal (*Setd5*$^{+/+}$, n = 8, 2.12 exits; *Setd5*$^{+/-}$, n = 8, 6.88 exits, $p = 0.047$). **c**, Ethogram of shelter exits during reward trials. Each row presents the trial of a single animal, filled and open dots represent exits into the threat zone or not, respectively. **di**, Reaction time (*Setd5*$^{+/-}$, 44 trials, r = 0.83, $p = 0.0001$). **dii**, escape vigour (*Setd5*$^{+/-}$, 44 trials, $p = 0.5116$) during repeated presentations of the loom. Trials when the animal was interacting with the reward were excluded. **f**, Number of shelter exits per animal (*Ptchd1*$^{Y/+}$, n = 4, 5.75 exits; *Ptchd1*$^{Y/-}$, n = 4, 9.75 exits, $p = 0.314$). **g**, as for **c** but for *Ptchd1* animals. **hi**, Reaction time (*Ptchd1*$^{Y/+}$, r = 0.815, $p = 0.002$; *Ptchd1*$^{Y/-}$, $p = 0.167$). **hii**, escape vigour (*Ptchd1*$^{Y/+}$, $p = 0.801$; *Ptchd1*$^{Y/-}$, r = -0.72, $p = 0.004$) during repeated presentations of the loom. **j**, Number of shelter exits per animal (*Cul3*$^{+/+}$, n = 11, 0.40 exits; *Cul3*$^{+/-}$, n = 11, 1.27 exits, $p = 0.501$). **k**, as for **c** but for *Cul3* animals. **li**, Reaction time (*Cul3*$^{+/-}$, p = 0.057). **lii**, escape vigour (*Cul3*$^{+/-}$, p = 0.343) during repeated presentations of the loom. Trials when the animal was interacting with the reward were excluded. Box-and-whisker plots show median, IQR and range. Error Bars represent the SEM. Trend lines are only drawn for significant correlations.

4.4 Learned suppression of escape

In the wild, while it is generally a better survival strategy to respond to all potential threats, performing an escape behaviour is an energetically expensive behaviour, and perhaps more importantly, prohibits the individual from engaging in other behaviours such as foraging, caring for young or defending territory that are of significant survival importance. For this reason, it is beneficial for an animal to learn to distinguish stimuli that, although they might appear to be potential threats, frequently do not lead to harm and suppress their innate defensive responses - a behaviour that has been described as 'learned suppression of escape (LSE)' (Fig. 4.8a, Lenzi et al. 2022). In the earlier parts of this chapter we observed that while the wild-type animals from our three models showed the typical sensitisation to the looming stimulus across repeated loom presentations (Evans 2017), the mutant animals from the Setd5 and Ptchd1 models did not (Fig. 4.5). In these experiments, the animals were exposed to sparse looming

stimuli across multiple days. We wondered whether enforced (exposure without the presence of a shelter), repeated exposure to the looming stimuli would lead to a suppression of the LAR in both the wild-type and mutant animals, and if so, how these adaptive responses of the wild-type animals might compare to the responses of the mutant animals at baseline. We chose to specifically investigate this effect in the *Setd5* model since these animals demonstrated the strongest sensitisation (in *Setd5*$^{+/+}$) and adaptation (in *Setd5*$^{+/-}$) in their LAR over days.

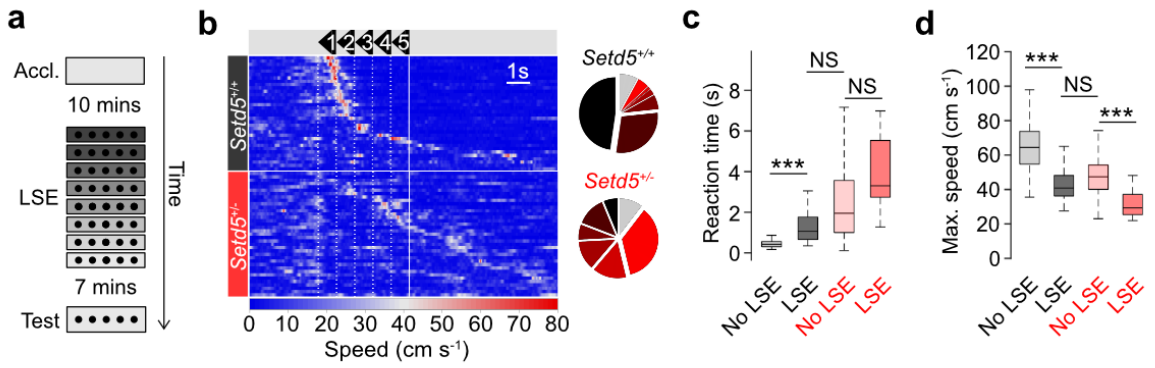

Figure 4.8 Adaptation in the generation of escape responses after rapid exposure to multiple looms in both *Setd5*$^{+/+}$ and *Setd5*$^{+/-}$ mice.

a, Learned suppression of escape (LSE) paradigm. **b**, Left, raster plot of mouse speed to the loom stimulus, as in Fig. 1.2 but after LSE. Right, proportion of trials where the mice respond within 1 of the 5-loom stimuli, after the 5th, or not at all in *Setd5*$^{+/+}$ (above) and *Setd5*$^{+/-}$ (below). **c**, LSE results in slower reaction times in *Setd5*$^{+/+}$ ($P < 0.001$, Kruskal-Wallis (K-W) test), comparable to that of *Setd5*$^{+/-}$ before LSE ($P = 0.319$, K-W test). LSE does not cause a significant change in the reaction time of *Setd5*$^{+/-}$ mice ($P = 0.082$, K-W test). **d**, LSE results in slower maximum speeds in both genotypes (*Setd5*$^{+/+}$, $P < 0.001$; *Setd5*$^{+/-}$, $P < 0.001$, K-W test). Max. speed after LSE in *Setd5*$^{+/+}$ is comparable to that of *Setd5*$^{+/-}$ before LSE ($P = 0.386$, K-W test). Box-and-whisker plots show median, IQR and range. Error Bars represent the SEM.

Following rapid exposure to multiple visual looms of increasing contrast we observed a progressive weakening in the escape responses generated by both *Setd5*$^{+/+}$ and *Setd5*$^{+/-}$ to subsequent stimulus presentations (Fig. 4.8). *Setd5*$^{+/+}$ animals became significantly slower in generating their escape response to the looming stimulus (Fig. 4.8c, *Setd5*$^{+/+}$ before LSE, 0.51s; *Setd5*$^{+/+}$ after LSE, 1.74s, $p < 0.001$, Kruskal-Wallis (KW) test with Dunn-sidak correction for multiple comparisons) and were statistically indistinguishable from the *Setd5*$^{+/-}$ mice before LSE conditioning (*Setd5*$^{+/-}$ before LSE, 2.56s, comparison with *Setd5*$^{+/+}$ after LSE, $p = 0.319$). The same trend was observed in the maximum speed of the escape responses generated by *Setd5*$^{+/+}$ and *Setd5*$^{+/-}$ before and after LSE (Fig. 4.8d, *Setd5*$^{+/+}$ before LSE, 65.9 cms^{-1}; *Setd5*$^{+/+}$ after LSE, 43.8cms^{-1}, $p < 0.001$; *Setd5*$^{+/-}$ before LSE, 48.3cms^{-1}, comparison with *Setd5*$^{+/+}$ after LSE, $p = 0.386$). *Setd5*$^{+/-}$ animals showed a non-significant trend towards slower reaction times after LSE conditioning and had significantly slower maximum escape speeds (*Setd5*$^{+/-}$ before LSE, 48.3cms^{-1}; *Setd5*$^{+/-}$ after LSE, 31.3cms^{-1}, $p < 0.001$). Intriguingly, these results suggest that the delayed responses observed in the *Setd5*$^{+/-}$ animals to high contrast stimuli with no or limited exposure to the looming stimulus are comparable to the responses observed in *Setd5*$^{+/+}$ animals after an intense adaptation conditioning protocol. This raises the possibility that the altered escape dynamics observed in the *Setd5*$^{+/-}$ animals at baseline could originate from a

misregulation of the mechanisms controlling the flexible expression of this behaviour in wild-types.

4.5 Summary

In this chapter, we investigated how the both natural, exploratory behaviour and stimulus-evoked escape responses adapt after exposure to a visual threat in both wild-type and mice haploinsufficient for autism-risk genes. We were able to extend our knowledge of the short-term sensitisation of escape behaviour in wild-type animals to longer periods of time, spanning multiple days. We showed that these mechanics of adaptation are different in our three mutant mouse models, with reduced formation of a conditioned place aversion, and even adaptation of the escape response in two of the three models (*Setd5*$^{+/-}$ and *Ptchd1*$^{Y/-}$). Additional experiments investigating the short-term adaptation of the LAR in these animals revealed the incredible robustness with which *Setd5*$^{+/-}$ and *Ptchd1*$^{Y/-}$ will generate escape responses in rapid succession with minimal adaptation, and continue to explore an arena when the motivation of an edible reward is present. Finally, by observing similarly delayed escape response in the wild-type animals conditioned to the looming stimulus we hypothesised that the behavioural differences observed in our mutant animals may arise from impairments in the neural circuits responsible for flexibly controlling this critical defensive behaviour.

Preface to chapters 5,6 & 7

The recent advancement in our understanding of the brain circuits responsible for the initiation and the control of visually-evoked defensive behaviours in rodents (See Chapter 1.3) presented us with the unprecedented opportunity to systematically dissect where along this defined neural axis differences could be emerging in our mutant animals. This rich characterisation provided us with a circuit-level framework upon which to select candidate brain loci that are functionally linked to distinct components of this rapid perceptual decision-making process. Given the strong behavioural phenotype and our greater knowledge of the molecular consequences of the genetic mutation, we decided to focus the majority of our circuit-level investigation on the *Setd5* model, however, where possible we attempted to corroborate our findings in the other two models, *Ptchd1* and *Cul3*.

The next three chapters contain the results from experiments that focus on understanding how three distinct 'checkpoints' along this neural pathway function in both our wild-type and mutant animals. In successive steps, we set out to investigate visual processing within the superficial superior colliculus (**Chapter 5**), sensorimotor transformations in the deep layers of the superior colliculus (**Chapter 6**) and the properties of the action initiation cells within the dorsal periaqueductal grey (**Chapter 7**). It was hoped that this systematic approach would facilitate the isolation of the locus, or loci, of disruption in this well-characterised subcortical neural pathway, that could potentially explain the behavioural differences observed in the chapters above.

5 Checkpoint 1: Visual processing in the superior colliculus

The superior colliculus is a highly-evolutionarily conserved midbrain region that is thought to be the main visual-processing centre in rodents and is strongly linked to subconscious visual behaviours in both rodents and humans. Its critical, and necessary, role in mediating defensive behavioural responses to the innately aversive visual looming stimulus has been well described (Westby et al. 1990; Shang et al. 2015, 2018; Evans et al. 2018). The superior colliculus formed an intriguing candidate for the behavioural effects observed in our *Setd5*$^{+/-}$ mice in response to the looming stimulus for several reasons that we expanded on in detail in Chapter 1 but will be summarised briefly here. Firstly, the *Setd5*$^{+/-}$ animals were previously characterised to have a misregulation in a number of genes linked to eye development. If the genetic mutation was affecting the development and subsequent function of the primary sense organ for receiving visual information then these differences should be obvious in this dominant retinorecipient area. Secondly, the SC has been strongly linked to subconscious visual processing of both salient and emotional stimuli in humans. Lastly, the SC has a well-established role in controlling gaze and visual attention, processes that are commonly impaired in autistic individuals and often used for early diagnosis of the condition. For these reasons we wanted to assess if visual response properties remained intact in the SC of *Setd5*$^{+/-}$ animals.

5.1 General properties of recorded cells

The first feature of visual processing we investigated within the SC was the baseline level of activity present in the absence of a visual stimulus. We found that, when observing a grey screen of equal luminance, neurons from across the recorded depths of the SC (0 to -1000um) in *Setd5*$^{+/+}$ and *Setd5*$^{+/-}$ animals had comparable maximum (Fig. 5.1b) and average firing rates (Fig. 5.1c).

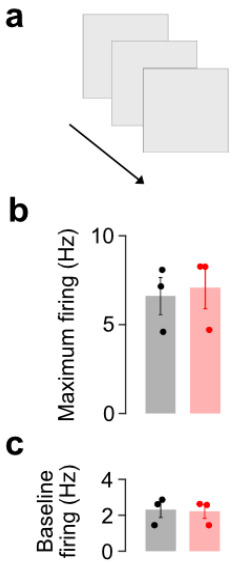

Figure 5.1 Baseline firing properties of SC neurons to a grey screen.

a, Schematic of the full-field grey screen stimulus presented at baseline. **b**, Average maximum firing rate (*Setd5*$^{+/+}$, n = 3, 323 units, 6.61 Hz; *Setd5*$^{+/-}$, n = 3, 479 units, 7.08 Hz, p = 0.781, two-sample Wilcoxon's ranked-sum test). **c**, Average firing rate (*Setd5*$^{+/+}$, n = 3, 2.31 Hz; *Setd5*$^{+/-}$, n = 3, 2.22 Hz, p = 0.880, two-sample Wilcoxon's ranked-sum test). Filled circles represent individual animals. Error bars are SEM.

5.2 Receptive fields from a full field shifting white noise stimulus

The visual receptive field (RF) of a neuron refers to the specific properties of light that reliably elicits the greatest change in activity of the cell. The RF is often described by both the location of the stimulus within the visual space and the specific features of the light present. The receptive field properties of a cell critically rely upon the connections and interactions between cells along the visual processing pathways. These properties are often thought to be inherited from, and emerge from the combination of, the cells from which the neuron of interest receives its visual input from. Within the SC, most cells within the sSC receive direct input from ~6 retinal ganglion cells (Chandrasekaran et al. 2007). Altered visual response properties in the earliest levels of the visual processing pathways will have cascading effects on downstream recipient targets. We hoped that by intercepting the flow of visual information within the SC and characterising visual responses *in situ*, we would be able to infer if the visual information being received from the retina, or the sensitivity of the RGC targets within the SC are impacted by the genetic mutation.

For each SC unit isolated from the extracellular recordings, we computed a spike-triggered average of the response of each cell to a full-field, shifting white noise stimulus (Fig. 5.2a). In order to quantitatively assess visual responsiveness, we generated a metric which generated a 'peak-to-noise' (P2N) value for each of the units. Briefly, this metric fitted a gaussian fit to the centre of the STA and compared the variance of this area with the variance in the outer boundary of the 2D array. After calculating this value for all units, from all animals, we defined visually-responsive (VR) units as those with P2N values in the 80th percentiles or above (Fig. 5.2c, top panel). Reassigning the units to each animal we found no difference in the proportion of VR SC units between *Setd5*$^{+/+}$ and *Setd5*$^{+/-}$ (Fig. 5.2b). We could also use these values to confirm the validity of our alignment of the position of the probe within the SC. By plotting the P2N value against the depth from the inflection depth (ID) found using current source density (CSD) analysis we could observe a clear clustering of cells with high P2N values within the 300 μm above and 50 μm below this depth, in line with previous characterisations (Stitt et al. 2013; Ito et al. 2017). We were able to do this for all the cells together (Fig. 5.2c) and sorted by animal (Fig. 5.2d).

The features of the visual space that drive a cell to respond can be analysed both in space and across time. 2D spatial receptive fields (Fig. 5.2g) were generated by reverse correlating the presented chequered images with the recorded neuron's spiking activity. The features of these spatial receptive fields could then be analysed to cluster the different RFs into functional groups. Units that showed the strongest change in activity to decreases in light levels were classified as 'OFF' RFs, whereas units that responded preferentially to increases in light were classified as 'ON' RFs. We observed a predominant proportion of OFF-centre RFs in both

Setd5$^{+/+}$ and *Setd5*$^{+/-}$ animals (Fig. 5.2e), in line with previous reports (Wang et al. 2010; Franceschi and Solomon 2018). When comparing the width of these RF centres, we found no difference between the average width in either genotype (Fig. 5.2f). Although uniphasic ON-centre cells were found in much lower numbers for both genotypes, the majority of cells that were classified as 'OFF-centre' RFs from their spatial RFs had biphasic ON-OFF profiles in their temporal RFs (Fig. 5.2h) indicating that they generated the strongest response to an decrease in light preceded by an increase in light. Preferences for the temporal presentation of light stimuli were analysed by clustering all temporal RFs together using a k-means analysis and investigating the proportion of each cluster that originates from each genotype (Fig. 5.2h,i). Using this method, five distinct clusters of unipolar ON and OFF cells, biphasic ON-OFF cells and cells with unclear temporal RF properties. All five clusters were found in both *Setd5*$^{+/+}$ and *Setd5*$^{+/-}$ recordings and showed largely overlapping response profiles (Fig.5.2i).

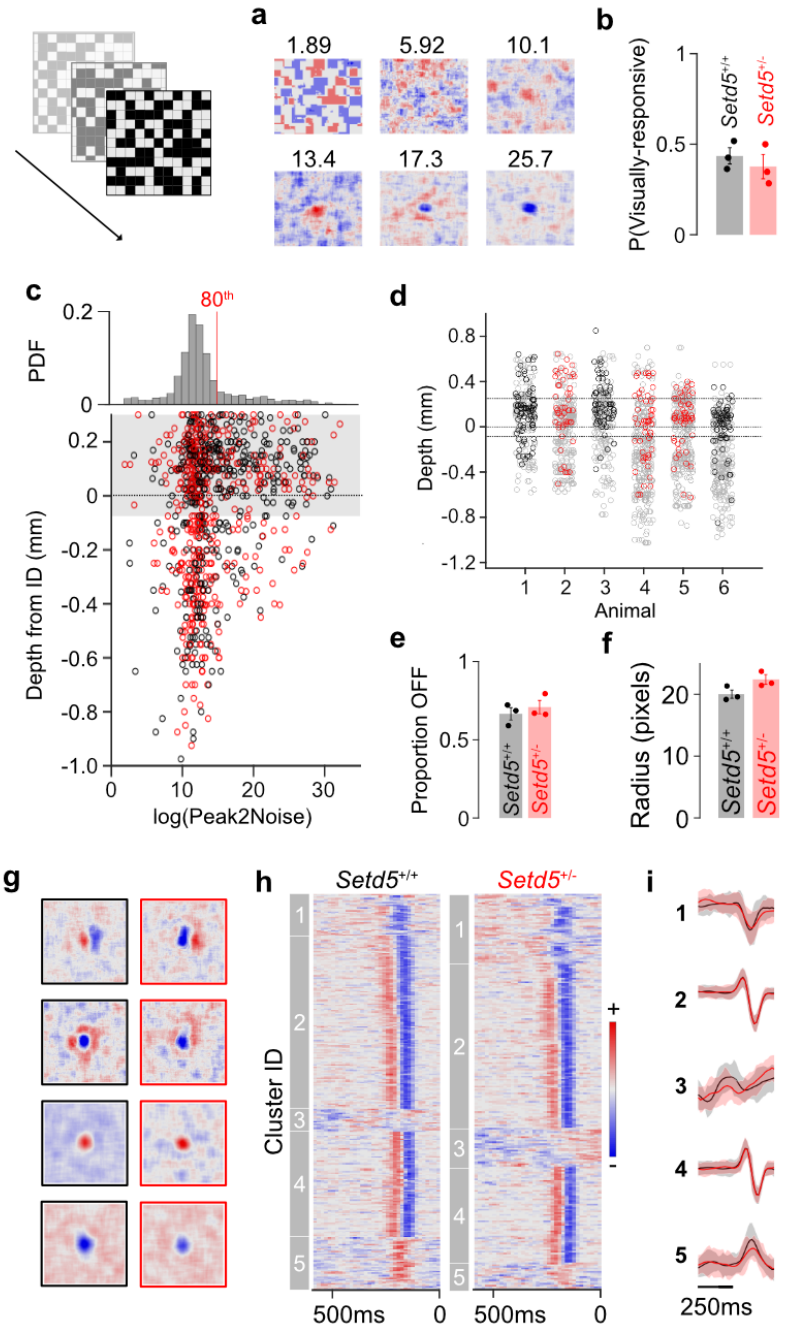

Figure 5.2 Visual response properties of SC neurons to a shifting white noise stimulus.

a, Example spatial receptive fields at different log(PeaktoNoise) values. **b**, Proportion of visually responsive neurons in the sSC (*Setd5*$^{+/+}$, n = 3, 0.4359; *Setd5*$^{+/-}$, n = 3, 0.3666, p = 0.400). **c**, Top, Distribution of log(PeaktoNoise) values of all cells. Red line indicates the 80th percentile. Below, Scatter plot of the log(PeaktoNoise) values of each recorded unit and its depth from the inflection depth (ID) found using a current source density (CSD) analysis. *Setd5*$^{+/+}$ units are in black, *Setd5*$^{+/-}$ units are in red, the grey shaded area represents the depths corresponding to the sSC. **d**, the depth of each recorded unit per animal. Non-visually responsive units are light grey, visually-responsive units are red (*Setd5*$^{+/-}$) and black (*Setd5*$^{+/+}$). **e**, Proportion of visually-responsive neurons in the superficial SC (sSC) that are OFF-centres (*Setd5*$^{+/+}$, 0.679; *Setd5*$^{+/-}$, 0.738, p = 0.700). **f**, Radius of OFF-centre cells in sSC (*Setd5*$^{+/+}$, 20.2 pixels; *Setd5*$^{+/-}$, 22.4 pixels, p = 0.100). **g**, Representative spatial receptive fields of *Setd5*$^{+/+}$ (left) and *Setd5*$^{+/-}$ (right), red areas indicate positive values and blue negative values. **h**, Temporal receptive fields of visually-responsive cells in *Setd5*$^{+/+}$ (left, n = 157) and *Setd5*$^{+/-}$ (right, n = 106) grouped by cluster

membership, as determined by k means (Distribution of clusters, $p = 0.9545$, two-sample Kolmogorov-Smirnov test). **i**, Mean of the temporal RFs in each cluster. Shaded areas and error bars represent the SEM.

5.3 Pupil dynamics and full field light responses

After characterising the individual response profiles of the recorded units from each genotype, we were interested to investigate if there were differences in the responses of these units to global changes in luminance, irrespective of the position of their RFs in space. To do this, we recorded responses to repeating sequences of 1s ON - 1s OFF flash stimuli and quantified a metric of responsivity using a previously published method (Montijn et al. 2021), see Methods). No difference was reported in the proportion of recorded units that were classified as 'flash-responsive' in any of the three models tested (Fig. 5.3a-c). Encouragingly, a similar proportion of flash-responsive cells were identified in all animals across the three models. We then used a similar k-means clustering approach to classify the flash responses of the individual units across animals (Fig.5.3d-i). For each model, all units from both the wild-type and mutant siblings were pooled and clustered. The response profiles and relative proportion of each group present in the population of wild-type and mutant units were then investigated.

For all models, units with previously characterised response profiles were identified, and the predominant response type was a weak, transient increase in activity to both the increase and decrease in light (Fig. 5.3e, *Setd5* group 1; Fig. 5.3g, *Ptchd1* group 6; Fig. 5.3i, *Cul3* group 4). Units with high baseline firing rates that displayed a sustained reduction in their firing in response to the flash stimulus were also observed across genotypes in all three models (Fig. 5.3e, *Setd5* group 4; Fig. 5.3g, *Ptchd1* groups 5,7 & 8; Fig. 5.3i, *Cul3* groups 2,6 & 8). Similarly, units with a sustained increase in their firing were also observed in all groups (Fig. 5.3e, *Setd5* group 2; Fig. 5.3g, *Ptchd1* group 4; Fig. 5.3i, *Cul3* group 7). All response clusters were found in both wild-type and mutant animals in all three models, except for one cluster in *Ptchd1*$^{Y/+}$ that displayed high baseline activity with a rapid light-induced reduction in firing, that was not observed in any *Ptchd1*$^{Y/-}$ units (Fig. 5.3g, group 5). This response profile was not observed in the *Setd5*$^{+/+}$ or *Cul3*$^{+/+}$ recordings either, suggesting it may be due to sampling biases or recording differences in the individual recordings.

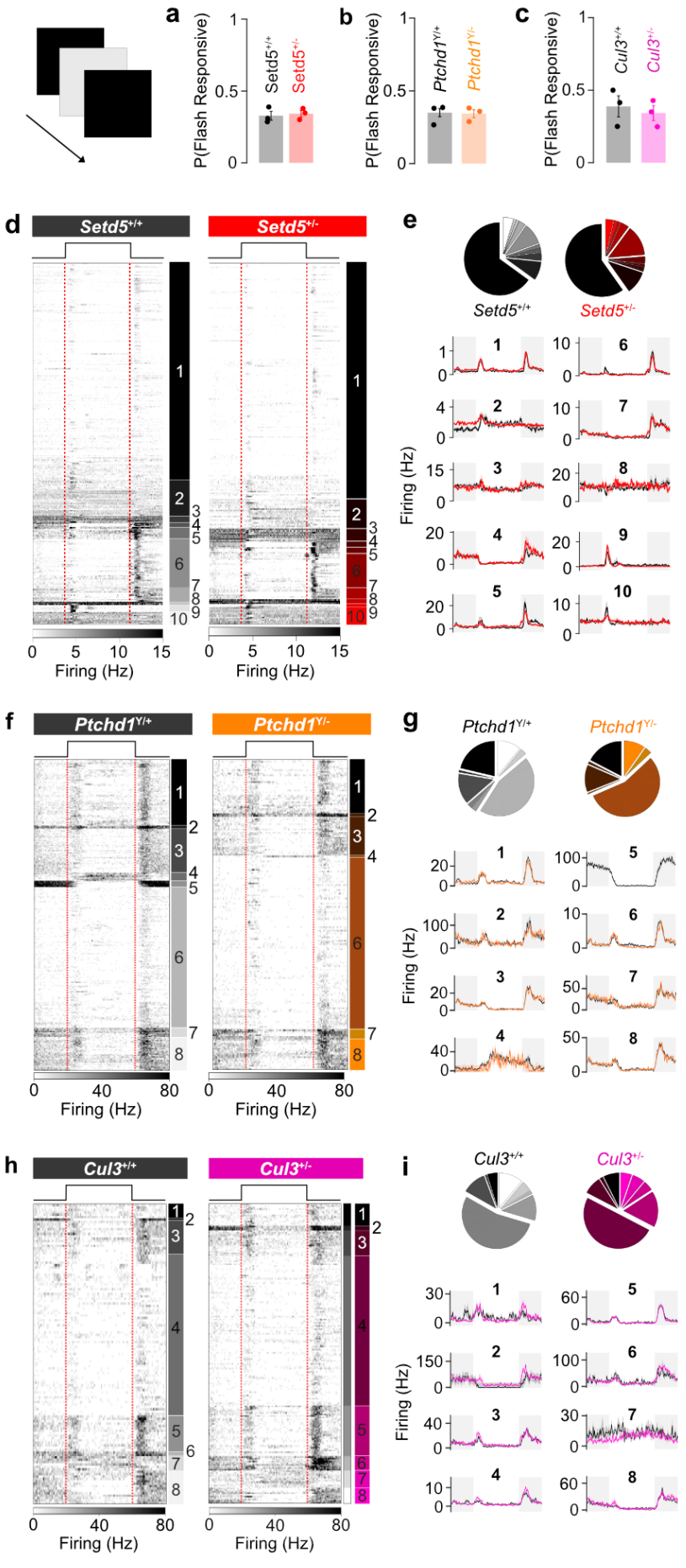
a
b
c
P(Flash Responsive)
Setd5+/+
Setd5+/-
Ptchd1Y/+
Ptchd1Y/-
Cul3+/+
Cul3+/-
d
e
f
g
h
i
Firing (Hz)

Figure 5.3 Visual response properties of SC neurons to a full field flash stimulus.

Proportion of flash responsive cells in the sSC of *Setd5* (**a**, *Setd5*$^{+/+}$, n = 3, 0.328; *Setd5*$^{+/-}$, n = 3, 0.342, $p > 0.995$, two-way *t*-test), *Ptchd1* (**b**, *Ptchd1*$^{Y/+}$, n = 3, 0.350; *Ptchd1*$^{Y/-}$, n = 3, 0.343, $p = 0.857$, two-way *t*-test) and *Cul3* (**c**, *Cul3*$^{+/+}$, n = 3, 0.388; *Cul3*$^{+/-}$, n = 3, 0.342, $p = 0.638$, two-way *t*-test) animals. **d**, Sorted raster plot of neural responses to a single flash stimulus. Vertical red dotted lines indicate the on and offset of the flash stimulus. **e**, Top, proportion of cells in each cluster. Bottom, mean ± SEM of the flash responses in each cluster (traces) for wild-type (black) and mutant (coloured). Shaded areas indicate 'light off' part of the flash and the central white area is the 'light on' segment. **f-g** and **h-i**, as for **d-e** but for *Ptchd1* and *Cul3* animals, respectively. Error Bars represent the SEM.

Mice, like humans, constrict their pupils in response to bright light to restrict the amount of light available to the retina. This reflexive action is called the pupillary light reflex, and can be used to assess the functionality of simple, light-induced behavioural responses. We observed that pupil responses were unaffected across genotypes in the *Setd5* model (Fig. 5.4a-b). Since it is known that behavioural states, such as running, can directly affect arousal levels and pupil dilation we only analysed pupil responses to single flash responses in trials where the animals were running for at least 50% of the flash presentation. It is also well known that the magnitude of responses to visual stimuli in both the visual cortex (Niell and Stryker 2010) and the superior colliculus (Ito et al. 2017; Savier et al. 2019) are affected by the running state of the animal, we investigated whether the locomotor behaviours of the *Setd5*$^{+/+}$ and *Setd5*$^{+/-}$ animals differed across the recordings. On average, both wild-type and mutant animals ran for about 25% of the recording time (Fig. 5.4c) and all animals ran more at the beginning of the recordings and declined over time (Fig. 5.4d).

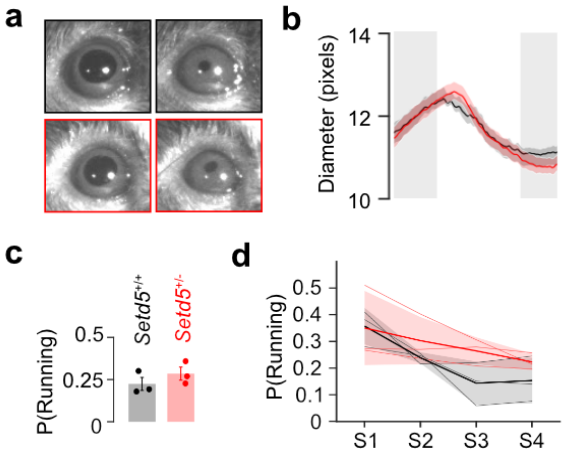

Fig. 5.4 Pupil dynamics to full field luminance changes in *Setd5* animals.

a, Pupil dilation in response to the full-field flash stimulus. Example images of dilated and constricted pupils in responses to the OFF (left) and ON (right) periods of the flash. **b**, Mean size of pupil diameter during one flash stimulus. The grey shaded areas represent the OFF period of the flash (Range in diameter: *Setd5*$^{+/+}$, n = 3, black, 2.36 pixels; Setd5$^{+/-}$, n = 3, red, 2.71 pixels, $p = 0.060$, two-sample Wilcoxon's ranked-sum). **c**, Proportion of time the mice were moving during the recording sessions ($p = 0.326$, student's two-way *t*-test. **d**, The proportion of time spent running in each of the four recording sessions (S1-S4). Thick lines represent the mean across all animals, thin red and black lines represent the values for individual *Setd5*$^{+/-}$ and *Setd5*$^{+/+}$ animals, respectively. Error Bars and shaded areas represent the SEM.

5.4 Neuronal responses to the looming stimulus

Visual responses to looming objects in the superior colliculus, and its non-mammalian homologue the optic tectum, have been well characterised and are known to be required for the effective generation of behavioural responses to looming visual threats. We were again interested in investigating whether the representation of looming stimuli within the visually-responsive regions of the superior colliculus were comparable between the wild-type and mutant animals in the *Setd5*, *Ptchd1* and *Cul3* models. We presented each animal with 25 individual looming stimuli at each depth recorded from. Similar to our analysis of the flash stimulus, the published ZETA test (Montijn et al. 2021) was again used to classify loom-responsive units. Using these values of responsivity we found no significant difference in the proportion of loom-responsive neurons between wild-type and mutant animals in any of the 3 models (Fig. 5.5a-c). We did however observe quite large variability in the proportion of loom responsive cells per animal, ranging from 0.15 to 0.65. This variability might stem from different experimental and recording conditions between animals. We then looked at the average response profiles and quantified the average firing rate, peak firing rate and the time to peak firing rate for all the loom-responsive units located within the sSC (Fig. 5.5d-u). In all models we found no obvious differences between wild-type and mutant animals, except in the timing of the responses in the *Ptchd1* model. Overall, however, all mice displayed clear neural responses to the looming stimuli in units recorded across the depths of the sSC showing that the behavioural delay observed in response to this stimulus does not arise from the absence or impairment in the transmission of visual information from the retina to the superior colliculus.

Fig. 5.5 Visual response properties of SC neurons to the looming stimulus. (Overleaf)

Proportion of loom responsive cells in the sSC of *Setd5* (**a**, *Setd5*$^{+/+}$, n = 3, 0.346; *Setd5*$^{+/-}$, n = 3, 0.337, p = 0.975, two-way *t*-test), *Ptchd1* (**b**, Ptchd1$^{Y/+}$*, n = 3, 0.619;* Ptchd1$^{Y/-}$*,* n = 3, 0.597*, P* = 0.728, two-way *t*-test*)* and *Cul3* (**c**, *Cul3*$^{+/+}$, 0.614; *Cul3*$^{+/-}$, 0.514, p = 0.534, two-way *t*-test*)* animals. **d**, Mean±SEM response of all and (**e**) of the 5 consecutive loom stimuli for Setd5$^{+/+}$ (black) and Setd5$^{+/-}$ (red) units. Average firing (**f**, *Setd5*$^{+/+}$, 6.35Hz; *Setd5*$^{+/-}$, 6.22Hz, p = 0.215), maximum firing (**g**, *Setd5*$^{+/+}$, 11.6Hz; *Setd5*$^{+/-}$, 12.7Hz, p = 0.100) and latency to peak spiking (**h**, *Setd5*$^{+/+}$, 0.190s; *Setd5*$^{+/-}$, 0.182s, p = 0.372) in *Setd5* units. **i,** Average firing to a single loom across the 5-loom stimulus (p = 0.732, two-way repeated measures (rm) ANOVA). **j**-**k**, as for **d**-**e** but for *Ptchd1*$^{Y/+}$ (black) and *Ptchd1*$^{Y/-}$ (orange) units. Average firing (**l**, *Ptchd1*$^{Y/+}$, 6.02Hz; *Ptchd1*$^{Y/-}$, 6.59Hz, p = 0.461), maximum firing (**m**, *Ptchd1*$^{Y/+}$, 46.1Hz; *Ptchd1*$^{Y/-}$, 44.5Hz, p = 0.100) and latency to peak spiking (**n**, *Ptchd1*$^{Y/+}$, 0.254s; *Ptchd1*$^{Y/-}$, 0.270s, p = 0.372) in *Ptchd1* units. **o**, Average firing to a single loom across the 5-loom stimulus (p = 0.758, two-way rmANOVA). **p**-**q**, as for **d**-**e** but for *Cul3*$^{+/+}$ (black) and *Cul3*$^{+/-}$ (magenta) units. Average firing (**r**, *Cul3*$^{+/+}$, 7.08Hz; *Cul3*$^{+/-}$, 7.50Hz, p = 0.214), maximum firing (**s**, *Cul3*$^{+/+}$, 43.9Hz; *Cul3*$^{+/-}$, 47.2HZ, p = 0.222) and latency to peak spiking (**t**, *Cul3*$^{+/+}$, 0.259s; *Cul3*$^{+/-}$, 0.259s, p = 0.879) in *Cul3* units. **u**, Average firing to a single loom across the 5-loom stimulus in *Cul3* animals (p = 0.758, two-way rmANOVA). Box-and-whisker plots show median, IQR and range. Error Bars represent the SEM. Unless otherwise stated p values are for Wilcoxon's ranked-sum tests.

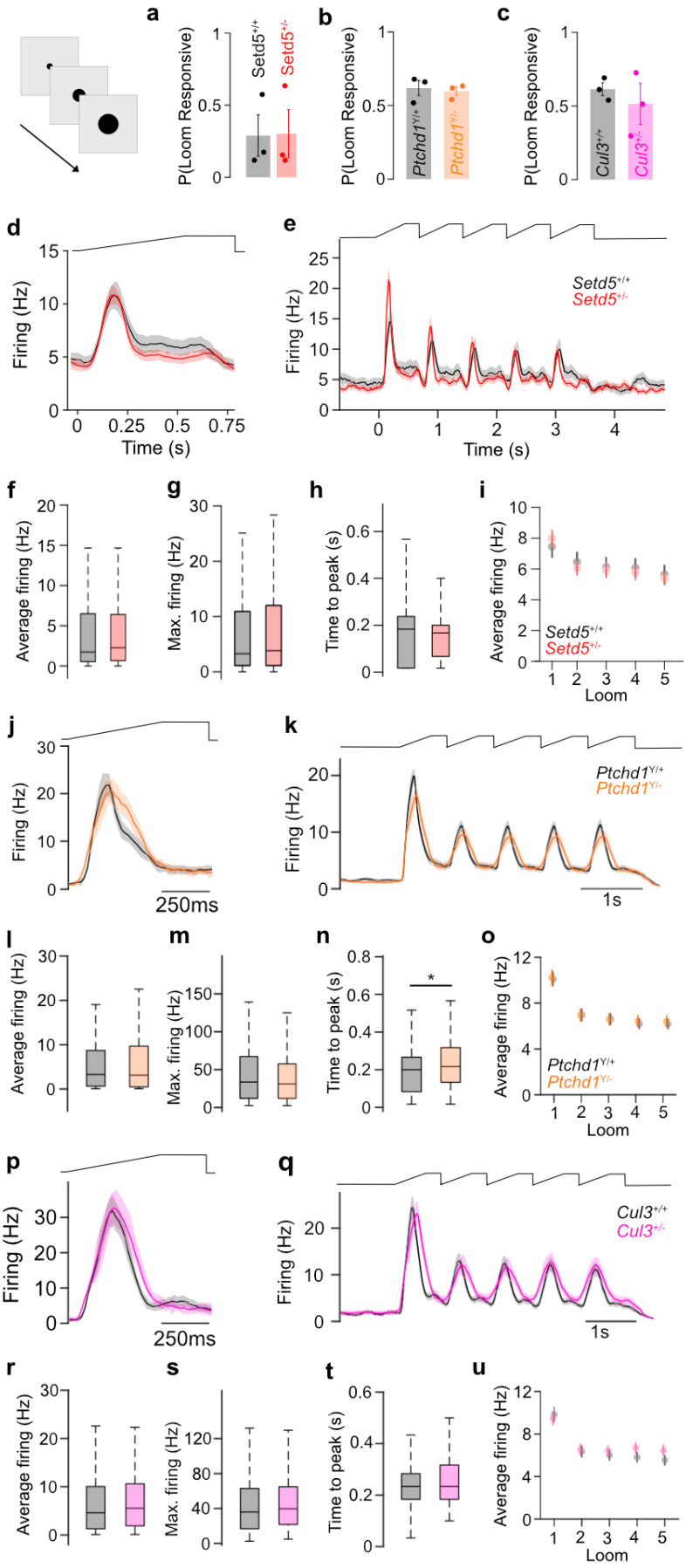
a
b
c
P(Loom Responsive)
Setd5+/+
Setd5+/-
Ptchd1Y/+
Ptchd1Y/-
Cul3+/+
Cul3+/-
d
e
Firing (Hz)
Time (s)
f
g
h
i
Average firing (Hz)
Max. firing (Hz)
Time to peak (s)
Loom
j
k
250ms
1s
l
m
n
o
*
p
q
r
s
t
u

5.5 Direction selectivity

Since the presentation of an expanding dark disc features a dynamic, directional expansion of a dark edge (in-to-out) we wanted to assess whether direction selectivity within the SC was affected in *Setd5*$^{+/-}$ animals. We presented both full-field square gratings (Fig. 5.6a-c) and a single moving bar stimulus (Fig. 5.6d-f) to *Setd5*$^{+/+}$ and *Setd5*$^{+/-}$ mice. Units from both genotypes displayed both direction-selective and non-direction selective cells to both forms of stimuli (Gratings: Fig.5.5b; Bars: Fig.5.5e). To quantitatively assess the direction selectivity of specific units, we generated a metric, the direction selectivity index (DSI), that compared the responses of the units to stimuli moving in each of the 8 cardinal directions across multiple presentations (See Methods: *Chapter 2.6.4.7*). This metric generated values in the range of 0 - 1, where 1 referred to a unit that had a highly direction selective response. Units classified as direction-selective neurons had DSI values in the 80th percentile or above. No difference was found in the proportion of direction-selective neurons between *Setd5*$^{+/+}$ or *Setd5*$^{+/-}$ mice (Fig. 5.6a,d), nor was there a difference in the mean DSI value or distribution in values between genotypes (Fig. 5.6c,f).

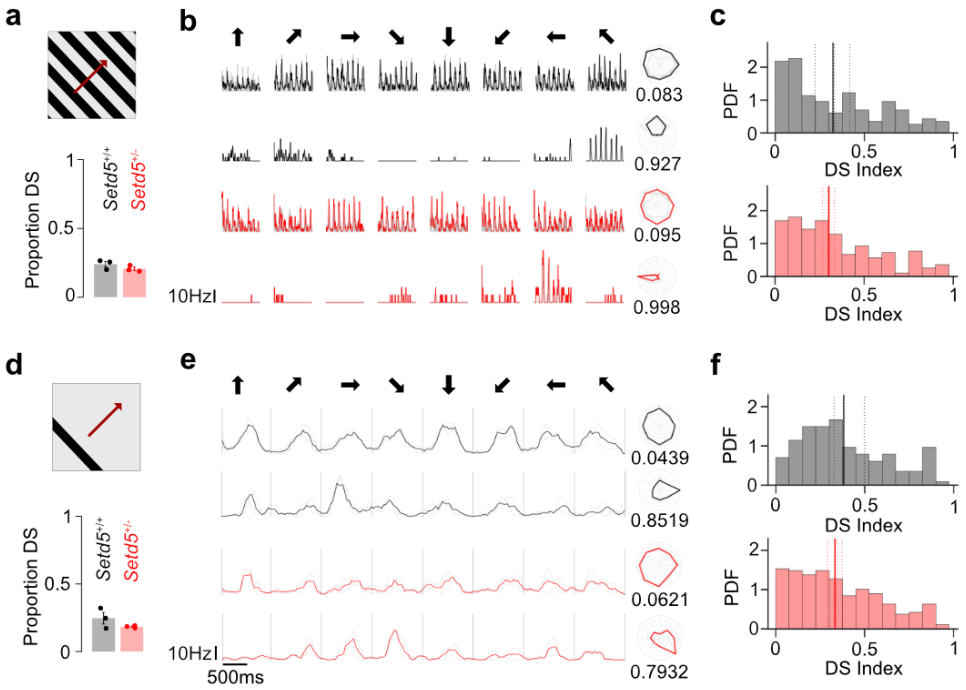

Fig. 5.6 Direction selectivity in SC cells in *Setd5*$^{+/+}$ and *Setd5*$^{+/-}$ mice.

a, Proportion of direction-selective SC cells (see Methods) to full field gratings (*Setd5*$^{+/+}$, n = 3, 87 of 153 units, 0.287; *Setd5*$^{+/-}$, n = 3, 159 of 259 units, 0.2432, $p = 0.322$, two-sample Wilcoxon's ranked-sum test). **b**, Firing rate of example units in response to full field gratings moving in 8 different directions for *Setd5*$^{+/+}$ (black) and *Setd5*$^{+/+}$ (red) with a summary polar plot of their direction selectivity (right) and the corresponding DSI value. Bold lines show the mean response across 3 repetitions (light grey lines). Spikes were binned into 1/60s time bins. **c**, Distribution of direction selectivity index (DSI) across SC units (top, *Setd5*$^{+/+}$, 153 units, median DSI = 0.323; bottom, Setd5$^{+/-}$, 259 units, median DSI = 0.3018, $p = 0.7054$, two-sample Kolmogorov-Smirnov test). Bold vertical lines represent the median DSI of all cells and dotted lines represent the median DSI of each animal. **d-f**, as for **a-c** but for single moving bar stimulus. Proportion of direction-selective SC cells (see Methods) to a moving bar stimulus (*Setd5*$^{+/+}$, 45 of 153 units, 0.243; *Setd5*$^{+/-}$, 57 of 259 units, 0.183, $p = 0.143$, Wilcoxon's test). **e**, as for **b**

but for the moving bar stimulus. **f**, Distribution of direction selectivity index (DSI) across SC units (top, *Setd5*$^{+/+}$, 153 units, median DSI = 0.478; Bottom, *Setd5*$^{+/-}$, 259 units, median DSI = 0.417, p = 0.244, two-sample Kolmogorov-Smirnov test). Bold vertical lines represent the median DSI of all cells and dotted lines represent the median DSI of each animal. Box-and-whisker plots show median, IQR and range. Error Bars represent the SEM.

5.6 Summary

In summary, electrophysiological analysis of the visual response properties of neurons within the sSC of *Setd5*, *Ptchd1* and *Cul3* animals did not reveal any substantial differences in the visual processing abilities of the superior colliculus in these mice. Strong visual responses were recorded with selectivity for different properties of light stimuli, and reflexive light-induced pupil responses were also observed in both *Setd5*$^{+/+}$ and *Setd5*$^{+/-}$ animals. These results suggest that the differences in the behavioural response to the looming stimulus observed in *Setd5*$^{+/-}$, *Ptchd1*$^{Y/-}$ and *Cul3*$^{+/-}$ animals are not the result of impaired preliminary visual processing in this sensorimotor process.

6 Checkpoint 2: Signal transmission out of the superior colliculus

Since the visual response properties of cells with the sSC appeared intact in *Setd5*$^{+/-}$ mice we speculated that the neural source of the behavioural differences observed between the genotypes in response to the LAR, was located downstream of the visual processing circuits located within the sSC. A previous study elegantly demonstrated the existence of a synaptic threshold mechanism between the deep layers of the SC and the dPAG, for generating escape responses in the mouse (Evans et al. 2018). They determined that critical to the execution of this mechanism is the weak and unreliable nature of the synaptic connection, so that only sufficiently large inputs, in the form of robust spiking activity within the dmSC, can drive the activation of the motor behaviour. This mechanism also acts to avoid the overactivation of these circuits and the unnecessary execution of this energetically expensive behaviour.

A previous studies have observed altered expression of genes related to synaptic transmission and postsynaptic density proteins in *Setd5*$^{+/-}$ (Deliu et al. 2018; Moore et al. 2019; Nakagawa et al. 2020) and our recordings of the visual responses in the sSC were not sufficient for us to examine if the propagation of visual information through the depths of the SC was intact in the mutant animals. These factors led us to speculate that perhaps aberrant transmission of information through the SC, or specific impairments in this 'critical' synapse might be causing the delayed responses observed in the LAR paradigm. To test this idea we decided to analyse the behavioural responses elicited to the artificial activation of excitatory dmSC neurons using optogenetics. Multiple studies have shown that stimulation of the intermediate and deep layers of the superior colliculus can mediate orienting and defensive responses, depending on the lateral or medial location of activation respectively (Comoli et al. 2012; Isa et al. 2020). Since it had previously been shown that the selective activation of excitatory glutamatergic neurons within the dmSC was sufficient to drive these responses (Shang et al. 2015; Evans et al. 2018) we injected *Setd5*$^{+/-}$::VGlut2-IRES-Cre and *Setd5*$^{+/+}$::VGlut2-IRES-Cre mice with a cre-dependent virus expressing Channelrhodopsin-2 (ChR2; Boyden et al. 2005) and delivered light stimulation *in vivo*. Given, the fraction of ChR2-infected spiking cells increases as a function of light intensity (Huber et al. 2008), we used a light intensity modulation assay to dynamically adjust the level of dmSC network activation in order to assess the dynamic range of behavioural expression in the two genotypes.

6.1 Incremental optogenetic activation of dmSC leads to divergent behavioural responses in *Setd5*$^{+/+}$ and *Setd5*$^{+/-}$ mice

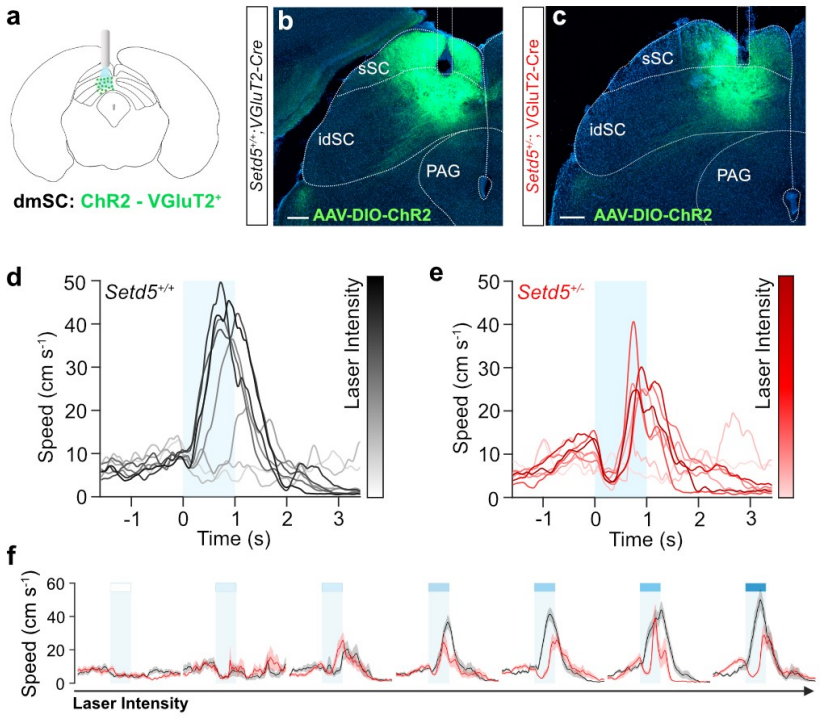

Fig. 6.1 Optogenetic stimulation of dmSC cells recapitulates the escape behaviours observed in *Setd5* mice to the visual looming stimulus and reveals divergent effects of network activation across genotypes.

a, Schematic of ChR2 expression in the dmSC and implantation of the optic fibre. **b-c**, Confocal micrographs of AAV-ChR2 expression in mSC and optic fibre location reconstruction in a *Setd5*$^{+/+}$ (**b**) and *Setd5*$^{+/-}$ (**c**) mouse. Scale bars = 200 µm. Mean speed responses to optogenetic stimulation at increasing laser intensities for *Setd5*$^{+/+}$ (**d**, n = 4, left) and *Setd5*$^{+/-}$ (**e**, n = 4, right). Blue shaded areas show the laser stimulation times. Darker lines represent higher laser intensities. Lines are the average across trials pooled across animals. **f**, Subplots of trials in **d** & **e** sorted by laser intensity (left to right, low to high intensity). Shaded areas represent the SEM.

By incrementally intensifying the level of dmSC network activation through stepwise increases in light intensity, we observed a dynamic range of evoked defensive responses in both *Setd5*$^{+/+}$ and *Setd5*$^{+/-}$ mice. At low levels of light stimulation, we observed the generation of a consistent risk assessment, 'arresting' behaviour, in both genotypes (Fig. 6.1d-e, light lines and f, panel second from the left). These levels of network activation were not sufficient to elicit an escape response, however they reliably generated a short secession in ongoing movement across animals. Similar low-to-mid levels of light stimulation evoked low vigour retreats back to the shelter in both wild-type and mutant animals. In all animals, by increasing the intensity of the light stimulation we were able to observe corresponding increases in the escape probability, maximum speed and time to maximum speed in both genotypes (Fig. 6.2a-c). Of note, however, was the fact that *Setd5*$^{+/-}$ animals required higher laser powers to reliably generate robust escape responses, reached lower maximal speeds and consistently took longer to reach their maximum acceleration (Fig. 6.2a-c). Unexpectedly, as we increased the intensity of the light stimulation, and the corresponding network activation, we began to observe a progressive divergence in the

behavioural responses of the wild-type and the mutant animals - most notably in the generation of an increasingly obvious arrest response in the *Setd5*$^{+/-}$ animals (Fig. 6.2d). Although optogenetic activation with the highest light intensities (maximum 12 mW mm^{-2}) generated robust, shelter-directed escape responses in both *Setd5*$^{+/+}$ and *Setd5*$^{+/-}$ animals, the response dynamics and kinematic profiles were reminiscent of the responses evoked by sensory threats (Fig. 3.1).

The arrest of ongoing locomotion has been observed in animals in response to the onset of a bright light stimulus (Liang et al. 2015; Roseberry and Kreitzer 2017). In order to observe if the arresting behaviour seen in the *Setd5*$^{+/-}$ mice was the result of a visually-driven reaction to ectopic light from the optogenetic stimulation, we tested the behavioural responses of animals to the same procedure but injected with a virus encoding GCaMP instead of the optogenetic protein ChR2. No behavioural changes, including arresting behaviours, were observed in mice from either genotype in these experiments (Fig. 6.3), indicating that the responses observed in Fig. 6.1 and Fig. 6.2 were due to network activation and not visual stimulation or experimental artefacts.

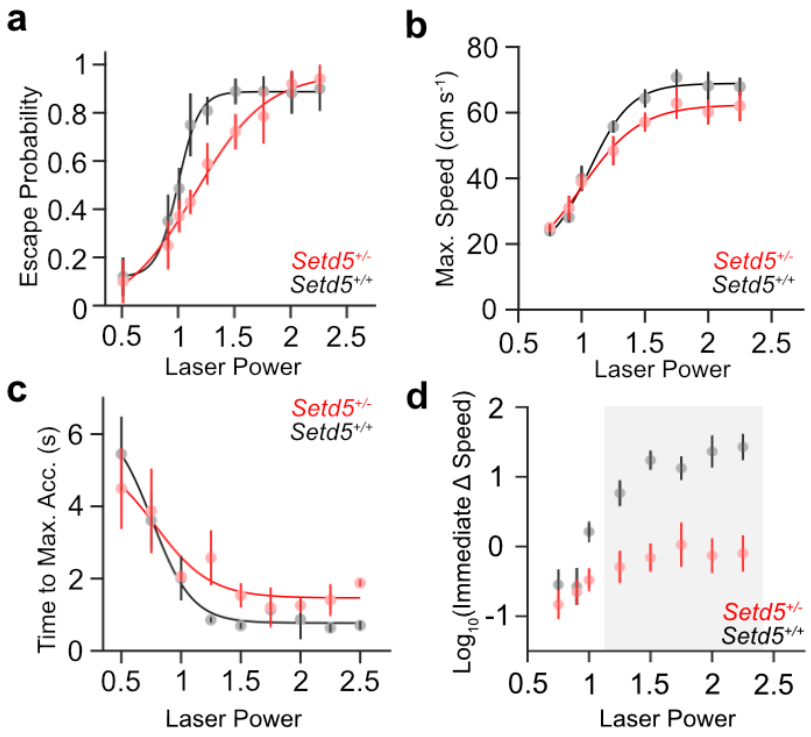

Fig. 6.2 Behavioural responses diverge at higher laser power intensities.

Psychometric, vigour and chronometric curves (**a**, *Setd5*$^{+/+}$, 312 trials, n = 4, slope = 4.62, 95% confidence interval (2.87, 6.37); *Setd5*$^{+/-}$, 291 trials, n = 4, slope = 1.36, 95 % confidence interval (0.62, 2.11); **b**, *Setd5*$^{+/+}$, 195 trials, n = 4, slope = 2.63, 95 % confidence interval (0.90, 4.36); *Setd5*$^{+/-}$, 171 trials, n = 4, slope = 1.88, 95 % confidence interval (0.44, 3.31); **c**, *Setd5*$^{+/+}$: 195 trials, n=4, slope = 2.58, 95 % confidence interval (0.94, 4.22); *Setd5*$^{+/-}$, 171 trials, n = 4, slope = 1.88, 95 % confidence interval (-1.99, 5.76). **d**, Mean ± SEM of the change in speed (300-800 ms after laser onset) at different intensities (between genotype distributions: $p < 0.001$; grey area denotes statistically significant difference through multiple comparisons test with Tukey-Kramer post-hoc test). Lines are sigmoidal fits pooled across trials from all mice and binned according to light intensities.

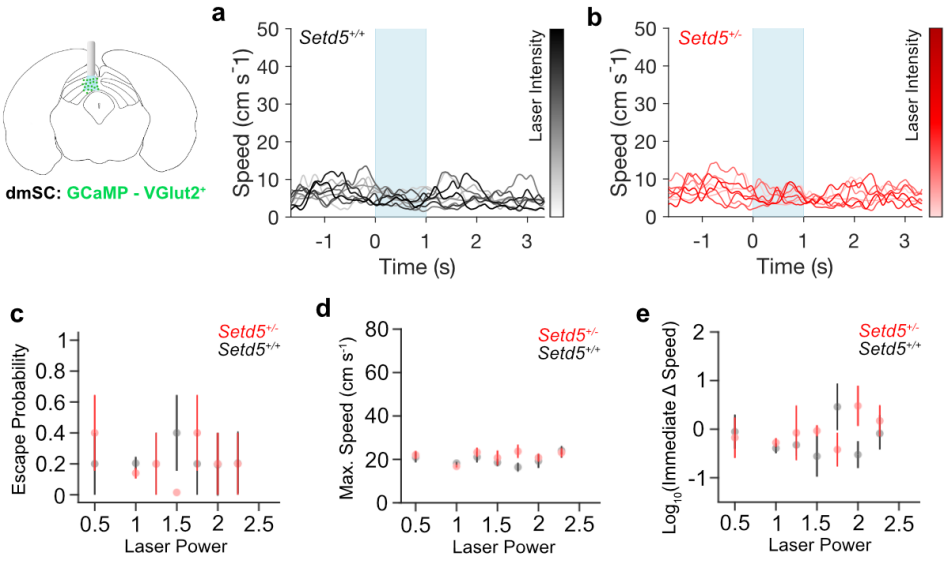

Fig. 6.3 Escape responses were not observed in control mice injected with a virus encoding the GCaMP protein.

Mean speed responses to optogenetic stimulation at increasing laser intensities in control *Setd5*$^{+/+}$ (**a**) and *Setd5*$^{+/-}$ (**b**) mice injected with AAV-GCaMP6m. Blue shaded areas show 1 s of 10 Hz light stimulation. **c**, Relationship between escape probability and laser power (*Setd5*$^{+/+}$, r = -0.005, p = 0.955; *Setd5*$^{+/-}$, r = -0.047, p = 0.577). **d**, Relationship between maximum speed and laser power (*Setd5*$^{+/+}$, r = -0.014, p = 0.871; *Setd5*$^{+/-}$, r = 0.011, p = 0.8986). **e**, Relationship between the Log_{10}(Immediate ΔSpeed) and laser power (*Setd5*$^{+/+}$, r = -0.057, p = 0.496; *Setd5*$^{+/-}$, r = 0.283, p = 0.149). p-values are Pearson's correlation. *Setd5*$^{+/+}$, n = 1, 147 trials; *Setd5*$^{+/-}$, n = 1, 145 trials. Error bars are SEM.

6.2 Extrapolating the graded effect hypothesis: behavioural adaptation to increasing stimulus uncertainty.

Slower and less vigorous behavioural responses to stimuli of increasing uncertainty, and weaker collicular responses to looming stimuli of decreasing contrast have been described in wild-type animals (Evans et al. 2018). These results suggest that visual stimulus contrast, SC network activation, and the generation of graded defensive responses are inextricably linked in wild-type mice. Having observed the expression of a shared behavioural arrest response in *Setd5*$^{+/+}$ and *Setd5*$^{+/-}$ and a similar progression of defensive behaviours to low levels of SC optogenetic activation, we were interested to assess whether we would observe a corresponding convergence in behavioural response to visual stimuli of decreasing certainty and reduced contrast.

Interestingly, exposing *Setd5*$^{+/+}$ and *Setd5*$^{+/-}$ mice to looms of variable contrast revealed a progressive convergence of their behavioural response to lower contrast stimuli (Fig. 6.4). Reaction times, escape probability and escape vigour decreased in animals of both genotypes to stimuli of decreasing contrast. At the lowest stimulus contrast (20%), *Setd5*$^{+/+}$ and *Setd5*$^{+/-}$ were indistinguishable in their reaction time and vigour. While *Setd5*$^{+/+}$ animals showed

marked improvements in their reaction and response kinetics with increasing stimulus contrast, the responses of *Setd5*$^{+/-}$ animals remained relatively unchanged. Whilst the probability of escape was higher in both genotypes with increasing contrast, it was consistently lower in *Setd5*$^{+/-}$ animals. Previous work observed that in wild-type mice it is the reaction, and not the detection, of the stimulus that is most affected in responses to lower contrast stimuli suggesting that the evaluation and action selection component of the PD are most affected, not the initial sensory processing of the stimulus (Evans et al. 2018).

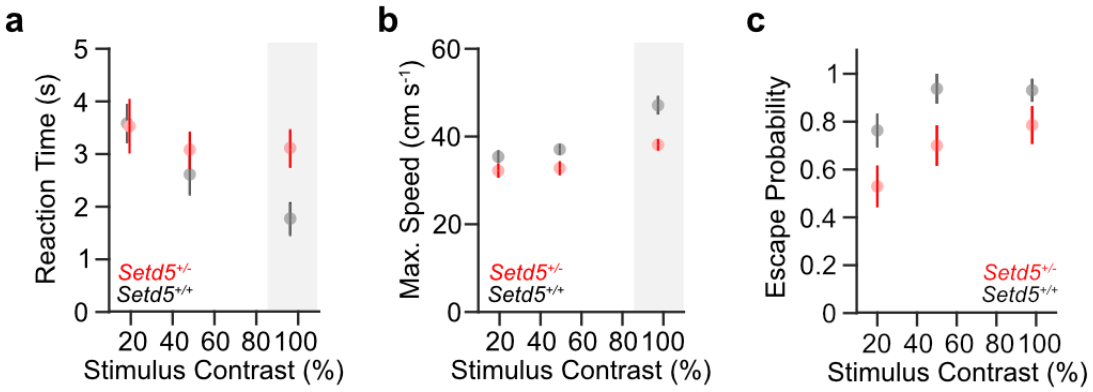

Fig. 6.4 Behavioural responses converge at higher stimulus contrasts in *Setd5* animals.

Summary of mean ± SEM of the (**a**) vigour, (**b**) reaction time and (**c**) escape probability of responses to LAR at different stimulus intensities. **a**, between genotypes: $p < 0.001$, between contrast: $p = 0.003$. *Setd5*$^{+/+}$, n = 13, 68 trials; *Setd5*$^{+/-}$, n = 13, 59 trials. **b,** between genotypes: p = 0.021, between contrast: p = 0.015. *Setd5*$^{+/+}$, n = 13, 68 trials; *Setd5*$^{+/-}$, n = 13, 59 trials. **c**, between genotypes: p < 0.001, between contrast: p = 0.005. *Setd5*$^{+/+}$, n = 13, 83 trials; *Setd5*$^{+/-}$, n = 13, 92 trials. Error bars and shaded areas represent SEM. *p*-values: Two-way repeated measures ANOVA with multiple comparisons with Tukey-Kramer correction. The grey area denotes statistically significant difference through multiple comparisons tests.

6.3 Summary

The generation of certain behavioural responses to visual stimuli, be it directed saccades or orienting body movements, is known to rely on the level of population activity within the SC (Basso and May 2017; Crapse et al. 2018; Jun et al. 2021). Graded collicular activation elicits increasingly intense behavioural responses (Evans et al. 2018), with the specific generation of an escape behaviour requiring an overall population level of activity over a designated threshold. In this section, we revealed that the progressive activation of the dmSC network evokes distinct behavioural responses in *Setd5*$^{+/-}$ and *Setd5*$^{+/+}$ mice at high, but not low, levels of stimulation. These results demonstrate that, firstly, activation of the neural circuitry downstream of the dmSC is not sufficient to overcome the behavioural deficits observed in *Setd5*$^{+/-}$ animals in response to visual threats and secondly, that the severity of the deficit observed in *Setd5*$^{+/-}$ is dependent on the intensity of the visual and neural stimulation. The observation of an intensity-dependent relationship underlying the behavioural divergence in mutant and wild-type animals to both optogenetic and visual stimulation, led us to hypothesise

that the origin of this behavioural deficit was linked to a selective dysfunction of the system at high levels of activation (Fig. 6.5).

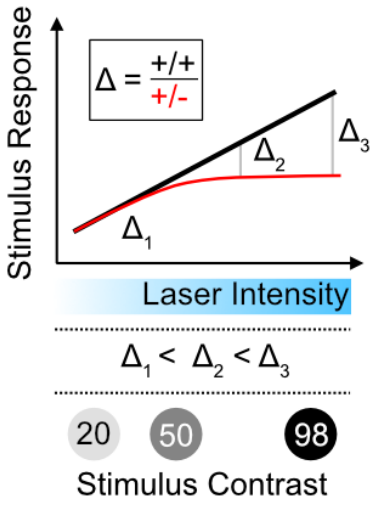

Fig. 6.5 Model of the graded stimulus-response relationship between the behavioural divergence in *Setd5*$^{+/+}$ and *Setd5*$^{+/-}$ animals.

This schematic represents the convergence in behavioural phenotypes of *Setd5*$^{+/+}$ and *Setd5*$^{+/-}$ at lower levels of circuit activation (left side of model), but an increasing divergence with increasing circuit activation either by laser-evoked optogenetic stimulation or sensory stimuli of higher contrast.

7 Checkpoint 3: Action initiation in the periaqueductal grey

With optogenetic activation of the dmSC output channels still retaining the evocation of the delayed escape response behaviour in *Setd5*$^{+/-}$ we decided to move our investigation to the underlying dorsal PAG (dPAG) that receives direct innervation from the dmSC cells and acts as a "gatekeeper" to the generation of escape responses in mice. Similar to dmSC activation, the graded stimulation of dPAG cells was previously shown to generate correspondingly vigorous escape responses, and the recruitment of dPAG cells is both necessary and sufficient to generate an escape response (Evans et al. 2018).

7.1 Synaptic input and intrinsic properties of dPAG cells

A feed-forward connection, with an 11:1 convergence, exists between predominantly excitatory cells within the dmSC and single dPAG cells (Evans et al. 2018). ChR2-assisted-circuit mapping experiments found this connection is weak and unreliable. These experiments revealed high failure rates in light-evoked excitatory postsynaptic currents (eEPSCs) in vGluT2+ dPAG neurons (20.3+/-8%, Evans et al. 2018), and analysis of relationship between spontaneous and miniature EPSCs in the presence of tetrodotoxin (TTX) revealed a low mean quantal content (2.3+/-0.6, Evans et al. 2018). To test the strength of this connection in *Setd5*$^{+/+}$ and *Setd5*$^{+/-}$ animals we performed similar ChR2-assisted-circuit mapping experiments and recorded the functional properties of this synapse using *in vitro* whole-cell patch-clamp recording whilst stimulating dmSC vGlut2^{+} cells by optogenetic activation (Fig. 7.1). Light pulses (0.2 ms, 10 Hz, 1 s) elicited monosynaptic excitatory postsynaptic currents (EPSCs), with an average current of −244±9.65 pA in *Setd5*$^{+/+}$ and -228±11.8 pA in *Setd5*$^{+/-}$, larger than previously reported (Evans et al. 2018). In contrast to previous work (Evans et al. 2018), no facilitation was observed in response to multiple light pulses in animals from either genotype.

Fig. 7.1 The synaptic connection strength between SC and PAG cells is unaffected in *Setd5*$^{+/-}$ animals.

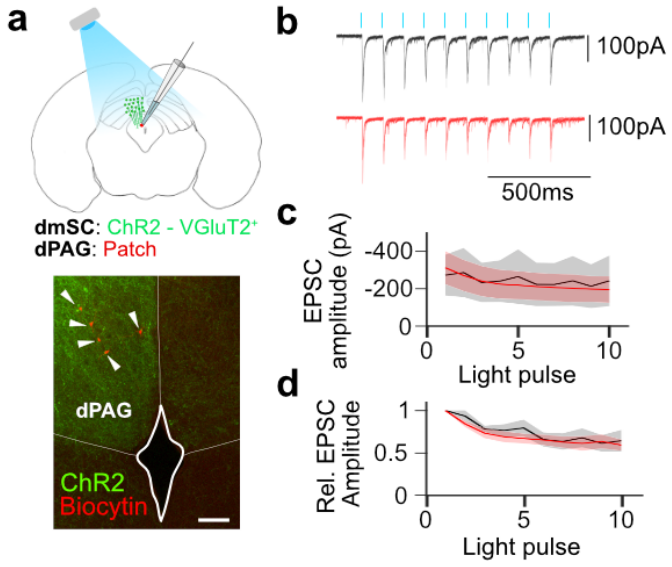

a, Schematic of the experimental approach, *in vitro* patch clamp recordings (top) and micrograph of VGluT2^{+} dmSC projections to the dPAG infected with AAV9-ires-DIO-ChR2 (green) with dPAG biocytin filled and recorded cells (red, arrows, scale bar: 100 µm). **b**, whole-cell voltage clamp traces of example *Setd5*$^{+/+}$ and *Setd5*$^{+/-}$ cells (black and red, respectively.) responding to 10 Hz light stimulation. **c**, EPSC amplitude (*Setd5*$^{+/+}$, n = 3, 6 cells; *Setd5*$^{+/-}$, n = 3, 10 cells, $p = 0.078$ for the effect of genotype in a repeated measures ANOVA (rmANOVA)) and **d**, relative EPSC amplitude (*Setd5*$^{+/+}$, n = 3, 6 cells; *Setd5*$^{+/-}$, n = 3, 10 cells, $p = 0.565$ for the effect of genotype in a repeated measures ANOVA (rmANOVA)) of responses to sequential light pulses in a 10 Hz train. Shaded areas represent SEM.

Spontaneous neurotransmission, as assessed through the examination of the frequency, amplitude and temporal dynamics of sEPCSs elicited at baseline, were indistinguishable between *Setd5*$^{+/+}$ and *Setd5*$^{+/-}$ animals (Fig. 7.2). The intrinsic properties of the dPAG cells were similarly unchanged between genotypes, with no notable differences in input resistance (Fig. 7.3a), the membrane decay constant (Fig. 7.3b), the membrane capacitance (Fig. 7.3c) or the resting membrane potential (Fig. 7.3d). Strikingly, however, we did observe a marked difference in the ability of *Setd5*$^{+/-}$ cells to generate action potentials in response to increasing injected current (Fig. 7.4a). Once again, we observed a dysfunction in the *Setd5*$^{+/-}$ animals that was related to the level of activation. At low current inputs (0 - 70pA), *Setd5*$^{+/-}$ and *Setd5*$^{+/+}$ dPAG cells generated similar levels of spiking activity and the current required to first spike (the rheobase current) was unaffected in *Setd5*$^{+/-}$ animals (Fig. 7.4b). Whilst at higher current inputs *Setd5*$^{+/-}$ cells showed a noticeable disruption in their ability to generate spikes at higher firing frequencies. Encouragingly, the current-firing relationship we observed in the *Setd5*$^{+/+}$ wild-type animals overlaps with previously recorded wild-type dPAG cells to a similar stimulation protocol (Evans et al. 2018).

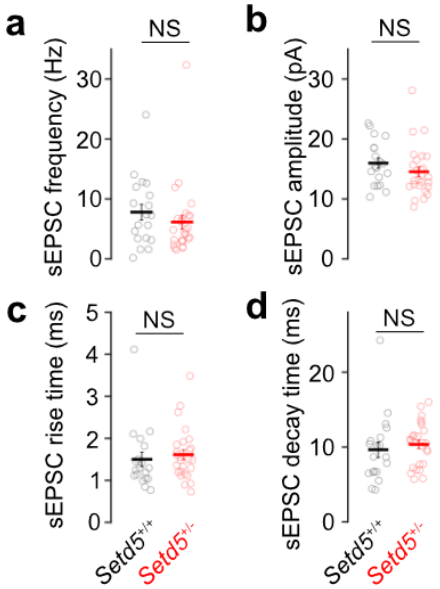

Fig. 7.2 dPAG sEPSC properties in *Setd5*$^{+/+}$ and *Setd5*$^{+/-}$ animals.

Spontaneous neurotransmission in dPAG (*Setd5*$^{+/+}$: n = 6, 19 cells; *Setd5*$^{+/-}$: n = 7, 21 cells). **a**, Average sEPSC frequency (*Setd5*$^{+/+}$: 7.8 Hz; *Setd5*$^{+/-}$: 5.0Hz, P = 0.7743); **b**, average sEPSC amplitude (*Setd5*$^{+/+}$: 16.0 pA; *Setd5*$^{+/-}$: 14.0 pA, P = 0.704); **c**, average sEPSC rise time (*Setd5*$^{+/+}$: 1.50 ms; *Setd5*$^{+/-}$: 1.60 ms, P = 0.948); **d**, average sEPSC decay time (*Setd5*$^{+/+}$: 9.64 ms; *Setd5*$^{+/-}$: 10.5 ms, P = 0.838). Error bars represent SEM. *p*-values are two-sample Wilcoxon's ranked-sum tests. Plotted points represent the values for individual cells.

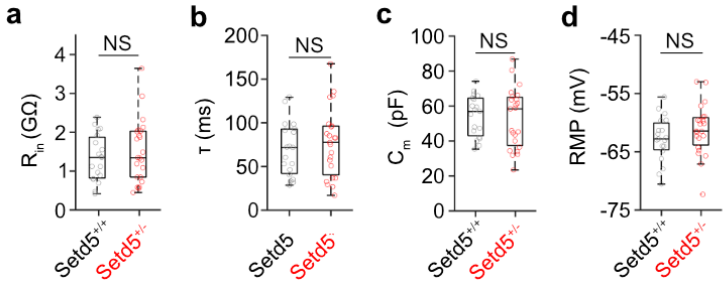

Fig. 7.3 Intrinsic properties of dPAG cells in *Setd5*$^{+/+}$ and *Setd5*$^{+/-}$ animals.

Box and whisker plots of the intrinsic response variables showing no significant difference in the input resistance (**a**, *Setd5*$^{+/+}$, n = 6, 19 cells; *Setd5*$^{+/-}$, n = 7, 21 cells, *p* = 0.6878), membrane constant tau (**b**, *Setd5*$^{+/+}$, n = 6, 19 cells; *Setd5*$^{+/-}$, n = 7, 21 cells, *p* = 0.6539), membrane capacitance (**c**, *Setd5*$^{+/+}$, n = 6, 19 cells; *Setd5*$^{+/-}$, n = 7, 21 cells, *p* = 0.6681) and resting membrane potential (**d**, *Setd5*$^{+/+}$, n = 6, 19 cells; *Setd5*$^{+/-}$, n = 7, 21 cells, *p* = 0.1046). Box-and-whisker plots show median, IQR and range. Error Bars represent the SEM. Plotted points represent the values for individual cells.

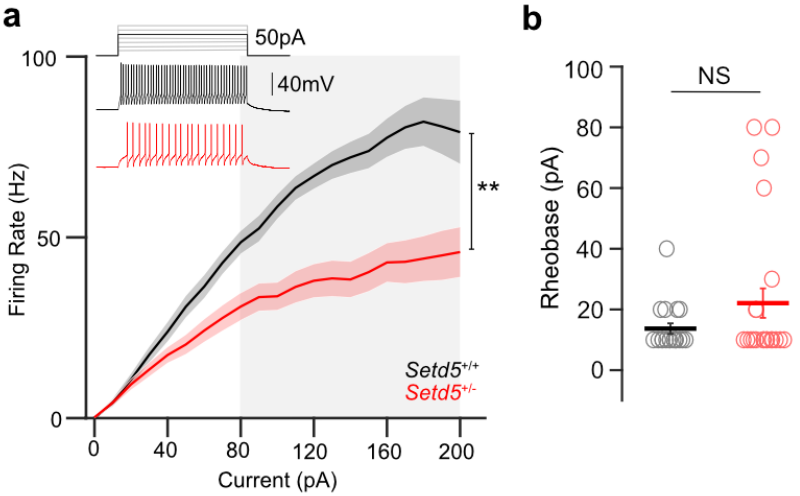

Fig. 7.4 *Setd5*$^{+/-}$ dPAG cells exhibit a hypoexcitability phenotype at higher, but not lower levels of current input.

a, Summary of the relationship between current-injection and action potential firing showing a strong reduction in firing (*Setd5*$^{+/+}$, n = 6, 19 cells; *Setd5*$^{+/-}$, n = 7, 21 cells, $p < 0.001$, repeated measures ANOVA). Inset, representative example traces to a 50 pA current injection in *Setd5*$^{+/+}$ (top, black) and *Setd5*$^{+/-}$ (bottom, red). Grey shaded area represent the current steps for which *Setd5*$^{+/+}$ and *Setd5*$^{+/-}$ have significantly different firing after a Tukey-Kramer multiple comparisons test. **b**, Rheobase current (*Setd5*$^{+/+}$: n = 6, 19 dPAG cells, 13.7pA; *Setd5*$^{+/-}$:

n = 7, 21 dPAG cells, 22.1 pA, P = 0.609). Error bars and shaded areas represent the SEM. Plotted points represent the values for individual cells.

This change in the ability to generate action potentials was accompanied by changes in the shape of the spikes produced during the rheobase sweep (Fig. 7.5). *Setd5*$^{+/-}$ spikes showed slightly higher depolarisation, less after-hyperpolarisation and an overall spike broadening due to slower rise and decay kinetics (Fig. 7.6).

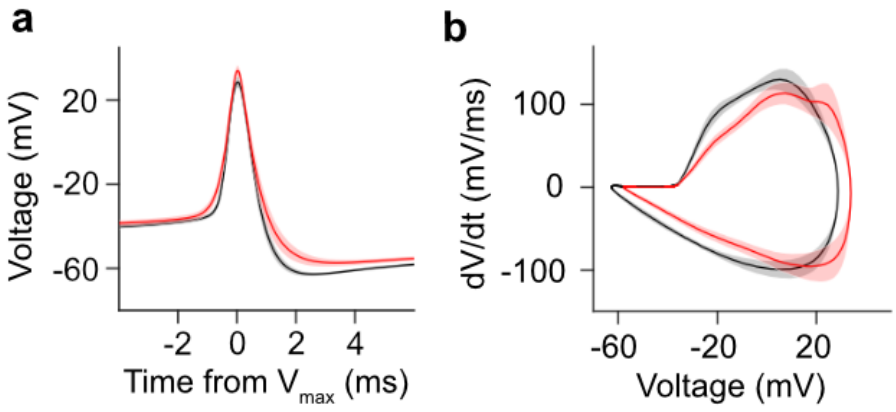

Fig. 7.5 Action potential shape and phase plane analysis of spikes generated by *Setd5*$^{+/+}$ and *Setd5*$^{+/-}$ PAG cells.

a, Average shape and (**b**) phase plane analysis of the action potentials generated in the rheobase sweep (*Setd5*$^{+/+}$, n = 6, 19 cells, 108 spikes; *Setd5*$^{+/-}$, n = 7, 21 cells, 127 spikes). Shaded areas represent the SEM.

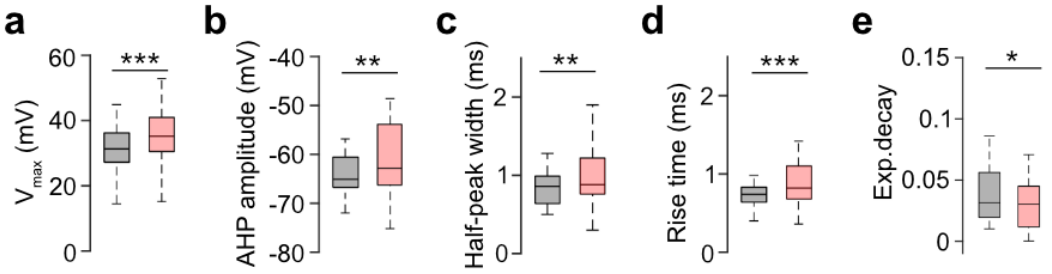

Fig. 7.6 Properties of spikes generated during the rheobase current by *Setd5*$^{+/+}$ and *Setd5*$^{+/-}$ PAG cells.

Summary of the action potential kinetics analysis. **a**, action potential amplitude (V_{max}) (*Setd5*$^{+/+}$, n = 6, 19 cells, 108 spikes; *Setd5*$^{+/-}$, n = 7, 21 cells, 127 spikes, $p < 0.001$); **b**, after-hyperpolarisation (AHP) amplitude (*Setd5*$^{+/+}$, n = 6, 19 cells, 108 spikes; *Setd5*$^{+/-}$, n = 7, 21 cells, 127 spikes, $p = 0.001$); **c**, width at half-peak (*Setd5*$^{+/+}$, n = 6, 19 cells, 108 spikes; *Setd5*$^{+/-}$, n = 7, 21 cells, 127 spikes, $p = 0.010$); **d**, action potential rise time (*Setd5*$^{+/+}$, n = 6, 19 cells, 108 spikes; *Setd5*$^{+/-}$, n = 7, 21 cells, 127 spikes, $p < 0.001$) and **e**, exponential decay constant (*Setd5*$^{+/+}$, n = 6, 19

cells, 108 spikes; *Setd5*$^{+/-}$, n = 7, 21 cells, 127 spikes, p = 0.032). Box-and-whisker plots show median, IQR and range.

7.2 The role of voltage-gated potassium channels in *Setd5*$^{+/-}$ dPAG hypoexcitability

The changes in excitability and spike kinetics observed in *Setd5*$^{+/-}$ dPAG cells are indicative of differences in channel composition that are part of adaptive homeostatic mechanisms (Zbili et al. 2021; Grubb & Burrone 2010), suggesting the influence of voltage-gated potassium channels (K_v). Previous analysis of the transcriptomic changes brought about by the *Setd5*$^{+/-}$ mutation revealed a significant upregulation in the expression of *Kcna1* which encodes the K_v1.1 potassium channel subtype (Deliu et al. 2018). To test whether an upregulation in K_v1.1 could be mediating the reduction in action potential firing observed in *Setd5*$^{+/-}$ dPAG cells to high current inputs, we applied the same stimulation protocol after the application of 100 nM of α-dendrotoxin (α-DTX), a blocker of the Kv1.1 channel. Remarkably, after α-DTX application the *Setd5*$^{+/-}$ dPAG cells were shown to fire at levels similar to that observed in *Setd5*$^{+/+}$ with or without α-DTX (Fig. 7.7). Analysis of the spike dynamics during the rheobase sweep confirmed major changes in the rise and decay kinetic in *Setd5*$^{+/-}$ cells (Fig. 7.7c-d). Interestingly, the application of α-DTX had a slight, but not significant, effect on the firing and spike properties of *Setd5*$^{+/+}$ cells.

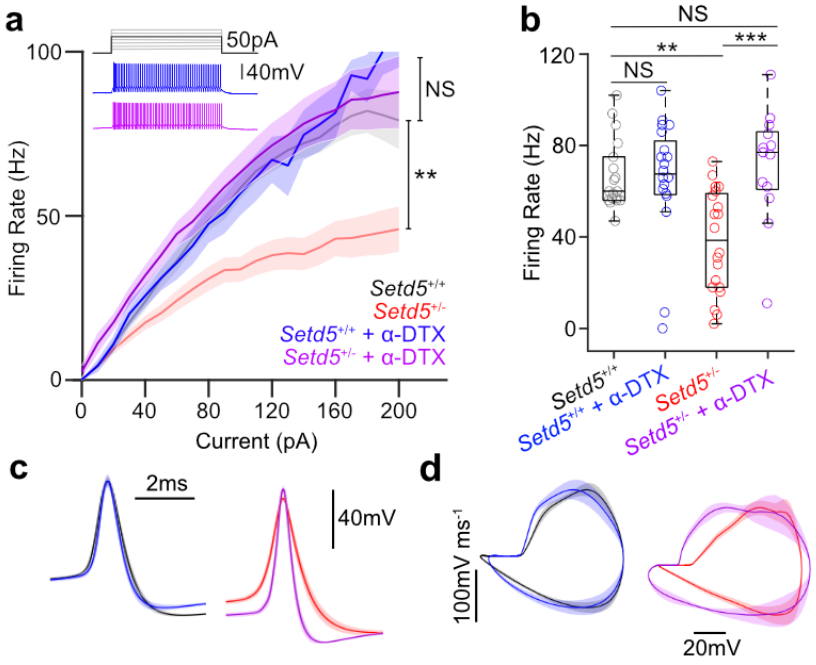

Fig. 7.7 Blocking voltage-gated potassium channels ameliorates current-induced firing in *Setd5*$^{+/-}$ PAG cells.

a, Summary of the relationship between current-injection and action potential firing as in Fig. 7.4a with the addition of *Setd5*$^{+/+}$ (blue) and *Setd5*$^{+/-}$ (purple) in the presence of α -Dendrotoxin, a Kv1.1, 1.2 and 1.6 blocker (α-DTX, 100 nM), ($p > 0.995$ and $p = 0.0147$ for the effect of α -DTX on *Setd5*$^{+/+}$ and *Setd5*$^{+/-}$ firing, respectively). **b**, Box and whisker plot of the firing rate to 120 pA current-injections (*Setd5*$^{+/+}$ without α -DTX, black, 63.3±15.3 Hz, n = 6, 18 cells; *Setd5*$^{+/+}$ with α -DTX, blue, 66.9±28.5 Hz, n = 3, 20 cells; *Setd5*$^{+/-}$ without α -DTX, red, 38.0±22.5 Hz, n = 7, 20 cells; *Setd5*$^{+/-}$ with α -DTX, purple, 71.5 ± 24.7 Hz, n = 3, 13 cells). **c**, Action potential shape and **d**, phase plane analysis of the action potentials generated in the rheobase current in *Setd5*$^{+/+}$ cells (without α -DTX, black, 19 cells; with α -DTX, blue, 12 cells), *Setd5*$^{+/-}$ cells (without α -DTX, red, 21 cells; with α-DTX, purple, 13 cells). Box-and-whisker plots show median, IQR and range. Shaded areas represent the SEM.

We tried to investigate if there we could identify changes in the $K_v1.1$ protein expression, in line with our electrophysiological results with α-DTX. We attempted to qualitatively examine $K_v1.1$ expression in the dPAG using immunohistochemical techniques (Fig. 7.8) and western blot analysis. However, we could not find any evidence for an increase in $K_v1.1$ in *Setd5*$^{+/-}$. In contrast, we even observed a trend towards a reduction in $K_v1.1$ in the PAG of *Setd5*$^{+/-}$ animals in the western blot analysis. No significant differences were observed when comparing samples from the SC or cortex (CTX), however these samples showed a non-significant trend towards an increase in $K_v1.1$ in *Setd5*$^{+/-}$ (Fig. 7.9). Histological examination of $K_v1.1$ staining in cerebellar basket pineau verified the ability of this antibody in labelling $K_v1.1$ in general. Qualitatively, we observed a similar pattern of $K_v1.1$ expression throughout the intermediate and deep layers of the SC, and especially in the dmPAG (Fig. 7.8).

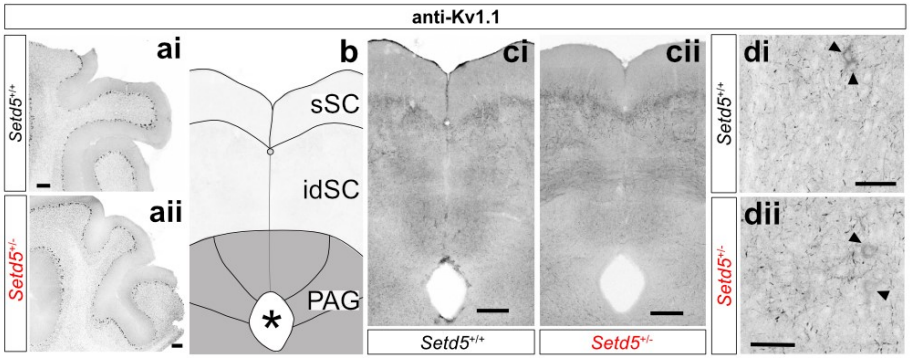

Fig. 7.8 Protein localisation of Kv1.1 in *Setd5*$^{+/+}$ and *Setd5*$^{+/-}$ mice.

Confocal micrographs of $K_v1.1$ staining in *Setd5*$^{+/+}$ and *Setd5*$^{+/-}$ tissue. **a**, Confirmation of strong $K_v1.1$ staining in cerebellar basket cell pinceau in *Setd5*$^{+/+}$ (left) and *Setd5*$^{+/-}$ (right). b, schematic of SC and PAG regions of interest. Immunohistochemical antibody stainings for $K_v1.1$ in *Setd5*$^{+/+}$ (**ci**, 55 µm projection; **di**, 30 µm projection) and *Setd5*$^{+/-}$ (**cii**, 55 µm projection; **dii**, 30 µm projection). Arrowheads indicate somas stained for $K_v1.1$. Scale bar: **c**, 200 µm; **d**, 50 µm.

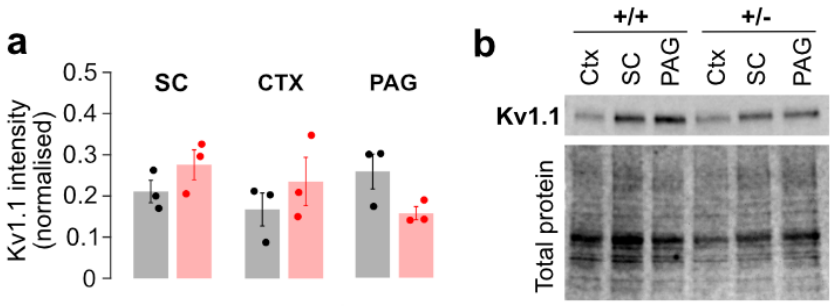

Fig. 7.9 Western blot analysis of Kv1.1 protein content in *Setd5*$^{+/+}$ and *Setd5*$^{+/-}$ mice.

a, Western blot analysis of Kv1.1 protein content within the superior colliculus (left, *Setd5*$^{+/+}$: n = 3, 0.210; *Setd5*$^{+/-}$: n = 3, 0.275, P = 0.226, two-tailed *t*-test), the cortex (middle, *Setd5*$^{+/+}$: n = 3, 0.167; *Setd5*$^{+/-}$: n = 3, 0.235, P = 0.392, two-tailed *t*-test) and the PAG of *Setd5*$^{+/+}$ (n = 3, 0.259) and *Setd5*$^{+/-}$ mice (n = 3, 0.157, P = 0.090, two-tailed *t*-test). **b**, Total protein blot for the three regions from an example pair of *Setd5*$^{+/+}$ and *Setd5*$^{+/-}$ animals. Error bars represent SEM.

7.3 Electrophysiological examination of *Setd5*$^{+/-}$ dmSC cells

We examined if the hypoexcitability phenotype observed in *Setd5*$^{+/-}$ dPAG cells was part of a wider hypoexcitability phenomenon across brain regions and patched dmSC neurons. Similar to the dPAG cells, we observed no difference in the intrinsic properties of the dmSC cells (Fig. 7.10). When performing the same stepwise examination of current-spiking excitability, we observed a weaker and non-significant hypoexcitability phenotype in the dmSC cells, together with no change in the rheobase current of the cells (Fig. 7.11). Morphologically, *Setd5*$^{+/-}$ showed similar soma sizes to the dmSC and dPAG cells in *Setd5*$^{+/+}$ mice (Fig. 7.12).

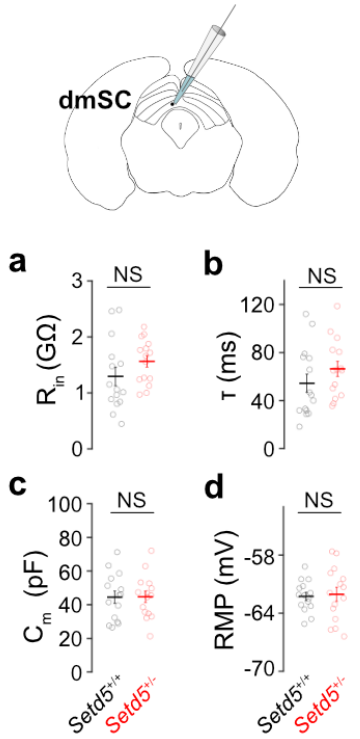

Fig. 7.10 Intrinsic membrane properties of SC cells *Setd5*$^{+/+}$ and *Setd5*$^{+/-}$ mice.

Intrinsic excitability of dmSC cells (*Setd5*$^{+/+}$: n = 4, 15 cells; *Setd5*$^{+/-}$: n = 4, 15 cells). **a**, Input resistance (*Setd5*$^{+/+}$: 1.29 GΩ; *Setd5*$^{+/-}$: 1.56 GΩ, p = 1721). **b**, Tau (*Setd5*$^{+/+}$: 54.5 ms; *Setd5*$^{+/-}$: 66.4 ms, p = 0.229). **c**, Membrane capacitance (*Setd5*$^{+/+}$: 44.4 pF; *Setd5*$^{+/-}$: 44.7 pF, p = 0.961). **d**, Resting membrane potential (*Setd5*$^{+/+}$: -62.3 mV; *Setd5*$^{+/-}$: -62.0 mV, p = 0.795). Error bars represent SEM. p values are from Wilcoxon's ranked sum test. Plotted points represent individual cells.

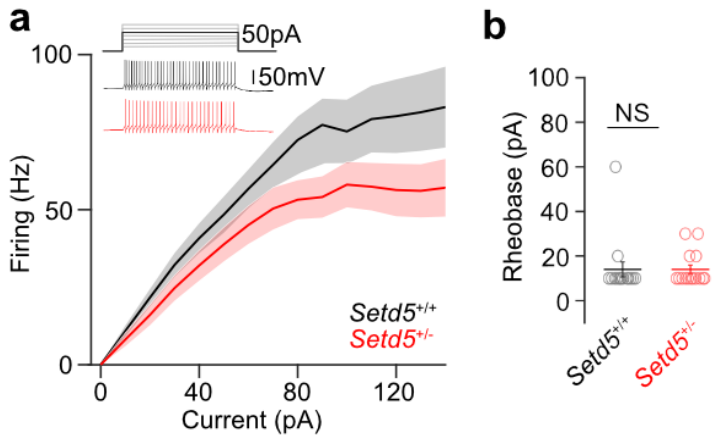

Fig. 7.11 Current-firing relationship in SC cells.

a, Summary of the relationship between current-injection and action potential firing in dmSC cells (*Setd5*$^{+/+}$, black, n = 15; *Setd5*$^{+/-}$, red, n = 15, p = 0.066 for a main effect of genotype, two-way repeated measures ANOVA). **b**,

rheobase current (*Setd5*$^{+/+}$: 15 dmSC cells, 14.0pA; *Setd5*$^{+/-}$: 15 dmSC cells, 14.0pA, $p > 0.999$, two-tailed *t*-test). Error bars and shaded areas represent SEM. Plotted points represent individual cells.

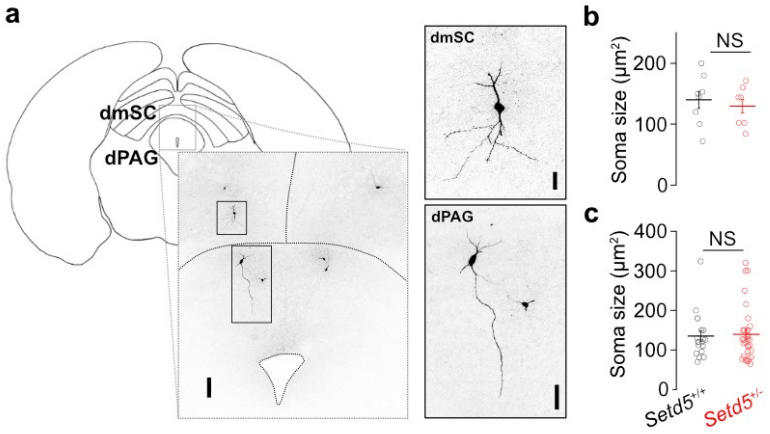

Fig. 7.12 Morphological analysis of *Setd5*$^{+/+}$ and *Setd5*$^{+/-}$ cells reveals no change in soma size between genotypes.

a, Location of dmSC and dPAG cells that were recorded and filled with biocytin (scale bar: 100 µm). Insets show close-ups of the biocytin-filled dPAG cells (top, scale bar: 50 µm) and dmSC cells (bottom, scale bar: 20 µm). **b**, dmSC soma size (*Setd5*$^{+/+}$: 9 dmSC cells, 139.9 µm; *Setd5*$^{+/-}$: 9 dmSC cells, 129.6 µm, $p = 0.609$, two-tailed *t*-test). **c**, dPAG soma size (*Setd5*$^{+/+}$: 19 dPAG cells, 135.3 µm; *Setd5*$^{+/-}$: 21 dPAG cells, 139.6 µm, $p = 0.899$, two-tailed *t*-test). Error bars represent SEM. Plotted points represent individual cells.

7.4 Electrophysiological properties of *Ptchd1*$^{Y/-}$ PAG cells

The convergent nature of the behavioural phenotype reported across the three autism mouse models investigated, as well as the lack of obvious SC visual processing deficits, led us to speculate that dPAG hypoexcitability might form part of a widespread mechanistic dysfunction. To test this possibility, we recorded dPAG neurons from both the *Ptchd1* and *Cul3* mouse models. In the *Ptchd1* line, we again observed no difference in the intrinsic properties of the dPAG neurons in the *Ptchd1*$^{Y/-}$ mutant animals (Fig. 7.13). We did however, observe a similar hypoexcitability phenotype in the *Ptchd1*$^{Y/-}$ dPAG cells during the stepwise current injection protocol (Fig. 7.14). Of further interest, was the observation of similarly delayed rise and decay kinetics in the mutant cells through action potential shape and phase plane analysis. In contrast to the *Setd5* model however, was that the application of α-DTX did not ameliorate the hypoexcitability phenotype in *Ptchd1*$^{Y/-}$ cells (cyan line in Fig. 7.14a), indicative of the fact that similar physiological phenotypes can arise from distinct molecular mechanisms. In line with this discrepancy, phase plane analysis of the spikes generated at rheobase indicates that delayed decay dynamics and insufficient after-hyperpolarisation are the predominant disruptions in *Ptchd*$^{Y/-}$ hypoexcitability, with no change in the maximum amplitude as seen in *Setd5*$^{+/-}$ (Fig. 7.6).

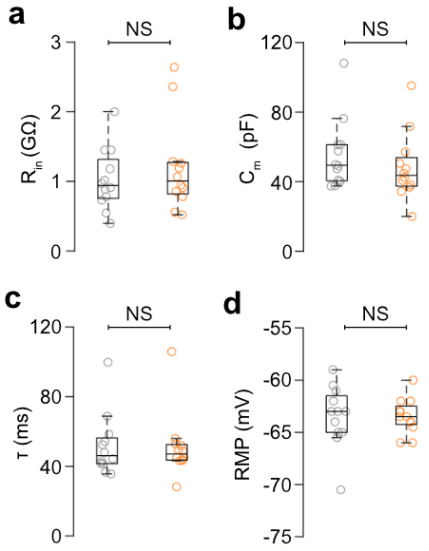

Fig. 7.13 Intrinsic properties of PAG cells in *Ptchd1*$^{Y/+}$ and *Ptchd1*$^{Y/-}$ mice.

Box and whisker plots of the intrinsic response variables showing no significant difference in the input resistance (**a**, *Ptchd1*$^{Y/+}$, n = 4, 12 cells, 1.03 GΩ; *Ptchd1*$^{Y/-}$, n = 4, 12 cells, 1.20 GΩ, $p = 0.623$), membrane capacitance (**b**, *Ptchd1*$^{Y/+}$, n = 4, 12 cells, 55.6 pF; *Ptchd1*$^{Y/-}$, n = 4, 12 cells, 48.2 pF, $p = 0.299$), membrane constant tau (**c**, *Ptchd1*$^{Y/+}$, n = 4, 12 cells, 52.0 ms; *Ptchd1*$^{Y/-}$, n = 4, 12 cells, 51.2 ms, $p = 0.795$) and resting membrane potential (**d**, *Ptchd1*$^{Y/+}$, n = 4, 12 cells, -63.5 mV; *Ptchd1*$^{Y/-}$, n = 4, 12 cells, -63.5 mV, $p = 0.749$). Points represent *Ptchd1*$^{Y/+}$ (grey) and *Ptchd1*$^{Y/-}$ (orange) dPAG cells. Box-and-whisker plots show median, IQR and range. *p*-values are two-sample Wilcoxon's ranked-sum tests.

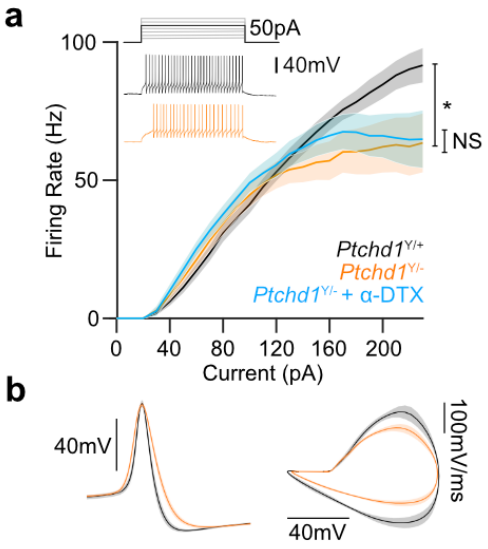

Fig. 7.14 Current-firing relationship, spike shape analysis and the effect of a-DTX on *Ptchd1* PAG cells.

a, Summary of the relationship between current-injection and action potential firing showing a strong reduction in firing. Effect of genotype without **α**-DTX: $p = 0.046$; effect of **α**-DTX on *Ptchd1*$^{Y/-}$ firing: $p = 0.680$. (*Ptchd1*$^{Y/+}$, n = 4, 16 cells; *Ptchd1*$^{Y/-}$, n = 4, 20 cells; *Ptchd1*$^{Y/-}$ with **α**-DTX , n = 3, 13 cells). Inset, representative example traces to a 50 pA current injection for *Ptchd1*$^{Y/+}$ (black, top) and *Ptchd1*$^{Y/-}$ (orange, bottom). **b**, Average shape (left) and

phase plane analysis (right) of the action potentials generated in the rheobase sweep (*Ptchd1*$^{Y/+}$, 16 cells, 58 spikes; *Ptchd1*$^{Y/-}$, 20 cells, 72 spikes). Shaded areas represent SEM.

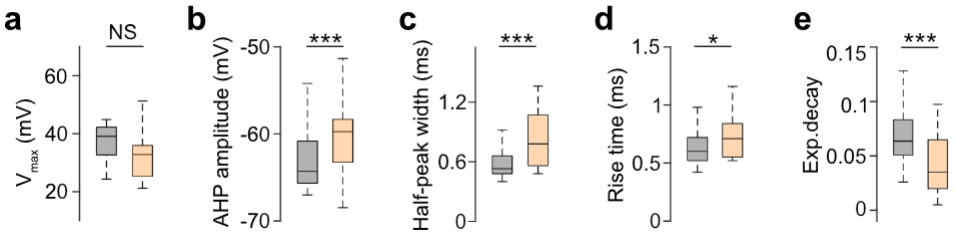

Fig. 7.15 Action potential properties in *Ptchd1* PAG cells.

Summary of the action potential kinetics analysis for the *Ptchd1* model. **a**, Action potential amplitude (V_{max}) (p = 0.092); **b**, after-hyperpolarisation (AHP) amplitude ($p < 0.001$), **c**, width at half-peak ($p < 0.001$), **d**, action potential rise time (p = 0.011) and **e**, exponential decay constant ($p < 0.001$). Box-and-whisker plots show median, IQR and range. *Ptchd1*$^{Y/+}$, n = 4, 16 cells; *Ptchd1*$^{Y/-}$, n = 4, 16 cells.

7.5 Electrophysiological properties of *Cul3*$^{+/-}$ PAG cells

In contrast to the *Setd5* and *Ptchd1* models, *Cul3* dPAG cells showed no differences in either their intrinsic properties (Fig. 7.16) or current-firing relationship (Fig. 7.17). Further analysis of their shape and phase plane profile of the spikes generated during their rheobase sweep showed no significant changes in any of the parameters measured (Fig. 7.18). In summary, these results indicate that hypoexcitability within the dPAG is unlikely to be the source of the behavioural delay observed in the *Cul3*$^{+/-}$ mice.

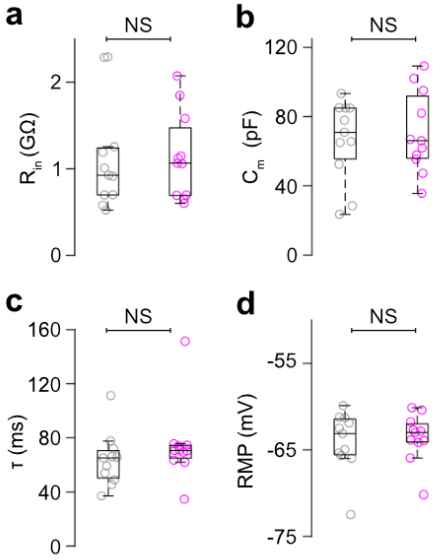

Fig. 7.16 Intrinsic properties of PAG cells in *Cul3*$^{+/+}$ and *Cul3*$^{+/-}$ mice.

a, Input resistance (*Cul3*$^{+/+}$, n = 3, 12 cells; *Cul3*$^{+/-}$, n = 3, 12 cells, p = 0.896), **b**, membrane capacitance (*Cul3*$^{+/+}$, n = 3, 12 cells; *Cul3*$^{+/-}$, n = 3, 12 cells, p = 0.896), **c**, membrane constant tau (*Cul3*$^{+/+}$, n = 3, 12 cells; *Cul3*$^{+/-}$, n = 3,

12 cells, p = 0.212) and **d**, resting membrane potential (*Cul3*$^{+/+}$, n = 3, 12 cells; *Cul3*$^{+/-}$, n = 3, 12 cells, p = 0.844). Points represent Cul3$^{+/+}$ (grey) and Cul3$^{+/-}$ (pink) dPAG cells. Box-and-whisker plots show median, IQR and range. p-values are two-sample Wilcoxon's ranked-sum tests.

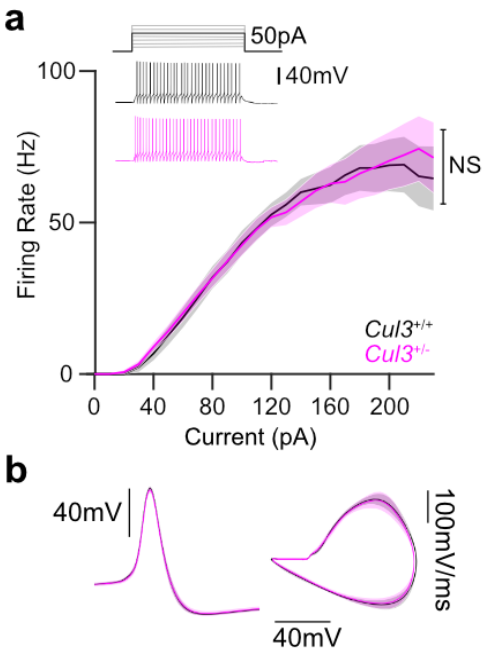

Fig. 7.17 Current-firing relationship and spike shape analysis of *Cul3* PAG cells.

a, Summary of the relationship between current-injection and action potential firing in *Cul3* dPAG cells (*Cul3*$^{+/+}$, grey, 12 cells, n = 3; *Cul3*$^{+/-}$, pink, 12 cells, n = 3, p = 0.683 for the effect of genotype, two-way rmANOVA). **b**, Average shape (left) and phase plane analysis (right) of the action potentials generated in the rheobase sweep for *Cul3*$^{+/+}$ (grey, 68 spikes) and *Cul3*$^{+/-}$ (pink, 73 spikes). Shaded areas represent SEM.

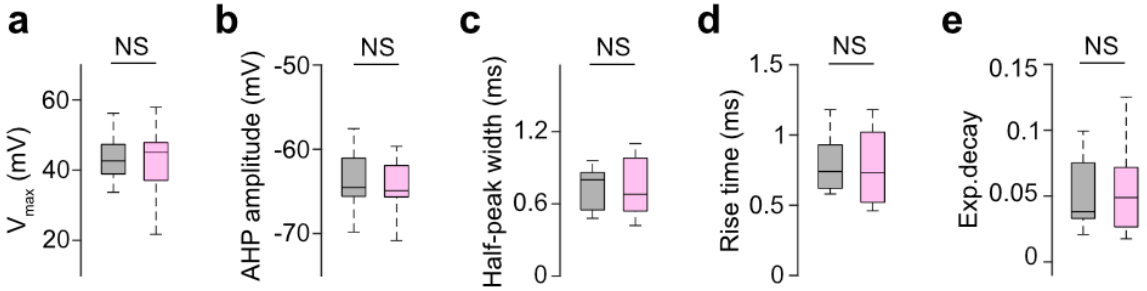

Fig. 7.18 Action potential properties in *Cul3* PAG cells.

Summary of the action potential kinetics analysis for the Cul3 model. **a**, Action potential amplitude (V_{max}) (*Cul3*$^{+/+}$, n = 3, 12 cells; *Cul3*$^{+/-}$, n = 3, 12 cells, p = 0.984); **b**, After-hyperpolarisation (AHP) amplitude (*Cul3*$^{+/+}$, n = 3, 12 cells; *Cul3*$^{+/-}$, n = 3, 12 cells, p = 0.296); **c**, Width at half-peak (*Cul3*$^{+/+}$, n = 3, 12 cells; *Cul3*$^{+/-}$, n = 3, 12 cells, p = 0.565); **d**, Action potential rise time (*Cul3*$^{+/+}$, n = 3, 12 cells; *Cul3*$^{+/-}$, n = 3, 12 cells, p = 0.399); **e**, Exponential decay constant (P = 0.867). Box-and-whisker plots show median, IQR and range. p-values are two-sample Wilcoxon's ranked-sum tests.

7.6 Summary

In this chapter, *in vitro* patch-clamp experiments identified a shared hypoexcitability phenotype in the dPAG cells of both *Setd5*$^{+/-}$ and *Ptchd1*$^{Y/-}$ animals that correlates with the magnitude of current input. This hypoexcitability seems to arise from intrinsic differences in the mechanisms controlling action potential dynamics in both cases. The hypoexcitability phenotype was rescued by the application of the selective pharmacological blocker (α-DTX) of several voltage-gated potassium channels (K_v1.1, K_v1.2 and K_v1.6) in *Setd5*$^{+/-}$ mice, but not in *Ptchd1*$^{Y/-}$ mice, indicating different underlying molecular causes. These differences, especially the graded nature of the dysfunction, are reminiscent of the divergent strength of the behavioural deficits observed in response to increasing stimulus contrast and optogenetic circuit activation (Chapter 6).

Altogether these results suggest that the delayed escape initiation observed in the *Setd5*$^{+/-}$ and *Ptchd1*$^{Y/-}$ animals might result from biophysical changes in dPAG cells that interrupt the flow of information through this subcortical circuit and impair the animal's ability to drive an appropriate behavioural response. In the framework of the LAR as a perceptual decision making process, it appears to be the level of the action selection / initiation that is specifically affected in these models. The absence of any electrophysiological differences in the biophysical properties of *Cul3*$^{+/-}$ dPAG cells suggests that a different underlying mechanism is responsible for the behavioural delay observed in these animals.

8 Summary of conclusions

In **Chapter 3**, we showed that the looming avoidance response (LAR) paradigm is a powerful system by which to study rapid perceptual decision-making in mouse models of autism. Behaviourally, we observed a consistent delay in initiating an escape response to an overhead looming stimulus across all three genetic models. This delay was due to the generation of an atypical biphasic mode of response involving an initial locomotor arrest followed by a subsequent shelter-directed escape.

Chapter 4 revealed a preference for this mode of response in mutant animals that was present from the first stimulus presentation. However, the selection of this response, the total time spent in the arrest phase, and the final vigour with which the escape response was performed were all affected by altered adaptation dynamics in the mutant animals. Mutant animals exhibited repetitive behavioural responses to the looming stimulus that weakened over time, inverse to the previously observed sensitisation to the looming stimulus that we recapitulated in the wild-type animals.

Visual responses within a key brain region for rapid visual processing, the superior colliculus (SC), were intact in haploinsufficient mice from all three models tested, as explored in **Chapter 5**. Visual responses to looming discs, moving bars, white noise checkers or full field flashes were indistinguishable between mice of both genotypes, indicating that visual responses and collicular dynamics are not affected in these models.

In **Chapter 6** we observed that artificial activation of this subcortical pathway at the point of SC output recapitulated the biphasic behavioural response, first arresting and then escaping, observed to visual stimuli. This indicated that the key node of dysfunction remained downstream of the SC, at least in the *Setd5*$^{+/-}$ mouse model. Graded activation of this circuit, either by optogenetic activation using different laser intensities or visual stimulation by different contrast looms, revealed a striking relationship between the level of circuit activation and the degree of behavioural divergence observed between the genotypes.

Electrophysiological investigation of the functional properties of the underlying dPAG cells in **Chapter 7** revealed a marked hypoexcitability phenotype in these cells in *Setd5*$^{+/-}$. A selective deficit in high frequency spiking was observed in these cells. Similar to the behavioural divergence observed with increasing circuit activation, the magnitude of this hypoexcitability phenotype was positively correlated with the amount of current injected. The use of a selective pharmacological blocker of voltage-gated potassium channels ($K_v1.1$, $K_v1.2$ & $K_v1.6$) rescued this hypoexcitability phenotype in *Setd5*$^{+/-}$ mice. Electrophysiological investigation of the *Cul3* and *Ptchd1* models revealed distinct molecular mechanisms that govern the expression of the shared behavioural deficit.

9 Discussion

The aims of this thesis were to assess (i) the impact of autism-risk genes on rapid, perceptual decision-making in ASD mouse models, (ii) to isolate the cellular and circuit mechanism mediating the behavioural differences, and finally (iii) to explore if we could use the behavioural differences observed in the autism models to deepen our biological understanding of rapid perceptual decision-making (PDM) in the context of responding to visual threats. In the sections below, I will comment on and discuss the findings presented in the chapters above.

9.1 Delayed escape initiation to visual threats in mouse models of autism.

While it has been widely reported that mice and other animals, including humans, generate robust behavioural responses to the PDM paradigm used in this study, it was unclear how genetic mouse models of the neurodevelopmental condition, autism, would perform. In humans with autism, perception and cognition are both affected. However, the perceptual abnormalities in autism are bidirectional with both hyper- and hypo-sensitivity to sensory stimuli reported. Our experiments showed that although both wild-type and mutant animals exhibit robust defensive responses to the looming stimulus (Fig. 3.2), mutant animals exhibit a consistent behavioural delay that arises from the performance of an atypical biphasic response. This biphasic defensive response consists of an initial locomotor arrest followed by a subsequent shelter-directed escape. The speed and reliability with which the mutant animals perform this arrest behaviour indicates that it is not the detection of the stimulus that is affected in these animals. Instead, it appears that difficulties in evaluating the available information or selecting a specific response give rise to this delayed response. The cessation of ongoing movement is thought to assist in the animal's ongoing risk assessment evaluation by allowing for more time to sample information from the environment, with the added benefit of simultaneously reducing the individual's saliency to potential predators (Blanchard et al. 2011). Similar biphasic responses have been observed in wild-type animals to low-contrast, ambiguous visual stimuli (Evans et al. 2018) and as a defensive strategy to low-level threats in the wild (Eilam 2005; Edut and Eilam 2003; Cresswell et al. 2009). In contrast to other studies, we did not observe sustained freezing (Wei et al. 2015; Shang et al. 2018) or tail rattling (Salay et al. 2018) in response to the looming stimulus. This could be due to the smaller dimensions and specific physical features of the arena and the shelter used in this study compared to the previous studies.

Given that arresting responses are often observed in response to lower-level threats, it is possible that the delay in behavioural response could arise from difficulties in evaluating the threat valence of the looming stimulus. As mentioned in Chapter 1, fear and the processing of threatening stimuli have frequently been identified as abnormal in autistic compared to neurotypical individuals. Although *Setd5*$^{+/-}$ and *Cul3*$^{+/-}$ animals were previously shown to have typical responses to a conditioned fear response paradigm (Deliu et al. 2018; Morandell et al. 2021), they could possess a selective impairment in the evaluation of visual, or specifically

looming, stimuli. Related to this, autistic children were slower and less accurate in classifying objects based on their cast shadow (Becchio et al. 2010), indicating that the mapping of reductionist visual features to their objects of origin might be selectively affected in autism. Similarly, the reduced influence of contextual information during the evaluation of sensory information, as hypothesised by Bayesian theories of perception in autism (Pellicano and Burr 2012), could impair the assignment of value to the looming stimulus. It is possible that impaired threat evaluation could impact the formation of appropriate fear memories, which in turn could affect response adaptation and the generation of flexible, threat-level appropriate, behavioural responses. Interestingly, we observed a strong link between the formation of place aversion to the threat zone and the severity of the decision delay in *Setd5*$^{+/-}$ and *Ptchd1*$^{Y/-}$ animals (Fig. 4.6). This result suggests that dysfunction in PAG circuits controlling perceptual decision-making can have far-reaching effects on seemingly unrelated behaviours and result in maladaptive responses to threats.

General decision-making difficulties have been described in a small number of experimental studies (Luke et al. 2012; Vella et al. 2018) and are widely reported anecdotally by autistic individuals (Grandin 2000; Lawson 2001; Sainsbury 2009). In these accounts, the phenomenon of decision paralysis is frequently described, especially when decisions need to be made quickly, and decision-making in general is thought to contribute to overall feelings of anxiety and exhaustion in autism. Decision-making difficulties might also directly contribute to the expression of repetitive behaviours and behavioural routines as a means by which individuals attempt to avoid decision-making situations. The identification of a PAG hypoexcitability phenotype in this study proposes a molecular mechanism by which both decision-making difficulties in autism and general decision fatigue might arise, and highlights the PAG as a region of interest for further investigation of these topics. Improving our understanding of the neurobiological mechanisms underlying altered decision-making in autism might help to improve overall awareness of the difficulties faced by affected individuals at performing seemingly ‘simple’ decision-making tasks.

9.2 The contribution of subcortical sensorimotor circuits to rapid PDM in autism mouse models.

9.2.1 Visual processing within the SC

Increasing interest has turned towards investigating the role of subcortical regions, such as the superior colliculus (SC) (Soares et al. 2017; Jure 2019; McFadyen et al. 2020), in the perceptual and visual attention deficits observed in autism. Its critical role in attentional control and multisensory integration and its dominant role in visual processing during the early stages of life, has led to it becoming a region of interest for the investigation of PDM abnormalities in autism (Jure 2019, 2022). Contrary to these expectations, however, in chapter 5 we observed no major differences in visual processing within the SC of our *Setd5*$^{+/-}$, *Cul3*$^{+/-}$ and *Ptchd1*$^{Y/-}$

mice. Using a shifting white noise stimulus (Gupta et al. 2022) we were able to resolve high-resolution receptive fields and identify similar spatial and temporal receptive field properties across mutant and the wild-type animals from all three models, similar to those previously described in the sSC (Wang et al. 2010; Franceschi and Solomon 2018; Lee et al. 2020). Responses to other types of visual features, including the looming stimulus, were indistinguishable across animals from all three mouse models. In contrast to previous studies that identified direction selectivity impairments in the visual cortex of Fragile X (*Fmr1*$^{-/-}$) mice (Goel et al. 2018), direction selectivity appears to be unaffected, at least in the *Setd5* model (Fig. 5.6). It is possible that the processing of motion, direction and orientation could be affected in the image-forming visual pathway through the thalamus and visual cortex which could lead to differences in slower PDM processes that require this type of visual evaluation. The absence of widespread visual processing deficits in the three models studied here suggests subcortical visual processing impairments are not universally expressed in autism and do not lead to the PDM behavioural deficits observed here.

9.2.2 The PAG as a novel locus of dysfunction in autism.

A key, and unexpected, finding of this research was the isolation of dPAG dysfunction in two molecularly distinct genetic models of autism. In this study, *in vitro* patch-clamp electrophysiological examination revealed a marked hypoexcitability to injected current in both *Setd5*$^{+/-}$ (Fig. 7.4) and *Ptchd1*$^{Y/-}$ dPAG cells (Fig. 7.14). To the best of our knowledge, only one paper has previously reported a direct link between PAG dysfunction and autism (Anstey et al. 2022), and the topic has, in general, received little direct attention. In agreement to the reduced defensive responses observed in the three autism mouse models in this study, Anstey et al. (2022) observed reduced freezing behaviour in rats with mutations in an additional autism-risk gene, neuroligin-3 (*Nlgn3*), to an auditory fear conditioning paradigm. However, in contrast to both of these results, the rats were faster at learning an active place avoidance task when subjected to foot shocks in a fixed region of the arena, and showed stronger jumping responses to aversive foot shocks. Functionally, dPAG but not ventral PAG (vPAG) cells were found to be hyperexcitable in this rat model (Anstey et al. 2022). The cause of the cellular hyperexcitability was found to be due to a reduction in the fast-afterhyperpolarisation potential (fAHP) of the spikes generated, which is known to be mediated by Ca^{2+}-activated large-conductance K^+ channels (BK) (Springer et al. 2014). It is interesting that in rodent models of different autism-risk genes, cells within the same brain region can have the inverse functional phenotype (hyperexcitability versus hypoexcitability) and lead to opposite behavioural outcomes (increased versus decreased defensive behaviours).

Although this study found a select impairment in the intrinsic excitability of dPAG cells in *Setd5*$^{+/-}$ and *Ptchd1*$^{Y/-}$ mice, other mutations linked to autism might indirectly affect PAG function, and PDM to visual threats, via disrupted inputs from other brain regions. The PAG receives strong afferent input from a multitude of regions, including higher cortical regions, that have the ability to modulate responses to threatening stimuli and alter the activity of cells within the PAG (Vianna and Brandao, 2003; Loyd and Murphy, 2013). Both the amygdala and

the prefrontal cortex (PFC) have been strongly linked to emotional and cognitive dysfunction in autism and send strong projections to the dPAG (Beitz 1982). Interestingly, afferent projections from the medial prefrontal cortex to the rostrolateral PAG were shown to modulate exploratory drive and motivation to hunt (Mota-Ortiz et al. 2009), it would be interesting to investigate the functional properties of lateral PAG cells as well to investigate whether a hyperactivity of these cells could be involved in the increased exploratory drive observed in the mutant *Setd5* and *Ptchd1* animals across test days. The PAG is similarly innervated by projections from neuromodulatory systems and PAG cells express a wide range of receptors for dopamine (Meyer et al. 2009; Vaaga et al. 2020; Ferrari et al. 2021), endocannabinoids (Saito and Moriera, 2010), opioids (McNally et al. 2004), adrenaline (Porter-Stransky et al. 2009) and serotonin (Deakin and Graeff, 1991). Pharmacological manipulations of serotonergic receptors *in vitro* mediated both increased and decreased the excitability of PAG cells depending on the region and receptor distribution (Jeong et al. 2013). The results presented in this study together with the known role of the PAG as an integrator and gatekeeper of many processes linked to autism pathophysiology, e.g. pain, sensory processing, fear and anxiety, indicates it may function as an appealing candidate for further study in autism research.

9.3 Contribution of PAG excitability to the adaptive control of defensive behaviours

The ability to flexibly respond to threats is critical for appropriately matching behavioural responses to the level of threat. Increasing levels of PAG stimulation has been linked to the selection of more severe defensive responses and the correspondingly intense performance of these behaviours, indicating that neuronal activity of PAG cell populations might modulate both the selection and expression of behavioural responses. In this study, we observed a specific behavioural abnormality in the mutant animals, to appropriately select and perform an escape response, which offered the unique opportunity to examine the circuit and cellular mechanisms driving adaptive control of this defensive behaviour. Since early neuronal stimulation studies observed the transition through increasingly defensive behaviours with increased PAG stimulation (Bittencourt et al. 2005), it was thought that distinct motor programmes - i.e. risk assessment, freezing, fleeing and defensive attack - were mediated by increasing levels of PAG activity. Similarly, populations that selectively encode stretch-attend risk-assessment behaviours, freezing, arresting, escape and defensive attack have all been exclusively isolated using *in vivo* extracellular recordings (Deng et al. 2016; La-Vu et al. 2022; Reis et al. 2021; Liu et al. 2022). Circuit mechanisms of flexible action selection propose that lateral inhibition between distinct excitatory output pathways of the PAG control the expression of distinct defensive strategies, i.e. freeze and flee (Tovote et al. 2016). Historically, this selection was explained by the PAG's columnar organisation (Depaulis et al. 1992; Keay and Bandler 2001) or the presence of parallel input-output pathways for active/passive defensive responses (Vianna and Brandão 2003; Gross and Canteras 2012). However, recent studies propose a new functional circuit motif by which extrinsic inputs are integrated within

the PAG to arbitrate between competing motor output circuits, enabling flexible switching between defensive behaviours in response to threats (Tovote et al. 2016; Fadok et al. 2017).

Our study unearthed intrinsic limitations to the maximum level of neuronal activity that can be generated by dPAG cells in *Ptchd1*$^{Y/-}$ (Fig. 7.14) and *Setd5*$^{+/-}$ animals (Fig. 7.4), and comparable impairments in the speed with which escape responses could be generated. Interestingly, observing an initial arrest followed by an escape in these animals, supports the idea that increasing levels of PAG activity are required to transition between low and high intensity responses. The retention of comparable defensive behaviours to low level threat stimuli (Fig. 6.4), or low levels of dmSC activation (Fig. 6.1) indicates that the circuits driving these behaviours are unaffected by these mutations. It is unclear from these experiments whether low level activation of the same excitatory dPAG cells that drive escape mediates the arrest behaviour, or if, as previous groups suggested (Deng et al. 2016; Reis et al. 2021), this is mediated by an additional circuit within the PAG that is unaffected in these mutant mouse models. We did not record from v/vlPAG cells, nor did we test the animals' responses to a paradigm selectively evoking freezing, such as the panning overhead disc (De Franceschi et al. 2016), so it is unclear if sustained freezing responses are also impaired in the mutant animals. It would be interesting to disentangle whether it is only the selection and performance of escape behaviours, or if freezing and fighting behaviours are also affected.

As well as selecting the most appropriate behavioural response, the flexible expression and performance of the chosen behaviour is critical for an organism to interact optimally with its environment (Lenzi et al. 2022). Here, we observed that animals that were unable to modulate the firing rates in their dPAG cells were similarly unable to perform an appropriate defensive response to an innately-threatening visual stimulus. In the *Setd5*$^{+/-}$ animals, the inability of their PAG cells to 'shift gears' into a higher firing state correlated with the animals' inability to generate suitably intense responses to high-level threats, even though their responses to lower level threats were unaffected. This selective impairment in response to high, but not low, intensity stimuli (Fig. 6.4) was also observed in the acoustic startle response of *Cul3*$^{+/-}$ mice (Rapanelli et al. 2021) and aligns with the coping difficulties of many individuals with ASD to high intensity sensory stimuli, such as bright lights or crowded places, but not to mellow sensory environments (McFadyen et al. 2020). It is interesting to speculate whether the impairment of homeostatic regulation of neuronal firing at higher levels of circuit activation might be a widespread feature in the neuropathophysiology of the sensory impairments in autism.

9.4 The role of potassium channels in adaptive behaviour ASD dysfunction

Voltage-gated potassium channels allow K^+ ions to exit the cell and therefore are commonly linked to hyperpolarisation of the plasma membrane, inhibition and reduced excitability. As mentioned in the section above, the excitability of the PAG cells seems to be critical to the generation of adaptive behavioural responses, however the molecular factors modulating this excitability and the mechanisms that regulate these changes over short and long time frames

are still unclear. This study identified voltage-gated potassium channel dysfunction as potential mediators of the perturbation of rapid sensorimotor processing observed in the *Setd5* model. Application of a pharmacological blocker of three subtypes of voltage-gated potassium channels (K_v1.1, K_v1.2 and K_v1.6) ameliorated the input-dependent hypoexcitability phenotype observed in *Setd5*$^{+/-}$ neurons to strong current injections. In line with the potential role of K_v channels in modulating PAG excitability, K_v1.1 was recently shown to regulate homeostatic control of hippocampal firing through functional modulation of the action initial segment (AIS) (Zbili et al. 2021). This modulatory control of hippocampal activity (Morgan et al. 2019; Zbili et al. 2021) and similarly adaptive changes in the behaviour of mice to the LAR paradigm were both observed in < 10 minutes (Lenzi et al. 2022), suggesting that homeostatic regulation of neuronal excitability through K_v channel regulation could be one mechanism by which the flexible control of defensive behaviours is achieved. It is already known that the selectivity of K_v channels fluctuates during development and in response to changing environmental conditions (Chen et al. 2014; Pliego and Pedroarena 2020), indicating that this modulatory mechanism might be applied to other adaptive processes as well.

Although the link between K_v channels in the PAG and sensorimotor dysfunction has not been previously described, the involvement of potassium channel dysfunction in autism is well-established (Guglielmi et al. 2015; Cheng, et al. 2021). Deleterious mutations in genes encoding diverse subtypes of potassium channels have been uncovered in genetic analyses of individuals with ASDs. Given Setd5's role as an epigenetic regulator, it is interesting that activity-dependent phosphorylation of potassium channels is able to modulate both the function, localisation and subunit composition of these channels, which in turn can modulate neuronal excitability (Misonou et al. 2004; Johnston et al. 2010). It could be that the *Setd5*$^{+/-}$ dPAG hypoexcitability phenotype could result from impaired homeostatic regulation of neuronal excitability caused by compromised epigenetic modulation, leading to aberrant post-translational modification (Winklhofer et al. 2003) or impaired interactions with auxiliary subunits (Niespodziany et al. 2019). K_v1.1 was the obvious target for initial investigation in the *Setd5* model given its widespread expression during development and in adulthood. However, it is possible that K_v1.2 or K_v1.6 might play a more influential role in the mechanism by which this mutation leads to dPAG hypoexcitability. Further investigation into the specific role of K_v1.1 using the more selective pharmacological agent, K-dendrotoxin (Robertson et al. 1996), or protein and transcriptional analyses of K_v1.2 and K_v1.6 are necessary to understand the exact molecular mechanism underlying this pathology. Although α-Dendrotoxin application was not able to rescue the hypoexcitability phenotype observed in *Ptchd1*$^{Y/-}$ animals, it is still possible that the observed hypoexcitability results from potassium channel dysfunction. A previous study linked the same mutation to a reduction in the conductance of a calcium-dependent potassium channel (SK channels) within a distinct thalamic nucleus (Wells et al. 2016). Application of a selective SK channel blocker, 1-EBIO (Pedarzani and Stocker 2008), would unveil the potential role of this channel in mediating the excitability changes observed in *Ptchd1*$^{Y/-}$ animals.

9.5 The use of the looming avoidance response paradigm to study rapid perceptual decision-making in ASD.

As elaborated in detail in chapter 1, autism spectrum disorders (ASDs) are ubiquitously observed in the global population and developments in genetic sequencing technologies have advanced our understanding of the genetic changes involved in the condition. However, insight into how these genetic alterations affect neural circuit function and behaviour is often hindered by the complexity of the neural circuits that drive the observed behavioural phenotypes, and the difficulty in interpreting the behavioural changes. This study attempted to overcome these shortcomings by attempting a top-down, neuroethological approach to investigate the impact of ASD-linked mutations on an innate, visually-driven behaviour with a well described, and relatively simple circuitry: the looming avoidance response.

This behavioural paradigm has several notable features that make it well-suited to this sort of systematic symptom-to-circuit approach. It is both simple and robust, and generates behavioural responses that are interpretable and quantifiable. Different features of these responses can then be mapped onto a defined circuit, providing a convergent framework upon which to compare responses across individuals. It can be considered an innate form of a "Go/No-Go" decision-making task that is transferable and ethologically relevant to both animals and humans (Fig. 1.5, Juavinett, Erlich, and Churchland 2018; Najafi and Churchland 2018). The fact that it does not require training makes it particularly appealing for investigating PDM in organisms that may have concomitant difficulties with learning or memory, such as models of intellectual disability or neurodegeneration, since these factors could obscure results found with a conventional conditioned PDM task. Moreover, with respect to its use in autism research, this task specifically investigates the role of covert, non-image forming visual processing on the pathophysiology of the sensory processing and visual attention differences observed in many autistic individuals. Practically, the simplicity and ease with which both the stimulus and environmental conditions can be modified enables incredible experimental flexibility. What's more, an even wider range of behavioural responses could be investigated by expanding the environmental complexity, i.e. by adding platforms to climb on, boulders to hide behind or holes to burrow in. Manipulating the number of animals in the arena would also allow for the investigation of collective decision-making or the effect of certain group dynamics, such as social hierarchies, on PDM.

In this study, we used this framework to identify a convergent behavioural phenotype: a delay in the initiation of an escape response, across three molecularly distinct mouse models of autism. Targeted dissection of the known underlying circuitry enabled us to isolate a node of dysfunction (dPAG) in one of these models (*Setd5*) and to link this phenotype back to a molecular target (voltage-gated potassium channels). With the knowledge gained from one model, we could then directly target this identified locus of dysfunction in the other two models to observe a conserved functional impairment in the *Ptchd1* model, and a divergent underlying aetiology in the *Cul3* model. Overall, this paradigm offers a unique behavioural and circuit-

level framework that facilitates the comparative study of PDM processes in both health and disease.

9.6 Concluding remarks

The ability to evaluate sensory information to guide behaviour is critical in order to effectively interact with the external world and urgent situations require rapid sensory evaluation in order to generate optimal responses. Previous work elucidating the critical role of a subcortical circuit through the SC and the PAG in mediating escape responses to visual threats provided a mechanistic framework from which we were able to systematically investigate the neuronal origin of a behavioural impairment in this particular PDM process.

In this study, we demonstrated the use of the innate LAR paradigm to study rapid PDM in mouse models of autism and identified interpretable and consistent differences in the initiation of defensive escape behaviours across the mutant animals from these genetic models. Correspondingly, electrophysiological analysis of the circuit node known to be required for the initiation of an escape response, the dPAG, revealed a reduction in the intrinsic excitability of these cells in the mutant *Setd5* and *Ptchd1* animals. The magnitude of this effect was proportional to the amount of current injected, reminiscent of the graded behavioural impairment observed to stimuli of increasing threat level. In the *Setd5* model, pharmacological blockade of select voltage-gated potassium channels recovered the frequency-current (f-I) relationship of dPAG cells. It is tempting to speculate, given the large effect of blocking these channels on the excitability of these neurons, that the recruitment or upregulation of these channels might comprise a mechanism to flexibly control the performance of this defensive behaviour. This work further proposes the PAG, and the regulation of potassium channels within the PAG, as topics of interest for further investigation into the molecular mechanisms underlying altered PDM in autism.

10 Appendix

10.1 An immersive behavioural environment for conducting visual attention paradigms and recording collicular activity in freely-moving animals in this immersive environment.

Initially this study aimed to investigate perceptual decision-making in a freely-moving environment whilst simultaneously recording neuronal activity in the SC using calcium imaging techniques. In order to achieve this goal, we built a behavioural arena with a domed lid that enabled visual stimuli to be presented onto the entire outer surface of the lid to generate an immersive visual experience. The animal's behaviour was tracked through an IR-transparent floor from below and neuronal activity was recorded using implanted graded index (GRIN) lenses and miniature endoscopes (Fig. 11.1a, Doric Lenses Inc.). We successfully designed and constructed both the physical setup and an integrated pipeline for controlling the presentation of the desired visual stimuli and the synchronised recording of calcium transients through the Doric (Doric Lenses Inc.) imaging software. We developed scripts for subsequent offline analysis of the behavioural data using DeepLabCut (Mathis et al. 2018), and the calcium imaging data using the CaImAn NoRMCorre module (Pnevmatikakis and Giovannucci 2017) and constrained nonnegative matrix factorization (CNMF) (Pnevmatikakis et al. 2016), for motion correction and signal extraction respectively (Fig. 11.1c). We generated MATLAB scripts to generate various visual stimuli to probe approach ('fluttering' dot), avoidance (looming disc) and optokinetic (moving gratings) behavioural responses (Fig. 11.1a,b). To record the activity of cells within the SC, we first tried recording from transgenic animals that expressed GCaMP6f before changing to the injection of viruses encoding GCaMP6s because of superior expression and fluorophore intensity (Fig.11.1c, top left).

However, despite the system being fully operational (Fig. 10.1), we encountered a number of difficulties in combining this setup with our desired behavioural experiments. A fundamental issue for using the arena in the study of visually-guided behaviours was its relatively small size (~30 cm diameter). The limited space available to the animal impaired its ability to perform specific behaviours, for example we never saw a defensive behaviour to the presentation of a looming stimulus, instead we often observed rearing to the looming stimulus. It is possible that the 'shelter-like' geometry of the environment resulted in the animal registering the dome itself as a place of refuge and therefore contextually, the animal did not perceive the visual stimulus as a threat. An additional issue was the uneven projection of visual stimuli onto the dome surface due to the dome material. Three projectors were used in order to fully cover the surface of the arena, however this resulted in light aberrations that we only discovered after some time and were more pronounced when viewing from the inside than the outside of the arena. It is possible that this sufficiently impaired the projected image the animals were viewing that their detection was not able to trigger an appropriate behavioural response. Overall, we switched to a more conventional 'box-shape' arena (Fig. 2.1) for eliciting the LAR.

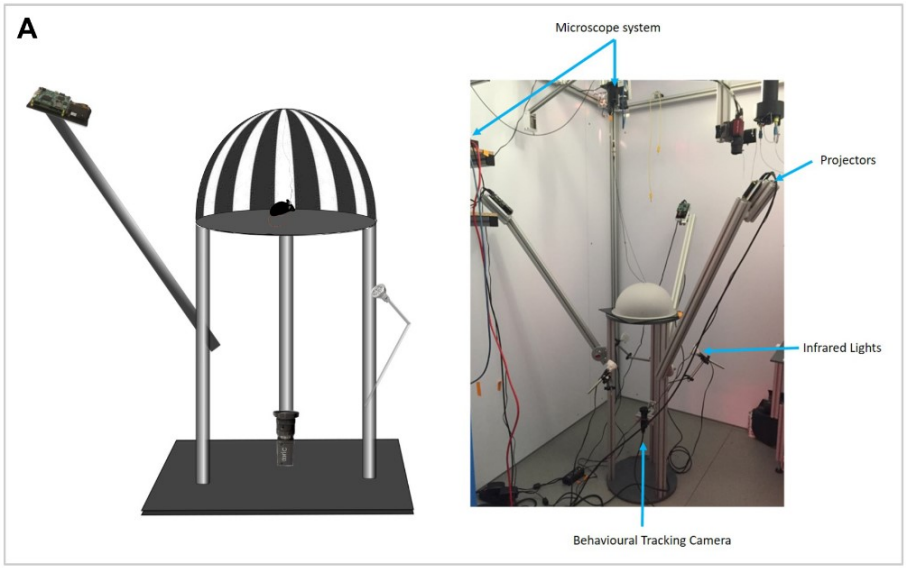
A
Microscope system
Projectors
Infrared Lights
Behavioural Tracking Camera

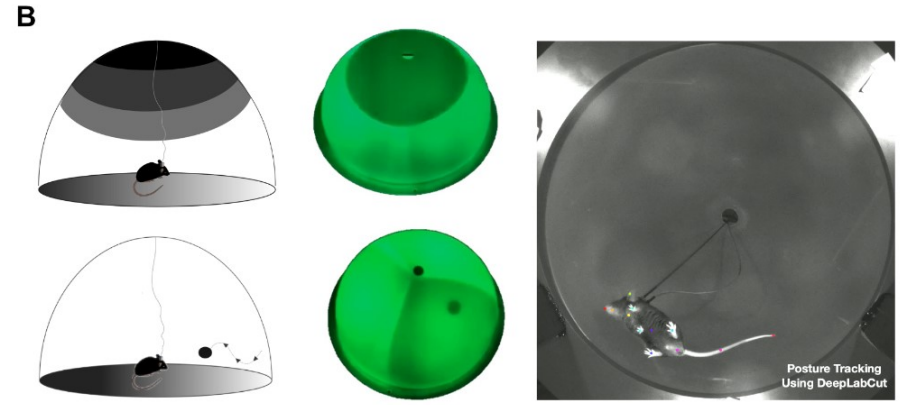
B
Posture Tracking
Using DeepLabCut

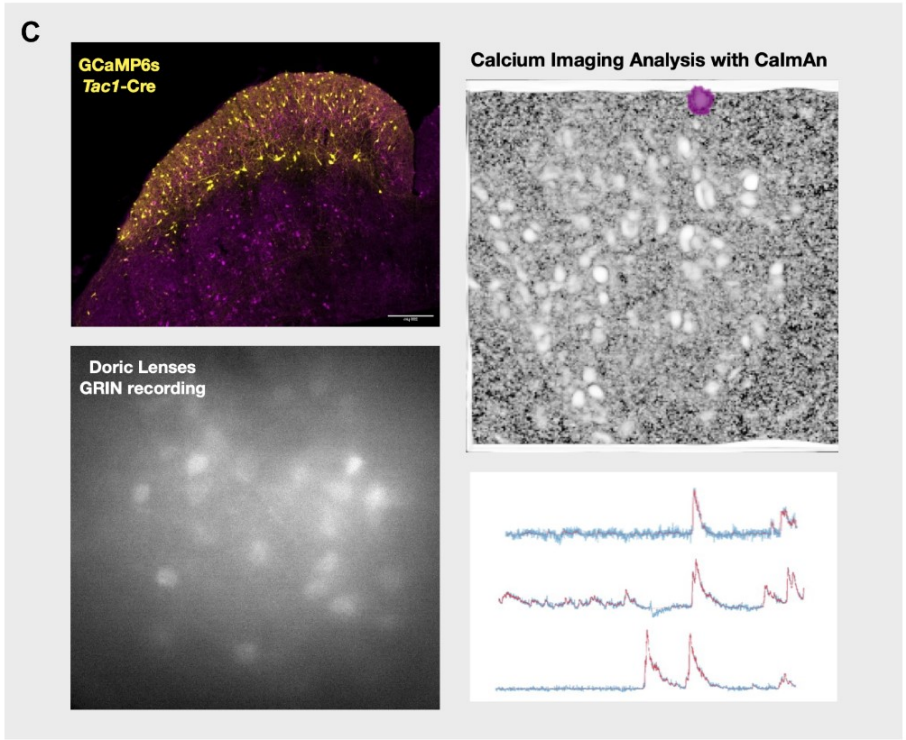
C
GCaMP6s
Tac1-Cre
Doric Lenses
GRIN recording
Calcium Imaging Analysis with CaImAn

Fig. 10.1 Domed behavioural arena for conducting freely-moving behavioural experiments and full-field visual stimulation. (Above)

a, A schematic of the setup built (left) showing the position of the mouse inside the domed roof, with a hole in the top for patch cables and optic fibres, back projection of the dome using DLP light projectors, illumination of the chamber using IR lights and behavioural recording using a near-IR camera from below. Right, shows a photograph of the completed setup. **b**, Both avoidance (i.e. the LAR) and approach (i.e. prey capture) behaviours could be tested within the arena. Left, experimental schematics of mice with a miniature endoscope attached and middle, photographs of stimulus presentation of the two types of stimuli on the external surface of the dome. Right, an example frame from a behavioural recording and the annotated body parts using DeepLabCut (Mathis et al. 2018). **c**, Top left, Confocal micrograph of one superior colliculus showing the infection of a cre-dependent virus encoding GCaMP6s (yellow) into a *Tac1*-Cre mouse. Parvalbumin positive cells are stained in magenta. Bottom left, an example frame from a video recording of GCaMP6s activity in the sSC of a mouse implanted with a Doric graded index (GRIN) lens. Top right, Example analysis of a different GCaMP recording using the CaImAn image analysis software. A selected cell of interest is segmented and highlighted in purple. Bottom right, Example traces exported from the CaImAn software.

11 References

Ahmadlou, Mehran, and J. Alexander Heimel. 2015. “Preference for Concentric Orientations in the Mouse Superior Colliculus.” *Nature Communications* 6 (April).

Ahmadlou, Mehran, Azadeh Tafreshiha, and J. Alexander Heimel. 2017. “Visual Cortex Limits Pop-Out in the Superior Colliculus of Awake Mice.” *Cerebral Cortex* 27 (12): 5772–83.

Ahmadlou, Mehran, Larry S. Zweifel, and J. Alexander Heimel. 2018. “Functional Modulation of Primary Visual Cortex by the Superior Colliculus in the Mouse.” *Nature Communications* 9 (1): 1–13.

Akechi, Hironori, Timo Stein, Atsushi Senju, Yukiko Kikuchi, Yoshikuni Tojo, Hiroo Osanai, and Toshikazu Hasegawa. 2014. “Absence of Preferential Unconscious Processing of Eye Contact in Adolescents with Autism Spectrum Disorder.” *Autism Research: Official Journal of the International Society for Autism Research* 7 (5): 590–97.

Al-Beltagi, Mohammed. 2021. “Autism Medical Comorbidities.” *World Journal of Clinical Pediatrics* 10 (3): 15–28.

Allen, Kathryne M., Jennifer Lawlor, Angeles Salles, and Cynthia F. Moss. 2021. “Orienting Our View of the Superior Colliculus: Specializations and General Functions.” *Current Opinion in Neurobiology* 71 (December): 119–26.

Amano, K., T. Tanikawa, H. Iseki, H. Kawabatake, M. Notani, H. Kawamura, and K. Kitamura. 1978. “Single Neuron Analysis of the Human Midbrain Tegmentum.” *Stereotactic and Functional Neurosurgery* 41 (1-4): 66–78.

Amano, K., T. Tanikawa, H. Kawamura, H. Iseki, M. Notani, H. Kawabatake, T. Shiwaku, T. Suda, H. Demura, and K. Kitamura. 1982. “Endorphins and Pain Relief.” *Stereotactic and Functional Neurosurgery* 45 (1-2): 123–35.

Amar, Megha, Akula Bala Pramod, Nam-Kyung Yu, Victor Munive Herrera, Lily R. Qiu, Patricia Moran-Losada, Pan Zhang, et al. 2021. “Autism-Linked Cullin3 Germline Haploinsufficiency Impacts Cytoskeletal Dynamics and Cortical Neurogenesis through RhoA Signaling.” *Molecular Psychiatry* 26 (7): 3586–3613.

Amoruso, Lucia, Antonio Narzisi, Martina Pinzino, Alessandra Finisguerra, Lucia Billeci, Sara Calderoni, Franco Fabbro, Filippo Muratori, Anna Volzone, and Cosimo Urgesi. 2019. “Contextual Priors Do Not Modulate Action Prediction in Children with Autism.” *Proceedings. Biological Sciences / The Royal Society* 286 (1908): 20191319.

Amso, Dima, Sara Haas, Elena Tenenbaum, Julie Markant, and Stephen J. Sheinkopf. 2014. “Bottom-up Attention Orienting in Young Children with Autism.” *Journal of Autism and Developmental Disorders* 44 (3): 664–73.

Andérica-Romero, Ana Cristina, Irma Gabriela González-Herrera, Abel Santamaría, and José Pedraza-Chaverri. 2013. “Cullin 3 as a Novel Target in Diverse Pathologies.” *Redox Biology*. Elsevier B.V. https://doi.org/10.1016/j.redox.2013.07.003.

Annaz, Dagmara, Ruth Campbell, Mike Coleman, Elizabeth Milne, and John Swettenham. 2012. “Young Children with Autism Spectrum Disorder Do Not Preferentially Attend to Biological Motion.” *Journal of Autism and Developmental Disorders* 42 (3): 401–8.

Annaz, Dagmara, Anna Remington, Elizabeth Milne, Mike Coleman, Ruth Campbell, Michael S. C. Thomas, and John Swettenham. 2010. “Development of Motion Processing in Children with Autism.” *Developmental Science* 13 (6): 826–38.

Anstey, Natasha J., Vijayakumar Kapgal, Shashank Tiwari, Thomas C. Watson, Anna K. H. Toft, Owen R. Dando, Felicity H. Inkpen, et al. 2022. “Imbalance of Flight-Freeze Responses and Their Cellular Correlates in the Nlgn3-/y Rat Model of Autism.” *Molecular Autism* 13 (1): 34.

An, X., R. Bandler, D. Ongür, and J. L. Price. 1998. “Prefrontal Cortical Projections to Longitudinal Columns in the Midbrain Periaqueductal Gray in Macaque Monkeys.” *The Journal of Comparative Neurology* 401 (4): 455–79.

Assareh, Neda, Mahsa Sarrami, Pascal Carrive, and Gavan P. McNally. 2016. “The Organization of Defensive Behavior Elicited by Optogenetic Excitation of Rat Lateral or Ventrolateral Periaqueductal Gray.” *Behavioral Neuroscience* 130 (4): 406–14.

Bakroon, Asmaa, and Vasudevan Lakshminarayanan. 2016. “Visual Function in Autism Spectrum Disorders: A Critical Review.” *Clinical & Experimental Optometry: Journal of the Australian*

Optometrical Association 99 (4): 297–308.
Balasco, Luigi, Giovanni Provenzano, and Yuri Bozzi. 2019. “Sensory Abnormalities in Autism Spectrum Disorders: A Focus on the Tactile Domain, From Genetic Mouse Models to the Clinic.” *Frontiers in Psychiatry / Frontiers Research Foundation* 10: 1016.
Ball, William, and Edward Tronick. 1971. “Infant Responses to Impending Collision: Optical and Real.” *Science* 171 (3973): 818–20.
Bandler, Richard, and Antoine Depaulis. 1991. “Midbrain Periaqueductal Gray Control of Defensive Behavior in the Cat and the Rat.” In *The Midbrain Periaqueductal Gray Matter: Functional, Anatomical, and Neurochemical Organization*, edited by Antoine Depaulis and Richard Bandler, 175–98. Boston, MA: Springer US.
Bandler, R., and M. T. Shipley. 1994. “Columnar Organization in the Midbrain Periaqueductal Gray: Modules for Emotional Expression?” *Trends in Neurosciences* 17 (9): 379–89.
Baron-Cohen, Simon, Emma Ashwin, Chris Ashwin, Teresa Tavassoli, and Bhismadev Chakrabarti. 2009. “Talent in Autism: Hyper-Systemizing, Hyper-Attention to Detail and Sensory Hypersensitivity.” *Philosophical Transactions of the Royal Society of London. Series B, Biological Sciences* 364 (1522): 1377–83.
Baron-Cohen, S., H. A. Ring, E. T. Bullmore, S. Wheelwright, C. Ashwin, and S. C. Williams. 2000. “The Amygdala Theory of Autism.” *Neuroscience and Biobehavioral Reviews* 24 (3): 355–64.
Basso, Michele A., and Paul J. May. 2017. “Circuits for Action and Cognition: A View from the Superior Colliculus.” *Annual Review of Vision Science* 3 (1): 197–226.
Becchio, Cristina, Morena Mari, and Umberto Castiello. 2010. “Perception of Shadows in Children with Autism Spectrum Disorders.” *PloS One* 5 (5). https://doi.org/10.1371/journal.pone.0010582.
Behbehani, M. M. 1995. “Functional Characteristics of the Midbrain Periaqueductal Gray.” *Progress in Neurobiology* 46 (6): 575–605.
Beitz, A. J. 1982. “The Organization of Afferent Projections to the Midbrain Periaqueductal Gray of the Rat.” *Neuroscience* 7 (1): 133–59.
Beltramo, Riccardo, and Massimo Scanziani. 2019. “A Collicular Visual Cortex: Neocortical Space for an Ancient Midbrain Visual Structure.” *Science* 363 (6422): 64–69.
Benarroch, Eduardo E. 2012. “Periaqueductal Gray: An Interface for Behavioral Control.” *Neurology* 78 (3): 210–17.
Benavidez, Nora L., Michael S. Bienkowski, Muye Zhu, Luis H. Garcia, Marina Fayzullina, Lei Gao, Ian Bowman, et al. 2021. “Organization of the Inputs and Outputs of the Mouse Superior Colliculus.” *Nature Communications* 12 (1): 4004.
Bertone, Armando, Laurent Mottron, Patricia Jelenic, and Jocelyn Faubert. 2005. “Enhanced and Diminished Visuo-Spatial Information Processing in Autism Depends on Stimulus Complexity.” *Brain: A Journal of Neurology* 128 (10): 2430–41.
Billington, Jac, Richard M. Wilkie, David T. Field, and John P. Wann. 2011. “Neural Processing of Imminent Collision in Humans.” *Proceedings. Biological Sciences / The Royal Society* 278 (1711): 1476–81.
Bittencourt, A. S., A. P. Carobrez, L. P. Zamprogno, S. Tufik, and L. C. Schenberg. 2004. “Organization of Single Components of Defensive Behaviors within Distinct Columns of Periaqueductal Gray Matter of the Rat: Role of N-Methyl-D-Aspartic Acid Glutamate Receptors.” *Neuroscience* 125 (1): 71–89.
Bittencourt, A. S., E. M. Nakamura-Palacios, H. Mauad, S. Tufik, and L. C. Schenberg. 2005. “Organization of Electrically and Chemically Evoked Defensive Behaviors within the Deeper Collicular Layers as Compared to the Periaqueductal Gray Matter of the Rat.” *Neuroscience* 133 (4): 873–92.
Blake, Randolph, Lauren M. Turner, Moria J. Smoski, Stacie L. Pozdol, and Wendy L. Stone. 2003. “Visual Recognition of Biological Motion Is Impaired in Children with Autism.” *Psychological Science* 14 (2): 151–57.
Blanchard, D. Caroline, Guy Griebel, Roger Pobbe, and Robert J. Blanchard. 2011. “Risk Assessment as an Evolved Threat Detection and Analysis Process.” *Neuroscience and Biobehavioral Reviews* 35 (4): 991–98.
Blanchard, D. C., G. Williams, E. M. C. Lee, and R. J. Blanchard. 1981. “Taming of Wild Rattus Norvegicus by Lesions of the Mesencephalic Central Gray.” *Physiological Psychology* 9 (2): 157–

63.
Blanchard, R. J., and D. C. Blanchard. 1989. “Attack and Defense in Rodents as Ethoexperimental Models for the Study of Emotion.” *Progress in Neuro-Psychopharmacology & Biological Psychiatry* 13 Suppl: S3–14.
Blanchard, R. J., M. Yang, C. I. Li, A. Gervacio, and D. C. Blanchard. 2001. “Cue and Context Conditioning of Defensive Behaviors to Cat Odor Stimuli.” *Neuroscience and Biobehavioral Reviews* 25 (7-8): 587–95.
Blanchard, Robert J., Kevin J. Flannelly, and D. Caroline Blanchard. 1986. “Defensive Behaviors of Laboratory and Wild Rattus Norvegicus.” *Journal of Comparative Psychology*. https://doi.org/10.1037/0735-7036.100.2.101.
Blanchard, Robert J., Kenneth K. Fukunaga, and D. Caroline Blanchard. 1976. “Environmental Control of Defensive Reactions to a Cat.” *Bulletin of the Psychonomic Society* 8 (3): 179–81.
Blumstein, Daniel T. 2003. “Flight-Initiation Distance in Birds Is Dependent on Intruder Starting Distance.” *The Journal of Wildlife Management* 67 (4): 852–57.
Bolles, Robert C., and Michael S. Fanselow. 1980. “A Perceptual-Defensive-Recuperative Model of Fear and Pain.” *The Behavioral and Brain Sciences* 3 (2): 291–301.
Borst, Alexander. 2014. “Fly Visual Course Control: Behaviour, Algorithms and Circuits.” *Nature Reviews. Neuroscience* 15 (9): 590–99.
Bothe, Maximilian S., Harald Luksch, Hans Straka, and Tobias Kohl. 2019. “Neuronal Substrates for Infrared Contrast Enhancement and Motion Detection in Rattlesnakes.” *Current Biology: CB* 29 (11): 1827–32.e4.
Boyden, Edward S., Feng Zhang, Ernst Bamberg, Georg Nagel, and Karl Deisseroth. 2005. “Millisecond-Timescale, Genetically Targeted Optical Control of Neural Activity.” *Nature Neuroscience* 8 (9): 1263–68.
Burack, J. A. 1994. “Selective Attention Deficits in Persons with Autism: Preliminary Evidence of an Inefficient Attentional Lens.” *Journal of Abnormal Psychology* 103 (3): 535–43.
Burgess, Christopher P., Armin Lak, Nicholas A. Steinmetz, Peter Zatka-Haas, Charu Bai Reddy, Elina A. K. Jacobs, Jennifer F. Linden, et al. 2017. “High-Yield Methods for Accurate Two-Alternative Visual Psychophysics in Head-Fixed Mice.” *Cell Reports* 20 (10): 2513–24.
Byun, Haewon, Soohyun Kwon, Hee-Jeong Ahn, Hong Liu, Douglas Forrest, Jonathan B. Demb, and In-Jung Kim. 2016. “Molecular Features Distinguish Ten Neuronal Types in the Mouse Superficial Superior Colliculus.” *The Journal of Comparative Neurology* 524 (11): 2300–2321.
Campatelli, G., R. R. Federico, F. Apicella, F. Sicca, and F. Muratori. 2013. “Face Processing in Children with ASD: Literature Review.” *Research in Autism Spectrum Disorders* 7 (3): 444–54.
Card, Gwyneth, and Michael H. Dickinson. 2008. “Visually Mediated Motor Planning in the Escape Response of Drosophila.” *Current Biology: CB* 18 (17): 1300–1307.
Chandrasekaran, Anand R., Ruchir D. Shah, and Michael C. Crair. 2007. “Developmental Homeostasis of Mouse Retinocollicular Synapses.” *The Journal of Neuroscience: The Official Journal of the Society for Neuroscience* 27 (7): 1746–55.
Chaudhry, A., A. Noor, B. Degagne, K. Baker, L. A. Bok, A. F. Brady, D. Chitayat, et al. 2015. “Phenotypic Spectrum Associated with PTCHD1 Deletions and Truncating Mutations Includes Intellectual Disability and Autism Spectrum Disorder.” *Clinical Genetics* 88 (3): 224–33.
Cheng, Ning, Eden Pagtalunan, Abdulrahman Abushaibah, Jessica Naidu, William K. Stell, Jong M. Rho, and Yves Sauvé. 2020. “Atypical Visual Processing in a Mouse Model of Autism.” *Scientific Reports* 10 (1): 12390.
Cheng, Peipei, Zilong Qiu, and Yasong Du. 2021. “Potassium Channels and Autism Spectrum Disorder: An Overview.” *International Journal of Developmental Neuroscience: The Official Journal of the International Society for Developmental Neuroscience* 81 (6): 479–91.
Chen, Haijun, Franck C. Chatelain, and Florian Lesage. 2014. “Altered and Dynamic Ion Selectivity of K+ Channels in Cell Development and Excitability.” *Trends in Pharmacological Sciences* 35 (9): 461–69.
Chen, Shanping, Huiying Tan, Zhijie Wang, Yu-Ting Tseng, Xiaotao Li, and Liping Wang. 2022. “Formation of the Looming-Evoked Innate Defensive Response during Postnatal Development in Mice.” *Neuroscience Bulletin* 38 (7): 741–52.
Chiang, J. A., V. Shumakova, and K. Greenfield. 2020. “Proposed Phenotype for Females with a

SETD5 Gene Variation: A Case Report." *Journal of Neurology*. https://www.itmedicalteam.pl/abstract/proposed-phenotype-for-females-with-a-setd5-gene-variation-a-case-report-107644.html.

Chou, Xiao-Lin, Xiyue Wang, Zheng-Gang Zhang, Li Shen, Brian Zingg, Junxiang Huang, Wen Zhong, Lukas Mesik, Li I. Zhang, and Huizhong Whit Tao. 2018. "Inhibitory Gain Modulation of Defense Behaviors by Zona Incerta." *Nature Communications* 9 (1): 1151.

Chung, Seungwon, and Jung Woo Son. 2020. "Visual Perception in Autism Spectrum Disorder: A Review of Neuroimaging Studies." *Journal of the Korean Academy of Child and Adolescent Psychiatry* 31 (3): 105–20.

Cléry, Justine C., David J. Schaeffer, Yuki Hori, Kyle M. Gilbert, Lauren K. Hayrynen, Joseph S. Gati, Ravi S. Menon, and Stefan Everling. 2020. "Looming and Receding Visual Networks in Awake Marmosets Investigated with fMRI." *NeuroImage* 215 (July): 116815.

Coker-Appiah, Dionne S., Stuart F. White, Roberta Clanton, Jiongjong Yang, Alex Martin, and R. J. R. Blair. 2013. "Looming Animate and Inanimate Threats: The Response of the Amygdala and Periaqueductal Gray." *Social Neuroscience* 8 (6): 621–30.

Comoli, Eliane, Véronique Coizet, Justin Boyes, J. Paul Bolam, Newton S. Canteras, Rachet H. Quirk, Paul G. Overton, and Peter Redgrave. 2003. "A Direct Projection from Superior Colliculus to Substantia Nigra for Detecting Salient Visual Events." *Nature Neuroscience* 6 (9): 974–80.

Comoli, Eliane, Plínio Das Neves Favaro, Nicolas Vautrelle, Mariana Leriche, Paul G. Overton, and Peter Redgrave. 2012. "Segregated Anatomical Input to Sub-Regions of the Rodent Superior Colliculus Associated with Approach and Defense." *Frontiers in Neuroanatomy* 6 (APRIL 2012): 1–19.

Courchesne, E., J. Townsend, N. A. Akshoomoff, O. Saitoh, R. Yeung-Courchesne, A. J. Lincoln, H. E. James, R. H. Haas, L. Schreibman, and L. Lau. 1994. "Impairment in Shifting Attention in Autistic and Cerebellar Patients." *Behavioral Neuroscience* 108 (5): 848–65.

Cowey, A., and V. H. Perry. 1980. "The Projection of the Fovea to the Superior Colliculus in Rhesus Monkeys." *Neuroscience* 5 (1): 53–61.

Crapse, Trinity B., Hakwan Lau, and Michele A. Basso. 2018. "A Role for the Superior Colliculus in Decision Criteria." *Neuron* 97 (1): 181–94.e6.

Crawley, Jacqueline N. 2012. "Translational Animal Models of Autism and Neurodevelopmental Disorders." *Dialogues in Clinical Neuroscience* 14 (3): 293–305.

Cresswell, W., S. Butler, M. J. Whittingham, and J. L. Quinn. 2009. "Very Short Delays Prior to Escape from Potential Predators May Function Efficiently as Adaptive Risk-Assessment Periods." *Behaviour* 146 (6): 795–813.

Dakin, Steven, and Uta Frith. 2005. "Vagaries of Visual Perception in Autism." *Neuron* 48 (3): 497–507.

Dalton, Kim M., Brendon M. Nacewicz, Tom Johnstone, Hillary S. Schaefer, Morton Ann Gernsbacher, H. H. Goldsmith, Andrew L. Alexander, and Richard J. Davidson. 2005. "Gaze Fixation and the Neural Circuitry of Face Processing in Autism." *Nature Neuroscience* 8 (4): 519–26.

Deakin, J. F., and F. G. Graeff. 1991. "5-HT and Mechanisms of Defence." *Journal of Psychopharmacology* 5 (4): 305–15.

Dean, P., I. J. Mitchell, and P. Redgrave. 1988. "Responses Resembling Defensive Behaviour Produced by Microinjection of Glutamate into Superior Colliculus of Rats." *Neuroscience* 24 (2): 501–10.

Dean, P., P. Redgrave, and G. W. Westby. 1989. "Event or Emergency? Two Response Systems in the Mammalian Superior Colliculus." *Trends in Neurosciences* 12 (4): 137–47.

De Franceschi, Gioia, Tipok Vivattanasarn, Aman B. Saleem, and Samuel G. Solomon. 2016. "Vision Guides Selection of Freeze or Flight Defense Strategies in Mice." *Current Biology: CB* 26 (16): 2150–54.

Deliu, Elena, Niccolò Arecco, Jasmin Morandell, Christoph P. Dotter, Ximena Contreras, Charles Girardot, Eva Lotta Käsper, et al. 2018. "Haploinsufficiency of the Intellectual Disability Gene SETD5 Disturbs Developmental Gene Expression and Cognition." *Nature Neuroscience* 21 (12): 1717–27.

Del Pino, Isabel, Beatriz Rico, and Oscar Marín. 2018. "Neural Circuit Dysfunction in Mouse Models

of Neurodevelopmental Disorders." *Current Opinion in Neurobiology* 48 (February): 174–82.
Dendrinos, Georgia, Marie Hemelt, and Asaf Keller. 2011. "Prenatal VPA Exposure and Changes in Sensory Processing by the Superior Colliculus." *Frontiers in Integrative Neuroscience* 5 (October): 68.
Deng, Hanfei, Xiong Xiao, and Zuoren Wang. 2016. "Periaqueductal Gray Neuronal Activities Underlie Different Aspects of Defensive Behaviors." *Journal of Neuroscience* 36 (29): 7580–88.
De Oca, B. M., J. P. DeCola, S. Maren, and M. S. Fanselow. 1998. "Distinct Regions of the Periaqueductal Gray Are Involved in the Acquisition and Expression of Defensive Responses." *The Journal of Neuroscience: The Official Journal of the Society for Neuroscience* 18 (9): 3426–32.
Depaulis, A., K. A. Keay, and R. Bandler. 1992. "Longitudinal Neuronal Organization of Defensive Reactions in the Midbrain Periaqueductal Gray Region of the Rat." *Experimental Brain Research. Experimentelle Hirnforschung. Experimentation Cerebrale* 90 (2): 307–18.
Dickinson, Abigail, Michael Bruyns-Haylett, Richard Smith, Myles Jones, and Elizabeth Milne. 2016. "Superior Orientation Discrimination and Increased Peak Gamma Frequency in Autism Spectrum Conditions." *Journal of Abnormal Psychology* 125 (3): 412–22.
Dillon, Shane C., Xing Zhang, Raymond C. Trievel, and Xiaodong Cheng. 2005. "The SET-Domain Protein Superfamily: Protein Lysine Methyltransferases." *Genome Biology* 6 (8): 227.
Dinstein, Ilan, David J. Heeger, Lauren Lorenzi, Nancy J. Minshew, Rafael Malach, and Marlene Behrmann. 2012. "Unreliable Evoked Responses in Autism." *Neuron* 75 (6): 981–91.
Dong, Zhaoqi, Wenbing Chen, Chao Chen, Hongsheng Wang, Wanpeng Cui, Zhibing Tan, Heath Robinson, et al. 2020. "CUL3 Deficiency Causes Social Deficits and Anxiety-like Behaviors by Impairing Excitation-Inhibition Balance through the Promotion of Cap-Dependent Translation." *Neuron* 105 (3): 475–90.e6.
Drager, U. C., and D. H. Hubel. 1975. "Responses to Visual Stimulation and Relationship between Visual, Auditory, and Somatosensory Inputs in Mouse Superior Colliculus." *Journal of Neurophysiology* 38 (3): 690–713.
Dräger, U. C., and D. H. Hubel. 1976. "Topography of Visual and Somatosensory Projections to Mouse Superior Colliculus." *Journal of Neurophysiology* 39 (1): 91–101.
Dunkeld, J., and T. G. Bower. 1980. "Infant Response to Impending Optical Collision." *Perception* 9 (5): 549–54.
Edut, Shahaf, and David Eilam. 2003. "Rodents in Open Space Adjust Their Behavioral Response to the Different Risk Levels during Barn-Owl Attack." *BMC Ecology* 3 (November): 10.
Eilam, David. 2005. "Die Hard: A Blend of Freezing and Fleeing as a Dynamic Defense--Implications for the Control of Defensive Behavior." *Neuroscience and Biobehavioral Reviews* 29 (8): 1181–91.
Ellard, C. G. 1996. "Laboratory Studies of Antipredator Behavior in the Mongolian Gerbil (Meriones Unguiculatus): Factors Affecting Response Attenuation with Repeated Presentations." *Journal of Comparative Psychology* 110 (2): 155–63.
Ellis, Erika M., Gregory Gauvain, Benjamin Sivyer, and Gabe J. Murphy. 2016. "Shared and Distinct Retinal Input to the Mouse Superior Colliculus and Dorsal Lateral Geniculate Nucleus." *Journal of Neurophysiology* 116 (2): 602–10.
Elsabbagh, Mayada, Janice Fernandes, Sara Jane Webb, Geraldine Dawson, Tony Charman, Mark H. Johnson, and British Autism Study of Infant Siblings Team. 2013. "Disengagement of Visual Attention in Infancy Is Associated with Emerging Autism in Toddlerhood." *Biological Psychiatry* 74 (3): 189–94.
Endevelt-Shapira, Yaara, Ofer Perl, Aharon Ravia, Daniel Amir, Ami Eisen, Vered Bezalel, Liron Rozenkrantz, et al. 2018. "Altered Responses to Social Chemosignals in Autism Spectrum Disorder." *Nature Neuroscience* 21 (1): 111–19.
Espenhahn, Svenja, Kate J. Godfrey, Sakshi Kaur, Maia Ross, Niloy Nath, Olesya Dmitrieva, Carly McMorris, et al. 2021. "Tactile Cortical Responses and Association with Tactile Reactivity in Young Children on the Autism Spectrum." *Molecular Autism* 12 (1): 26.
Esteban Masferrer, Maria, Bianca A. Silva, Kensaku Nomoto, Susana Q. Lima, and Cornelius T. Gross. 2020. "Differential Encoding of Predator Fear in the Ventromedial Hypothalamus and Periaqueductal Grey." *The Journal of Neuroscience: The Official Journal of the Society for*

Neuroscience 40 (48): 9283–92.
Evans, DA. 2017. “A MIDBRAIN MECHANISM FOR COMPUTING ESCAPE DECISIONS IN THE MOUSE.” Thesis. Cambridge University Press.
Evans, David W., Kristin Canavera, F. Lee Kleinpeter., Elise Maccubbin, and Ken Taga. 2005. “The Fears, Phobias and Anxieties of Children with Autism Spectrum Disorders and Down Syndrome: Comparisons with Developmentally and Chronologically Age Matched Children.” *Child Psychiatry and Human Development* 36 (1): 3–26.
Evans, Dominic A., A. Vanessa Stempel, Ruben Vale, and Tiago Branco. 2019. “Cognitive Control of Escape Behaviour.” *Trends in Cognitive Sciences* 23 (4): 334–48.
Evans, Dominic A., A. Vanessa Stempel, Ruben Vale, Sabine Ruehle, Yaara Lefler, and Tiago Branco. 2018. “A Synaptic Threshold Mechanism for Computing Escape Decisions.” *Nature* 558 (7711): 590–94.
Ewert, Jörg-Peter. 1987. “Neuroethology of Releasing Mechanisms: Prey-Catching in Toads.” *The Behavioral and Brain Sciences* 10 (3): 337–68.
Fadok, Jonathan P., Sabine Krabbe, Milica Markovic, Julien Courtin, Chun Xu, Lema Massi, Paolo Botta, et al. 2017. “A Competitive Inhibitory Circuit for Selection of Active and Passive Fear Responses.” *Nature* 542 (7639): 96–100.
Fang, Qi, Xiao Lin Chou, Bo Peng, Wen Zhong, Li I. Zhang, and Huizhong Whit Tao. 2020. “A Differential Circuit via Retino-Colliculo-Pulvinar Pathway Enhances Feature Selectivity in Visual Cortex through Surround Suppression.” *Neuron* 105 (2): 355–69.e6.
Fanselow, M. S. 1991. “The Midbrain Periaqueductal Gray as a Coordinator of Action in Response to Fear and Anxiety.” *The Midbrain Periaqueductal Gray Matter*. https://link.springer.com/chapter/10.1007/978-1-4615-3302-3_10.
Feigin, Helen, Shir Shalom-Sperber, Ditza A. Zachor, and Adam Zaidel. 2021. “Increased Influence of Prior Choices on Perceptual Decisions in Autism.” *eLife* 10 (July). https://doi.org/10.7554/eLife.61595.
Feinberg, Evan H., and Markus Meister. 2015. “Orientation Columns in the Mouse Superior Colliculus.” *Nature* 519 (7542): 229–32.
Felgerolle, Chloé, Betty Hébert, Maryvonne Ardourel, Géraldine Meyer-Dilhet, Arnaud Menuet, Kimberley Pinto-Morais, Jean Charles Bizot, Jacques Pichon, Sylvain Briault, and Olivier Perche. 2019. “Visual Behavior Impairments as an Aberrant Sensory Processing in the Mouse Model of Fragile X Syndrome.” *Frontiers in Behavioral Neuroscience* 13 (October): 228.
Feria Pliego, Jessica Abigail, and Christine M. Pedroarena. 2020. “Kv1 Potassium Channels Control Action Potential Firing of Putative GABAergic Deep Cerebellar Nuclear Neurons.” *Scientific Reports* 10 (1): 6954.
Fernandes, Isabella R., Ana C. P. Cruz, Adriano Ferrasa, Dylan Phan, Roberto H. Herai, and Alysson R. Muotri. 2018. “Genetic Variations on *SETD5* Underlying Autistic Conditions.” *Developmental Neurobiology* 78 (5): 500–518.
Fernandez de Molina, A., and R. W. Hunsperger. 1962. “Organization of the Subcortical System Governing Defence and Flight Reactions in the Cat.” *The Journal of Physiology* 160 (2): 200–213.
Filges, I., B. Röthlisberger, A. Blattner, N. Boesch, P. Demougin, F. Wenzel, A. R. Huber, K. Heinimann, P. Weber, and P. Miny. 2011. “Deletion in Xp22.11: PTCHD1 Is a Candidate Gene for X-Linked Intellectual Disability with or without Autism.” *Clinical Genetics* 79 (1): 79–85.
Filosa, Alessandro, Alison J. Barker, Marco Dal Maschio, and Herwig Baier. 2016. “Feeding State Modulates Behavioral Choice and Processing of Prey Stimuli in the Zebrafish Tectum.” *Neuron* 90 (3): 596–608.
Flanders, M. 1985. “Visually Guided Head Movement in the African Chameleon.” *Vision Research* 25 (7): 935–42.
Foss-Feig, Jennifer H., Duje Tadin, Kimberly B. Schauder, and Carissa J. Cascio. 2013. “A Substantial and Unexpected Enhancement of Motion Perception in Autism.” *The Journal of Neuroscience: The Official Journal of the Society for Neuroscience* 33 (19): 8243–49.
Franceschi, Gioia, and Samuel G. Solomon. 2018. “Visual Response Properties of Neurons in the Superficial Layers of the Superior Colliculus of Awake Mouse.” *The Journal of Physiology* 596 (24): 6307–32.
Franklin, Tamara B., Bianca A. Silva, Zinaida Perova, Livia Marrone, Maria E. Masferrer, Yang Zhan,

Angie Kaplan, et al. 2017. “Prefrontal Cortical Control of a Brainstem Social Behavior Circuit.” *Nature Neuroscience* 20 (2): 260–70.
Fratzl, Alex, Alice M. Koltchev, Nicole Vissers, Yu Lin Tan, Andre Marques-Smith, A. Vanessa Stempel, Tiago Branco, and Sonja B. Hofer. 2021. “Flexible Inhibitory Control of Visually Evoked Defensive Behavior by the Ventral Lateral Geniculate Nucleus.” *Neuron*, October. https://doi.org/10.1016/j.neuron.2021.09.003.
Fricano-Kugler, Catherine, Aaron Gordon, Grace Shin, Kun Gao, Jade Nguyen, Jamee Berg, Mary Starks, and Daniel H. Geschwind. 2019. “CYFIP1 Overexpression Increases Fear Response in Mice but Does Not Affect Social or Repetitive Behavioral Phenotypes.” *Molecular Autism* 10 (June): 25.
Frith, U., and F. Happé. 1994. “Autism: Beyond ‘Theory of Mind.’” *Cognition* 50 (1-3): 115–32.
Frost, R. O., and D. L. Shows. 1993. “The Nature and Measurement of Compulsive Indecisiveness.” *Behaviour Research and Therapy* 31 (7): 683–92.
Furigo, I. C., W. F. de Oliveira, A. R. de Oliveira, E. Comoli, M. V. C. Baldo, S. R. Mota-Ortiz, and N. S. Canteras. 2010. “The Role of the Superior Colliculus in Predatory Hunting.” *Neuroscience* 165 (1): 1–15.
Gabbiani, Fabrizio, Holger G. Krapp, Christof Koch, and Gilles Laurent. 2002. “Multiplicative Computation in a Visual Neuron Sensitive to Looming.” *Nature* 420 (6913): 320–24.
Gabbiani, F., H. G. Krapp, and G. Laurent. 1999. “Computation of Object Approach by a Wide-Field, Motion-Sensitive Neuron.” *The Journal of Neuroscience: The Official Journal of the Society for Neuroscience* 19 (3): 1122–41.
Gale, Samuel D., and Gabe J. Murphy. 2014. “Distinct Representation and Distribution of Visual Information by Specific Cell Types in Mouse Superficial Superior Colliculus.” *Journal of Neuroscience* 34 (40): 13458–71.
Gepner, B., D. Mestre, G. Masson, and S. de Schonen. 1995. “Postural Effects of Motion Vision in Young Autistic Children.” *Neuroreport* 6 (8): 1211–14.
Gibson, William T., Carlos R. Gonzalez, Conchi Fernandez, Lakshminarayanan Ramasamy, Tanya Tabachnik, Rebecca R. Du, Panna D. Felsen, Michael R. Maire, Pietro Perona, and David J. Anderson. 2015. “Behavioral Responses to a Repetitive Visual Threat Stimulus Express a Persistent State of Defensive Arousal in Drosophila.” *Current Biology: CB* 25 (11): 1401–15.
Gilbert, Charles D., and Wu Li. 2013. “Top-down Influences on Visual Processing.” *Nature Reviews. Neuroscience* 14 (5): 350–63.
Goel, Anubhuti, Daniel A. Cantu, Janna Guilfoyle, Gunvant R. Chaudhari, Aditi Newadkar, Barbara Todisco, Diego de Alba, et al. 2018. “Impaired Perceptual Learning in a Mouse Model of Fragile X Syndrome Is Mediated by Parvalbumin Neuron Dysfunction and Is Reversible.” *Nature Neuroscience* 21 (10): 1404–11.
Grandin, Temple. 2000. “My Mind Is a Web Browser: How People with Autism Think.” *Cerebrum: The Dana Forum on Brain Science* 2 (1): 14–22.
Green, Claire, Joshua Willoughby, and Meena Balasubramanian. 2017. “De Novo SETD5 Loss-of-Function Variant as a Cause for Intellectual Disability in a 10-Year Old Boy with an Aberrant Blind Ending Bronchus.” *American Journal of Medical Genetics. Part A* 173 (12): 3165–71.
Gross, Cornelius T., and Newton Sabino Canteras. 2012. “The Many Paths to Fear.” *Nature Reviews. Neuroscience* 13 (9): 651–58.
Grozeva, Detelina, Keren Carss, Olivera Spasic-Boskovic, Michael J. Parker, Hayley Archer, Helen V. Firth, Soo-Mi Park, et al. 2014. “De Novo Loss-of-Function Mutations in SETD5, Encoding a Methyltransferase in a 3p25 Microdeletion Syndrome Critical Region, Cause Intellectual Disability.” *American Journal of Human Genetics* 94 (4): 618–24.
Grubb, M.S. & Burrone, J. 2010. “Activity-Dependent Relocation of the Axon Initial Segment Fine-Tunes Neuronal Excitability.” *Nature*, no. 465: 1070–74.
Gruber-Dujardin, Eva. 2010. “Chapter 8.1 - Role of the Periaqueductal Gray in Expressing Vocalization.” In *Handbook of Behavioral Neuroscience*, edited by Stefan M. Brudzynski, 19:313–27. Elsevier.
Guglielmi, Luca, Ilenio Servettini, Martino Caramia, Luigi Catacuzzeno, Fabio Franciolini, Maria Cristina D’Adamo, and Mauro Pessia. 2015. “Update on the Implication of Potassium Channels in Autism: K(+) Channelautism Spectrum Disorder.” *Frontiers in Cellular Neuroscience* 9 (March):

34.
Gupta, Divyansh, Wiktor Młynarski, Olga Symonova, Jan Svatoň, and Maximilian Joesch. 2022. “Panoramic Visual Statistics Shape Retina-Wide Organization of Receptive Fields.” *bioRxiv*. https://doi.org/10.1101/2022.01.11.475815.
Guy, Jacalyn, Laurent Mottron, Claude Berthiaume, and Armando Bertone. 2019. “A Developmental Perspective of Global and Local Visual Perception in Autism Spectrum Disorder.” *Journal of Autism and Developmental Disorders* 49 (7): 2706–20.
Hadjikhani, Nouchine, Jakob Åsberg Johnels, Nicole R. Zürcher, Amandine Lassalle, Quentin Guillon, Loyse Hippolyte, Eva Billstedt, Noreen Ward, Eric Lemonnier, and Christopher Gillberg. 2017. “Look Me in the Eyes: Constraining Gaze in the Eye-Region Provokes Abnormally High Subcortical Activation in Autism.” *Scientific Reports* 7 (1): 1–7.
Halewa, Judith, Sylviane Marouillat, Manon Dixneuf, Rose-Anne Thépault, Dévina C. Ung, Nicolas Chatron, Bénédicte Gérard, et al. 2021. “Novel Missense Mutations in PTCHD1 Alter Its Plasma Membrane Subcellular Localization and Cause Intellectual Disability and Autism Spectrum Disorder.” *Human Mutation* 42 (7): 848–61.
Happé, Francesca, and Uta Frith. 2006. “The Weak Coherence Account: Detail-Focused Cognitive Style in Autism Spectrum Disorders.” *Journal of Autism and Developmental Disorders* 36 (1): 5–25.
Hausen, Klaus, and Martin Egelhaaf. 1989. “Neural Mechanisms of Visual Course Control in Insects.” In *Facets of Vision*, 391–424. Springer Berlin Heidelberg.
Heinemans & Moita. 2022. “Looming Stimuli Reliably Drive Innate, but Not Learned, Defensive Responses in Rats.”
Hikidi, Yuto, Noritaka Hirohashi, Takashi Kasugai, and Noriyosi Sato. 2020. “An Elaborate Behavioural Sequence Reinforces the Decoy Effect of Ink during Predatory Attacks on Squid.” *Journal of Ethology* 38 (2): 155–60.
Holstege, G., R. Bandler, and C. B. Saper. 1996. “The Emotional Motor System.” *Progress in Brain Research* 107: 3–6.
Huang, Yan, Lei Li, Kun Dong, Hongsi Tang, Qingning Yang, Xianglian Jia, Yundan Liao, et al. 2020. “Topological Shape Changes Weaken the Innate Defensive Response to Visual Threat in Mice.” *Neuroscience Bulletin* 36 (4): 427–31.
Huang, Yiting, Mark Vangel, Helen Chen, Maya Eshel, Ming Cheng, Tao Lu, and Jian Kong. 2022. “The Impaired Subcortical Pathway From Superior Colliculus to the Amygdala in Boys With Autism Spectrum Disorder.” *Frontiers in Integrative Neuroscience* 16 (June): 666439.
Huber, Daniel, Leopoldo Petreanu, Nima Ghitani, Sachin Ranade, Tomás Hromádka, Zach Mainen, and Karel Svoboda. 2008. “Sparse Optical Microstimulation in Barrel Cortex Drives Learned Behaviour in Freely Moving Mice.” *Nature* 451 (7174): 61–64.
Hulbert, S. W., and Y-H Jiang. 2016. “Monogenic Mouse Models of Autism Spectrum Disorders: Common Mechanisms and Missing Links.” *Neuroscience* 321 (May): 3–23.
Hunsperger, R. W. 1956. “Role of Substantia Grisea Centralis Mesencephali in Electrically-Induced Rage Reactions.” *Progress in Neurobiology*, no. 2: 289–94.
Hu, Yu, Zhuoming Chen, Lu Huang, Yue Xi, Bingxiao Li, Hong Wang, Jiajian Yan, et al. 2017. “A Translational Study on Looming-Evoked Defensive Response and the Underlying Subcortical Pathway in Autism.” *Scientific Reports* 7 (1): 14755.
Ibrahim, Karim, Jeffrey A. Eilbott, Pamela Ventola, George He, Kevin A. Pelphrey, Gregory McCarthy, and Denis G. Sukhodolsky. 2019. “Reduced Amygdala–Prefrontal Functional Connectivity in Children With Autism Spectrum Disorder and Co-Occurring Disruptive Behavior.” *Biological Psychiatry: Cognitive Neuroscience and Neuroimaging* 4 (12): 1031–41.
Inayat, Samsoon, Jad Barchini, Hui Chen, Liang Feng, Xiaorong Liu, and Jianhua Cang. 2015. “Neurons in the Most Superficial Lamina of the Mouse Superior Colliculus Are Highly Selective for Stimulus Direction.” *The Journal of Neuroscience: The Official Journal of the Society for Neuroscience* 35 (20): 7992–8003.
Inman, Callen M. 2020. “Visual Recognition of Prey and Predators.” In *Encyclopedia of Animal Cognition and Behavior*, edited by Jennifer Vonk and Todd Shackelford, 1–7. Cham: Springer International Publishing.
Isa, Kaoru, Thongchai Sooksawate, Kenta Kobayashi, Kazuto Kobayashi, Peter Redgrave, and

Tadashi Isa. 2020. “Dissecting the Tectal Output Channels for Orienting and Defense Responses.” *eNeuro* 7 (5). https://doi.org/10.1523/ENEURO.0271-20.2020.
Isa, Tadashi, and William C. Hall. 2009. “Exploring the Superior Colliculus in Vitro.” *Journal of Neurophysiology* 102 (5): 2581–93.
Ito, Shinya, and David A. Feldheim. 2018. “The Mouse Superior Colliculus: An Emerging Model for Studying Circuit Formation and Function.” *Frontiers in Neural Circuits* 12 (February): 10.
Ito, Shinya, David A. Feldheim, and Alan M. Litke. 2017. “Segregation of Visual Response Properties in the Mouse Superior Colliculus and Their Modulation during Locomotion.” *Journal of Neuroscience* 37 (35): 8428–43.
Iwafuchi, Sota, Atsuo Kikuchi, Wakaba Endo, Takehiko Inui, Yu Aihara, Kazuhito Satou, Tadashi Kaname, and Shigeo Kure. 2021. “A Novel Stop-Gain CUL3 Mutation in a Japanese Patient with Autism Spectrum Disorder.” *Brain & Development* 43 (2): 303–7.
Jao Keehn, R. Joanne, Ellyn B. Pueschel, Yangfeifei Gao, Afrooz Jahedi, Kalekirstos Alemu, Ruth Carper, Inna Fishman, and Ralph-Axel Müller. 2020. “Underconnectivity Between Visual and Salience Networks and Links With Sensory Abnormalities in Autism Spectrum Disorder.” *Journal of the American Academy of Child and Adolescent Psychiatry* 0 (0). https://doi.org/10.1016/j.jaac.2020.02.007.
Jeong, Hyo-Jin, Karen Lam, Vanessa A. Mitchell, and Christopher W. Vaughan. 2013. “Serotonergic Modulation of Neuronal Activity in Rat Midbrain Periaqueductal Gray.” *Journal of Neurophysiology* 109 (11): 2712–19.
Johnson, Mark H., Richard Griffin, Gergely Csibra, Hanife Halit, Teresa Farroni, Michelle de Haan, Leslie A. Tucker, Simon Baron-Cohen, and John Richards. 2005. “The Emergence of the Social Brain Network: Evidence from Typical and Atypical Development.” *Development and Psychopathology* 17 (3): 599–619.
Johnson, Shannon A., Eldad Yechiam, Robin R. Murphy, Sarah Queller, and Julie C. Stout. 2006. “Motivational Processes and Autonomic Responsivity in Asperger’s Disorder: Evidence from the Iowa Gambling Task.” *Journal of the International Neuropsychological Society: JINS* 12 (5): 668–76.
Johnston, Jamie, Ian D. Forsythe, and Conny Kopp-Scheinpflug. 2010. “Going Native: Voltage-Gated Potassium Channels Controlling Neuronal Excitability.” *The Journal of Physiology* 588 (Pt 17): 3187–3200.
Juavinett, Ashley L., Jeffrey C. Erlich, and Anne K. Churchland. 2018. “Decision-Making Behaviors: Weighing Ethology, Complexity, and Sensorimotor Compatibility.” *Current Opinion in Neurobiology*. Elsevier Ltd. https://doi.org/10.1016/j.conb.2017.11.001.
Jun, Elizabeth J., Alex R. Bautista, Michael D. Nunez, Daicia C. Allen, Jung H. Tak, Eduardo Alvarez, and Michele A. Basso. 2021. “Causal Role for the Primate Superior Colliculus in the Computation of Evidence for Perceptual Decisions.” *Nature Neuroscience*, June, 1–11.
Jure, Rubin. 2019. “Autism Pathogenesis: The Superior Colliculus.” *Frontiers in Neuroscience* 13 (JAN): 1029.
Jure, Rubin. 2022. “The ‘Primitive Brain Dysfunction’ Theory of Autism: The Superior Colliculus Role.” *Frontiers in Integrative Neuroscience* 16 (May): 797391.
Kanner, Leo, and Others. 1943. “Autistic Disturbances of Affective Contact.” *The Nervous Child* 2 (3): 217–50.
Kawakubo, Yuki, Kiyoto Kasai, Shinji Okazaki, Miyuki Hosokawa-Kakurai, Kei-Ichiro Watanabe, Hitoshi Kuwabara, Michiko Ishijima, et al. 2007. “Electrophysiological Abnormalities of Spatial Attention in Adults with Autism during the Gap Overlap Task.” *Clinical Neurophysiology: Official Journal of the International Federation of Clinical Neurophysiology* 118 (7): 1464–71.
Kawamura, K., and T. Konno. 1979. “Various Types of Corticotectal Neurons of Cats as Demonstrated by Means of Retrograde Axonal Transport of Horseradish Peroxidase.” *Experimental Brain Research. Experimentelle Hirnforschung. Experimentation Cerebrale* 35 (1): 161–75.
Kay, Rachel B., Nicole A. Gabreski, and Jason W. Triplett. 2018. “Visual Subcircuit-Specific Dysfunction and Input-Specific Mispatterning in the Superior Colliculus of Fragile X Mice.” *Journal of Neurodevelopmental Disorders* 10 (1). https://doi.org/10.1186/s11689-018-9241-1.
Keay, K. A., and R. Bandler. 2001. “Parallel Circuits Mediating Distinct Emotional Coping Reactions

to Different Types of Stress." *Neuroscience and Biobehavioral Reviews* 25 (7-8): 669–78.
Keehn, Brandon, Ralph-Axel Müller, and Jeanne Townsend. 2013. "Atypical Attentional Networks and the Emergence of Autism." *Neuroscience and Biobehavioral Reviews* 37 (2): 164–83.
Keehn, Brandon, Vanessa Vogel-Farley, Helen Tager-Flusberg, and Charles A. Nelson. 2015. "Atypical Hemispheric Specialization for Faces in Infants at Risk for Autism Spectrum Disorder." *Autism Research: Official Journal of the International Society for Autism Research* 8 (2): 187–98.
Ketter-Katz, Hadas, Tidhar Lev-Ari, and Gadi Katzir. 2020. "Vision in Chameleons-A Model for Non-Mammalian Vertebrates." *Seminars in Cell & Developmental Biology* 106 (October): 94–105.
King, Sheila M., and Alan Cowey. 1992. "Defensive Responses to Looming Visual Stimuli in Monkeys with Unilateral Striate Cortex Ablation." *Neuropsychologia* 30 (11): 1017–24.
Kleinhans, Natalia M., Todd Richards, L. Clark Johnson, Kurt E. Weaver, Jessica Greenson, Geraldine Dawson, and Elizabeth Aylward. 2011. "FMRI Evidence of Neural Abnormalities in the Subcortical Face Processing System in ASD." *NeuroImage* 54 (1): 697–704.
Klin, Ami, Sarah Shultz, and Warren Jones. 2015. "Social Visual Engagement in Infants and Toddlers with Autism: Early Developmental Transitions and a Model of Pathogenesis." *Neuroscience and Biobehavioral Reviews* 50 (March): 189–203.
Koffka, K. (1935). *Principles of Gestalt psychology*. Harcourt, Brace.
Kogan, C. S., A. Bertone, K. Cornish, I. Boutet, V. M. Der Kaloustian, E. Andermann, J. Faubert, and A. Chaudhuri. 2004. "Integrative Cortical Dysfunction and Pervasive Motion Perception Deficit in Fragile X Syndrome." *Neurology* 63 (9): 1634–39.
Kong, Augustine, Michael L. Frigge, Gisli Masson, Soren Besenbacher, Patrick Sulem, Gisli Magnusson, Sigurjon A. Gudjonsson, et al. 2012. "Rate of de Novo Mutations and the Importance of Father's Age to Disease Risk." *Nature* 488 (7412): 471–75.
Krauzlis, Richard J., Lee P. Lovejoy, and Alexandre Zénon. 2013. "Superior Colliculus and Visual Spatial Attention." *Annual Review of Neuroscience* 36 (1): 165–82.
Krysko, Kristen M., and M. D. Rutherford. 2009. "A Threat-Detection Advantage in Those with Autism Spectrum Disorders." *Brain and Cognition* 69 (3): 472–80.
Kuechler, Alma, Alexander M. Zink, Thomas Wieland, Hermann Josef Lüdecke, Kirsten Cremer, Leonardo Salviati, Pamela Magini, et al. 2015. "Loss-of-Function Variants of SETD5 Cause Intellectual Disability and the Core Phenotype of Microdeletion 3p25.3 Syndrome." *European Journal of Human Genetics: EJHG* 23 (6): 753–60.
Kunchulia, Marina, Tamari Tatishvili, Khatuna Parkosadze, Nino Lomidze, and Roland Thomaschke. 2019. "Children with Autism Spectrum Disorder Show Increased Sensitivity to Time-Based Predictability." *International Journal of Developmental Disabilities* 66 (3): 214–21.
Lack, David. 1939. "The Behaviour of the Robin.—Part I. The Life-History, with Special Reference to Aggressive Behaviour, Sexual Behaviour, and Territory. Part II. A Partial Analysis of Aggressive and Recognitional Behaviour." *Proceedings of the Zoological Society of London* A109 (2-3): 169–219.
La-Vu, Mimi Q., Ekayana Sethi, Sandra Maesta-Pereira, Peter J. Schuette, Brooke C. Tobias, Fernando M. C. V. Reis, Weisheng Wang, et al. 2022. "Sparse Genetically Defined Neurons Refine the Canonical Role of Periaqueductal Gray Columnar Organization." *eLife* 11 (June). https://doi.org/10.7554/eLife.77115.
Lawson, Rebecca P., Geraint Rees, and Karl J. Friston. 2014. "An Aberrant Precision Account of Autism." *Frontiers in Human Neuroscience* 8 (MAY). https://doi.org/10.3389/fnhum.2014.00302.
Lawson, Wendy. 2001. *Understanding and Working with the Spectrum of Autism: An Insider's View*. Jessica Kingsley Publishers.
Lee, Kyu Hyun, Alvita Tran, Zeynep Turan, and Markus Meister. 2020. "The Sifting of Visual Information in the Superior Colliculus." *eLife* 9 (April). https://doi.org/10.7554/eLife.50678.
Lees, Rebecca Nicole, Armaan Fazal Akbar, and Tudor Constantin Badea. 2020. "Retinal Ganglion Cell Defects Cause Decision Shifts in Visually Evoked Defense Responses." *Journal of Neurophysiology* 124 (5): 1530–49.
Lefler, Yaara, Dario Campagner, and Tiago Branco. 2020. "The Role of the Periaqueductal Gray in Escape Behavior." *Current Opinion in Neurobiology*. Elsevier Ltd. https://doi.org/10.1016/j.conb.2019.11.014.
Lenzi, Stephen C., Lee Cossell, Benjamin Grainger, Sarah F. Olesen, Tiago Branco, and Troy W.

Margrie. 2022. “Threat History Controls Flexible Escape Behavior in Mice.” *Current Biology: CB* 0 (0). https://doi.org/10.1016/j.cub.2022.05.022.
Lettvin, J. Y., H. R. Maturana, W. S. McCulloch, and W. H. Pitts. 1959. “What the Frog’s Eye Tells the Frog's Brain.” *Proceedings of the IRE* 47 (11): 1940–51.
Liang, Feixue, Xiaorui R. Xiong, Brian Zingg, Xu Ying Ji, Li I. Zhang, and Huizhong W. Tao. 2015. “Sensory Cortical Control of a Visually Induced Arrest Behavior via Corticotectal Projections.” *Neuron*. https://doi.org/10.1016/j.neuron.2015.03.048.
Liu, Denghui, Shouhao Li, Liqing Ren, Xinyu Liu, Xiaoyuan Li, and Zhenlong Wang. 2022. “Different Coding Characteristics between Flight and Freezing in Dorsal Periaqueductal Gray of Mice during Exposure to Innate Threats.” *Animal Models and Experimental Medicine*, October. https://doi.org/10.1002/ame2.12276.
Liu, Yong Jun, Qian Wang, and Bing Li. 2011. “Neuronal Responses to Looming Objects in the Superior Colliculus of the Cat.” *Brain, Behavior and Evolution* 77 (3): 193–205.
Li, Yi, Jiawei Zeng, Juen Zhang, Chenyu Yue, Weixin Zhong, Zhixiang Liu, Qiru Feng, and Minmin Luo. 2018. “Hypothalamic Circuits for Predation and Evasion.” *Neuron* 97 (4): 911–24.e5.
Lock, T. M., J. S. Baizer, and D. B. Bender. 2003. “Distribution of Corticotectal Cells in Macaque.” *Experimental Brain Research. Experimentelle Hirnforschung. Experimentation Cerebrale* 151 (4): 455–70.
Lorenz, K. 1939. “Vergleichende Verhaltensforschung.” *Verhandlungen Der Deutschen Zoologischen Gesellschaft, Zoologischer Anzeiger Supplementband* 12: 69–102.
Lorteije, Jeannette A. M., Ariel Zylberberg, Brian G. Ouellette, Chris I. De Zeeuw, Mariano Sigman, and Pieter R. Roelfsema. 2015. “The Formation of Hierarchical Decisions in the Visual Cortex.” *Neuron* 87 (6): 1344–56.
Loyd, Dayna R., and Anne Z. Murphy. 2013. “Forebrain Modulation of the Periaqueductal Gray and Its Role in Pain.” In *Encyclopedia of Pain*, edited by Gerald F. Gebhart and Robert F. Schmidt, 1297–1303. Berlin, Heidelberg: Springer Berlin Heidelberg.
Luke, Lydia, Isabel C. H. Clare, Howard Ring, Marcus Redley, and Peter Watson. 2012. “Decision-Making Difficulties Experienced by Adults with Autism Spectrum Conditions.” *Autism: The International Journal of Research and Practice* 16 (6): 612–21.
Macari, Suzanne L., Angelina Vernetti, and Katarzyna Chawarska. 2021. “Attend Less, Fear More: Elevated Distress to Social Threat in Toddlers With Autism Spectrum Disorder.” *Autism Research: Official Journal of the International Society for Autism Research* 14 (5): 1025–36.
Madipakkam, Apoorva Rajiv, Marcus Rothkirch, Isabel Dziobek, and Philipp Sterzer. 2017. “Unconscious Avoidance of Eye Contact in Autism Spectrum Disorder.” *Scientific Reports* 7 (1): 13378.
Maior, Rafael S., Etsuro Hori, Carlos E. Uribe, Patricia G. Saletti, Taketoshi Ono, Hisao Nishijo, and Carlos Tomaz. 2012. “A Role for the Superior Colliculus in the Modulation of Threat Responsiveness in Primates: Toward the Ontogenesis of the Social Brain.” *Reviews in the Neurosciences* 23 (5-6): 697–706.
Manning, Catherine, Cameron D. Hassall, Laurence T. Hunt, Anthony M. Norcia, Eric-Jan Wagenmakers, Nathan J. Evans, and Gaia Scerif. 2022. “Behavioural and Neural Indices of Perceptual Decision-Making in Autistic Children during Visual Motion Tasks.” *Scientific Reports* 12 (1): 6072.
Mantyh, P. W. 1982. “The Midbrain Periaqueductal Gray in the Rat, Cat, and Monkey: A Nissl, Weil, and Golgi Analysis.” *The Journal of Comparative Neurology* 204 (4): 349–63.
Marco, Elysa J., Leighton B. N. Hinkley, Susanna S. Hill, and Srikantan S. Nagarajan. 2011. “Sensory Processing in Autism: A Review of Neurophysiologic Findings.” *Pediatric Research* 69 (5 Pt 2): 48R – 54R.
Markram, Henry. 2007. “The Intense World Syndrome – an Alternative Hypothesis for Autism.” *Frontiers in Neuroscience* 1 (1): 77–96.
Markram, Kamila, Tania Rinaldi, Deborah La Mendola, Carmen Sandi, and Henry Markram. 2008. “Abnormal Fear Conditioning and Amygdala Processing in an Animal Model of Autism.” *Neuropsychopharmacology: Official Publication of the American College of Neuropsychopharmacology* 33 (4): 901–12.
Marquez-Legorreta, Emmanuel, Lena Constantin, Marielle Piber, Itia A. Favre-Bulle, Michael A.

Taylor, Ann S. Blevins, Jean Giacomotto, Dani S. Bassett, Gilles C. Vanwalleghem, and Ethan K. Scott. 2022. “Brain-Wide Visual Habituation Networks in Wild Type and fmr1 Zebrafish.” *Nature Communications* 13 (1): 895.

Marshall, Christian R., Abdul Noor, John B. Vincent, Anath C. Lionel, Lars Feuk, Jennifer Skaug, Mary Shago, et al. 2008. “Structural Variation of Chromosomes in Autism Spectrum Disorder.” *American Journal of Human Genetics* 82 (2): 477–88.

Masterson, S. P., N. Zhou, B. K. Akers, W. Dang, and M. E. Bickford. 2019. “Ultrastructural and Optogenetic Dissection of V1 Corticotectal Terminal Synaptic Properties.” *The Journal of Comparative Neurology* 527 (4): 833–42.

Masullo, Laura, Letizia Mariotti, Nicolas Alexandre, Paula Freire-Pritchett, Jerome Boulanger, and Marco Tripodi. 2019. “Genetically Defined Functional Modules for Spatial Orienting in the Mouse Superior Colliculus.” *Current Biology: CB* 29 (17): 2892–2904.e8.

Mathis, Alexander, Pranav Mamidanna, Kevin M. Cury, Taiga Abe, Venkatesh N. Murthy, Mackenzie Weygandt Mathis, and Matthias Bethge. 2018. “DeepLabCut: Markerless Pose Estimation of User-Defined Body Parts with Deep Learning.” *Nature Neuroscience* 21 (9): 1281–89.

May, Paul J. 2006. “The Mammalian Superior Colliculus: Laminar Structure and Connections.” *Progress in Brain Research*. Elsevier. https://doi.org/10.1016/S0079-6123(05)51011-2.

McFadyen, Jessica, Raymond J. Dolan, and Marta I. Garrido. 2020. “The Influence of Subcortical Shortcuts on Disordered Sensory and Cognitive Processing.” *Nature Reviews. Neuroscience* 21 (5): 264–76.

Milne, Elizabeth, John Swettenham, Peter Hansen, Ruth Campbell, Helen Jeffries, and Kate Plaisted. 2002. “High Motion Coherence Thresholds in Children with Autism.” *Journal of Child Psychology and Psychiatry, and Allied Disciplines* 43 (2): 255–63.

Mirza, M. Berk, Rick A. Adams, Karl Friston, and Thomas Parr. 2019. “Introducing a Bayesian Model of Selective Attention Based on Active Inference.” *Scientific Reports* 9 (1): 1–22.

Misonou, Hiroaki, Durga P. Mohapatra, Eunice W. Park, Victor Leung, Dongkai Zhen, Kaori Misonou, Anne E. Anderson, and James S. Trimmer. 2004. “Regulation of Ion Channel Localization and Phosphorylation by Neuronal Activity.” *Nature Neuroscience* 7 (7): 711–18.

Mobbs, Dean, Predrag Petrovic, Jennifer L. Marchant, Demis Hassabis, Nikolaus Weiskopf, Ben Seymour, Raymond J. Dolan, and Christopher D. Frith. 2007. “When Fear Is near: Threat Imminence Elicits Prefrontal-Periaqueductal Gray Shifts in Humans.” *Science* 317 (5841): 1079–83.

Montijn, Jorrit S., Koen Seignette, Marcus H. Howlett, J. Leonie Cazemier, Maarten Kamermans, Christiaan N. Levelt, and J. Alexander Heimel. 2021. “A Parameter-Free Statistical Test for Neuronal Responsiveness.” *eLife* 10 (September). https://doi.org/10.7554/eLife.71969.

Mooney, R. D., X. Huang, and R. W. Rhoades. 1992. “Functional Influence of Interlaminar Connections in the Hamster’s Superior Colliculus.” *The Journal of Neuroscience: The Official Journal of the Society for Neuroscience* 12 (6): 2417–32.

Moore, Spencer M., Jason S. Seidman, Jacob Ellegood, Richard Gao, Alex Savchenko, Ty D. Troutman, Yohei Abe, et al. 2019. “Setd5 Haploinsufficiency Alters Neuronal Network Connectivity and Leads to Autistic-like Behaviors in Mice.” *Translational Psychiatry* 9 (1): 1–12.

Morandell, Jasmin, Lena A. Schwarz, Bernadette Basilico, Saren Tasciyan, Georgi Dimchev, Armel Nicolas, Christoph Sommer, et al. 2021. “Cul3 Regulates Cytoskeleton Protein Homeostasis and Cell Migration during a Critical Window of Brain Development.” *Nature Communications* 12 (1): 3058.

Morgan, Peter James, Romain Bourboulou, Caroline Filippi, Julie Koenig-Gambini, and Jérôme Epsztein. 2019. “Kv1.1 Contributes to a Rapid Homeostatic Plasticity of Intrinsic Excitability in CA1 Pyramidal Neurons in Vivo.” *eLife* 8 (November): e49915.

Morin, Lawrence P., and Keith M. Studholme. 2014. “Retinofugal Projections in the Mouse.” *The Journal of Comparative Neurology* 522 (16): 3733–53.

Moschovakis, A. K. 1996. “The Superior Colliculus and Eye Movement Control.” *Current Opinion in Neurobiology* 6 (6): 811–16.

Mota-Ortiz, S. R., Sukikara, M. H., Felicio, L. F., & Canteras, N. S. (2009). Afferent connections to the rostrolateral part of the periaqueductal gray: a critical region influencing the motivation drive to hunt and forage. Neural plasticity.

Müller, James R., Marios G. Philiastides, and William T. Newsome. 2005. “Microstimulation of the Superior Colliculus Focuses Attention without Moving the Eyes.” *Proceedings of the National Academy of Sciences of the United States of America* 102 (3): 524–29.
Münch, Thomas A., Rava Azeredo da Silveira, Sandra Siegert, Tim James Viney, Gautam B. Awatramani, and Botond Roska. 2009. “Approach Sensitivity in the Retina Processed by a Multifunctional Neural Circuit.” *Nature Neuroscience* 12 (10): 1308–16.
Murakami, Yuki, Yukio Imamura, Kuniaki Saito, Daisuke Sakai, and Jun Motoyama. 2019. “Altered Kynurenine Pathway Metabolites in a Mouse Model of Human Attention-Deficit Hyperactivity/autism Spectrum Disorders: A Potential New Biological Diagnostic Marker.” *Scientific Reports* 9 (1): 13182.
Najafi, Farzaneh, and Anne K. Churchland. 2018. “Perceptual Decision-Making: A Field in the Midst of a Transformation.” *Neuron* 100 (2): 453–62.
Nakagawa, Tadashi, Satoko Hattori, Risa Nobuta, Noriko Osumi, Keiichi I. Nakayama, and Keiko Nakayama. 2020. “The Autism-Related Protein SETD5 Controls Neural Cell Proliferation through Epigenetic Regulation of rDNA Expression.” https://doi.org/10.1016/j.isci.2020.101030.
Nakajima, Miho, L. Ian Schmitt, Guoping Feng, and Michael M. Halassa. 2019. “Combinatorial Targeting of Distributed Forebrain Networks Reverses Noise Hypersensitivity in a Model of Autism Spectrum Disorder.” *Neuron* 104 (3): 488–500.e11.
Nakashima, Mitsuko, Mitsuhiro Kato, Masaru Matsukura, Ryutaro Kira, Lock-Hock Ngu, Klaske D. Lichtenbelt, Koen L. I. van Gassen, Satomi Mitsuhashi, Hirotomo Saitsu, and Naomichi Matsumoto. 2020. “De Novo Variants in CUL3 Are Associated with Global Developmental Delays with or without Infantile Spasms.” *Journal of Human Genetics* 65 (9): 727–34.
Nashold, B. S., Jr, W. P. Wilson, and D. G. Slaughter. 1969. “Sensations Evoked by Stimulation in the Midbrain of Man.” *Journal of Neurosurgery* 30 (1): 14–24.
Nguyen, Minh Nui, Jumpei Matsumoto, Etsuro Hori, Rafael Souto Maior, Carlos Tomaz, Anh H. Tran, Taketoshi Ono, and Hisao Nishijo. 2014. “Neuronal Responses to Face-like and Facial Stimuli in the Monkey Superior Colliculus.” *Frontiers in Behavioral Neuroscience* 8 (March): 85.
Niell, Cristopher M., and Michael P. Stryker. 2010. “Modulation of Visual Responses by Behavioral State in Mouse Visual Cortex.” *Neuron* 65 (4): 472–79.
Niespodziany, Isabelle, Brice Mullier, Véronique Marie André, Philippe Ghisdal, Eric Jnoff, David Moreno-Delgado, Dominique Swinnen, Zara Sands, Martyn Wood, and Christian Wolff. 2019. “Discovery of a Small Molecule Modulator of the Kv1.1/Kvβ1 Channel Complex That Reduces Neuronal Excitability and in Vitro Epileptiform Activity.” *CNS Neuroscience & Therapeutics* 25 (4): 442–51.
Noor, Abdul, Annabel Whibley, Christian R. Marshall, Peter J. Gianakopoulos, Amelie Piton, Andrew R. Carson, Marija Orlic-Milacic, et al. 2010. “Disruption at the PTCHD1 Locus on Xp22.11 in Autism Spectrum Disorder and Intellectual Disability.” *Science Translational Medicine* 2 (49): 49ra68.
Odoemene, Onyekachi, Sashank Pisupati, Hien Nguyen, and Anne K. Churchland. 2018. “Visual Evidence Accumulation Guides Decision-Making in Unrestrained Mice.” *The Journal of Neuroscience: The Official Journal of the Society for Neuroscience* 38 (47): 10143–55.
Olds, M. E., and J. Olds. 1962. “Approach-Escape Interactions in Rat Brain.” *The American Journal of Physiology* 203 (November): 803–10.
Oliva, Damián, Violeta Medan, and Daniel Tomsic. 2007. “Escape Behavior and Neuronal Responses to Looming Stimuli in the Crab Chasmagnathus Granulatus (Decapoda: Grapsidae).” *The Journal of Experimental Biology* 210 (Pt 5): 865–80.
Orefice, Lauren L., Amanda L. Zimmerman, Anda M. Chirila, Steven J. Sleboda, Joshua P. Head, and David D. Ginty. 2016. “Peripheral Mechanosensory Neuron Dysfunction Underlies Tactile and Behavioral Deficits in Mouse Models of ASDs.” *Cell* 166 (2): 299–313.
O’Roak, Brian J., Laura Vives, Santhosh Girirajan, Emre Karakoc, Niklas Krumm, Bradley P. Coe, Roie Levy, et al. 2012. “Sporadic Autism Exomes Reveal a Highly Interconnected Protein Network of de Novo Mutations.” *Nature* 485 (7397): 246–50.
Otero Coronel, Santiago, Nicolás Martorell, Martín Beron de Astrada, and Violeta Medan. 2020. “Stimulus Contrast Information Modulates Sensorimotor Decision Making in Goldfish.” *Frontiers in Neural Circuits* 14 (May): 23.

Palmer, Colin J., Rebecca P. Lawson, and Jakob Hohwy. 2017. “Bayesian Approaches to Autism: Towards Volatility, Action, and Behavior.” *Psychological Bulletin* 143 (5): 521–42.
Panagiotidi, Maria, Paul G. Overton, and Tom Stafford. 2017. “Multisensory Integration and ADHD-like Traits: Evidence for an Abnormal Temporal Integration Window in ADHD.” *Acta Psychologica* 181 (November): 10–17.
Pastore, Stephen F., Sangyoon Y. Ko, Paul W. Frankland, Paul A. Hamel, and John B. Vincent. 2022. “PTCHD1: Identification and Neurodevelopmental Contributions of an Autism Spectrum Disorder and Intellectual Disability Susceptibility Gene.” *Genes* 13 (3). https://doi.org/10.3390/genes13030527.
Pedarzani, P., and M. Stocker. 2008. “Molecular and Cellular Basis of Small--and Intermediate-Conductance, Calcium-Activated Potassium Channel Function in the Brain.” *Cellular and Molecular Life Sciences: CMLS* 65 (20): 3196–3217.
Pellicano, Elizabeth, and David Burr. 2012. “When the World Becomes ‘Too Real’: A Bayesian Explanation of Autistic Perception.” *Trends in Cognitive Sciences*. Elsevier Current Trends. https://doi.org/10.1016/j.tics.2012.08.009.
Pirrone, Angelo, Abigail Dickinson, Rosanna Gomez, Tom Stafford, and Elizabeth Milne. 2017. “Understanding Perceptual Judgment in Autism Spectrum Disorder Using the Drift Diffusion Model.” *Neuropsychology* 31 (2): 173–80.
Platt, Michael L., Brian Lau, and Paul W. Glimcher. 2003. “Situating the Superior Colliculus within the Gaze Control Network.” *The Superior Colliculus: New Approaches for Studying Sensorimotor Integration. CRC Press, Boca Raton*, 1–34.
Pnevmatikakis, Eftychios A., and Andrea Giovannucci. 2017. “NoRMCorre: An Online Algorithm for Piecewise Rigid Motion Correction of Calcium Imaging Data.” *Journal of Neuroscience Methods* 291 (November): 83–94.
Pnevmatikakis, Eftychios A., Daniel Soudry, Yuanjun Gao, Timothy A. Machado, Josh Merel, David Pfau, Thomas Reardon, et al. 2016. “Simultaneous Denoising, Deconvolution, and Demixing of Calcium Imaging Data.” *Neuron* 89 (2): 285–99.
Pollack, J. G., and T. L. Hickey. 1979. “The Distribution of Retino-Collicular Axon Terminals in Rhesus Monkey.” *The Journal of Comparative Neurology* 185 (4): 587–602.
Qi, Song, Demis Hassabis, Jiayin Sun, Fangjian Guo, Nathaniel Daw, and Dean Mobbs. 2018. “How Cognitive and Reactive Fear Circuits Optimize Escape Decisions in Humans.” *Proceedings of the National Academy of Sciences of the United States of America* 115 (12): 3186–91.
Rapanelli, Maximiliano, Tao Tan, Wei Wang, Xue Wang, Zi-Jun Wang, Ping Zhong, Luciana Frick, et al. 2021. “Behavioral, Circuitry, and Molecular Aberrations by Region-Specific Deficiency of the High-Risk Autism Gene Cul3.” *Molecular Psychiatry* 26 (5): 1491–1504.
Razak, Khaleel A., Devin K. Binder, and Iryna M. Ethell. 2021. “Neural Correlates of Auditory Hypersensitivity in Fragile X Syndrome.” *Frontiers in Psychiatry / Frontiers Research Foundation* 12 (October): 720752.
Reichert, H., and J. J. Wine. 1982. “Neural Mechanisms for Serial Order in a Stereotyped Behaviour Sequence.” *Nature* 296 (5852): 86–87.
Reinhard, Katja, Chen Li, Quan Do, Emily G. Burke, Steven Heynderickx, and Karl Farrow. 2019. “A Projection Specific Logic to Sampling Visual Inputs in Mouse Superior Colliculus.” *eLife* 8 (November). https://doi.org/10.7554/eLife.50697.
Reis, Fernando Mcv, Johannes Y. Lee, Sandra Maesta-Pereira, Peter J. Schuette, Meghmik Chakerian, Jinhan Liu, Mimi Q. La-Vu, et al. 2021. “Dorsal Periaqueductal Gray Ensembles Represent Approach and Avoidance States.” *eLife* 10 (May). https://doi.org/10.7554/eLife.64934.
Reis, Fernando M. C. V., Jinhan Liu, Peter J. Schuette, Johannes Y. Lee, Sandra Maesta-Pereira, Meghmik Chakerian, Weisheng Wang, Newton S. Canteras, Jonathan C. Kao, and Avishek Adhikari. 2021. “Shared Dorsal Periaqueductal Gray Activation Patterns during Exposure to Innate and Conditioned Threats.” *The Journal of Neuroscience: The Official Journal of the Society for Neuroscience* 41 (25): 5399–5420.
Remington, Anna, and Jake Fairnie. 2017. “A Sound Advantage: Increased Auditory Capacity in Autism.” *Cognition* 166 (September): 459–65.
Remington, Anna M., John G. Swettenham, and Nilli Lavie. 2012. “Lightening the Load: Perceptual

Load Impairs Visual Detection in Typical Adults but Not in Autism." *Journal of Abnormal Psychology* 121 (2): 544–51.
Remington, Anna, John Swettenham, Ruth Campbell, and Mike Coleman. 2009. "Selective Attention and Perceptual Load in Autism Spectrum Disorder." *Psychological Science* 20 (11): 1388–93.
Reyn, Catherine R. von, Patrick Breads, Martin Y. Peek, Grace Zhiyu Zheng, W. Ryan Williamson, Alyson L. Yee, Anthony Leonardo, and Gwyneth M. Card. 2014. "A Spike-Timing Mechanism for Action Selection." *Nature Neuroscience* 17 (7): 962–70.
Rigoli, Francesco, Michael Ewbank, Tim Dalgleish, and Andrew Calder. 2016. "Threat Visibility Modulates the Defensive Brain Circuit Underlying Fear and Anxiety." *Neuroscience Letters* 612 (January): 7–13.
Robertson, B., D. Owen, J. Stow, C. Butler, and C. Newland. 1996. "Novel Effects of Dendrotoxin Homologues on Subtypes of Mammalian Kv1 Potassium Channels Expressed in Xenopus Oocytes." *FEBS Letters* 383 (1-2): 26–30.
Robertson, Caroline E., and Simon Baron-Cohen. 2017. "Sensory Perception in Autism." *Nature Reviews. Neuroscience* 18 (11): 671–84.
Rosa Salva, O., U. Mayer, and G. Vallortigara. 2015. "Roots of a Social Brain: Developmental Models of Emerging Animacy-Detection Mechanisms." *Neuroscience and Biobehavioral Reviews* 50 (March): 150–68.
Roseberry, Thomas, and Anatol Kreitzer. 2017. "Neural Circuitry for Behavioural Arrest." *Philosophical Transactions of the Royal Society of London. Series B, Biological Sciences* 372 (1718). https://doi.org/10.1098/rstb.2016.0197.
Ross, P. Joel, Wen-Bo Zhang, Rebecca S. F. Mok, Kirill Zaslavsky, Eric Deneault, Lia D'Abate, Deivid C. Rodrigues, et al. 2020. "Synaptic Dysfunction in Human Neurons With Autism-Associated Deletions in PTCHD1-AS." *Biological Psychiatry* 87 (2): 139–49.
Rotschafer, Sarah Elizabeth. 2021. "Auditory Discrimination in Autism Spectrum Disorder." *Frontiers in Neuroscience* 15 (June): 651209.
Rowland, B. A., W. Jiang, and B. E. Stein. 2007. "Cortical Afferents of the Superior Colliculus Guide the Development of Multisensory Integration in Visual Localization." *Investigative Ophthalmology & Visual Science* 48 (13): 3763–3763.
Ruediger, Sarah, and Massimo Scanziani. 2020. "Learning Speed and Detection Sensitivity Controlled by Distinct Cortico-Fugal Neurons in Visual Cortex." *eLife* 9. https://doi.org/10.7554/eLife.59247.
Sacrey, Lori-Ann R., Vickie L. Armstrong, Susan E. Bryson, and Lonnie Zwaigenbaum. 2014. "Impairments to Visual Disengagement in Autism Spectrum Disorder: A Review of Experimental Studies from Infancy to Adulthood." *Neuroscience and Biobehavioral Reviews* 47 (November): 559–77.
Sahibzada, N., P. Dean, and P. Redgrave. 1986. "Movements Resembling Orientation or Avoidance Elicited by Electrical Stimulation of the Superior Colliculus in Rats." *The Journal of Neuroscience: The Official Journal of the Society for Neuroscience* 6 (3): 723–33.
Sainsbury, Clare. 2009. *Martian in the Playground: Understanding the Schoolchild with Asperger's Syndrome*. Sage Publications.
Salay, Lindsey D., and Andrew D. Huberman. 2021. "Divergent Outputs of the Ventral Lateral Geniculate Nucleus Mediate Visually Evoked Defensive Behaviors." *Cell Reports* 37 (1): 109792.
Salay, Lindsey D., Nao Ishiko, and Andrew D. Huberman. 2018. "A Midline Thalamic Circuit Determines Reactions to Visual Threat." *Nature* 557 (7704): 183–89.
Salkić, Naim, Zulfo Ahmetović, Safet Velić, and Lara Krnojelac. 2022. "Difficulties of the Tactile Sensory System Sensory Integration of Children with Autism." *Technium Social Sciences Journal* 27 (January): 502–10.
Sans-Dublanc, Arnau, Anna Chrzanowska, Katja Reinhard, Dani Lemmon, Bram Nuttin, Théo Lambert, Gabriel Montaldo, Alan Urban, and Karl Farrow. 2021. "Optogenetic fUSI for Brain-Wide Mapping of Neural Activity Mediating Collicular-Dependent Behaviors." *Neuron* 109 (11): 1888–1905.e10.
Savier, Elise L., Hui Chen, and Jianhua Cang. 2019. "Effects of Locomotion on Visual Responses in the Mouse Superior Colliculus." *The Journal of Neuroscience: The Official Journal of the Society for Neuroscience* 39 (47): 9360–68.

Schiff, W., J. A. Caviness, and J. J. Gibson. 1962. “Persistent Fear Responses in Rhesus Monkeys to the Optical Stimulus of ‘Looming.’” *Science* 136 (3520): 982–83.
Schleidt, Wolfgang, Michael D. Shalter, and Humberto Moura-Neto. 2011. “The Hawk/goose Story: The Classical Ethological Experiments of Lorenz and Tinbergen, Revisited.” *Journal of Comparative Psychology* 125 (2): 121–33.
Schneider, Keith A., and Sabine Kastner. 2005. “Visual Responses of the Human Superior Colliculus: A High-Resolution Functional Magnetic Resonance Imaging Study.” *Journal of Neurophysiology* 94 (4): 2491–2503.
Scott, Kaela E., Ashley L. Schormans, Katharine Y. Pacoli, Cleusa De Oliveira, Brian L. Allman, and Susanne Schmid. 2018. “Altered Auditory Processing, Filtering, and Reactivity in the Cntnap2 Knock-Out Rat Model for Neurodevelopmental Disorders.” *The Journal of Neuroscience: The Official Journal of the Society for Neuroscience* 38 (40): 8588–8604.
Seamone, Scott, Tristan Blaine, and Timothy E. Higham. 2014. “Sharks Modulate Their Escape Behavior in Response to Predator Size, Speed and Approach Orientation.” *Zoology* 117 (6): 377–82.
Sefton, A. J., A. Mackay-Sim, L. A. Baur, and L. J. Cottee. 1981. “Cortical Projections to Visual Centres in the Rat: An HRP Study.” *Brain Research* 215 (1-2): 1–13.
Senju, Atsushi, Yukiko Kikuchi, Hironori Akechi, Toshikazu Hasegawa, Yoshikuni Tojo, Hiroo Osanai, and Mark H. Johnson. 2011. “Atypical Modulation of Face-Elicited Saccades in Autism Spectrum Disorder in a Double-Step Saccade Paradigm.” *Research in Autism Spectrum Disorders* 5 (3): 1264–69.
Seo, Changwoo, Akash Guru, Michelle Jin, Brendan Ito, Brianna J. Sleezer, Yi Yun Ho, Elias Wang, et al. 2019. “Intense Threat Switches Dorsal Raphe Serotonin Neurons to a Paradoxical Operational Mode.” *Science* 363 (6426): 539–42.
Shang, Congping, Zijun Chen, Aixue Liu, Yang Li, Jiajing Zhang, Baole Qu, Fei Yan, et al. 2018. “Divergent Midbrain Circuits Orchestrate Escape and Freezing Responses to Looming Stimuli in Mice.” *Nature Communications* 9 (1): 1232.
Shang, Congping, Zhihui Liu, Zijun Chen, Yingchao Shi, Qian Wang, Su Liu, Dapeng Li, and Peng Cao. 2015. “A Parvalbumin-Positive Excitatory Visual Pathway to Trigger Fear Responses in Mice.” *Science* 348 (6242): 1472–77.
Shapse, Steven N. 2008. “THE DIAGNOSTIC AND STATISTICAL MANUAL OF MENTAL DISORDERS I.” shapse.com. 2008. http://shapse.com/articles/dsm.pdf.
Shi, Xuefeng, Jad Barchini, Hector Acaron Ledesma, David Koren, Yanjiao Jin, Xiaorong Liu, Wei Wei, and Jianhua Cang. 2017. “Retinal Origin of Direction Selectivity in the Superior Colliculus.” *Nature Neuroscience* 20 (4): 550–58.
Siegel, Markus, Andreas K. Engel, and Tobias H. Donner. 2011. “Cortical Network Dynamics of Perceptual Decision-Making in the Human Brain.” *Frontiers in Human Neuroscience* 5 (February): 21.
Siemann, Justin K., Jeremy Veenstra-VanderWeele, and Mark T. Wallace. 2020. “Approaches to Understanding Multisensory Dysfunction in Autism Spectrum Disorder.” *Autism Research: Official Journal of the International Society for Autism Research* 13 (9): 1430–49.
Sillery, Emma, Richard G. Bittar, Matthew D. Robson, Timothy E. J. Behrens, John Stein, Tipu Z. Aziz, and Heidi Johansen-Berg. 2005. “Connectivity of the Human Periventricular-Periaqueductal Gray Region.” *Journal of Neurosurgery* 103 (6): 1030–34.
Singer, J. D., M. Gurian-West, B. Clurman, and J. M. Roberts. 1999. “Cullin-3 Targets Cyclin E for Ubiquitination and Controls S Phase in Mammalian Cells.” *Genes & Development* 13 (18): 2375–87.
Smolka, Jochen, Jochen Zeil, and Jan M. Hemmi. 2011. “Natural Visual Cues Eliciting Predator Avoidance in Fiddler Crabs.” *Proceedings. Biological Sciences / The Royal Society* 278 (1724): 3584–92.
Soares, Sandra C., Rafael S. Maior, Lynne A. Isbell, Carlos Tomaz, and Hisao Nishijo. 2017. “Fast Detector/first Responder: Interactions between the Superior Colliculus-Pulvinar Pathway and Stimuli Relevant to Primates.” *Frontiers in Neuroscience*. Frontiers Research Foundation. https://doi.org/10.3389/fnins.2017.00067.
Solié, Clément, Alessandro Contestabile, Pedro Espinosa, Stefano Musardo, Sebastiano Bariselli,

Chieko Huber, Alan Carleton, and Camilla Bellone. 2022. “Superior Colliculus to VTA Pathway Controls Orienting Response and Influences Social Interaction in Mice.” *Nature Communications* 13 (1): 1–15.
Sparks, D. L. 1986. “Translation of Sensory Signals into Commands for Control of Saccadic Eye Movements: Role of Primate Superior Colliculus.” *Physiological Reviews* 66 (1): 118–71.
Sparks, D. L., and R. Hartwich-Young. 1989. “The Deep Layers of the Superior Colliculus.” *Reviews of Oculomotor Research* 3: 213–55.
Springer, Steven J., Brian J. Burkett, and Laura A. Schrader. 2014. “Modulation of BK Channels Contributes to Activity-Dependent Increase of Excitability through MTORC1 Activity in CA1 Pyramidal Cells of Mouse Hippocampus.” *Frontiers in Cellular Neuroscience* 8: 451.
Srinivasan, M. V., M. Poteser, and K. Kral. 1999. “Motion Detection in Insect Orientation and Navigation.” *Vision Research* 39 (16): 2749–66.
Stein, Barry E. 1984. “DEVELOPMENT OF THE SUPERIOR COLLICULUS.” Vol. 7.
Stitt, Iain, Edgar Galindo-Leon, Florian Pieper, Gerhard Engler, and Andreas K. Engel. 2013. “Laminar Profile of Visual Response Properties in Ferret Superior Colliculus.” *Journal of Neurophysiology* 110 (6): 1333–45.
Summerfield, C., and A. Blangero. 2017. “Chapter 12 - Perceptual Decision-Making: What Do We Know, and What Do We Not Know?” In *Decision Neuroscience*, edited by Jean-Claude Dreher and Léon Tremblay, 149–62. San Diego: Academic Press.
Tamietto, Marco, and Beatrice de Gelder. 2010. “Neural Bases of the Non-Conscious Perception of Emotional Signals.” *Nature Reviews. Neuroscience* 11 (10): 697–709.
Temizer, Incinur, Joseph C. Donovan, Herwig Baier, and Julia L. Semmelhack. 2015. “A Visual Pathway for Looming-Evoked Escape in Larval Zebrafish.” *Current Biology: CB* 25 (14): 1823–34.
Terburg, David, Diego Scheggia, Rodrigo Triana Del Rio, Floris Klumpers, Alexandru Cristian Ciobanu, Barak Morgan, Estrella R. Montoya, et al. 2018. “The Basolateral Amygdala Is Essential for Rapid Escape: A Human and Rodent Study.” *Cell* 175 (3): 723–35.e16.
Thye, Melissa D., Haley M. Bednarz, Abbey J. Herringshaw, Emma B. Sartin, and Rajesh K. Kana. 2018. “The Impact of Atypical Sensory Processing on Social Impairments in Autism Spectrum Disorder.” *Developmental Cognitive Neuroscience*. Elsevier Ltd. https://doi.org/10.1016/j.dcn.2017.04.010.
Tinbergen, N. 1939. “Why Do Birds Behave the Way They Do.” *Bird Lore*.
Tinbergen, N. 1951. “The Study of Instinct” 237. https://psycnet.apa.org/fulltext/2004-16480-000.pdf.
Tora, David, Andrea M. Gomez, Jean-Francois Michaud, Patricia T. Yam, Frédéric Charron, and Peter Scheiffele. 2017. “Cellular Functions of the Autism Risk Factor PTCHD1 in Mice.” *The Journal of Neuroscience: The Official Journal of the Society for Neuroscience* 37 (49): 11993–5.
Torre-Ubieta, Luis de la, Hyejung Won, Jason L. Stein, and Daniel H. Geschwind. 2016. “Advancing the Understanding of Autism Disease Mechanisms through Genetics.” *Nature Medicine* 22 (4): 345–61.
Tovote, Philip, Maria Soledad Esposito, Paolo Botta, Fabrice Chaudun, Jonathan P. Fadok, Milica Markovic, Steffen B. E. Wolff, et al. 2016. “Midbrain Circuits for Defensive Behaviour.” *Nature* 534 (7606): 206–12.
Tsutsui-Kimura, Iku, Naoshige Uchida, and Mitsuko Watabe-Uchida. 2022. “Dynamical Management of Potential Threats Regulated by Dopamine and Direct- and Indirect-Pathway Neurons in the Tail of the Striatum.” *bioRxiv*. https://doi.org/10.1101/2022.02.05.479267.
Uexküll, Jakob von. 2013. *A Foray into the Worlds of Animals and Humans: With A Theory of Meaning*. U of Minnesota Press.
Ung, D. C., G. Iacono, H. Méziane, E. Blanchard, M-A Papon, M. Selten, J-R van Rhijn, et al. 2018. “Ptchd1 Deficiency Induces Excitatory Synaptic and Cognitive Dysfunctions in Mouse.” *Molecular Psychiatry* 23 (5): 1356–67.
Vagnoni, Eleonora, Stella F. Lourenco, and Matthew R. Longo. 2012. “Threat Modulates Perception of Looming Visual Stimuli.” *Current Biology*. Cell Press. https://doi.org/10.1016/j.cub.2012.07.053.
Vale, Ruben, Dominic A. Evans, and Tiago Branco. 2017. “Rapid Spatial Learning Controls Instinctive

Defensive Behavior in Mice." *Current Biology: CB* 27 (9): 1342–49.
Van der Hallen, Ruth, Kris Evers, Katrien Brewaeys, Wim Van den Noortgate, and Johan Wagemans. 2015. "Global Processing Takes Time: A Meta-Analysis on Local–global Visual Processing in ASD." *Psychological Bulletin* 141 (3): 549–73.
Vargas, L. C., T. A. Marques, and L. C. Schenberg. 2000. "Micturition and Defensive Behaviors Are Controlled by Distinct Neural Networks within the Dorsal Periaqueductal Gray and Deep Gray Layer of the Superior Colliculus of the Rat." *Neuroscience Letters* 280 (1): 45–48.
Vaughn, Eric, Stephen Eichhorn, Won Jung, Xiaowei Zhuang, and Catherine Dulac. 2022. "Three-Dimensional Interrogation of Cell Types and Instinctive Behavior in the Periaqueductal Gray." *bioRxiv*. https://doi.org/10.1101/2022.06.27.497769.
Vella, Lydia, Howard A. Ring, Mike Rf Aitken, Peter C. Watson, Alexander Presland, and Isabel Ch Clare. 2018. "Understanding Self-Reported Difficulties in Decision-Making by People with Autism Spectrum Disorders." *Autism: The International Journal of Research and Practice* 22 (5): 549–59.
Vianna, D. M. L., and M. L. Brandão. 2003. "Anatomical Connections of the Periaqueductal Gray: Specific Neural Substrates for Different Kinds of Fear." *Brazilian Journal of Medical and Biological Research = Revista Brasileira de Pesquisas Medicas E Biologicas / Sociedade Brasileira de Biofisica ... [et Al.]* 36 (5): 557–66.
Wang, Fei, E. Li, Lei De, Qiwen Wu, and Yifeng Zhang. 2021. "OFF-Transient Alpha RGCs Mediate Looming Triggered Innate Defensive Response." *Current Biology: CB* 31 (11): 2263–73.e3.
Wang, Lupeng, Rashmi Sarnaik, Krsna Rangarajan, Xiaorong Liu, and Jianhua Cang. 2010. "Visual Receptive Field Properties of Neurons in the Superficial Superior Colliculus of the Mouse." *The Journal of Neuroscience: The Official Journal of the Society for Neuroscience* 30 (49): 16573–84.
Wang, Quan, Joseph Chang, and Katarzyna Chawarska. 2020. "Atypical Value-Driven Selective Attention in Young Children With Autism Spectrum Disorder." *JAMA Network Open* 3 (5): e204928.
Wang, Shuo, Ming Jiang, Xavier Morin Duchesne, Elizabeth A. Laugeson, Daniel P. Kennedy, Ralph Adolphs, and Qi Zhao. 2015. "Atypical Visual Saliency in Autism Spectrum Disorder Quantified through Model-Based Eye Tracking." *Neuron* 88 (3): 604–16.
Wang, Tianyun, Hui Guo, Bo Xiong, Holly A. F. Stessman, Huidan Wu, Bradley P. Coe, Tychele N. Turner, et al. 2016. "De Novo Genic Mutations among a Chinese Autism Spectrum Disorder Cohort." *Nature Communications* 7 (November): 13316.
Wang, Y. C., S. Jiang, and B. J. Frost. 1993. "Visual Processing in Pigeon Nucleus Rotundus: Luminance, Color, Motion, and Looming Subdivisions." *Visual Neuroscience* 10 (1): 21–30.
Wang, Yuxi C., Marta Bianciardi, Lorena Chanes, and Ajay B. Satpute. 2020. "Ultra High Field fMRI of Human Superior Colliculi Activity during Affective Visual Processing." *Scientific Reports* 10 (1): 1331.
Wässle, H., and R. B. Illing. 1980. "The Retinal Projection to the Superior Colliculus in the Cat: A Quantitative Study with HRP." *The Journal of Comparative Neurology* 190 (2): 333–56.
Wei, Pengfei, Nan Liu, Zhijian Zhang, Xuemei Liu, Yongqiang Tang, Xiaobin He, Bifeng Wu, et al. 2015. "Processing of Visually Evoked Innate Fear by a Non-Canonical Thalamic Pathway." *Nature Communications* 6 (April): 6756.
Wells, Michael F., Ralf D. Wimmer, L. Ian Schmitt, Guoping Feng, and Michael M. Halassa. 2016. "Thalamic Reticular Impairment Underlies Attention Deficit in Ptchd1(Y/-) Mice." *Nature* 532 (7597): 58–63.
Wendt, Julia, Andreas Löw, Mathias Weymar, Martin Lotze, and Alfons O. Hamm. 2017. "Active Avoidance and Attentive Freezing in the Face of Approaching Threat." *NeuroImage* 158 (September): 196–204.
Westby, G. W., K. A. Keay, P. Redgrave, P. Dean, and M. Bannister. 1990. "Output Pathways from the Rat Superior Colliculus Mediating Approach and Avoidance Have Different Sensory Properties." *Experimental Brain Research. Experimentelle Hirnforschung. Experimentation Cerebrale* 81 (3): 626–38.
Wheatcroft, Thomas, Aman B. Saleem, and Samuel G. Solomon. 2022. "Functional Organisation of the Mouse Superior Colliculus." *Frontiers in Neural Circuits* 16 (April): 792959.
Wilming, Niklas, Peter R. Murphy, Florent Meyniel, and Tobias H. Donner. 2020. "Large-Scale

Dynamics of Perceptual Decision Information across Human Cortex." *Nature Communications* 11 (1): 5109.
Winklhofer, M., K. Matthias, G. Seifert, M. Stocker, S. Sewing, T. Herget, C. Steinhäuser, and S. Saaler-Reinhardt. 2003. "Analysis of Phosphorylation-Dependent Modulation of Kv1.1 Potassium Channels." *Neuropharmacology* 44 (6): 829–42.
Winter, Matt. 2011. *Asperger Syndrome - What Teachers Need to Know: Second Edition*. Jessica Kingsley Publishers.
Wiśniowiecka-Kowalnik, Barbara, and Beata Anna Nowakowska. 2019. "Genetics and Epigenetics of Autism Spectrum Disorder-Current Evidence in the Field." *Journal of Applied Genetics* 60 (1): 37–47.
Wu, Le Qing, Yu Qiong Niu, Jin Yang, and Shu Rong Wang. 2005. "Tectal Neurons Signal Impending Collision of Looming Objects in the Pigeon." *The European Journal of Neuroscience* 22 (9): 2325–31.
Wurtz, R. H., and J. E. Albano. 1980. "Visual-Motor Function of the Primate Superior Colliculus." *Annual Review of Neuroscience* 3: 189–226.
Wyart, Valentin, and Catherine Tallon-Baudry. 2009. "How Ongoing Fluctuations in Human Visual Cortex Predict Perceptual Awareness: Baseline Shift versus Decision Bias." *The Journal of Neuroscience: The Official Journal of the Society for Neuroscience* 29 (27): 8715–25.
Xie, Zhiyong, Huating Gu, Meizhu Huang, Xinyu Cheng, Congping Shang, Ting Tao, Dapeng Li, et al. 2022. "Mechanically Evoked Defensive Attack Is Controlled by GABAergic Neurons in the Anterior Hypothalamic Nucleus." *Nature Neuroscience* 25 (1): 72–85.
Yamawaki, Yoshifumi, and Yoshihiro Toh. 2009. "Responses of Descending Neurons to Looming Stimuli in the Praying Mantis Tenodera Aridifolia." *Journal of Comparative Physiology. A, Neuroethology, Sensory, Neural, and Behavioral Physiology* 195 (3): 253–64.
Yang, Xing, Qingqing Liu, Jinling Zhong, Ru Song, Lin Zhang, and Liping Wang. 2020. "A Simple Threat-Detection Strategy in Mice." *BMC Biology* 18 (1): 93.
Ydenberg, R. C., and L. M. Dill. 1986. "The Economics of Fleeing from Predators." In *Advances in the Study of Behavior*, edited by Jay S. Rosenblatt, Colin Beer, Marie-Claire Busnel, and Peter J. B. Slater, 16:229–49. Academic Press.
Yilmaz, Melis, and Markus Meister. 2013. "Rapid Innate Defensive Responses of Mice to Looming Visual Stimuli." *Current Biology: CB* 23 (20): 2011–15.
Zacarias, Ricardo, Shigehiro Namiki, Gwyneth M. Card, Maria Luisa Vasconcelos, and Marta A. Moita. 2018. "Speed Dependent Descending Control of Freezing Behavior in Drosophila Melanogaster." *Nature Communications* 9 (1): 3697.
Zbili, Mickaël, Sylvain Rama, Maria-José Benitez, Laure Fronzaroli-Molinieres, Andrzej Bialowas, Norah Boumedine-Guignon, Juan José Garrido, and Dominique Debanne. 2021. "Homeostatic Regulation of Axonal Kv1.1 Channels Accounts for Both Synaptic and Intrinsic Modifications in the Hippocampal CA3 Circuit." *Proceedings of the National Academy of Sciences of the United States of America* 118 (47). https://doi.org/10.1073/pnas.2110601118.
Zhang, Yifeng, In-Jung Kim, Joshua R. Sanes, and Markus Meister. 2012. "The Most Numerous Ganglion Cell Type of the Mouse Retina Is a Selective Feature Detector." *Proceedings of the National Academy of Sciences of the United States of America* 109 (36): E2391–98.
Zhao, Xinyu, Mingna Liu, and Jianhua Cang. 2014. "Visual Cortex Modulates the Magnitude but Not the Selectivity of Looming-Evoked Responses in the Superior Colliculus of Awake Mice." *Neuron* 84 (1): 202–13.
Zhou, Z., Xuemei Liu, Shanping Chen, Zhijian Zhang, Yuanming Liu, Quentin Montardy, Yongqiang Tang, et al. 2019. "A VTA GABAergic Neural Circuit Mediates Visually Evoked Innate Defensive Responses." *Neuron* 103 (3): 473–88.e6.
Zingg, Brian, Xiao Lin Chou, Zheng Gang Zhang, Lukas Mesik, Feixue Liang, Huizhong Whit Tao, and Li I. Zhang. 2017. "AAV-Mediated Anterograde Transsynaptic Tagging: Mapping Corticocollicular Input-Defined Neural Pathways for Defense Behaviors." *Neuron* 93 (1): 33–47.